

**MIXTURE PREPARATION PROCESS IN SI ENGINES
WITH PARTICULAR REFERENCE TO AN AIR-
ASSISTED FUEL VAPORISER**

by
Simon David Jackson

Submitted for the Degree of Doctor of Philosophy

**University College London
Department of Mechanical Engineering**

1996

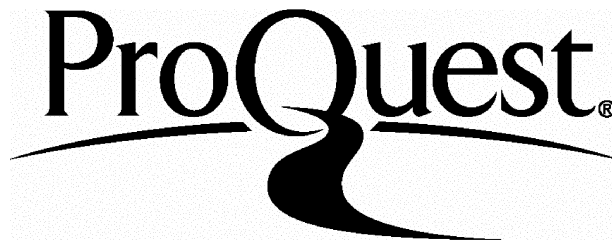
ProQuest Number: 10106880

All rights reserved

INFORMATION TO ALL USERS

The quality of this reproduction is dependent upon the quality of the copy submitted.

In the unlikely event that the author did not send a complete manuscript and there are missing pages, these will be noted. Also, if material had to be removed, a note will indicate the deletion.



ProQuest 10106880

Published by ProQuest LLC(2016). Copyright of the Dissertation is held by the Author.

All rights reserved.

This work is protected against unauthorized copying under Title 17, United States Code.
Microform Edition © ProQuest LLC.

ProQuest LLC
789 East Eisenhower Parkway
P.O. Box 1346
Ann Arbor, MI 48106-1346

ABSTRACT

This thesis describes the problems encountered during cold-start operation of a SI engine and details an alternative fuelling system designed to reduce unburned hydrocarbon emissions throughout this period. The system is able to produce vaporised fuel during start-up conditions by incorporating an electrical heating element which may be switched off once the catalyst has reached its light-off temperature. Air assistance has been incorporated into the design to ensure good atomisation of the liquid fuel when operating with the heating element disabled.

Characterisation of the liquid fuel spray and measurement of the efficiency of the heating element was performed. The device was tested to characterise its performance and applied to an engine to provide comparison of UHC emissions during a cold-start with the standard fuel system. Further tests were performed to analyse the vapour flow of fuel within the intake port of a running engine of the device in both air atomisation and fuel vaporisation modes and compared with that obtained from the standard pintle injector. Two major factors influence the mixture preparation, namely backflow and port temperature. These effects were isolated and removed for the final test programme by the use of a pulsating flow rig.

A means of procuring a pressurised air supply for the device instead of relying on an atmospheric bleed was also investigated. The method was to provide a tapping into the combustion chamber via a restriction so to control the bleed rate.

The tests identified reduction of engine out UHC emissions during the cold-start period of operation. Results from intake port FRFID tests indicated the vapour flow of fuel within the port, clarified the mixture preparation process and identified the major contributors to fuel vapour formation and movement. The cylinder pressure tapping experiments revealed the possibilities and benefits of such an arrangement.

ACKNOWLEDGEMENTS

The author would like to thank both Paul Williams and Chris Nightingale for their unfailing and enthusiastic support and guidance.

The UCL technical staff for their continued efforts in deciphering all submitted technical drawings, especially Phil Jeavons, John Inns and Richard Winn.

Tom Ma of the Ford Motor Company for the numerous suggestions and ideas that kept the work progressing, and to Tim Sweet, also of the Ford Motor Company, for the supply of many pieces of necessary hardware.

Thanks are also extended to the EPSRC and the Ford Motor Company for funding the research.

Finally I would like to thank my parents for their support and my sister and brother in law for providing somewhere to live throughout the duration of the work.

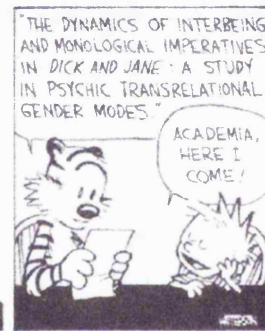
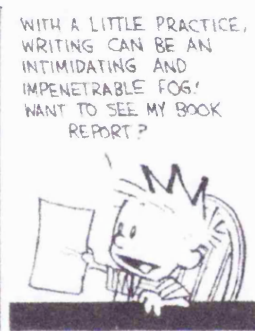
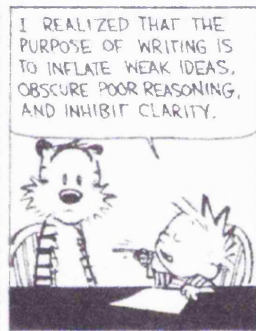


TABLE OF CONTENTS

Abstract.....	ii
Acknowledgements.....	iii
Table of contents.....	v
List of figures.....	ix
List of tables.....	xv
Nomenclature.....	xvi
CHAPTER 1, A LITERATURE SURVEY.....	1
1.1 INTRODUCTION.....	2
1.2 FOUR-STROKE SI ENGINE ANALYSIS.....	3
1.3 EMISSIONS, EMISSION REGULATIONS AND EXHAUST GAS TREATMENT.....	6
1.3.1 Introduction.....	6
1.3.2 HC: Pollutant.....	6
1.3.3 HC: Formation.....	6
1.3.4 Oxides of nitrogen (NO _x): Pollutant.....	7
1.3.5 NO formation.....	8
1.3.6 NO ₂ formation.....	9
1.3.7 Carbon monoxide/dioxide: Emissions.....	9
1.3.8 CO ₂ /CO formation.....	9
1.3.9 Emissions regulations.....	10
1.3.10 Cold-start emissions.....	12
1.3.11 Exhaust gas treatment.....	13
1.3.12 Closing comments on emissions.....	21
1.4 MIXTURE PREPARATION/ FUEL SPRAYS.....	22
1.4.1 Carburettors.....	22
1.4.2 Multi-point fuel injection.....	23
1.4.3 Single-point fuel injection.....	24
1.4.4 Drop size.....	25
1.4.5 Problems associated with the Sauter mean diameter.....	26
1.4.6 An alternative to the Sauter mean diameter.....	26
1.4.7 Droplet size distributions.....	27
1.4.8 Fuel transportation properties.....	28
1.4.8a Droplet impaction: Carburettors & single-point fuel injection.....	28
1.4.8b Fuel film behaviour.....	31
1.4.8c Vaporised mixtures.....	32
1.4.8d Vaporised mixtures applied to fully warm engines.....	32
1.4.9 Fuel injector sprays.....	34
1.4.9a Port injection.....	34
1.4.9b Air-assisted atomisers.....	37
1.4.9c Vaporised mixtures applied during cold-starting and warm up.....	41
1.4.10 Closing comments on mixture preparation.....	45
1.5 HEAT TRANSFER THEORY.....	47
1.5.1 Introduction.....	47
1.5.2 Dimensional analysis applied to heat transfer by forced convection.....	48
1.5.3 Heat transfer with change of phase.....	50
1.5.4 Closing comments on heat transfer theory.....	53
1.6.1 Introduction.....	55
1.6.3 Laser diffraction particle sizing.....	57
1.6.4 Problems of evaporation.....	57
1.6.5 Vapour concentration measurement.....	59
1.6.6 Closing comments on spray measurement techniques.....	64
1.6.6a Footnote on laser induced fluorescent techniques.....	65

1.7 RESEARCH PROGRAMME.....	67
1.8 REFERENCES.....	70
CHAPTER 2, CHARACTERISATION OF FUEL/AIR MIXTURE	
PREPARATION.....	78
2.1 AIR-ASSISTED FUEL VAPORISER (AAFV): DESIGN.....	79
2.2 THEORY.....	81
2.2.1 Compressible flow equations.....	81
2.2.2 Heat transfer.....	83
2.2.3 Calculation of C_{pf}	83
2.2.4 Flow restriction.....	84
2.3 DISCUSSION I.....	85
2.3.1 Operating criteria.....	85
2.3.2 Time delay to leading edge formation.....	86
2.3.3 Liquid fuel/air-atomisation operation: Spray duration.....	87
2.3.4 Fuel droplet size.....	88
2.3.5 Modulation of air flow.....	89
2.4 CONCLUSIONS FROM INITIAL TESTING.....	90
2.5 DISCUSSION II.....	91
2.5.1 Vaporised fuel operation.....	91
2.5.2 Geometric influences on vaporisation.....	91
2.5.3 Heat transfer.....	92
2.5.4 Nozzle mass flow rates.....	93
2.5.5 Spray duration.....	96
2.5.6 Drop size evaluation.....	97
2.5.7 Vapour detection.....	97
2.5.8 Spray cone angles.....	98
2.6 CONCLUSIONS FROM VAPOUR TESTING.....	99
2.7 CONCLUDING STATEMENT.....	99
2.8 REFERENCES.....	101
APPENDIX A2.....	102
A2.1 SIMULATED ENGINE CONDITIONS.....	102
A2.1.1 Idle.....	102
A2.1.2 Road load.....	102
A2.1.3 Full load.....	102
A2.2 GLOW PLUG TEMPERATURE DATA.....	103
A2.2.1 Glow plug temperature measurements points.....	103
A2.3 LASER DIAGNOSTIC PARTICLE SIZING.....	106
A2.3.1 Background and limitations.....	106
A2.3.2 Theory.....	107
A2.3.3 Malvern 2600c.....	109
A2.4 AAFV FUEL SPRAY CONE ANGLES.....	111
A2.4.1 Fuel spray cone angle testing.....	111
A2.5 RATIO OF SPECIFIC HEATS FOR GASOLINE/AIR MIXTURES.....	112
CHAPTER 3, COLD-START TESTING.....	114
3.1 INTRODUCTION.....	114
3.2 TEST DETAILS.....	117
3.2.1 Installation.....	117
3.2.2 Testbed.....	117
3.2.3 Operating system.....	118
3.2.4 Data-logging system.....	118
3.3 EXPERIMENTAL PROCEDURE.....	118
3.4 TEST RESULTS AND DISCUSSION.....	120

3.5 CONCLUSIONS	127
3.6 REFERENCES	128
APPENDIX A3	130
A3.1 DATA LOGGING	130
CHAPTER 4, AAFV DEVELOPMENT PROGRAMME	135
4.1 INTRODUCTION	136
4.2 CHANGES TO THE ORIGINAL UNIT	136
4.3 INSTALLATION IMPROVEMENTS	137
4.4 CONCLUSIONS	139
APPENDIX A4	141
A4.1 GLOW PLUG CONTROLLER FUNCTION	141
A4.2 FUNCTION DIAGRAMS	142
A4.2.1 Normal operation	142
A4.2.2 Premature start	142
A4.2.3 Start after safety cut-off	143
A4.2.4 Unsuccessful start	143
CHAPTER 5, INTAKE & EXHAUST PORT UNBURNED HYDROCARBON CONCENTRATION SAMPLING	145
5.1 INTRODUCTION	145
5.2 TEST PROGRAMME MEASUREMENT APPARATUS	150
5.2.1 Combustion high frequency response flame ionisation detector, HFRFID	150
5.2.2 Design of cylinder head sample sites	153
5.3 EXTERNAL AIR-ASSISTANCE FOR THE AAFV	154
5.3.1 Air pump	155
5.3.2 Cylinder Pressure Tapping, CPT	155
5.4 FIGURE GUIDE	158
5.4.1 Key to figures	158
5.4.2 HFRFID sampling sites:	158
5.5 DISCUSSION	159
5.5.1 HFRFID tests: 1500 rev/min, road load, 35.9 kPa intake pressure	159
5.5.1a Intake port sampling, vapour, atmospheric bleed	159
5.5.1b Intake port sampling, vapour, cylinder pressure tapping 1 & 2	161
5.5.1c Intake port sampling, air-atomisation (i.e. no heat applied), cylinder pressure tapping 1 & 2	163
5.5.1d Intake port sampling, backflow, standard, air-atomisation & vapour, atmospheric bleed	166
5.5.2 HFRFID exhaust port sampling	169
5.5.2a Exhaust port sampling, 1500 rev/min, road load, 35.9 kPa intake pressure, standard, air-atomisation & vapour, atmospheric bleed	170
5.5.2b Exhaust port sampling, air-atomisation, cylinder pressure tapping 1 & 2	172
5.5.3 HFRFID intake port sampling: 800 rev/min, idle, 52.3 kPa intake pressure	173
5.5.3a Intake port sampling, vapour, atmospheric bleed	173
5.5.3b Intake port sampling, vapour, cylinder pressure tapping 1 & 2	175
5.5.3c Intake port sampling, air-atomisation, cylinder pressure tapping 1 & 2	177
5.5.3d Intake port sampling, backflow, standard, air-atomisation & vapour, atmospheric bleed	179
5.5.6 HFRFID intake port sampling: 1650 rev/min, full load, 0 kPa intake pressure	182
5.5.6a Intake port sampling, standard, air-atomisation & vapour, cylinder pressure tapping 2	182
5.6 CONCLUSIONS	185
5.7 REFERENCES	187

APPENDIX A5	189
A5.1 GENERAL	189
A5.2 ENGINE SPECIFICATION:	189
A5.2.1 Valve timing	189
A5.3 TEST DATA	190
A5.3.1 Engine variables.....	190
A5.3.2 Idle settings.....	190
A5.3.3 Road load setting.....	190
A5.3.4 Full load settings.....	190
CHAPTER 6, INLET PORT UHC TRACES, ENGINE VS. PULSATING FLOW RIG	192
6.1 INTRODUCTION.....	192
6.2 TEST RESULTS AND DISCUSSION.....	194
6.2.1 800 rev/min idle (53.2 kPa manifold depression), sample sites B & D.....	194
6.2.2 1500 rev/min road load (35.9 kPa manifold depression), sample sites B & D	198
6.2.3 1650 rev/min full load (0 kPa manifold depression), sample sites B & D.....	203
6.3 CONCLUSIONS	206
6.4 REFERENCES.....	207
CHAPTER 7, MOTORED-START & INJECTOR INTERRUPT TESTS	209
7.1 INTRODUCTION.....	209
7.2 TEST PROGRAMME.....	212
7.3 DISCUSSION	213
7.3.1 Motored-start tests, (idling conditions, 52.3 kPa manifold depression), standard fuel system, open & closed valve injection strategy	213
7.3.2 Motored-start tests, (idling conditions, 52.3 kPa manifold depression), AAFV, air- atomisation, open & closed valve injection strategy.....	215
7.3.3 Motored-start tests, (idling conditions, 52.3 kPa manifold depression), AAFV, fuel vaporisation, open & closed valve injection strategy.....	217
7.4 INJECTOR INTERRUPT TESTS.....	219
7.4.1 Curve fitting program as applied to injector interrupt test measurements.....	219
7.4.2 Injector interrupt tests, (idling conditions, 52.3 kPa manifold depression), standard fuel system, open & closed valve injection strategy	221
7.5 CONCLUSIONS.....	224
7.6 REFERENCES.....	225
APPENDIX A7	226
A7.1 INJECTOR INTERRUPT DECAY AND CUMULATIVE UHC TRACES.....	226
CHAPTER 8, CONCLUSIONS AND SUGGESTIONS FOR FUTURE WORK	228
8.1 SUMMARY OF CONCLUSIONS FROM PRECEDING CHAPTERS.....	228
8.1.1 Steady flow rig tests	228
8.1.2 Cold-start engine tests.....	228
8.1.3 Intake port HFRFID sampling: engine tests.....	229
8.1.4 Intake port HFRFID sampling; PFR tests	229
8.1.5 Motored-start and injector interrupt tests.....	230
8.2 FURTHER DEVELOPMENT POSSIBILITIES FOR THE AAFV.....	231
8.2.1 Recommendations for further research	232
8.3 CLAIMS OF ORIGINALITY	233
APPENDIX A8	234
A8.1 GLOW PLUG POWER CONTROLLER.....	234

LIST OF FIGURES

Figure 1.1, The Otto cycle.....	3
Figure 1.2, Variation of exhaust NO concentration with air/fuel ratio	8
Figure 1.3, Variation of HC, CO and No _x with air/fuel ratio.....	9
Figure 1.4, FTP driving schedule.....	12
Figure 1.5, HC emission and catalyst temperature vs. time during Urban Drive Cycle.....	13
Figure 1.6, Schematic of EGI system	15
Figure 1.7, Flammability of cold exhaust/air mixture	17
Figure 1.8, Catalyst heating options.....	18
Figure 1.9, Reduction of emissions due to catalyst heating.....	18
Figure 1.10, Experimental cold-start hydrocarbon collection exhaust routing	19
Figure 1.11, FTP cold-start hydrocarbon collection	20
Figure 1.12, Schematic of an elementary carburettor.....	22
Figure 1.13, Cross section of pintle type fuel injector	23
Figure 1.14, Electronic multi-point port fuel injection system	24
Figure 1.15, Cutaway drawing of a two injector throttle-body	25
Figure 1.16a, Regions of engine load and speed range where extensive pools or puddles, liquid films or rivulets were observed on the manifold plenum floor.....	29
Figure 1.16b, Regions of engine load and speed range where extensive pools or puddles, liquid films or rivulets were observed in the manifold runner.....	29
Figure 1.17a, Percentage of indolene fuel evaporated at equilibrium at one pressure of atmosphere.....	30
Figure 1.17b, Effect of pressure on amount of indolene fuel evaporated	30
Figure 1.18a, Predicted behaviour of the fuel film for an uncompensated step change in engine operating conditions.....	31
Figure 1.18b, Observed variation in air/fuel ratio for uncompensated throttle opening	31
Figure 1.19, Gasoline injection valves.....	35
Figure 1.20, Structure of a two-stream injector.....	36
Figure 1.21, Start performance (-30° C) of a four-valve engine using standard pintle and two-stream injector	37
Figure 1.22, Lucas air-assisted fuel injector with air bleed upstream of the fuel metering orifice.....	38
Figure 1.23, Nippondenso air-assisted fuel injector with air bleed downstream of the fuel metering orifice	38
Figure 1.24, Sectioned view of air-assisted atomiser.....	39
Figure 1.25, Fuel spray mean droplet diameter.....	40
Figure 1.26, Variation of droplet size with air pressure	40
Figure 1.27, Influence of injection timing and spray quality on part load engine performance.....	41
Figure 1.28, NEL fuel vaporiser.....	42
Figure 1.29, Comparison of HC emissions from a 16-valve engine during cold-starting using liquid and vaporised fuel	42
Figure 1.30, Heater power required to vaporise fuel at various pulse widths and injection frequencies	43
Figure 1.31, PTC honeycomb EFE heater	44
Figure 1.32, PTC manifold heater.....	44
Figure 1.33, Modified exhaust cam.....	45
Figure 1.34, Modified and standard camshaft diagrams	45
Figure 1.35, The four regimes of pool boiling in water at atmospheric pressure	48
Figure 1.36, Influence of valve temperature on rates of heat transfer to air/fuel mixtures.....	51
Figure 1.37, Percentage of liquid fuel remaining along a heated duct.....	53
Figure 1.38, Droplet temperature along a heated duct.....	53

Figure 1.39, Typical PDA optical set-up	56
Figure 1.51, Dimensionless energy distribution of diffracted light.....	58
Figure 1.41, Infra-red transmission range of various hydrocarbon molecules	59
Figure 1.42, Partition of space into concentric annuli for axisymmetric geometries.....	60
Figure 1.43, Radial variation of total IR transmission at 3.39 μm in the axial plane of a 1.48 MPa n-heptane spray	61
Figure 1.44, Radial variation of the fuel vapour concentration in an n-heptane spray	61
Figure 1.45, Effects of injector timing on the cycle to cycle repeatability of fuel vapour concentrations.....	62
Figure 1.46, Influence of engine temperature on in-cylinder fuel vapour concentration.....	63
Figure 1.47, Vapour mole fraction measured as a function of test section position, light loading case.....	64
Figure 1.48, Vapour mole fraction measured as a function of test section position, heavy loading case.....	64
Figure 2.1, Sectioned view of the UCL air-assisted fuel vaporiser	79
Figure 2.2, Light obscuration vs. time delay after injector trigger, 0.8, 1.5 & 2.3 mm nozzles, 1500 rev/min, passive air bleed.....	86
Figure 2.3, Light obscuration vs. time delay after injector trigger, 0.8, 1.5 & 2.3 mm nozzles, 2000 rev/min, 35 kPa air bleed pressure	86
Figure 2.4, Light obscuration vs. time delay after injector trigger, 0.8, 1.5 & 2.3 mm nozzles, 2000 rev/min, 70 kPa air bleed pressure	87
Figure 2.5, Fuel spray drop size (Smd) vs. time delay after injector trigger, 0.8, 1.5 & 2.3 mm nozzles, 1500 rev/min, passive air bleed.....	88
Figure 2.6, Fuel spray drop size (Smd) vs. time delay after injector trigger, 0.8, 1.5 & 2.3 mm nozzles, 2000 rev/min, full load, 35 kPa air bleed pressure.....	88
Figure 2.7, Fuel spray drop size (Smd) vs. time delay after injector trigger, 0.8, 1.5 & 2.3 mm nozzles, 2000 rev/min, 70 kPa air bleed pressure.....	89
Figure 2.8, Light obscuration vs. time delay after injector trigger, 1.2 & 1.5 mm nozzles, 2000 rev/min, full load, 70 kPa air bleed pressure.....	97
Figure 2.9, Fuel spray drop size (Smd) vs. time delay after injector trigger, 1.2 & 1.5 mm nozzles, 2000 rev/min, full load, 70 kPa air bleed pressure.....	97
Figure 2.10, Image of fuel spray into quiescent air, 1.5 mm nozzle, 12 kPa air-assistance....	98
Figure 2.11, Image of fuel spray into quiescent air, 1.5 mm nozzle, 70 kPa air-assistance....	98
Figure A2.1, Variation of γ_{mixture} with respect to air/fuel ratio across lines of constant mixture temperature.....	112
Figure 3.1, Cold-start gravimetric air/fuel ratio, 7° C start temperature.....	121
Figure 3.2, Cold-start gravimetric air/fuel ratio, 0° C start temperature.....	121
Figure 3.3, Cold-start hydrocarbon emissions, optimum results from standard injector and AAFV tests, 7° C start temperature.....	121
Figure 3.4, Cold-start hydrocarbon emissions, optimum results from standard injector and AAFV tests, 0° C start temperature.....	121
Figure 3.5, Cold-start carbon monoxide emissions, 0° C start temperature	122
Figure 3.6, Cold-start hydrocarbon emissions, 7° C start temperature	122
Figure 3.7, Cold-start hydrocarbon emissions, 0° C start temperature	122
Figure 3.8, Typical rise of engine speed and manifold depression with respect to time.....	123
Figure 3.9, Engine speed with respect to time, standard injectors, 7° C start temperature...	124
Figure 3.10, Engine speed with respect to time, AAFV, 7° C start temperature.....	124
Figure 3.11, Typical electrical power requirements for a 6-cylinder installation of the AAFVs	125
Figure A3.1, Response characteristics of Horiba HC/CO analyser to a step change in engine fuelling.....	134
Figure A3.2, Horiba unburned hydrocarbon calibration.....	134
Figure A3.3, Horiba carbon monoxide calibration.....	134

Figure A3.4, Horiba carbon monoxide calibration, 4% spanned to 1.5 V.....	134
Figure A3.5, Jaguar air flow meter calibration.....	134
Figure 4.1, Explode view of the redesigned AAFV.....	138
Figure 4.2, Computer generated model of the redesigned AAFV installation on the Zetec engine.....	139
Figure 4.3, Zetec engine equipped with the redesigned AAFV installation.....	139
Figure 4.4, Computer generated model of the redesigned AAFV installation on the Sigma engine.....	140
Figure 4.5, Sigma engine equipped with the redesigned AAFV installation.....	140
Figure 5.1, Comparison of a conventional FID and the Combustion HFRFID.....	151
Figure 5.2, Sectioned view of the Combustion HFRFID.....	152
Figure 5.3, View of the intake port showing the HFRFID, probe sites B & C.....	153
Figure 5.4, Overall view of the engine test bed.....	154
Figure 5.5a, CPT schematic.....	156
Figure 5.5b, View of the cylinder pressure tapping pipe work cylinder head and the HFRFID probe sites B, C & D.....	157
Figure 5.6, Closed valve injection, fuel vaporisation, 1500 rev/min road load, $\lambda = 1$, (sample sites C & D).....	159
Figure 5.7, Open valve injection, fuel vaporisation, 1500 rev/min road load, $\lambda = 1$, (sample sites C & D).....	159
Figure 5.8, Closed valve injection, fuel vaporisation, 1500 rev/min road load, $\lambda = 1$, (sample sites B & C).....	160
Figure 5.9, Open valve injection, fuel vaporisation, 1500 rev/min road load, $\lambda = 1$, (sample sites B & C).....	160
Figure 5.10, Closed valve injection, CPT1, fuel vaporisation, 1500 rev/min road load, $\lambda = 1$, (sample sites B & C).....	162
Figure 5.11, Closed valve injection, CPT2, fuel vaporisation, 1500 rev/min road load, $\lambda = 1$, (sample sites B & C).....	162
Figure 5.12, Open valve injection, CPT1, fuel vaporisation, 1500 rev/min road load, $\lambda = 1$, (sample sites B & C).....	162
Figure 5.13, Open valve injection, CPT2, fuel vaporisation, 1500 rev/min road load, $\lambda = 1$, (sample sites B & C).....	162
Figure 5.14, CPT1 bleed pressure, fuel vaporisation, 1500 road load, $\lambda = 1$	163
Figure 5.15, CPT2 bleed pressure, fuel vaporisation, 1500 road load, $\lambda = 1$	163
Figure 5.16, Closed valve injection, CPT1, air-atomisation, 1500 rev/min road load, $\lambda = 1$, (sample sites B & C).....	164
Figure 5.17, Closed valve injection, CPT2, air-atomisation, 1500 rev/min road load, $\lambda = 1$, (sample sites B & C).....	164
Figure 5.18, Open valve injection, CPT1, air-atomisation, 1500 rev/min road load, $\lambda = 1$, (sample sites B & C).....	164
Figure 5.19, Open valve injection, CPT2, air-atomisation, 1500 rev/min road load, $\lambda = 1$, (sample sites B & C).....	164
Figure 5.20, CPT1 bleed pressure, air-atomisation, 1500 road load, $\lambda = 1$	165
Figure 5.21, CPT2 bleed pressure, air-atomisation, 1500 road load, $\lambda = 1$	165
Figure 5.22, Closed valve injection, standard injector, 1500 rev/min road load, $\lambda = 1$, (sample site D).....	166
Figure 5.23, Open valve injection, standard injector, 1500 rev/min road load, $\lambda = 1$, (sample site D).....	166
Figure 5.24, Closed valve injection, air-atomisation, 1500 rev/min road load, $\lambda = 1$, (sample site D).....	167
Figure 5.25, Open valve injection, air-atomisation, 1500 rev/min road load, $\lambda = 1$, (sample site D).....	167

Figure 5.26, Closed valve injection, fuel vaporisation, 1500 rev/min road load, $\lambda = 1$, (sample site D).....	167
Figure 5.27, Open valve injection, fuel vaporisation, 1500 rev/min road load, $\lambda = 1$, (sample site D).....	167
Figure 5.28, Typical exhaust HFRFID trace	169
Figure 5.29, Closed valve injection, standard injector, 1500 rev/min road load, $\lambda = 1$, (sample site A).....	171
Figure 5.30, Open valve injection, standard injector, 1500 rev/min road load, $\lambda = 1$, (sample site A).....	171
Figure 5.31, Closed valve injection, air-atomisation, 1500 rev/min road load, $\lambda = 1$, (sample site A).....	171
Figure 5.32, Open valve injection, air-atomisation, 1500 rev/min road load, $\lambda = 1$, (sample site A).....	171
Figure 5.33, Closed valve injection, fuel vaporisation, 1500 rev/min road load, $\lambda = 1$, (sample site A).....	171
Figure 5.34, Open valve injection, fuel vaporisation, 1500 rev/min road load, $\lambda = 1$, (sample site A).....	171
Figure 5.35, Closed valve injection, CPT1, air-atomisation, 1500 rev/min road load, $\lambda = 1$, (sample site A).....	172
Figure 5.36, Open valve injection, CPT1, air-atomisation, 1500 rev/min road load, $\lambda = 1$, (sample site A).....	172
Figure 5.37, Closed valve injection, fuel vaporisation, 800 rev/min idle, $\lambda = 1$, (sample sites C & D).....	174
Figure 5.38, Open valve injection, fuel vaporisation, 800 rev/min idle, $\lambda = 1$, (sample sites C & D).....	174
Figure 5.39, Closed valve injection, fuel vaporisation, 800 rev/min idle, $\lambda = 1$, (sample sites B & C).....	174
Figure 5.40, Open valve injection, fuel vaporisation, 800 rev/min idle, $\lambda = 1$, (sample sites B & C).....	174
Figure 5.41, Closed valve injection, CPT1, fuel vaporisation, 800 rev/min idle, $\lambda = 1$, (sample sites B & C).....	176
Figure 5.42, Closed valve injection, CPT2, fuel vaporisation, 800 rev/min idle, $\lambda = 1$, (sample sites B & C).....	176
Figure 5.43, Open valve injection, CPT1, fuel vaporisation, 800 rev/min idle, $\lambda = 1$, (sample sites B & C).....	176
Figure 5.44, Open valve injection, CPT2, fuel vaporisation, 800 rev/min idle, $\lambda = 1$, (sample sites B & C).....	176
Figure 5.45, CPT1 bleed pressure, fuel vaporisation, 800 rev/min idle, $\lambda = 1$	177
Figure 5.46, CPT2 bleed pressure, fuel vaporisation, 800 rev/min idle, $\lambda = 1$	177
Figure 5.47, Closed valve injection, CPT1, air-atomisation, 800 rev/min idle, $\lambda = 1$, (sample sites B & C).....	178
Figure 5.48, Closed valve injection, CPT2, air-atomisation, 800 rev/min idle, $\lambda = 1$, (sample sites B & C).....	178
Figure 5.49, Open valve injection, CPT2, air-atomisation, 800 rev/min idle, $\lambda = 1$, (sample sites B & C).....	178
Figure 5.50, Open valve injection, CPT2, air-atomisation, 800 rev/min idle, $\lambda = 1$, (sample sites B & C).....	178
Figure 5.51, CPT1 bleed pressure, air-atomisation, 800 rev/min idle, $\lambda = 1$	179
Figure 5.52, CPT2 bleed pressure, air-atomisation, 800 rev/min idle, $\lambda = 1$	179
Figure 5.53, Closed valve injection, standard injector, 800 rev/min idle, $\lambda = 1$, (sample site D).....	180
Figure 5.54, Open valve injection, standard injector, 800 rev/min idle, $\lambda = 1$, (sample site d)	180

Figure 5.55, Closed valve injection, air-atomisation, 800 rev/min idle, $\lambda = 1$, (sample site D).....	180
Figure 5.56, Open valve injection, air-atomisation, 800 rev/min idle, $\lambda = 1$, (sample site D).....	180
Figure 5.57, Closed valve injection, fuel vaporisation, 800 rev/min idle, $\lambda = 1$, (sample site D).....	180
Figure 5.58, Open valve injection, fuel vaporisation, 800 rev/min idle, $\lambda = 1$, (sample site D).....	180
Figure 5.59, Closed valve injection, standard injector, 1650 rev/min full load, 13.5:1 AFR, (sample sites B & C).....	182
Figure 5.60, Open valve injection, standard injector, 1650 rev/min full load, 13.5:1 AFR, (sample sites B & C).....	182
Figure 5.61, Closed valve injection, CPT2, air-atomisation, 1650 rev/min full load, 13.5:1 AFR (sample sites B & C).....	183
Figure 5.62, Open valve injection, CPT2, air-atomisation, 1650 rev/min full load, 13.5:1 AFR (sample sites B & C).....	183
Figure 5.63, Closed valve injection, CPT2, fuel vaporisation, 1650 rev/min full load, 13.5:1 AFR (sample sites B & C).....	183
Figure 5.64, Open valve injection, CPT2, fuel vaporisation, 1650 rev/min full load, 13.5:1 AFR (sample sites B & C).....	183
Figure 5.65, CPT2 bleed pressure, air-atomisation, 1650 rev/min full load, 13.5:1 AFR.....	184
Figure 6.1, Engine test. Open valve injection, standard injector, 800 rev/min idle.....	194
Figure 6.2, Engine test. Closed valve injection, standard injector, 800 rev/min idle	194
Figure 6.3, Engine test. Open valve injection, air-atomisation, 800 rev/min idle	195
Figure 6.4, Engine test. Closed valve injection, air-atomisation, 800 rev/min idle.....	195
Figure 6.5, Engine test. Open valve injection, vaporised fuel, 800 rev/min idle.....	195
Figure 6.6, Engine test. Closed valve injection, vaporised fuel, 800 rev/min idle.....	195
Figure 6.7, PFR test. Closed valve injection, standard injector, 800 rev/min idle.....	196
Figure 6.8, PFR test. Closed valve injection, standard injector, 800 rev/min idle.....	196
Figure 6.9, PFR test. Open valve injection, air-atomisation, 800 rev/min idle.....	197
Figure 6.10, PFR test. Closed valve injection, air-atomisation, 800 rev/min idle	197
Figure 6.11, PFR test. Open valve injection, vaporised fuel, 800 rev/min idle	197
Figure 6.12, PFR test. Closed valve injection, vaporised fuel, 800 rev/min idle	197
Figure 6.13, Engine test. Open valve injection, standard injector, 1500 rev/min road load.....	200
Figure 6.14, Engine test. Closed valve injection, standard injector, 1500 rev/min road load.....	200
Figure 6.15, Engine test. Open valve injection, air-atomisation, 1500 rev/min road load..	200
Figure 6.16, Engine test. Closed valve injection, air-atomisation, 1500 rev/min road load	200
Figure 6.17, Engine test. Open valve injection, vaporised fuel, 1500 rev/min road load	200
Figure 6.18, Engine test. Closed valve injection, vaporised fuel, 1500 rev/min oad load....	200
Figure 6.19, PFR test. Open valve injection, standard injector, 1500 rev/min road load.....	201
Figure 6.20, PFR test. Closed valve injection, standard injector, 1500 rev/min road load ..	201
Figure 6.21, PFR test. Open valve injection, air-atomisation, 1500 rev/min road load.....	202
Figure 6.22, PFR test. Closed valve injection, air-atomisation, 1500 rev/min road load.....	202
Figure 6.23, PFR test. Open valve injection, vaporised fuel, 1500 rev/min road load.....	202
Figure 6.24, PFR test. Closed valve injection, vaporised fuel, 1500 rev/min road load.....	202
Figure 6.25, Engine test, Open valve injection, standard injector, 1650 rev/min full load...	203
Figure 6.26, Engine test. Closed valve injection, standard injector, 1650 rev/min full load	203
Figure 6.27, Engine test. Open valve injection, air-atomisation, 1650 rev/min full load	204
Figure 6.28, Engine test. Closed valve injection, air-atomisation, 1650 rev/min full load..	204
Figure 6.29, Engine test. Open valve injection, vaporised fuel, 1650 rev/min full load.....	204

Figure 6.30, Engine test. Closed valve injection, vaporised fuel, 1650 rev/min full load....	204
Figure 6.31, PFR test. Open valve injection, standard injector, 1650 rev/min full load	205
Figure 6.32, PFR test. Closed valve injection, standard injector, 1650 rev/min full load....	205
Figure 6.33, PFR test. Open valve injection, air-atomisation, 1650 rev/min full load.....	205
Figure 6.34, PFR test. Closed valve injection, air-atomisation, 1650 rev/min full load	205
Figure 6.35, PFR test. Open valve injection, vaporised fuel, 1650 rev/min full load	205
Figure 6.36, PFR test. Closed valve injection, vaporised fuel, 1650 rev/min full load	205

Figure 7.1, Motored start unburned exhaust hydrocarbon concentration vs. time after injector enabled, standard injector, 800 rev/min, open valve injection, 10.5:1 air/fuel ratio.....	214
Figure 7.2, Motored start unburned exhaust hydrocarbon concentration vs. time after injector enabled, standard injector, 800 rev/min, closed valve injection, 10.5:1 air/fuel ratio.....	214
Figure 7.3, Motored start unburned exhaust hydrocarbon concentration vs. time after injector enabled, standard injector, 800 rev/min, open valve injection, 11.5:1 air/fuel ratio.....	214
Figure 7.4, Motored start unburned exhaust hydrocarbon concentration vs. time after injector enabled, standard injector, 800 rev/min, closed valve injection, 11.5:1 air/fuel ratio.....	214
Figure 7.5, Motored start unburned exhaust hydrocarbon concentration vs. time after injector enabled, standard injector, 800 rev/min, open valve injection, 12.5:1 air/fuel ratio.....	214
Figure 7.6, Motored start unburned exhaust hydrocarbon concentration vs. time after injector enabled, standard injector, 800 rev/min, closed valve injection, 12.5:1 air/fuel ratio.....	214
Figure 7.7, Motored start unburned exhaust hydrocarbon concentration vs. time after injector enabled, air-atomisation, 800 rev/min, open valve injection, 10.5:1 air/fuel ratio	216
Figure 7.8, Motored start unburned exhaust hydrocarbon concentration vs. time after injector enabled, air-atomisation, 800 rev/min, closed valve injection, 10.5:1 air/fuel ratio	216
Figure 7.9, Motored start unburned exhaust hydrocarbon concentration vs. time after injector enabled, air-atomisation, 800 rev/min, open valve injection, 11.5:1 air/fuel ratio	216
Figure 7.10, Motored start unburned exhaust hydrocarbon concentration vs. time after injector enabled, air-atomisation, 800 rev/min, closed valve injection, 11.5:1 air/fuel ratio	216
Figure 7.11, Motored start unburned exhaust hydrocarbon concentration vs. time after injector enabled, air-atomisation, 800 rev/min, open valve injection, 12.5:1 air/fuel ratio	216
Figure 7.12, Motored start unburned exhaust hydrocarbon concentration vs. time after injector enabled, air-atomisation, 800 rev/min, closed valve injection, 12.5:1 air/fuel ratio	216
Figure 7.13, Motored start unburned exhaust hydrocarbon concentration vs. time after injector enabled, fuel vaporisation, 800 rev/min, open valve injection, 13.5:1 air/fuel ratio.....	218
Figure 7.14, Motored start unburned exhaust hydrocarbon concentration vs. time after injector enabled, fuel vaporisation, 800 rev/min, closed valve injection, 13.5:1 air/fuel ratio.....	218
Figure 7.15, Motored start unburned exhaust hydrocarbon concentration vs. time after injector enabled, fuel vaporisation, 800 rev/min, open valve injection, stoichiometric air/fuel ratio.....	218
Figure 7.16, Motored start unburned exhaust hydrocarbon concentration vs. time after injector enabled, fuel vaporisation, 800 rev/min, closed valve injection, stoichiometric air/fuel ratio.....	218
Figure 7.17, Typical UHC decay after injector interrupt, raw data & curve fit, standard injector, closed valve injection, stoichiometric fuelling	220
Figure 7.18, Typical UHC decay after injector interrupt, raw data & curve fit, air-atomisation, closed valve injection, 800 rev/min, stoichiometric fuelling	220
Figure 7.19, Typical UHC decay after injector interrupt, raw data & curve fit, vaporised fuel, closed valve injection, 800 rev/min, stoichiometric fuelling	220
Figure 7.20, UHC decay after injector interrupt, exponential decay curve fit, standard injector, closed valve injection, 800 rev/min, stoichiometric fuelling	222
Figure 7.21, UHC decay after injector interrupt, exponential decay curve fit, air-atomisation, closed valve injection, 800 rev/min, stoichiometric fuelling	222
Figure 7.22, UHC decay after injector interrupt, exponential decay curve fit, vaporised fuel, closed valve injection, 800 rev/min, stoichiometric fuelling	222
Figure 7.23, Calculated cumulative UHC, standard injector, closed valve injection, 800 rev/min, stoichiometric fuelling	222

Figure 7.24, Calculated cumulative UHC, air-atomisation, closed valve injection, 800 rev/min, stoichiometric fuelling	222
Figure 7.25, Calculated cumulative UHC, vaporised fuel, closed valve injection, 800 rev/min, stoichiometric fuelling	222
Figure A7.1, UHC decay after injector interrupt, exponential decay curve fit, standard injector, open valve injection, 800 rev/min, stoichiometric fuelling.....	226
Figure A7.2, UHC decay after injector interrupt, exponential decay curve fit, air-atomisation, open valve injection, 360 mm Hg manifold pressure (absolute), 800 rev/min, stoichiometric fuelling.....	226
Figure A7.3, UHC decay after injector interrupt, exponential decay curve fit, vaporised fuel, open valve injection, 800 rev/min, stoichiometric fuelling.....	226
Figure A7.4, Calculated cumulative UHC, standard injector, closed valve injection, 800 rev/min, stoichiometric fuelling.....	226
Figure A7.5, Calculated cumulative UHC, air-atomisation, open valve injection, 800 rev/min, stoichiometric fuelling	226
Figure A7.6, Calculated cumulative UHC, vaporised fuel, open valve injection, 800 rev/min, stoichiometric fuelling	226
Figure A8.1, Circuit diagram for glow plug modulation	235
Figure A8.2, Glow plug driver circuit.....	236

LIST OF TABLES

Table 1.1, Atmospheric pollutant levels and their sources	8
Table 1.2, California exhaust emissions standards.....	10
Table 1.3, FTP driving schedule summary	11
Table 1.4, Cold-start emissions with preheated catalyst and air injection.....	14
Table 1.5, Comparative results for the emissions during Bag 1, Cycle 1 of the FTP Drive Cycle	16
Table 1.6, FTP cold-start hydrocarbon collection	20
Table 1.7, Liquid spray droplet distribution.....	52
Table 2.1, AAFV exit nozzle air mass flow rates for idle and 1500 rev/min road load	90
Table 2.2, Energy balance results for 1.2 mm & 1.5 mm nozzles at idle and 1500 rev/min road load	92
Table 2.3, 1.2 mm nozzle diameter mass flow rates, measured & calculated at idle and 1500 rev/min road load.....	94
Table 2.4, 1.2 mm nozzle diameter nozzle mixture mass flow rates at idle and 1500 rev/min road load, measured & calculated (using a calculated value of γ for the mixture).....	96
Table A2.1, Glow plug temperature vs. applied power, 30 mm glow plug heated in quiescent air	103
Table A2.2, Glow plug temperature vs. applied power, 20 mm glow plug heated in quiescent air	104
Table A2.3, Glow plug expansion vs. applied power, 30 mm glow plug heated in quiescent air	105
Table A2.4, AAFV fuel spray cone angles for a range of ΔP across the exit nozzle.....	111
Table 3.1, Per cylinder comparison of AAFV & EHCs.....	125

NOMENCLATURE

General abbreviations

AAFV	air-assisted fuel vaporiser
ABDC	after bottom dead centre
ADC	analogue-to-digital converter
AFR	air/fuel ratio
ATDC	after top dead centre
BBDC	before bottom dead centre
BDC	bottom dead centre
BMEP	brake mean effective pressure
BTDC	before bottom dead centre
CA	crank angle
CCD	charge coupled device
CO	carbon monoxide
CO ₂	carbon dioxide
COV	coefficient of variation
CU	control unit
Dev Aid	development aid
EC	European Community
ECEP2	Emissions Consortium Project Engine 2
ECU	electronic control unit
EFE	early fuel evaporation
EGI	exhaust gas ignition
EGR	exhaust gas recirculation
EHC	electrically heated catalyst
EMS	engine management system
EVC	exhaust valve closure
EVO	exhaust valve opening
FID	flame ionisation detector
FTP	Federal Test Procedure
HC	hydrocarbon
IC	internal combustion
IMEP	indicated mean effective pressure
IR	infra-red absorption
IVC	intake valve closure
IVO	intake valve opening
LEV	low emission vehicle
LD	laser diffraction
LIF	laser induced fluorescent
M	Mach number
MBT	minimum advance for best torque
NDIR	non-dispersive infra-red
NMHC	non-methane hydrocarbons
NO	nitric oxide
NO ₂	nitrogen dioxide
NO _x	oxides of nitrogen
Nu	Nusselt number
P	pressure

pC	pico coulomb
PC	personal computer
PDA	phase-doppler anemometry
Pr	Prandtl number
PTC	positive temperature coefficient
Re	reynolds number
SAE	Society of Automotive Engineers
SI	spark ignition
Smd	Sauter mean diameter
TDC	top dead centre
tml	terminal
ULEV	ultra low emission vehicle
UHC	unburned hydrocarbon

Symbols

A	area
C_d	coefficient of discharge
C_p	specific heat capacity at constant pressure
C_v	specific heat capacity at constant volume
E	energy of system
γ	ratio of specific heats, C_p/C_v
h	specific, molar enthalpy
H	enthalpy
id	internal diameter
l_{he}	latent heat of evaporation
m	mass flow rate
Q	net heat per unit mass
R	gas constant
u	specific, molar internal energy
U	internal energy
\mathcal{R}	universal, molar gas constant
W	work
v	velocity
ω	molecular weight
x	upper limit of glow plug expansion

Subscripts

1	upstream
2	downstream
a	air
f	fuel
m	mixture
ϕ	equivalence ratio, $(F/A_{\text{actual}})/(F/A_{\text{stoichiometric}})$

CHAPTER 1
A LITERATURE SURVEY

CHAPTER 1

A LITERATURE SURVEY

1.1 INTRODUCTION

The internal combustion engine has now been subjected to over a century of continuous development and its accessibility to the general public has changed substantially. The dramatic increase in vehicle ownership has focused attention on the environmental impact of automobile use and necessitated legislation to curb toxic emissions. Legislation was first introduced in America with the 1966 Clean Air Act in an effort to combat growing pollution problems. Legislative control was later adopted by European countries which, in conjunction with spiralling petrol prices throughout the 1970s, forced the engine designer to strive for 'clean', fuel efficient power plants.

With increasingly stringent engine emission control, research work now extends to all processes involved in IC engine operation. Mixture preparation, combustion and exhaust gas treatment are all required to interact harmoniously if proposed emission levels for the end of the century and beyond are to be met.

In an attempt to reduce the problems associated with both cold-start emissions and mixture preparation an air assisted fuel vaporiser, AAFV, has been designed to replace the existing port mounted fuel injector. The device is able to produce vaporised fuel during start-up conditions by incorporating an electrical heating element which may be switched off once the catalyst has reached its light-off temperature. Air assistance has been incorporated into the design to ensure good atomisation of the liquid fuel when operating with the heating element disabled.

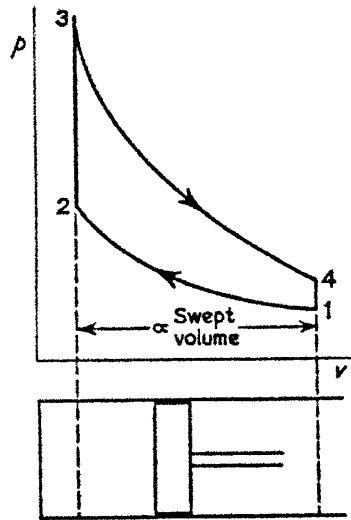
The following literature survey was undertaken to gain knowledge of alternative systems aimed at addressing the areas of cold-start emissions and mixture preparation and how to measure and quantify their performance.

1.2 FOUR-STROKE SI ENGINE ANALYSIS

The most common form of automotive power plant is based on the four-stroke Otto cycle. Figure 1.1 indicates the idealised four non-flow processes which form one complete cycle.

Figure 1.1
The Otto cycle, from Rogers & Mayhew, 1980

- 1-2 Air is compressed isentropically through a volume ratio, known as the compression ratio, r_v .
- 2-3 Heat is added at constant volume until the air is at state 3.
- 3-4 The air is expanded isentropically to the original volume.
- 4-1 Heat is rejected at constant volume until the cycle is completed.



Assuming an ideal cycle and constant ratio of specific heats (γ) for air, the efficiency (η) of the Otto cycle may be expressed in terms of its compression ratio as:

$$\eta = 1 - \frac{1}{r_v^{\gamma-1}} \quad \text{equation 1.1}$$

To maximise the thermal efficiency of a spark ignition engine, it is desirable for combustion to occur when the piston is at top dead centre, TDC, coinciding with the minimum volume within the combustion chamber. Restrictions exist due to the finite time required for the chemical reactions of combustion and therefore, spark initiation is necessary prior to TDC. If combustion is too early, the work transfer to the gases

during the compression stroke is too large while late combustion reduces the peak cylinder pressure, decreasing the work transfer from the gas to the piston during the expansion stroke. Engine efficiency is therefore dependent upon the optimum ignition timing that achieves minimum advance for best torque, MBT, which is specific for each engine operating condition of speed, mixture composition and load, Stone, 1992a.

At the instant of spark initiation, an arc is produced across the electrodes of the sparking plug creating some active chemical species which, in turn, initiate the process of combustion. Three phases of combustion exist, firstly the development phase, in which the spherical flame kernel, formed around the sparking plug, evolves into a highly wrinkled sheet due to air turbulence within the cylinder. Secondly, the developed, 'turbulent' flame undergoes a rapid-burning phase during which most of the mixture is burnt as the flame propagates across the combustion chamber. Finally, the flame front is extinguished by the boundary layer at the cylinder walls, leaving a thin layer of unburned gas which acts as an insulator to the combustion chamber and protects the mechanical components from the peak gas temperatures which may reach 2800 K. Burn rates during the rapid-burning phase accelerate with in-cylinder turbulence and the turbulence increases with engine speed. Combustion is usually complete within 30-90° of crank angle rotation dependent upon operating conditions.

Turbulence is usually increased by generating in-cylinder gas motion, either swirling or tumbling or a component of each. Tumble refers to swirl that occurs about an axis normal to that of the cylinder and is generally associated with four-valve engine designs. Due to the increased flow area associated with this design, the kinetic energy of the intake charge is insufficient to create significant in-cylinder turbulence at low operating speeds. In addition, low inlet velocities encourage poor mixture preparation since insufficient shear forces are present to atomise the fuel. Increased wall wetting in the port can arise, due to the inlet tract division slowing fuel transportation between the injector and combustion chamber and therefore requires

increased transient compensatory fuel if lean excursions are to be avoided during this operating period.

The four-valve engine is now favoured due to its superior volumetric efficiency at high speed, however, designers of modern four-valve Otto cycle engines have to address the problems of low inlet velocities at low speeds and increased fuel wetting of the inlet tract due to the port divide wall.

1.3 EMISSIONS, EMISSION REGULATIONS AND EXHAUST GAS TREATMENT

1.3.1 Introduction

Combustion of hydrocarbon fuels produces three main types of pollutants, unburned hydrocarbons (HC), oxides of nitrogen (NO_x) and carbon monoxide (CO), in addition to the basic products of combustion, namely carbon dioxide (CO₂) and water. The pollutant by-products form the majority of the emissions which fall under legislative control. In order to tackle the problem, an understanding of the types of pollutants formed and their formation processes is required.

1.3.2 HC: Pollutant

Hydrocarbon emissions, some of which are known to be carcinogenic, are the consequence of incomplete combustion. Photochemical smog may be produced if the hydrocarbons mix with oxides of nitrogen under certain atmospheric conditions. Typical levels of unburned hydrocarbons present in the exhaust gas of a SI engine are between 1 and 2.5 percent of the fuel flow into the engine, Heywood, 1988a.

1.3.3 HC: Formation

Four mechanisms exist for the production of unburned hydrocarbons in SI engines:

(1) *Flame quenching, at the walls of the combustion chamber.* As the flame front propagates through the mixture, a thin layer of hydrocarbons is left unburned at the comparatively cool cylinder wall due to the heat sink effect quenching the flame and the relatively low rates of mass transfer that occur within the boundary layer.

(2) *Crevice volumes acting as traps.* Small crevice regions in the combustion chamber exist around the spark plug thread and electrode, between the valves and

their seats, around the head gasket, and the largest region being between piston, piston rings and cylinder wall. During compression, the pressure within the combustion chamber forces unburned mixture into these small crevices and the high ratio of surface area to volume of these regions, cools the mixture. Throughout combustion, this mixture remains largely unburned and is released into the exhaust gases as the cylinder pressure drops when the exhaust valves open.

(3) ***Fuel vapour absorption/desorption into the engine oil during compression and expansion respectively.*** A thin layer of engine lubricant is deposited on the cylinder walls as the piston reciprocates. This oil film absorbs fuel vapour from the mixture during the compression stroke. Throughout combustion and the ensuing expansion stroke, the concentration of fuel vapour in the burning gases drops essentially to zero and the cylinder pressure falls towards atmospheric leading to the desorption of the fuel vapour into the combustion products. Fuel vapour which desorbs late in the cycle, when the bulk gas is relatively cool, does not oxidise and so contributes to emissions of unburned hydrocarbons.

(4) ***Incomplete combustion.*** Poor combustion quality can be caused by extinction of the flame due to bulk quenching. Under certain conditions, the temperature of the unburned mixture can decrease to a low level during the expansion stroke. If this temperature drop is sufficient, the burn rate will decrease and the flame front may be extinguished. Bulk quenching is more likely to occur when the residual gas fraction is high due to either low speed, light load operating conditions or if the mixture is too lean during throttle opening transients.

1.3.4 Oxides of nitrogen (NO_x): Pollutant

The predominant oxide of nitrogen, NO_x, emission is nitric oxide, NO. NO_x pollutants are associated with respiratory illness such as asthma and can lead to acid rain and chemical erosion most notably to ancient buildings and artwork. Goldsmith, 1989, stated that in 1982 transportation accounted for over 50% of the total amount of NO_x measured in urban areas, see table 1.1.

Table 1.1
Atmospheric pollutant levels and their sources
measured in a West German city, from Goldsmith, 1989

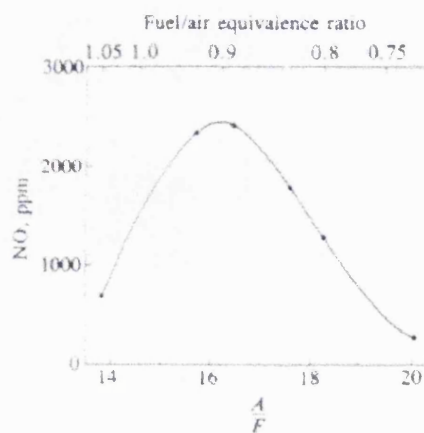
Pollutant	Share of impact as Percentage of Total			
	Transport	Industry	Heating Plants	Households
Hydrocarbons (HCs)	33.0 (0.59)	28.0 (0.47)	0.6 (0.09)	32.4 (0.49)
Nitrogen Oxides (NO _x)	54.6 (1.63)	14.0 (0.43)	27.7 (0.86)	3.7 (0.11)
Carbon Monoxide (CO)	65.0 (5.40)	13.6 (1.13)	0.4 (0.03)	21.0 (1.74)

N.B. The figures given in brackets are the weight of emissions in million tonnes per year. It is interesting to note that NO_x has increased from 2 million tonnes in 1960 to 3 million tonnes in 1982.

1.3.5 NO formation

NO is formed as a consequence of combustion in the IC engine as opposed to being formed during combustion itself. The majority of NO is produced in the post-flame gases, with only a small percentage formed in the flame front itself due to the short residence time of the gas within the flame reaction zone at the high pressures associated with IC engines. Variation of air/fuel ratio greatly affects NO formation due to the changes of in-cylinder temperature and oxygen concentration, see figure 1.2. The basic mechanisms of NO formation are the dissociation of nitrogen and oxygen molecules to form atoms which recombine to form NO. Higher combustion temperatures lead to higher concentrations of NO. One method of reducing NO emissions is to recirculate exhaust gas through the combustion chamber to act as a thermal sink and thereby reduce the peak temperature of combustion.

Figure 1.2
Variation of exhaust NO
concentration with air/fuel ratio. SI
engine, 1600 rev/min, MBT timing,
from Heywood, 1988a



1.3.6 NO₂ formation

NO₂ is formed in the post-flame combustion process but, in general for SI engines, chemical equilibrium, using the extended Zeldovich reactions, suggests that the ratio of NO₂/NO is negligible for typical flame temperatures, Heywood, 1988a.

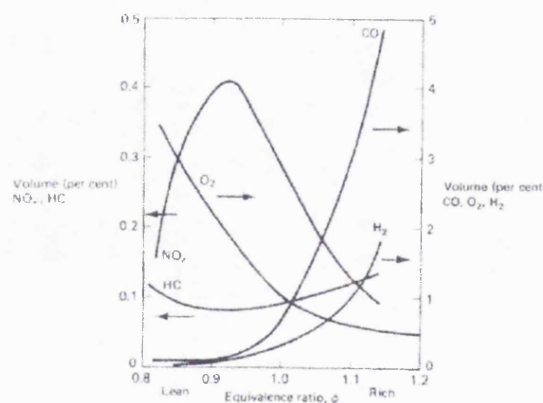
1.3.7 Carbon monoxide/dioxide: Emissions

Carbon monoxide, CO, is absorbed into the blood in preference to oxygen thereby causing suffocation at high concentration levels. Lower concentrations tend to cause drowsiness and headaches. Carbon dioxide, CO₂, is formed in far greater quantities than CO. It is not toxic but it is one of the 'greenhouse' gases which potentially can lead to global warming.

1.3.8 CO₂/CO formation

CO emissions from an IC engine are primarily determined by the air/fuel ratio. For rich of stoichiometric mixtures, insufficient air exists to achieve complete combustion of the fuel. This leads to high CO concentrations in the exhaust gases. Very little CO is formed when mixtures are burnt lean of stoichiometric as excess oxygen is present to convert CO to CO₂, see figure 1.3.

Figure 1.3
Variation of HC, CO and NO_x
concentration in the exhaust of a
conventional SI engine with air/fuel ratio,
from Stone, 1992a



1.3.9 Emissions regulations

Limits for engine emissions are determined by legislative bodies. The most significant recent challenge for the SI engine was stipulated by the Californian Air Research Board (CARB) for introduction in 1997 which defined the Ultra Low Emissions Vehicle (ULEV). The ULEV is described as one which produces a maximum of 0.20 g/mile of NO_x, 1.70 g/mile CO and 0.40 g/mile of non-methane hydrocarbons (NMHC), see table 1.2, which compares with the 1990 Clean Air Amendments Act, which specified 0.41 g/mile for NMHC, 1.00 g/mile NO_x and 3.40 g/mile for CO. Wright, 1990, suggested that increasingly strict legislation was responsible for a 96% fall in tail-pipe emissions since 1970 in the US, excluding CO₂, and a doubling of fuel efficiency.

Table 1.2
California exhaust emissions standards,
from Heimrich, Albu & Osborn, 1991

Vehicle Category	Exhaust Emissions, g/mi		
	NMOG	CO	NO _x
Adopted for 1993	0.250	3.4	0.40
TLEV	0.125	3.4	0.40
LEV	0.075	3.4	0.20
ULEV	0.040	1.7	0.20
TLEV, LEV, ULEV standards adopted September 1990			

Legislation in the form of the EEC Council Directive 91/441/EEC, which came into force at the end of 1992 as an amendment to Directive 87/76/EEC, required tail-pipe emissions to be below 2.72 g/km CO and 0.97 g/km for HC and NO_x combined. Tail-pipe emissions are those measured at the point of exhaust pipe exit to atmosphere as opposed to 'engine-out' emissions which are measured in the exhaust manifold. Consequently, these figures take into account the benefits of ancillary components such as catalysts. The 1999 EC Directive, ECD3, closes the gap between Europe and the United States by including an emissions test from -7°C, with sampling recorded from cranking. 160,000 km catalyst durability also forms part of the European test.

It is interesting to note at this point that in Europe a great deal of pressure was brought to bear on the member states of the EEC prior to the 'Luxembourg Agreement' of 1985, ratified in 1987, not to follow the US in the fitment of catalytic

converters. Whilst there is little question of their capability in reducing emissions, they were at the time subject to a number of operational problems of misuse or mis-fuelling and they require accurate stoichiometric engine fuelling to achieve satisfactory conversion levels and avoid contamination. Instead the 'lean burn' engine was proposed, offering a more elegant and cost-effective solution. It had potential for excellent fuel economy, lifetime durability for emission control and decreased CO₂ formation, the main contributor to global warming. However, agreement was eventually reached between the Council of Ministers to press towards standards in line with those already adopted in the States which has inevitably led to the adoption of catalytic converters.

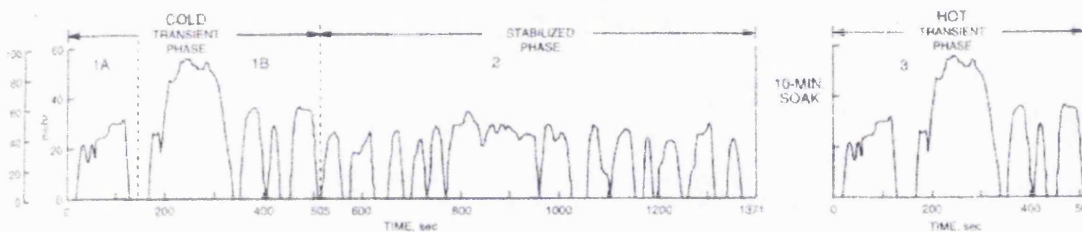
Testing of vehicle emission performance is achieved using a certified drive cycle and chassis dynamometer. In the United States this operating cycle is known as the Federal Test Cycle, FTP. The FTP uses a 1372-second duration urban driving cycle divided into two segments, a 505-second cold transient followed by an 867-second cold stabilised portion. The vehicle is then subjected to a ten-minute soak to achieve normal operating temperatures. A hot transient test of 505 seconds duration completes the test. In order to study the effects on emissions due to the different temperature regimes encountered throughout the test cycle, it is split into three 'Bags' for exhaust gas analysis. Bag 1 is split further into Bags 1A and 1B, representing the first 140 seconds and the remaining 140-505 seconds of the cold transient segment respectively. The FTP driving schedule with hot and cold transient test segments is shown in figure 1.4. The drive cycle duration, driving distances and average speeds are shown in table 1.3.

Table 1.3
FTP driving schedule summary, from
Heimrich, Albu & Osborn, 1991

Segment	Duration, seconds	Distance, miles	Average Speed, miles/hr
Transient Phase	505	3.60	25.7
Stabilized Phase	867	3.90	16.2
UDDS	1372	7.50	19.7

Whilst the difficulties faced by the engine designer due to increasingly stringent legislation become more severe, the benefits of enforced emissions legislation are clear, though they pose tremendous technical challenges.

Figure 1.4
FTP driving schedule showing test segments ,
from Heimrich, Albu & Osborn, 1991



1.3.10 Cold-start emissions

The first 140 seconds of the FTP cycle after the cold-start contributes some 70-80% of the total tail pipe CO and HC emissions collected throughout the entire test, Hurley *et al.* Section 1.3.3 outlined the predominant causes of HC emissions in a fully warm SI engine which are generally accentuated during cold-start and warm-up conditions, whilst other factors unique to this period of engine operation add to the levels of HC emissions.

Fuel enrichment is required in order to achieve steady combustion in a cold engine. Combustion will only occur if a combustible mixture of fuel vapour and air are present at the sparking plug at the time of spark initiation. When the engine is warm the majority of fuel vaporisation occurs due to the spray impinging upon the back of the inlet valves and hot intake port surfaces, however, under cold-start conditions the metal surfaces are at ambient temperatures requiring that secondary processes such as flash evaporation of the fuel's light fractions and evaporation from wetted port surfaces must be enough to produce sufficient fuel vapour. Consequently significant fuel enrichment is required during cold cranking and the early stages of engine warm-

up with the effect that throughout this period high levels of unburned hydrocarbons are emitted.

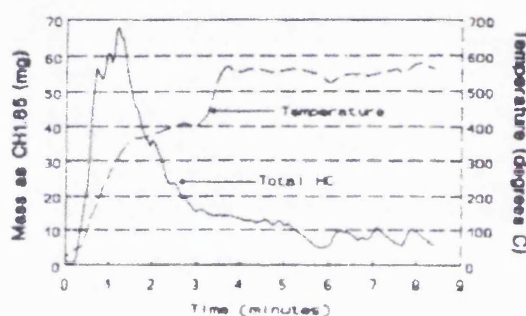
To compound the problem of cold-start emissions still further, the exhaust catalyst is ineffective until its 'light-off' temperature has been reached. The term 'light-off' is most often used to describe the temperature at which the catalyst reaches 50% HC conversion efficiency, typically 300-500°C, and as figure 1.5 shows, this normally occurs up to two minutes after stable engine operation has been achieved, Hurley *et al*, 1991.

1.3.11 Exhaust gas treatment

Electrically-heated catalysts (EHC) have been the subject of in-depth investigation to reduce the period of low catalytic conversion, Hurley *et al*, 1991 and Heimrich, Albu and Osborn, 1991. Heimrich, Albu and Osborn, investigated two different configurations of electrically-heated catalysts, each being fitted to then current production vehicles and subjected to the FTP emissions tests. Electrically-heated catalysts are pre-heated prior to engine cranking to achieve temperatures sufficient for catalytic activity from cranking, consequently reducing cold-start and warm-up emissions. The catalyst may also be subjected to additional heating once the engine has started in order to maintain a pre-set operating temperature. The duration of post heating depends upon the location and size of the EHC.

Due to the cold-start enrichment, emissions of HC and CO are high with relatively low concentrations of O₂ present. O₂ is required for satisfactory oxidation levels of both HC and CO, therefore air must be injected upstream of the EHC if such a system

Figure 1.5
Total HC emission and catalyst
temperature vs. time for Urban Drive
Cycle, from Hurley *et al*, 1991



is to operate at its full potential though a detrimental effect on NO_x emissions will be incurred if either the volume flow rate of air is too great, or it is supplied for an excessive period of time. Table 1.4 shows the results of altering the air flow rates supplied to the EHC performed by Heimrich, Albu and Osborn, 1991, for the cold-start portion of the FTP emissions tests. The researchers stated that the unexpectedly low value of NO_x at the highest air flow rates was presumed to be an anomaly, and reported high scatter for the data collected. Catalyst cooling due to excess air was thought to be the reason for the increase in CO levels at the highest air flow rates. Emission levels of the vehicle measured during the FTP test cycle for both standard and the EHC systems averaged reductions of non-methane hydrocarbons (NMHC) of up to 75% and 85% for CO are extremely impressive and approach the ULEV emission levels, though the increase in NO_x appears to be unavoidable. Concerns include electrical power requirements as high as 3-8 kW, durability and the delay in reaching operating temperature, Hurley *et al*, 1991, Anon, 1994a and Anon, 1994b.

Table 1.4
Cold-start emissions with preheated catalyst and air injection,
3.8 litre V-6, from Heimrich, Albu and Osborn, 1991

Bag 1A Emissions, g/mi	Air Injection Flowrate, L/min			
	No Air ^a	170	300	370
HC	1.50	0.36	0.40	0.42
CO	9.68	1.96	1.16	2.92
NO _x	2.24	2.80	2.61	1.80

^aHeat only.
Air Injection for 75 seconds.
Average of repeat tests at 300 L/min.

Hurley *et al*, 1991, investigated the problem of durability but only looked as far as 4000 miles. The reduction in emission levels of both new and aged EHCs were substantial when compared with the 'baseline' catalyst system, however, whilst the aged catalyst still produced lower emission levels after aging than the baseline system it suffered an increase of 115% of NMHC emissions and CO output rose by 250%. The drop in conversion efficiency is clearly worrying considering the proposed

160,000 km durability emissions tests. Hurley *et al* suggests that repositioning of the EHC further downstream of the exhaust manifold and downstream of the three-way catalyst may provide a level of protection from both exhaust contamination and high exhaust temperatures, thereby increasing durability. This repositioning incurs electrical power penalties due to the loss of exhaust gas heating which requires the electrical power be maintained for a period of time after the engine has fired. The current requirement averaged approximately 650W for a duration of 20 seconds when pre-heating the catalyst and throughout the post-heating period.

Ma, Collings and Hands, 1992, describe an alternative method for the rapid heating of the exhaust catalyst known as Exhaust Gas Ignition (EGI). Operational catalyst temperatures were reached by utilising an afterburner situated just upstream of the catalyst, see figure 1.6. The engine was calibrated to run extremely rich to provide a sufficiently flammable hydrogen concentration in the exhaust gas when mixed with an auxiliary air supply pumped into the exhaust.

Figure 1.6

Schematic of EGI system, from Ma, Collings & Hands, 1992

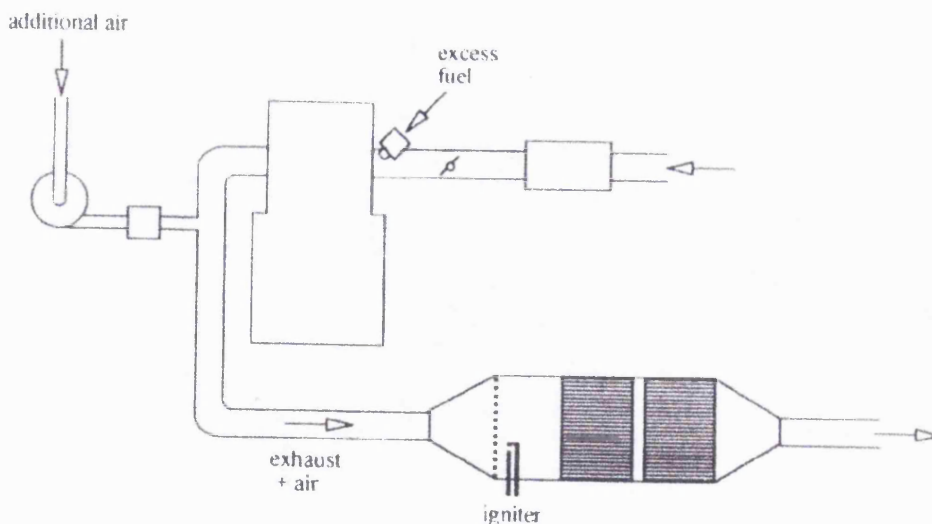


Table 1.5

Comparative results for the emissions during Bag 1, Cycle 1 of the FTP Drive Cycle, from Ma, Collings & Hands, 1992

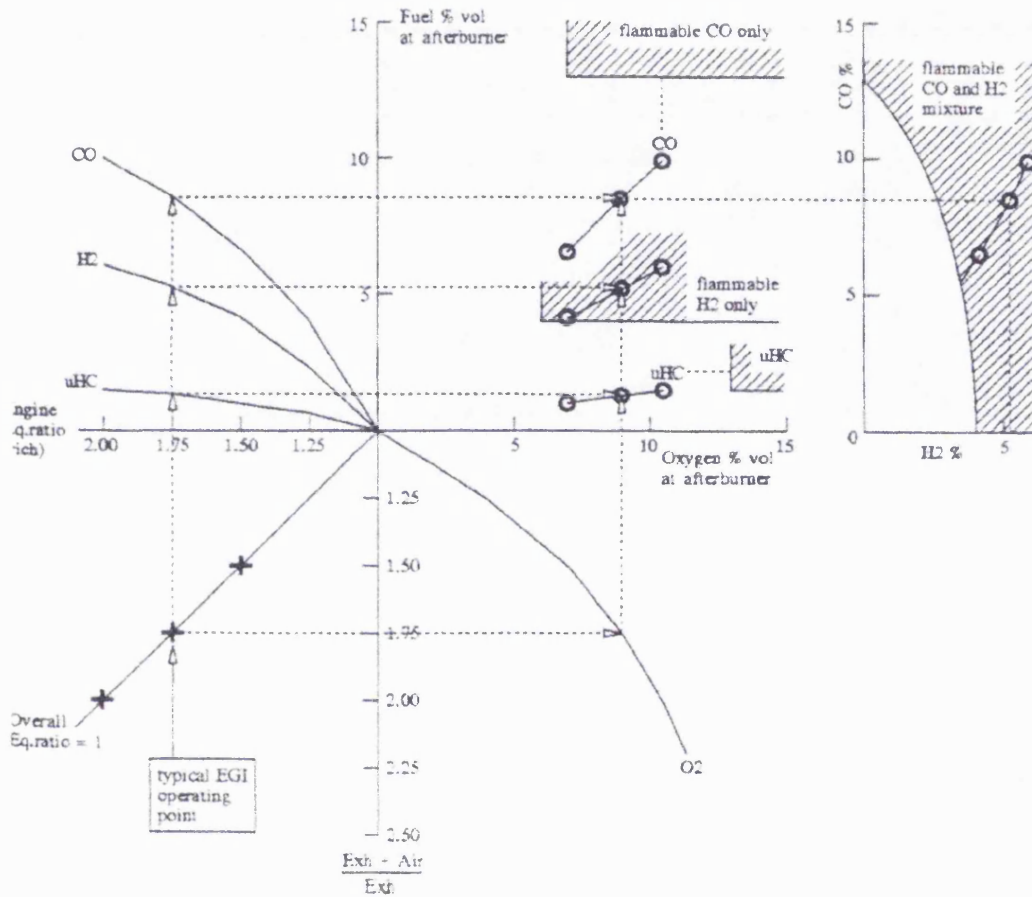
grams/mile	HC	CO	NO_x
No EGI	4.1	31.3	2.4
With EGI	1.0	4.8	1.3
Reduction	76%	85%	54%

The rich fuelling excursion was required to achieve a flammable exhaust air/fuel ratio such that ignition within the afterburner was achieved. Details of fuel mapping for the cold-start and warm-up conditions were not disclosed, although light off time for the catalyst was reduced from 100 seconds to 20 seconds indicating a rich excursion time of approximately the same duration. Results recorded for Bag 1, Cycle 1 of the FTP Drive Cycle show substantial reductions, see table 1.5, however, these gains are not achieved without penalty. Heavy carbon deposits, increased roughness, poor fuel economy and performance were cited by the authors as some of the adverse effects. The arrangement also required a substantial volume of air pumped into the exhaust to achieve reliable afterburner ignition, with the required flow rate equalling that of the engine air flow rate. Figure 1.7 shows the difficulties in achieving a flammable exhaust mixture. Whilst this study was prompted by the expected durability failings of EHCs no durability tests of the EGI system were discussed, in addition, there may be problems of oil dilution and coke deposits due to the rich mixture required throughout the initial period of operation which will adversely affect the engine's longevity. The afterburner required an idling period of 20 seconds to achieve catalyst light-off temperatures, Anon, 1994a.

Both BMW and Mercedes Benz took the concept of an exhaust burner further by the use of a separate fuel supply introduced to the exhaust system just upstream of the catalyst, see figure 1.8. Unlike the afterburner system of Ma, Collings and Hands, the

Figure 1.7

Flammability of cold exhaust/air mixture, from Ma, Collings & Hands, 1992



intallation required no modification of the engine's operating strategy. Figure 1.9 shows the reduction of emissions, comparing a variety of catalytic converter heating methods. The principal benefit of this system was the reduction in the energy conversion efficiency when compared to an EHC. Whilst it may appear wasteful to put neat fuel into the exhaust, burning it directly in the exhaust to provide heat allows a higher heating efficiency than burning it in the combustion chamber. SI engines operate at approximately 25% thermal efficiency which is then used drive the alternator to provide electrical power, with an associated efficiency of some 75%, before being used to power the heating elements within the EHC. One of the principal concern regarding the exhaust burner system was that of obtaining reliable

operation in service, with failure to achieve ignition resulting in higher emissions than with a conventional closed-loop catalyst. BMW also cited the problem of coke build-up in the injector nozzle with an associated deterioration in the air/fuel mixture presented to the ignition unit due to the short duration of operation of the burner (< 1% of the vehicle's service life), Anon, 1994a. For the remainder of the time the injector was subjected to the hot flow of exhaust gases which burn any residual fuel creating the coke deposits.

Figure 1.8
Catalyst heating options,
from Anon, 1994a

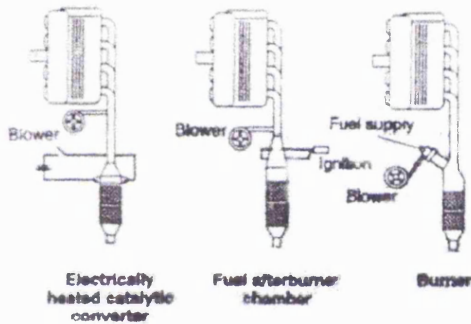
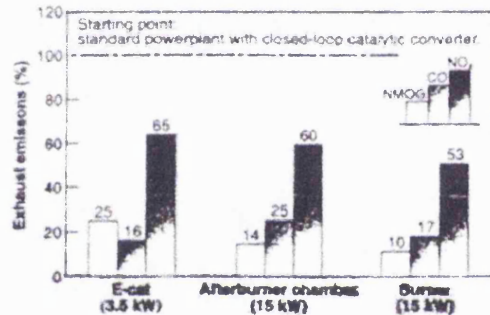


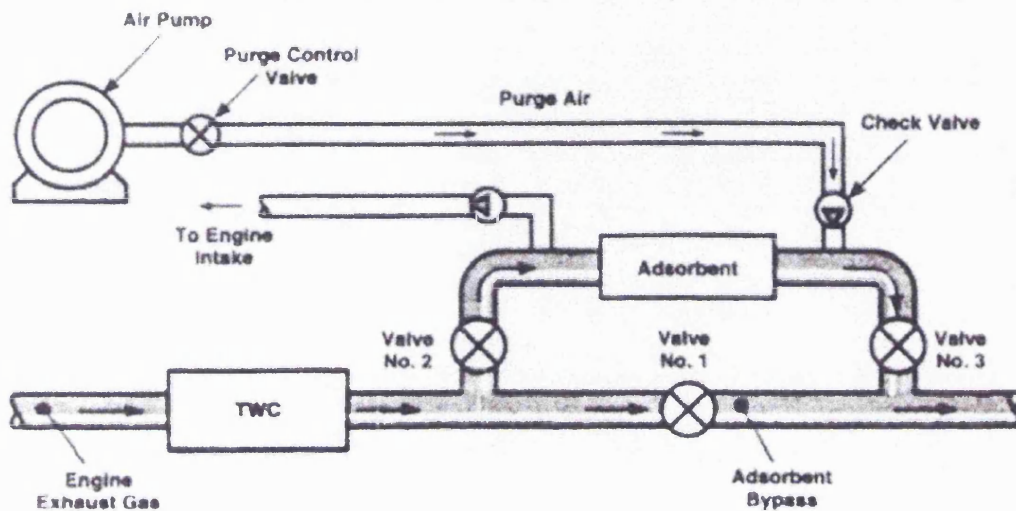
Figure 1.9
Reduction of emissions due to catalyst
heating, from Anon, 1994b



A further alternative to the EHC was proposed by Hiemrich, Smith & Kitowshi, 1992. A method of hydrocarbon collection was suggested and tested using a zeolite molecular sieve situated in the exhaust system. Since the catalyst is below operating temperature under cold-start conditions, the unburned hydrocarbons pass through the catalyst and into the sieve. Zeolites are highly porous aluminosilicate crystals. The collector, a standard type of catalyst substrate with a zeolite coating, readily adsorbed certain sizes of molecules and therefore collecting the UHC emissions until the catalyst reached light-off temperature. The sieve was then purged using exhaust gas which fed back into the inlet manifold as a form of EGR. Zeolite has a desorption temperature of 83°C and must be situated in the exhaust at a point where this temperature will not be reached prior to catalyst light-off. The exhaust system configuration is shown in figure 1.10 and subjected to the FTP Cold-Start test with

Figure 1.10

Experimental cold-start hydrocarbon collection exhaust routing, from Hiemrich, Smith & Kitowshi, 1992



HC measurements taken both upstream and downstream of the adsorption unit. Bag 1 of the test was split into two parts, with Bag 1A representing the first 140 seconds of the 505-second duration cycle, see figure 1.11. It can be seen from this figure that desorption occurs at temperatures between 45-50°C, well below the predicted 83°C desorption temperature and thought to have been due to higher than expected HC concentrations, contamination from other exhaust gas pollutants or short containment times within the sieve caused by the exhaust gas velocity during engine transients. Regardless of the system's inability to function as predicted, a 35% reduction in cold-start HC emissions during this 140-second period was recorded, table 1.6. Areas for further study were cited as the long term durability of such a system and development of the chemical adsorption kinetics to produce a successful adsorbent that can readily target specific species following a cold-start.

Figure 1.11

FTP cold-start hydrocarbon collection, 1.9 litre Honda Accord, from Hiemrich, Smith & Kitowshi, 1992

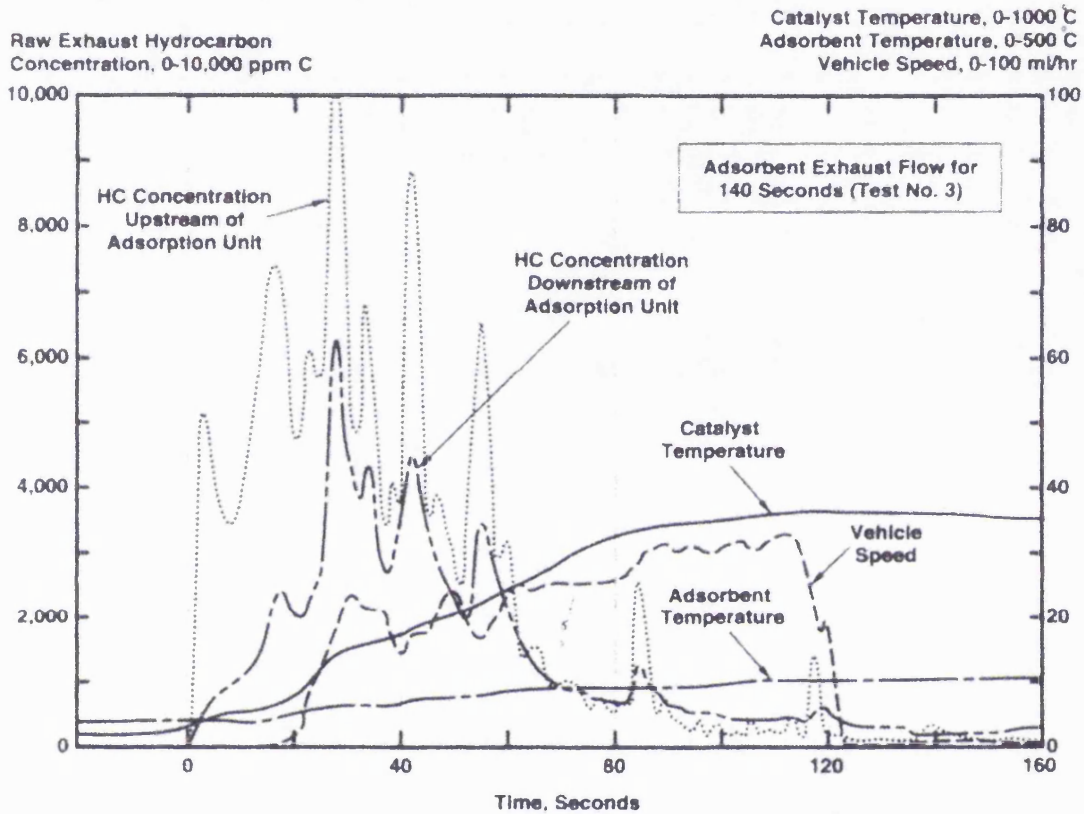


Table 1.6

FTP cold-start hydrocarbon collection, 1.9 litre Honda Accord, cumulative emission levels, from Hiemrich, Smith & Kitowshi, 1992

Test Number	Cold-Start Hydrocarbon Collection	Collection Time, sec	Hydrocarbon Emissions, grams	Improvement over Baseline, %
			Bag 1A (0-140 sec)	
1	No	0	1.72	—
2	Yes	70	1.11	35
3	Yes	140	1.11	35

1.3.12 Closing comments on emissions

Clearly a number of options exist for reducing the level of emissions during the cold-start and warm-up periods of engine operation. These options fall into two groups representing pre- and post-combustion treatments. The EHC, EGI, HC trap and exhaust afterburner, all forms of post-combustion emissions treatment, offer improved emissions during the critical phase of operation, though only the HC collector and EHC will not increase these levels if an operational failure of the system occurs. Problems of longevity were cited for all of the exhaust gas treatment processes, now a major concern in light of the 1997 legislation including durability testing of any emissions equipment.

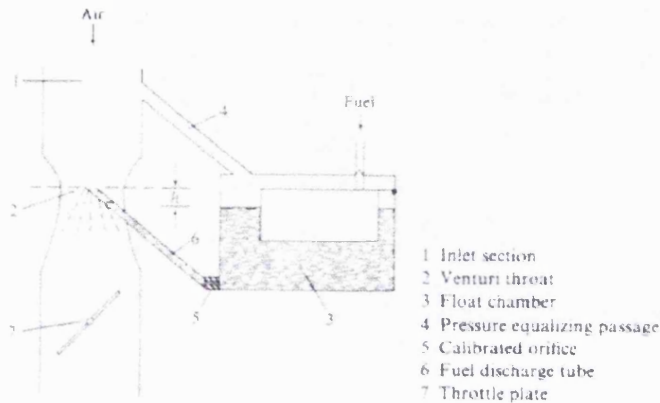
In reality, it is likely that no one solution can provide the reductions necessary at the current level of development. The exhaust gas treatments proposed must also be presented with reasonably low pollutant levels from the combustion process if they are to function efficiently. To this end, it is vital that the mixture preparation prior to combustion is good in order to minimise 'engine out' emissions. The essential features of mixture preparation are therefore discussed in the following section.

1.4 MIXTURE PREPARATION/ FUEL SPRAYS

1.4.1 Carburettors

Figure 1.12

Schematic of an elementary carburettor, from Heywood, 1988b

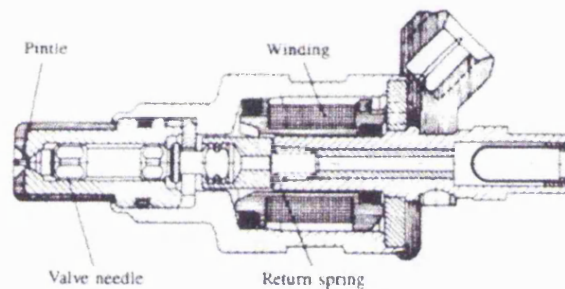


Until the late 1980s, fuel flow into a SI engine intake system was controlled by a carburettor on nearly every application. Figure 1.12 shows the fundamental components of an elementary carburettor. Air flows first through a filter in order to remove suspended dust particles and then into the carburettor inlet, commonly a convergent-divergent section, or venturi, which is incorporated to increase the air velocity with a corresponding drop in static pressure from the condition at the carburettor inlet. The pressure drop is used to induce fuel into the air stream from the float chamber with the liquid fuel atomised by the moving air stream and then slowing as it enters the divergent section of the venturi, providing a partial pressure recovery of the fuel-air mixture which then passes the throttle plate and enters the inlet manifold plenum chamber. At part load conditions, further atomisation occurs as liquid deposits are stripped from the throttle disc forming sprays with characteristic drop sizes of the order of $20\ \mu\text{m}$ in diameter, Nightingale, 1985. However, as wide open throttle (WOT) conditions are approached the droplet sizes increase as atomisation only occurs within the venturi. Whilst many changes and improvements have been made to achieve a more comprehensive and efficient fuel mapping to the engine's requirements, the principles remain the same. Modern carburettors include cold-start enrichment, altitude compensation for changes in air density, accelerator

pumps to overcome transient delay times during rapid throttle opening, as well as power enrichment and idle systems to ensure the appropriate air/fuel ratio is maintained throughout the engine's operating range. In spite of all of these improvements, the modern carburettor still suffers from cylinder-to-cylinder fuel mal-distribution and transport delay problems as the fuel has to negotiate the intake manifold before it reaches the engine.

1.4.2 Multi-point fuel injection

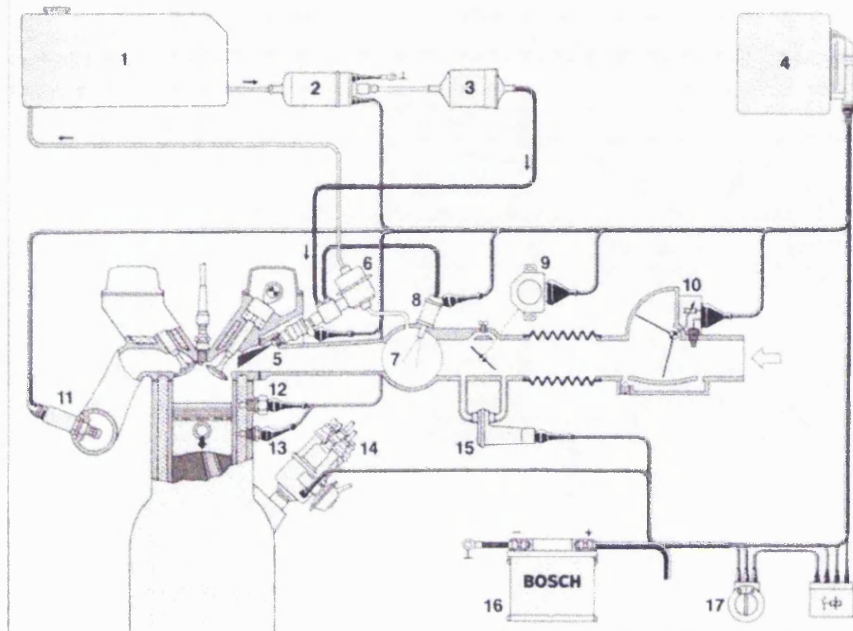
Figure 1.13
Cross section of pintle type fuel injector, from Griener,
Roman & Stienbrenner, 1987



Fuel injection systems have been developed to overcome the problems of fuel transport delay times, metering accuracy and cylinder-to-cylinder mal-distribution. An injector is placed in each intake port close to the inlet valves and contains a metering valve opened by an electrically-operated solenoid with fuel supplied to the injector at a constant pressure relative to the inlet manifold. The volume of fuel delivered to the cylinder is controlled by the duration of solenoid excitation. The most common types of injector are the pintle injector, see figure 1.13, which has a pintle valve shaped to promote atomisation of the fuel and is designed to produce a hollow spray cone and the hole-type injector where the needle valve is lifted by a solenoid and the fuel then passes through an atomising orifice of either single or multiple hole design. An electronic control unit, ECU, is used to set the appropriate pulse width of solenoid coil excitation, based on input signals received from a number of sensors. Figure 1.14 shows a schematic layout for a multi-point fuel injection system.

Figure 1.14

**Electronic multi-point port fuel injection system with air-flow meter,
(Bosch L-Jetronic) , from Lembke, 1988a**



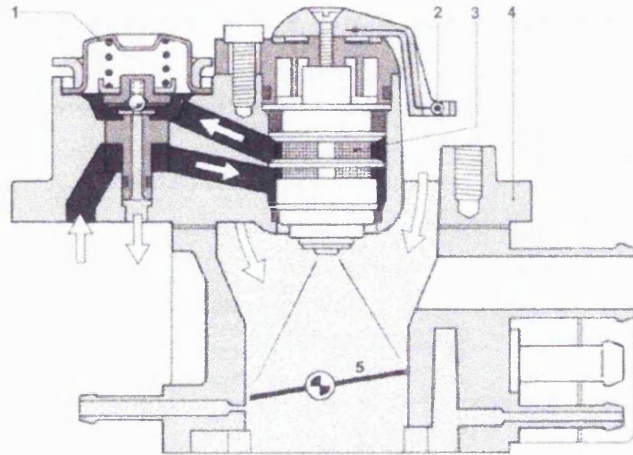
1 Fuel tank, 2 electric fuel pump, 3 fuel filter, 4 ECU, 5 injection valve, 6 fuel rail & pressure regulator, 7 intake manifold, 8 cold-start valve, 9 throttle-valve switch, 10 air-flow sensor, 11 lambda sensor, 12 thermo-time switch, 13 engine temperature sensor, 14 ignition distributor, 15 auxiliary-air device, 16 battery, 17 ignition & starting switch

1.4.3 Single-point fuel injection

Single-point fuel injection, see figure 1.15, offers a lower cost alternative to the multi-point systems providing the delivery control of multi-point systems but with the slower fuel transport times and distribution problems associated with a carburettor. One or two injectors are used and are fired either simultaneously or alternately. Increased air velocities over the throttle plate downstream of the injectors assists atomisation of the fuel droplets as with the carburettor and improves the mixture uniformity in the inlet manifold. Single-point injection systems are able to use a lower pressure fuel supply than that associated with multi-point systems due to the atomising effect created by the throttle plate at part load. The primary cost saving of single-point injection systems is due to the reduced fuel delivery pressure significantly affecting the pump manufacturing costs.

Figure 1.15

Cutaway drawing of a two injector throttle-body electronic fuel injection system, from Lembke, 1988b



1 pressure regulator, 2 air-temperature sensor, 3 solenoid-operated injector, 4 throttle-valve housing, 5 throttle valve

1.4.4 Drop size

Characterisation of fuel sprays is achieved using drop size distributions and mean diameters. The most widely used measured mean is the Sauter mean diameter, S_{md} or $d_{3,2}$, defined as:-

$$D_{SM} = \left(\int D_d^3 dn \right) / \left(\int D_d^2 dn \right) \quad \text{equation 1.2}$$

where dn is the number of droplets with diameter D_d in the range $D_d - dD_d / 2 < D_d < D_d + dD_d / 2$. The integration is usually performed over a number of drop size groups and represents the droplet diameter from a mono-sized spray with the same ratio of surface area/volume as that of the measured spray, Stone, 1992b. The definition is particularly relevant in measuring evaporative fuel sprays since the rate of evaporation is a function of the surface area.

1.4.5 Problems associated with the Sauter mean diameter

The potential problem of Smd quoted in isolation has been highlighted by Miller & Nightingale, 1990, and Williams, 1994, and is due to its extreme sensitivity to the presence of small droplets due to the square-law relationship between surface area and volume of a sphere. Miller and Nightingale, 1994, reported a 30% increase in Smd, from 33.68 μm to 47.67 μm , achieved by redistribution of droplets smaller than 2.6 μm which represented only 1.1% of the total spray by volume. Due to the Smd's sensitivity to the presence of small droplets, and given that droplets in the smaller size bands are difficult to measure and are of little importance to the overall spray, its use is unsuitable for some SI engine spray analysis.

1.4.6 An alternative to the Sauter mean diameter

Williams, 1994, outlined the problems stated above and proposed alternative spray characterisation parameters without the Smd's sensitivity to small droplets using a simple model of the evaporation process. Characterisation was achieved using the d-squared evaporation law and ignored complicated manifold geometry, varying air and fuel velocities, wall film interactions and multi-component fuels. The equivalent drop size, $d_{e,x}$ is given by:

$$d_{e,x} = [K(t_y - t_x)/(1-z)]^{1/2} \quad \text{equation 1.3}$$

where, $z = (1-y/100)^{2/3}/(1-x/100)^{2/3}$ and x & y are the percentage of the spray (by volume) evaporated at times t_x and t_y respectively. K is related to the fuel properties and the ambient conditions and is obtained by plotting the percentage evaporation versus time, however, the equivalent diameter is independent of K , provided that the same value is used in the evaluation of t_y and t_x . Complete derivation of the governing equations may be found by consulting Spalding, 1979, whilst Williams, 1994, contains the derivation of the evaporation model.

The model was used in an iterative computer program to calculate the size of a mono-disperse spray which had the same time to achieve an arbitrary band width of evaporation exhibited by the measured spray, and it was suggested by Williams, 1994, that 0-10, 50 and 90% evaporation times would be most appropriate to modelling combustion in port-injected SI engines.

1.4.7 Droplet size distributions

Both the droplet size and distribution are required to characterise fully the spray. Rosin & Rammler proposed an equation to describe the variation of particle size of crushed coal in the 1920s which has been successfully applied to fuel sprays and is the most commonly used in this field. It takes the form of:

$$VF = e^{-(D/\bar{D})^n} \quad \text{equation 1.4}$$

where VF is the volume fraction of droplets with a diameter greater than D. \bar{D} is a constant representing the characteristic diameter of droplets and n is the measure of the spread, i.e., for a spray of droplets of uniform size, $n = \infty$, Miller & Nightingale, 1990. The characteristic diameter \bar{D} is related to the Sauter mean diameter by;

$$D_{32} = \frac{\bar{D}}{\Gamma\left(1 - \frac{1}{n}\right)} \quad \text{equation 1.5}$$

where Γ is the gamma function obtained from tables. Lefebvre, 1989, noted that the expression allowed data to be extrapolated into the range of very fine droplets corresponding to the point where accurate measurement was most difficult, however, it was suggested that before it could be used with confidence a good fit to the experimental data was required. The Rosin-Rammler distribution has the merit of simplicity whilst assuming an infinite range of droplet sizes.

Further relationships for drop size variation include the Nukiyama-Tanasawa, Log-probability, Log-normal and Normal distributions. Mugele & Evans, 1951, reviewed the relationships with the exception of the normal distributions, suggesting that the Rosin-Rammler distribution sometimes calculated a different Sauter mean diameter from that obtained by summation of the experimental data. Mugele & Evans proffered a further alternative, the upper limit distribution, however, all these drop size distributions are linked by the assumption of a mono-modal distribution. An analysis model exists, known as Model Independent, which makes no prior, assumption of the data allowing multi-modal volume distributions, Levebvre, 1989.

No one distribution can be described as better than the others. Lefebvre unsurprisingly suggested that the most appropriate selection was the distribution which best fitted the experimental data for the particular system under observation.

1.4.8 Fuel transportation properties

1.4.8a Droplet impact: Carburettors & single-point fuel injection

Fuel flow from either a carburettor or a single-point fuel injection system follows a tortuous path before entering the combustion chamber. The majority of fuel either inducted or injected into the air stream impacts upon the throttle plate until WOT or near WOT conditions are approached though the liquid droplets are still required to negotiate the intake manifold and port walls.

In a carburettor the venturi creates air stream velocities in excess of 100 m/s at higher air flow conditions and the associated shear forces ensure reasonable atomisation of the fuel. Boam & Finlay, 1979, and Yun & Lo, 1976, state that 2-15% fuel evaporation occurs as the fuel passes through the venturi section of the carburettor, and this caused a reduction in mixture temperature of up to 30°C due to evaporative cooling. In a single-point fuel injection system the velocity of the spray as it exits the injector is sufficient to provide partial atomisation. The liquid fuel impacts upon the

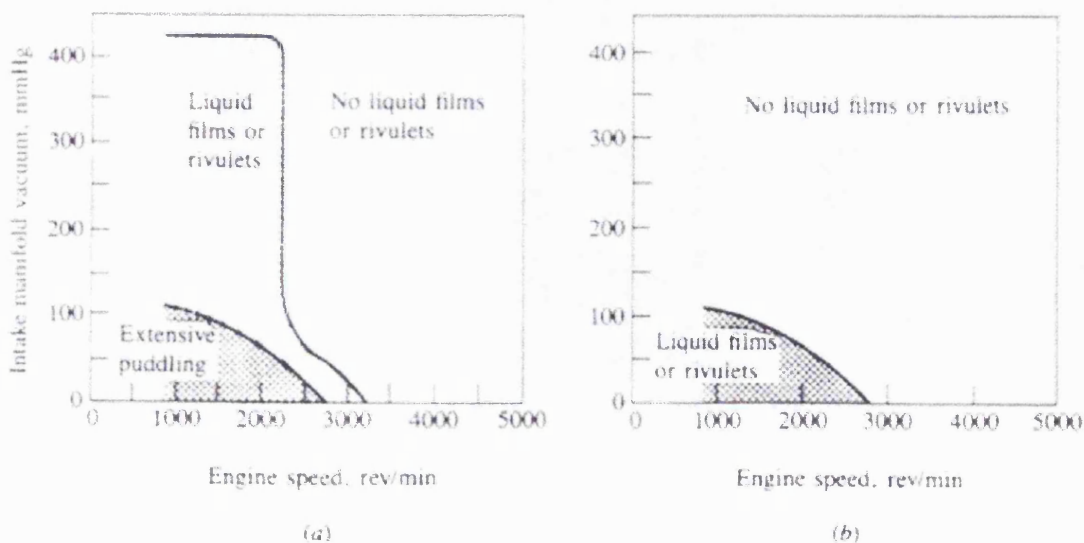
throttle disc during light load conditions and is subsequently re-entrained into the air stream as it shears off the edges of the throttle into the high-speed air flow

From the throttle plate, the air/fuel mixture enters the inlet manifold and feeds through to each cylinder via the manifold branches with walls heated by either engine coolant or exhaust gas. Many of the fuel droplets are too large to be fully entrained in the air stream. Nogi *et al*, 1988, showed that droplets with diameters greater than 30 μm flowing through the manifold with an air stream velocity of 10 m/s could not be suspended in the flow, and were consequently deposited on the passage floor.

Fuel approaches the inlet valves in its vapour form, as droplets and also as liquid films and rivulets. Figure 1.16 shows the extent and location of puddling and wall wetting as a function of inlet manifold depression and that puddling is also highly dependent upon manifold temperature.

Figure 1.16

Regions of engine load and speed range where extensive pools or puddles, liquid films or rivulets were observed: (a) on the manifold plenum floor and (b) in the manifold runner, on a four cylinder SI automobile engine. Manifold heated by coolant to 90°C, from Heywood, 1988b



Gasoline is made up from thousands of different hydrocarbons, each with its associated boiling point. This causes the liquid to have a boiling range as opposed to a single boiling point with a range typically between 30°C and 200°C. Figure 1.17 shows the evaporation effect on a specific gasoline (indolene) with varying temperatures and manifold depressions, however, insufficient residence time of the fuel within the manifold exists to achieve the levels of evaporation suggested. A residence time of only 10 ms is available at 6000 rev/min, and 100 ms at 600 rev/min. Studies suggest that only droplets with diameters of less than 10 μm will evaporate at 6000 rev/min, whilst drops exceeding 100μm will not fully vaporise at any speed, Heywood, 1988b, original reference, Trayser *et al*, 1969.

Figure 1.17 (a)

Percentage of indolene fuel evaporated at equilibrium at one pressure of atmosphere, from Heywood, 1988b, original reference, Trayser *et al*, 1969

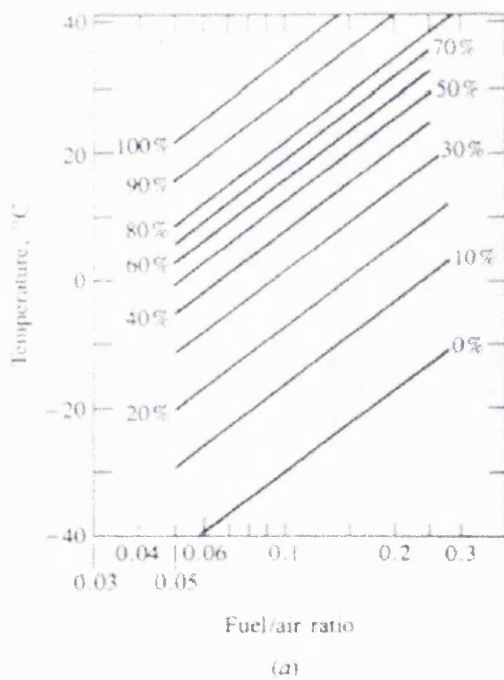
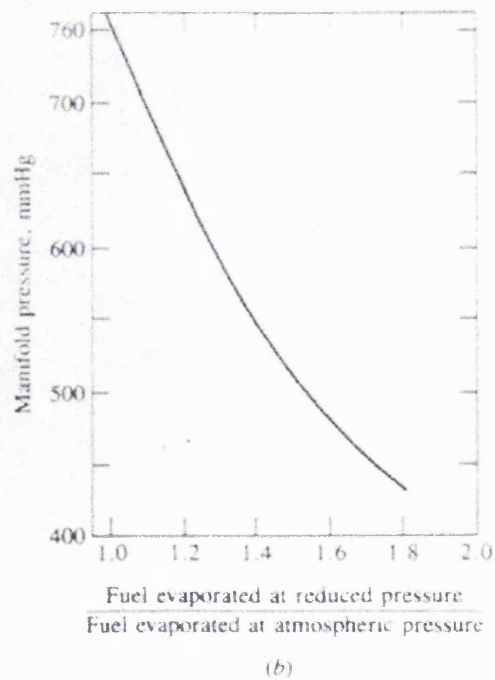


Figure 1.17 (b)

Effect of pressure on amount of indolene fuel evaporated, from Heywood, 1988b, original reference, Trayser *et al*, 1969



1.4.8b Fuel film behaviour

Liquid fuel films on the manifold walls can lead to disparity between the amount of fuel entering the combustion chamber and that required by the engine. If the rate of vaporisation from films and puddles is insufficient the liquid fuel residing in the intake manifold will build up and add a phase lag between fuel and air flows during engine transients due to the slower transportation times associated with the liquid. Since only part of the fuel is suspended in the air stream, unless compensation is provided a lean excursion or spike will occur during rapid throttle openings, conversely, a rich spike is possible on throttle closing, see figure 1.18.

Carburetted and single point injection systems require that the inlet manifold be designed to transport equal amounts of air and fuel between each cylinder to avoid cylinder-to-cylinder air/fuel ratio variations. A multi-point injection system only requires the air flow to be equally divided.

Figure 1.18 (a)

Predicted behaviour of the fuel film for an uncompensated step change in engine operating conditions, from Heywood, 1988b, original reference Hires & Overington, 1981

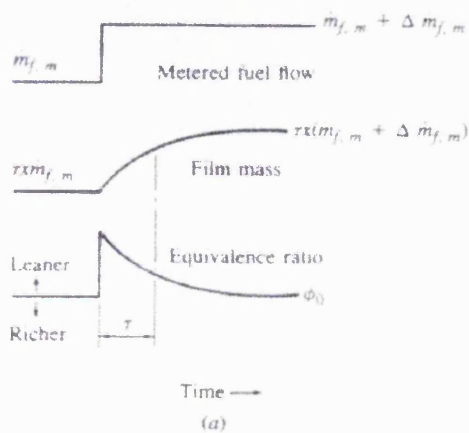
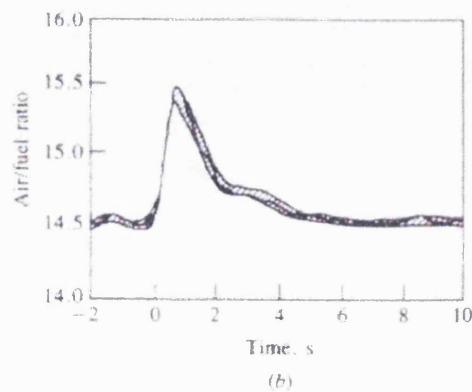


Figure 1.18 (b)

Observed variation in air/fuel ratio for uncompensated throttle opening @ 1600 rev/min which increased manifold pressure from 48 to 61 Hg, from Heywood, 1988b, original reference Hires & Overington, 1981



The variation in air/fuel ratio for carburetted engines can be between 5-15% of the mean value for light load and WOT conditions respectively which reduces the safe lean limit of engine operation if a lean burn strategy is adopted, Heywood, 1988b, original reference Kay, 1978, and Blackmore & Thomas, 1977. Whilst the range of variation is reduced for multi-point injection systems, manufacturing tolerances still result in variations in fuel mass flow rates between injectors.

1.4.8c Vaporised mixtures

The problems associated with wall film behaviour on carburetted engines have led a number of researchers to investigate the performance improvements that can be obtained from using pre-vaporised mixtures. The research work has tended to fall into two categories:

(i) Work performed mainly during the 1960s and 1970s to investigate possible improvements in fuel economy and emissions when using pre-vaporised mixtures on fully-warm engines. The base engine in this case would normally have been fitted with a carburettor.

(ii) More recent work to quantify the improvements in emissions possible during the starting and warm-up phases of engine operation carried out in response to the inclusion of cold-starting in the emissions test procedures, as described in section 1.3.9. The studies have been carried out primarily on engines that would normally be fitted with multi-point fuel injection due to the degree of fuelling control required to meet the emissions legislation.

1.4.8d Vaporised mixtures applied to fully warm engines

A number of studies have been made of the effects of using a homogeneous charge in SI engines at normal operating temperatures, achieved by using a pre-vaporised air-fuel mixture, Robison & Brehob, 1965, Dodd & Wisdom, 1968, Lindsay *et al*, 1971,

Matthes & McGill, 1976, and Burt, Roberts & Woodworth, 1979. The gaseous mixture eliminated wall wetting thereby reducing variation of both the cycle-to-cycle and cylinder-to-cylinder air/fuel ratio allowing either a leaner mixture to be used prior to the onset of misfire or more exhaust gas recirculation if a stoichiometric tune had been adopted.

Robison & Brehob, 1965, measured the cylinder-to-cylinder air/fuel ratio spread on a carburetted 6-cylinder engine, of unspecified displacement, using a single carburettor. Mixture mal-distribution was in the range of 0.65 of an air/fuel ratio at 1200 rev/min road load and 3.4 at 3200 rev/min road load. WOT fuel distribution variations were large at both 1200 and 2400 rev/min engine speeds, with a 4.5-6.4 air/fuel ratio spread though no one cylinder was consistently the richest or leanest as distribution changed with engine condition. Use of a fully vaporised mixture reduced the range to 0.6 of a ratio over all conditions whilst the cycle-to-cycle pressure fluctuations decreased indicating diminished mixture variations with respect to time.

Dodd & Wisdom, 1968, performed a similar series of tests using single cylinder engines. Like Robison & Brehob, they found that the lean misfire limit could be extended using a fully vaporised mixture, however, the expected reductions in HC emissions due to the improved mixture homogeneity were not realised. Dodd & Wisdom experienced difficulties in obtaining acceptable levels of repeatability between tests though the overall trend appears to indicate little benefit in the use of a fully vaporised mixture for reducing unburned HCs on an engine operating at normal coolant temperatures.

Lindsay *et al*, 1971, chose to study the effects of a vaporised mixture on NO and CO emissions. By substantially extending the lean limit, they showed that it was possible to achieve a reduction in the concentrations of both of these pollutants when the engine was operated at air/fuel ratios in excess of 20:1, accompanied by increased HC emissions.

In 1973 the National Engineering Laboratory in conjunction with Shell Research developed the 'Vapipe' to evaluate the use of a vaporised mixture with the conclusion that there was little benefit in exhaust emissions and fuel economy to be gained when operating at conventional mixture strengths though improvements during the warm-up period were noted, Lindsay Thomas & Wilson, 1973. It is possible to conclude therefore that the principal advantage of utilising a vaporised mixture is to remove mixture inhomogeneity between cylinders. Whilst this is of interest to vehicles fitted with carburettors and single-point fuel injection, the current trend towards multi-point injection systems greatly reduces the need for such a preparation process. It is also worth noting that, with current legislation and technology, lean-burn engines are unable to meet emission targets due to the lack of an effective lean NO_x converter.

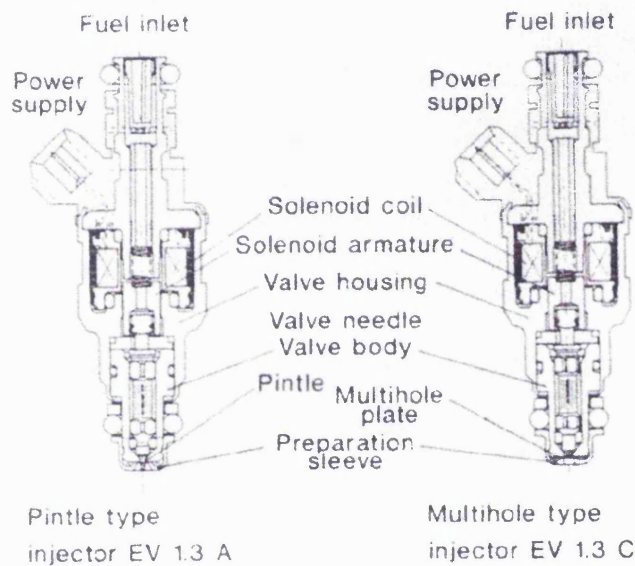
1.4.9 Fuel injector sprays

1.4.9a Port injection

Port fuel injection goes some way to relieving the problems of cylinder-to-cylinder variation associated with carburettors and single-point injection systems without the need to adopt vaporised fuelling. The principal problem associated with port injection is the possible reduction in atomisation and evaporation of the fuel spray prior to combustion due to the greatly reduced path length from injector to combustion when compared to carburetted engines, hence there is potentially less residence time within the inlet manifold for evaporation to occur prior to combustion. Since hydrocarbon fuels will not burn unless in a gaseous form, the degree of evaporation is of prime importance when trying to reduce HC emissions. In order to increase evaporation levels, the fuel is sprayed onto the back of the inlet valve which at normal operating temperatures is hot enough to achieve almost complete evaporation at light loads when closed valve injection is used. Open valve injection reduces the rate of evaporation by up to 20%, Martins & Finlay, 1992.

The two most common types of injector, pintle and hole, are shown in figure 1.19. Single hole-type injectors produce a coherent pencil jet whilst the pintle injector develops a hollow cone spray. The hole-type injector has been improved by the use of two and four-hole designs where interaction between sprays serves to break up the liquid jets to form a similar spray cone to that found with the pintle injector.

Figure 1.19
Gasoline injection valves, from Simon, Ardnt & Ziegler, 1992



Evaporation rates become important during cold-start conditions when insufficient inlet valve temperatures are present to vaporise the fuel and an enriched mixture is required to achieve the level of evaporation necessary for combustion within the time available. Any reduction in the level of enrichment will have a significant effect on the vehicle's performance during Bag 1 of the emissions test cycle. Kishiyawa et al, 1990, established an astonishing reduction in cranking time, reduced from 110 to 3 seconds, when the mean drop size was reduced from 176 μm to 85 μm at -30°C .

Good atomisation of any fuel spray in a four-valve engine is hindered by the port divide wall between the two inlet valve passages creating increased levels of wall

wetting, reducing mixture quality and increasing the engine's transient response times, Okamoto *et al*, 1992 and Heywood, 1988b, original reference Hires & Overington, 1981. Accordingly, a two-stream injector is required to reduce fuel impaction on the divide wall. Development work by Hitachi, Okamoto *et al*, 1992, produced a nose adapter for their single-stream swirl-type injector which used an unpartitioned spectacle-shaped single outlet orifice to split the fuel into two distinct streams for four-valve engines, see figure 1.20. A comparison of the drop size between the modified and standard injectors was not provided, though the text indicated that a reduction was obtained. The fuel spray emanating from the twin-stream injector was measured by laser diffraction particle sizing to produce an average drop diameter of approximately 100 μm . High injector swirl rates were reported as assisting in attaining this value. The improved mixture preparation provided a 17% reduction in transient response times measured by the time taken for the engine to reach 4000 rev/min from 1200 rev/min road load conditions after achieving WOT. Cold cranking times and fuel enrichment were also improved, see figure 1.21, though no description of engine type or definition of 'complete fire' was given.

Figure 1.20

Structure of a two-stream injector, from Okamoto *et al*, 1992

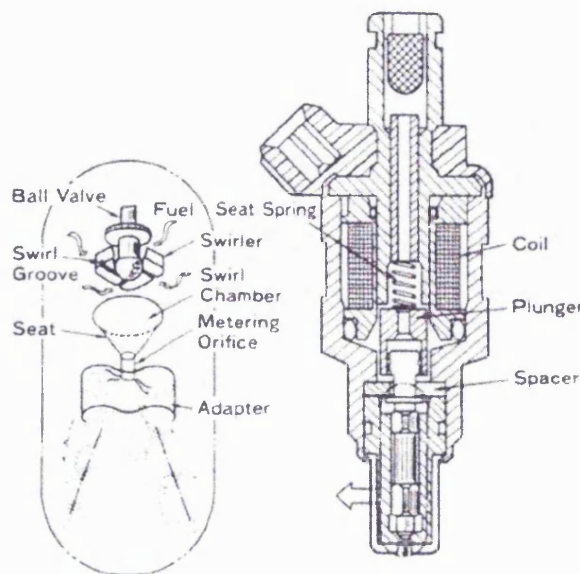
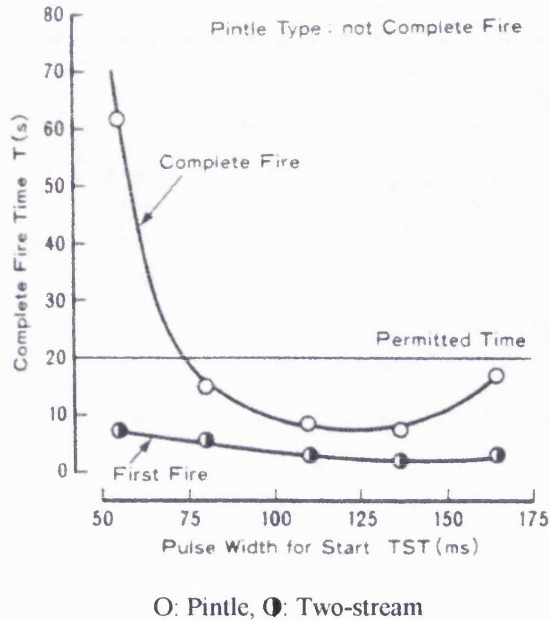


Figure 1.21

Start performance (-30° C) of a four-valve engine using standard pintle and two-stream injector, from Okamoto *et al*, 1992



1.4.9b Air-assisted atomisers

Improved performance of the standard pintle or plate injectors may be simply obtained through application of air-assistance. Fuel delivered by the standard injector is shattered into very fine droplets using a high velocity air stream. Two main configurations of air-assistance exist which are defined by the point of mixing between the air and fuel. Figure 1.22 shows the air and fuel mixing prior to a downstream atomising orifice, the alternative is to provide an air shroud around the fuel as it exits the injector, see figure 1.23. The shear surface between the fuel and air assists in atomising the fuel and tends to keep the droplets from impacting on the port walls improving the engine's transient performance by decreasing compensatory fuel requirement. Improved starting and enrichment reductions during warm-up may also realised, Rokita, Bandel & Herzog, 1993 and Emmenthal *et al*, 1985.

Figure 1.22

Lucas air-assisted fuel injector with air bleed upstream of the fuel metering orifice, from Fry 1994

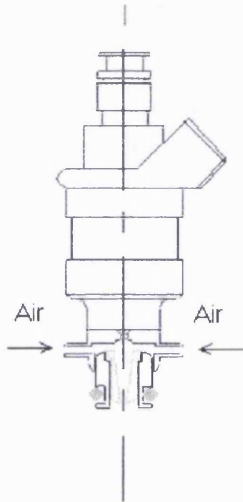
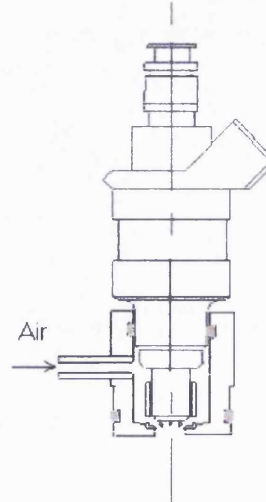


Figure 1.23

Nippondenso air-assisted fuel injector with air bleed downstream of the fuel metering orifice, from Fry 1994



Problems associated with air assistance are primarily due to idle and low speed control when an auxiliary air supply is utilised as the means of procuring a sufficient quantity of air at an appropriate pressure throughout the engine's operating range.

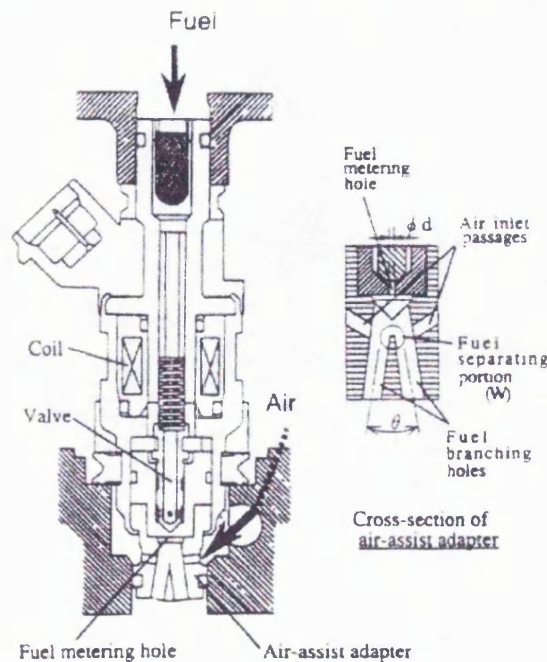
Emmanthal *et al*, 1985, applied the principles of air-assisted atomisation to a single-point fuel injection system for small displacement engines to address the relatively poor performance associated with carburettors during warm-up and obtain the uniformity of mixture preparation without the expense of a multi-point injection system. The air-forced injection relied heavily on carburettor technology for metering the fuel by incorporating a standard venturi, choke and throttle plate. Air was drawn out of the metered venturi flow by an electric pump and mixed with fuel metered by the pressure signal of the air passing through the venturi after which the pressurised mixture was divided between the cylinders using knife-edge ports and distributed by flexible hoses. The air drawn into the mixing process was approximately 15% of the idle air flow.

Droplet diameters in the range of 25-50 μm were recorded, measured using a holographic technique, and these compare very favourably with a multi-point injection system. Cylinder-to-cylinder air/fuel ratio variation was reduced to $\pm 4\%$ under all conditions, however, problems were encountered during low speed transient operation with poor fuel metering created by the heavily pulsating air flow at low engine speeds.

Toyota developed a twin-spray air-assisted atomiser for application to four-valve engines, see figure 1.24. The air supply was taken from the engine's intake system downstream of the metering unit at the near atmospheric conditions upstream of the throttle plate. Air was drawn through the injector due to the pressure drop between the throttle plate and the intake port. Whilst the pressure difference between the conditions upstream and downstream of the throttle fell ostensibly to zero at WOT conditions the mixture preparation was claimed to offer an improvement over the standard injector due to the dividing nozzle helping to break up the fuel, see figure 1.25. Since the flow area through the injector was significant and the supply

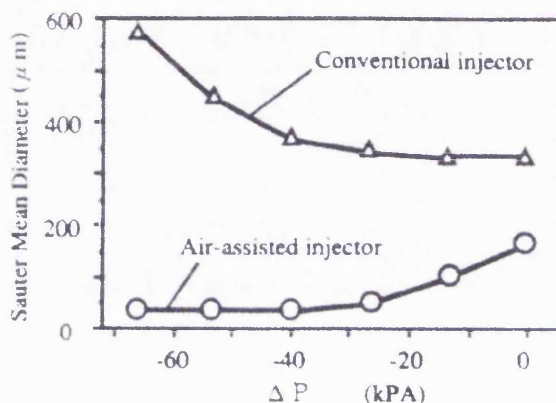
Figure 1.24

Sectioned view of air-assisted atomiser, from Harada *et al*, 1992



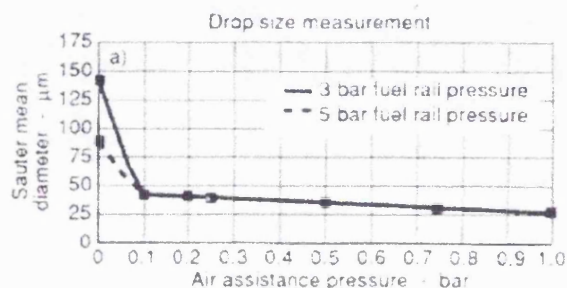
unthrottled, an auxiliary idle speed control valve, ISCV, was required to maintain satisfactory idling performance. A 30% reduction in transient compensatory fuel requirements was claimed using this system during open valve injection. Reductions in HC emissions of 10-15% measured over a standard drive cycle and decreased idle roughness were found and attributed to better combustion achieved by the homogeneous air-fuel mixture.

Figure 1.25
Fuel spray mean droplet diameter,
from Harada *et al*, 1992



Rokita, Bandel & Hezog, 1993, tested an air-assisted atomiser, differing from the Toyota design in that the air jets surrounded the pintle of a standard injector and impinged upon the fuel spray as it emerged into the inlet port. The standard injector utilised was of multi-hole design, though originally produced two separate fuel sprays which air-assistance reduced to a single wide-angle atomised spray cone. Varying the air pressure from 0-100 kPa reduced the Smd of the spray from 140 µm to 25 µm, whilst as little as 10 kPa was sufficient to obtain droplet diameters of 40 µm, see figure 1.26. The mixture preparation was optimised using an optical flow rig to modify parameters such as injector position, spray cone angle and injector timings and the effects were measured in

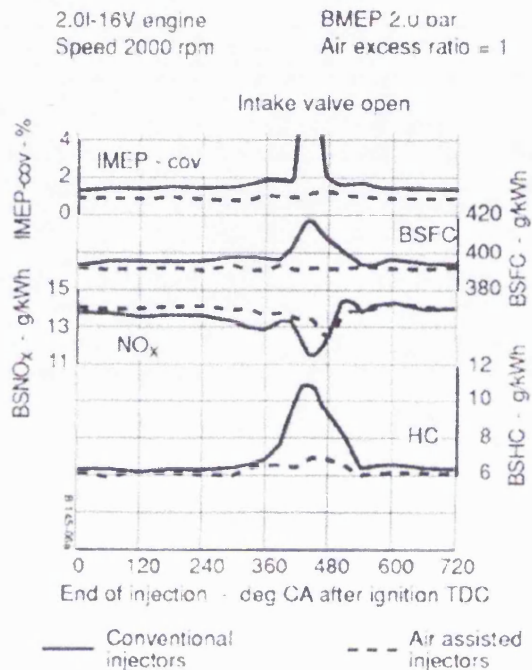
Figure 1.26
Variation of droplet size with air
pressure, from Rokita, Bandel & Herzog,
1993



terms of coefficient of variation, COV, of the indicated mean effective pressure, IMEP, NO_x and HC levels per cycle, see figure 1.27. Rokita stated that the reductions in emission levels and the increased stability were due to the low levels of wall wetting and improved mixture quality. It was also suggested that with standard injectors, the fuel entered the combustion chamber as a liquid, leading to charge inhomogeneity accounting for the high HC levels and lower stability of the original installation though no measurements were made to validate this claim.

Figure 1.27

Influence of injection timing and spray quality on part load engine performance, from Rokita, Bandel & Herzog, 1993



1.4.9c Vaporised mixtures applied during cold-starting and warm up

Boyle, Boam and Finlay, 1993, proposed a system which introduced an electrically-heated shroud to the fuel injector. The injected fuel was driven by two compressed air jets, supplied by an external source, forcing the liquid fuel into a helical flow around the shroud and forming a vapour due to heat transfer between the heated surface and the liquid fuel, see figure 1.28. Stoichiometric fuelling strategies are possible during starting and warm-up if pre-vaporisation occurs prompting a reduction in the level of HC emissions but incurring the penalty of a significant electrical power requirement. The reduction of UHC emissions during cold cranking followed by constant speed engine operation at idle can be seen in figure 1.29. Boyle, Boam and Finlay also explored the transient operating characteristics of the vaporiser by introducing a step change in engine fuelling from an air/fuel ratio of 17.5:1 to

12.5:1 at an engine speed of 1000 rev/min. It was reported that the engine reacted to the change of input within two engine cycles, measurement of the air/fuel ratio being taken in the exhaust pipe and that 90% of the final air/fuel ratio was achieved within a further two cycles. A more interesting measurement may have been a rich to lean system response allowing greater insight into the fuel stored within the heated section of the injector. No mention was made of the means of procuring the compressed air supply.

Figure 1.28
NEL fuel vaporiser, from Boyle, Boam and
Finlay, 1993

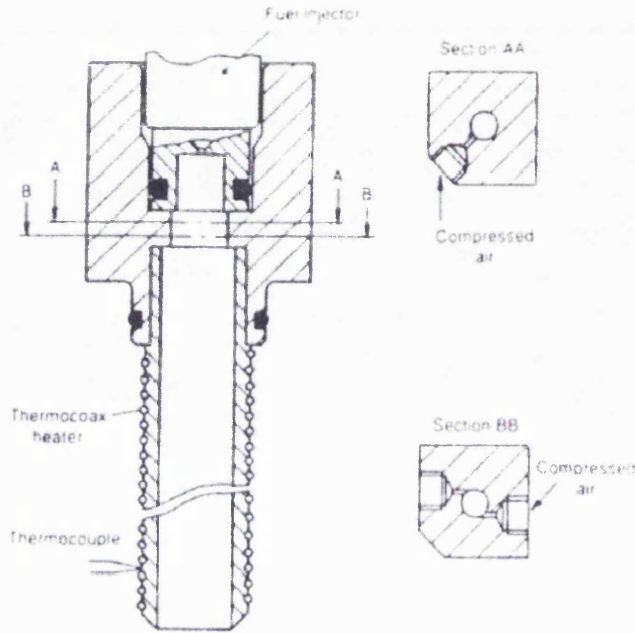


Figure 1.29
Comparison of HC emissions from a 16-valve engine during cold-starting using
liquid and vaporised fuel, from Boyle, Boam and Finlay, 1993

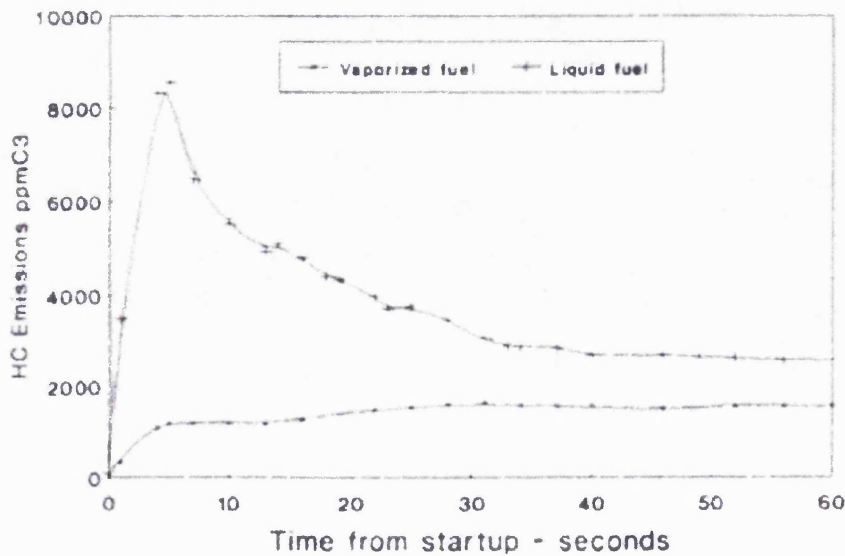
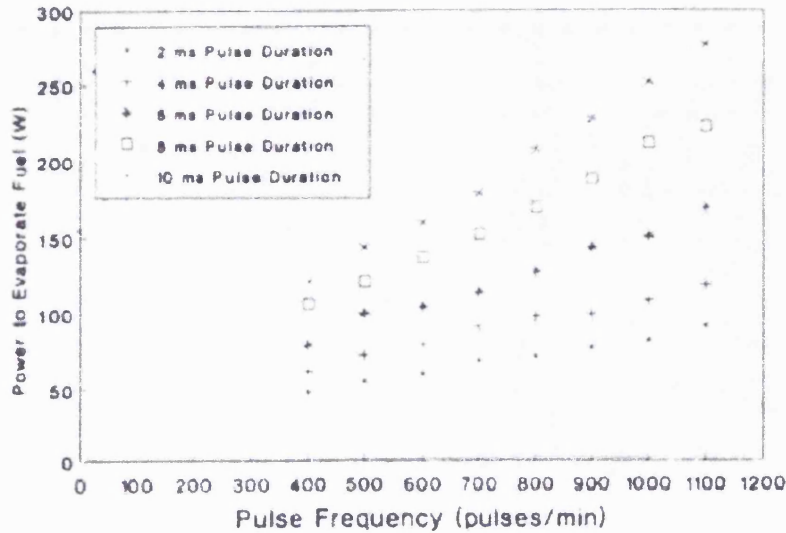


Figure 1.30

Heater power required to vaporise fuel at various pulse widths and injection frequencies, from Boyle, Boam and Finlay, 1993



The power required by a single NEL vaporiser to achieve full vaporisation over a range of fuel flow rates is shown in figure 1.30, however, it is likely that the power requirements of the unit will be far higher than those suggested due to the thermal inertia associated with the vaporiser construction necessitating that the units be overdriven to achieve adequate response during engine transients. It should be noted that whilst full vaporisation was claimed for each fuel flow rate no means of measurement was described. To operate during the FTP cold-start test the vaporisers would be required to function with fuel flows varying from idle to WOT. The thermal inertia of the unit can be used to an advantage during engine transients, but this would require careful development. Once the catalyst reaches light-off temperature, the power may be removed, however, it is not clear whether the vaporiser was intended for fitting in conjunction with or as a replacement for the standard fuel system. If the vaporisers were adopted as the sole fuel system it is likely that the spray produced when unheated would be very poor. Additionally the engine management system would have to make allowance for the air bled in through the two jets, stated as being some 90% of the idling air flow rate per cylinder with some form of idle speed control.

The NEL vaporiser was used for part of the studies by Fox *et al*, 1992, into mixture preparation under cold-start conditions and they concluded that the pre-vaporised mixture procured reliable starting under test conditions without the need for fuel enrichment. The power required to achieve what was claimed to be full fuel vaporisation of a stoichiometric mixture at 900 rev/min WOT was 200 W for a 500 cc single-cylinder engine.

Paganelli, 1984, described a range of Positive Temperature Coefficient, PTC, heating elements for Early Fuel Evaporation, EFE, used as a means of increasing the amount of fuel vapour present within the inlet manifold of carburetted or single point injection engines. Two types exist, either heating the air/fuel mixture as it exited the primary barrel of the carburettor or injector unit, or as it passed over the manifold floor, see figures 1.31 and 1.32. Both of these are fairly low power devices, being in the range of 200-600 W and they rely predominantly upon heat transfer by convection to the air and subsequently to the fuel in order to achieve their goal. As such they only offer minor improvements to the cold-startability due to the small increases in vapour concentration with a limited reduction in emission levels.

Figure 1.31

PTC honeycomb EFE heater, from Paganelli, 1984

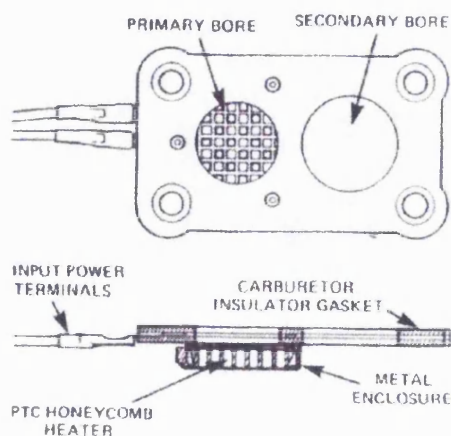
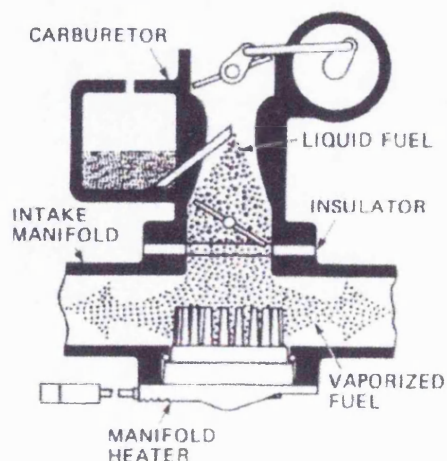


Figure 1.32

PTC manifold heater, from Paganelli, 1984



A novel means of assisting vaporisation of the mixture was proposed by Rao, Bardon & Gardiner, 1989 & 1991, which used an additional lobe at the base of the exhaust cam as a means for re-introducing exhaust gases into the combustion chamber late in the inlet stroke, known as prompt EGR, see figures 1.33 and 1.33. The re-circulated gases were those last evacuated from the combustion chamber and contained high levels of unburned HCs due to the late release in the exhaust stroke of the fuel trapped in crevice volumes. The mixture was at a temperature well above the fresh inlet charge and assisted in-cylinder fuel vaporisation. The method has been used to improve the cold-start combustion of methanol and gasoline fuelled engines with reductions being claimed for all three exhaust pollutants during both warm-up and at normal operating temperatures. The auxiliary lobe remained in place throughout the entire range of engine operation and was claimed to reduce emissions under all conditions though no evidence to back this claim was provided nor was there any data relating to the likely reduction in power output due to the decreased volumetric efficiency.

Figure 1.33

Modified exhaust cam, from Rao, Bardon & Gardiner, 1989

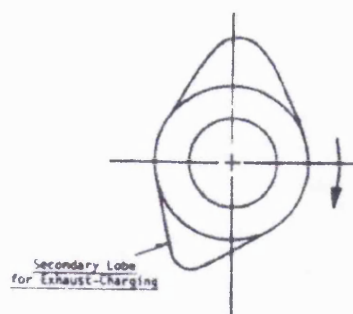
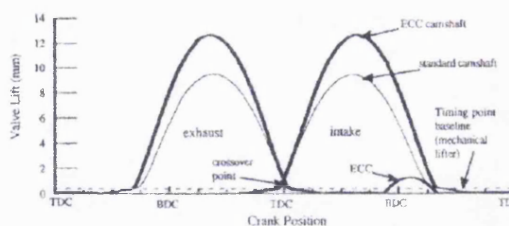


Figure 1.34

Modified and standard camshaft diagrams, from Rao, Bardon & Gardiner, 1989



1.4.10 Closing comments on mixture preparation

The use of a pre-vaporised mixture at normal engine operating temperature conditions has been proven to offer little reduction in emissions when a stoichiometric air/fuel ratio is retained. The principal benefit of using a vaporised mixture preparation

process at normal operating temperatures is to eliminate cylinder-to-cylinder variations when the engine is equipped with either single point fuel injection or a carburettor.

The option of air-assistance to improve mixture preparation by reducing the overall drop size appears to offer the potential of reduced emissions from port-injected engines attributed to improved combustion through a greater degree of homogeneity of the inlet charge and increased fuel atomisation. The swirl-type injector offers similar benefits but with the undesirable effect of increasing the spray angle if substantial reductions in droplet size are to be realised, consequently, an increase in the wall-wetting arises with an associated deterioration in transient response.

Whilst the potential of air-assisted injectors to reduce emissions under certain operating conditions exists, it is unlikely to be sufficient when the tightening legislation is considered, however, the benefits of improved idle stability and transient response are desirable. Reductions in transient response times improve not only the 'driveability' of the vehicle but also decrease the fuelling compensation, assisting in reducing UHC emissions and fuel consumption. The benefits of vaporisation during the engine's operation prior to catalyst light-off have already been stated, but it would seem appropriate to restrict this form of mixture preparation to the cold-start period and rely on air-assistance to procure the gains at normal operating temperatures.

1.5 HEAT TRANSFER THEORY

1.5.1 Introduction

Vaporisation of automotive gasoline is required prior to combustion since gasoline will not burn as a liquid. Studies of vaporisation rates and two-phase flows have been undertaken, Habib, 1983, Martins & Finlay, 1990, Troy, 1990 and Finlay Boam & Bannell, 1979, which enabled the heat transfer and liquid vaporisation rates to be predicted. Heat transfer from a solid to a liquid may be divided into four regimes;

1	Film Evaporation	$T_s \leq T_{sat}$
2	Vaporisation/Boiling	$T_{sat} \leq T_s \leq T_{bp}$
3	Transition	$T_{bp} \leq T_s \leq T_L$
4	Spheroidal Evaporation/Leidenfrost	$T_s \leq T_L$

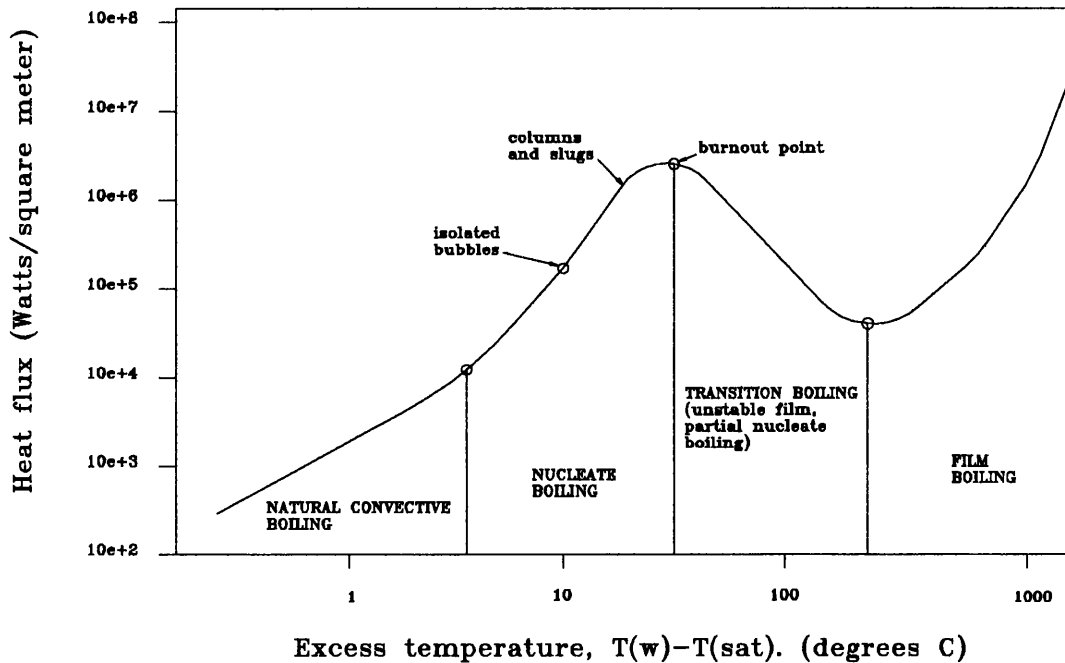
where s = surface, sat = saturation, bp = burnout point, L = Liedenfrost temperature.

Figure 1.35 indicates these regimes for water, though the shape is characteristic of the evaporation of other liquids.

Analysis of liquid gasoline forced to flow past a heating element to provide fuel vapour under cold-start conditions is a complex problem, combining bubble formation and motion from the liquid sweeping the heated surface. The heat transfer mechanism is a combination of film boiling and forced convection incorporating two-phase flow of varying periodicity, which is multi-component and either laminar or turbulent. Before the effects can be discussed, a brief overview of the interdependence of the governing variables is required.

Figure 1.35

**The four regimes of pool boiling in water at atmospheric pressure,
from Bejan, 1993**



1.5.2 Dimensional analysis applied to heat transfer by forced convection

Fluid flows involving heat transfer are generally represented in terms of the Nusselt number, Nu , a dimensionless number being a function of both the Prandtl, Pr , and Reynolds, Re , numbers. Its relevance and its derivation are given in the following.

The rate of heat transfer, \dot{Q} , from a surface of area, A , with a temperature difference of ΔT between the surface and the surrounding fluid, may be described by;

$$\dot{Q} = hA\Delta T \quad \text{equation 1.6}$$

where h represents the heat transfer coefficient at the surface boundary.

For forced convection, h may be described as a function of a number of variables;

$$h = \phi(u, \rho, \mu, k, c_p, \Delta T, l) \quad \text{equation 1.7}$$

where: $\rho = \text{density of fluid}$

$\mu = \text{viscosity of fluid}$

$k = \text{thermal conductivity of fluid}$

$c_p = \text{specific heat capacity of fluid}$

$\Delta T = \text{change in temperature}$

$l = \text{length}$

$u = \text{velocity of fluid}$

The relationship may be reduced into a manageable form using dimensional analysis if two further fundamental quantities are taken in addition to mass, M , length, L , and time, t . These two quantities are temperature, θ , and heat, H . Heat, according to the first law of thermodynamics, is interchangeable with work where there is no measurable interchange between thermal and mechanical quantities and the thermal effects from the fluid friction are negligible compared to the heat transfer from the surface to the fluid, Collins, 1980. Consequently, there are now eight quantities, see equation 1.7, defined in terms of five fundamentals which are listed below together with the exponents of the fundamental quantities:

		M	L	t	θ	H
<i>heat transfer coefficient</i>	$[h]$	0	-2	-1	-1	1
<i>velocity</i>	$[u]$	0	1	-1	0	0
<i>viscosity</i>	$[\mu]$	1	-1	-1	0	0
<i>density</i>	$[\rho]$	1	-3	0	0	0
<i>length</i>	$[l]$	0	1	0	0	0
<i>specific heat capacity</i>	$[c_p]$	-1	0	0	-1	1
<i>thermal conductivity</i>	$[k]$	0	-1	-1	-1	1
<i>change in temperature</i>	$[\Delta T]$	0	0	0	1	0

By choosing the variables l , ρ , μ , k and ΔT , which contain all the fundamental quantities and cannot form their own dimensionless group, the fundamentals may be defined as:

$$\begin{aligned} [M] &= [\rho l^3] \\ [L] &= [l] \\ [t] &= [\mu^{-1} \rho l^2] \\ [\theta] &= [\Delta T] \\ [H] &= [k \rho l^3 \Delta T \mu^{-1}] \end{aligned}$$

Recasting h , u and c_p from these definitions gives three dimensionless groups, $\pi_{1,2 \text{ \& } 3}$.

$$[h] = [k l^{-1}] \quad \text{hence } \pi_1 = \frac{hl}{k} = \text{Nusselt number, Nu.}$$

$$[u] = [\mu l^{-1} \rho^{-1}] \quad \text{hence } \pi_2 = \frac{\rho l u}{\mu} = \text{Reynolds number, Re.}$$

$$[c_p] = [k \mu^{-1}] \quad \text{hence } \pi_3 = \frac{c_p \mu}{k} = \text{Prandtl number, Pr.}$$

The Nusselt number gives a measure of heat transfer by convection, and can be described physically as the ratio of the temperature gradient in the fluid immediately in contact with the surface to a reference temperature gradient. The Prandtl number is the ratio of physical properties of the fluid relevant to heat transfer, while the Reynolds number can be considered to be the ratio of inertia to viscous forces in the flow. In order to calculate heat transferred by forced convection, it is necessary to determine h by using the following generalised relationship:

$$\text{Nu} = f(\text{Re})(\text{Pr})$$

1.5.3 Heat transfer with change of phase

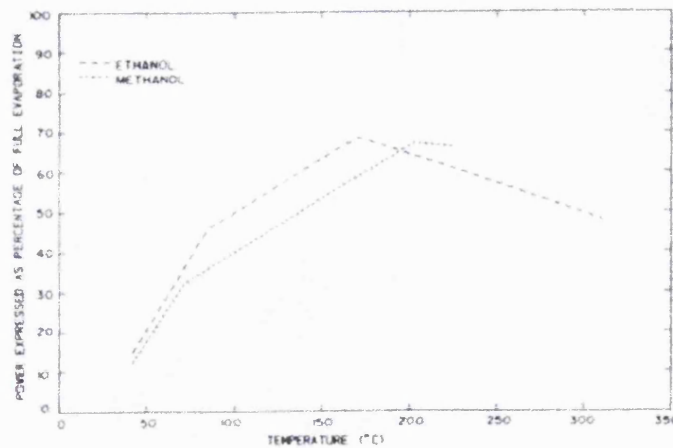
The theory in the preceding section applies to heat transfer by forced convection when there is no change of phase, however, a change of phase occurs when the fuel is

vaporised. There is no single relationship describing the convective heat transfer coefficient, h , under these circumstances, instead the behaviour is divided into the regimes shown in figure 1.35.

Martins and Finlay, 1990, assessed the heat transfer to liquid fuel injected into heated ducts and across heated intake valves. A coherent pencil jet spray was used for the experiment providing relatively accurate fuel impaction. One of the most interesting results was that of the evaporation levels with respect to the surface temperature of the inlet valve which showed that the evaporation peaked at only 70% with a surface temperature of 170-200°C depending on the type of fuel used, figure 1.36. Experimental observation indicated that the evaporation levels were limited due to the “drying out” of the valve surface, corresponding to the transition boiling regime as shown in figure 1.35.

Figure 1.36

Influence of valve temperature on rates of heat transfer to air/fuel mixtures expressed as a percentage of the power required to achieve complete fuel evaporation, 2 g/sec air flow rate, from Martins & Finlay, 1979



Relationships were established by Martins & Finlay between Nu , Re and Pr for flow past the inlet valves with dry air but no correlation was put forward to include gasoline in the air stream. Habib, 1983, used established turbulent flow relations, Kays & Crawford, 1980, to calculate the heat transfer coefficient, h ,

for investigations into cold liquid gasoline injected into a moving air stream. The primary objective of the study was to investigate the cooling effect on the droplets caused by the evaporation process using two theoretical fuel sprays with the same volume but split by differing droplet size groups, see table 1.7. Figure 1.37 shows the

Table 1.7

Liquid spray droplet distributions for two theoretical sprays, Habib, 1983

droplet \varnothing	17.19 μm	droplet \varnothing	8.59 μm
	32.32 μm		16.16 μm
(mean \varnothing)	50.00 μm	(mean \varnothing)	25.00 μm
	77.56 μm		38.68 μm
	145.45 μm		72.72 μm

(The number of droplets in each size group chosen such that each size contributes 20% of the total liquid mass.)

percentage of liquid fuel that remained as a function of the distance travelled along the duct. The flow was heated as it passed through a section along the duct at a temperature of some 833 K. It can be seen from figure 1.37 that between 75-95% of the fuel was calculated to remain in the liquid state, and the droplet temperature along the duct is shown in figure 1.38. It should be noted that the fuel type was unspecified, though it was unlikely to be gasoline due to the high temperatures applied to the duct indicating that the analysis was applied to diesel fuel in which case the extremely low levels of evaporation become more realistic.

Finlay *et al*, 1979, demonstrated the need for accurate modelling of fuel properties when considering theoretical evaporation processes of gasoline by assuming sixteen components to describe the fuel composition. In reality gasoline is made up of literally thousands of different hydrocarbons. The gasoline mixture model was found to give five times the level of evaporation when compared to n-octane demonstrating that investigation based on single component hydrocarbons may not represent behaviour with gasoline. The use of sixteen components may have been sufficient for the investigations in hand since only small temperature variations were considered though it is unlikely that it would be adequate if a larger temperature range had been involved.

Figure 1.37

**Percentage of liquid fuel remaining
along the duct, gas velocity: 7.62 m/s,
duct temperature: 278 K,
from Habib, 1983**

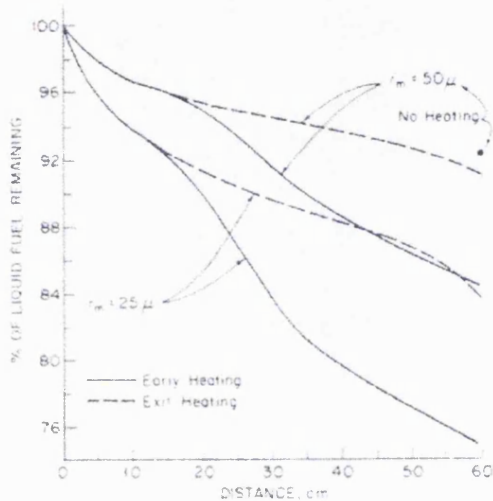
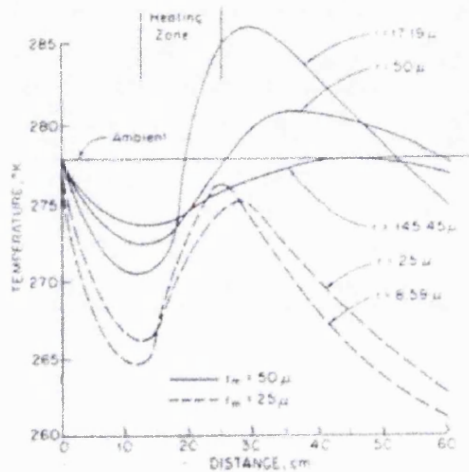


Figure 1.38

**Droplet temperature along the
duct, gas velocity: 7.62 m/sec,
duct temperature: 278 K,
from Habib, 1983**



Kusumowardhoyo and Subiakto, 1994, proposed a correlation to predict the boiling heat-transfer coefficient of both single fuels and multi-component mixtures, the mixtures being predominantly ethanol-gasoline. It is somewhat surprising, therefore, that whilst experimental data was presented for the validation of the proposed correlation, none referred to ethanol-gasoline mixtures.

1.5.4 Closing comments on heat transfer theory

Great difficulty is experienced in obtaining a satisfactory theoretical solution to the problem of two-phase heat flux of any real system due to the complexity of the flow fields and the process of heat transfer. The best that could be hoped for is an empirically-derived relationship between the salient parameters of Re and Nu numbers. Even this form of solution suffers from the difficulties of experimental verification because of the arduous task of obtaining accurate measurements,

consequently, it might be necessary to adopt a grossly simplified model for the purposes of theoretical analysis and to accept a limited accuracy.

The problem of accurate instrumentation is one which cannot be considered lightly. Any temperature measurements must be regarded with caution if they are made within a two-phase flow due to the averaging effect created between liquid and gaseous states of the fluid flow and the cooling of sensors or probes due to impingement and evaporation from the surface. Ideally a measured value of vapour concentration is required for the analysis as well as accurate measurement of droplet size and spray density.

1.6 DROP SIZE MEASUREMENT

1.6.1 Introduction

Previous sections have demonstrated the importance of good mixture preparation in the reduction of emissions from IC engines and it is therefore necessary to have a means of accurately measuring and characterising the liquid sprays produced by a fuel system. The most important criteria for drop size measurement techniques is that any results obtained are representative of the observed process, can be recorded instantly, have a sufficient size range for droplet size measurement and are non-intrusive, Williams, 1993.

Fuel spray measurement techniques fall into two groups, temporal and spatial. Temporal sampling is the measurement of individual droplets as they pass through a fixed volume during a specified time interval. Spatial sampling refers to the measurement of droplets contained within a small pre-described volume assuming the contents do not change throughout the duration of each measurement.

1.6.2 Phase-Doppler particle sizing

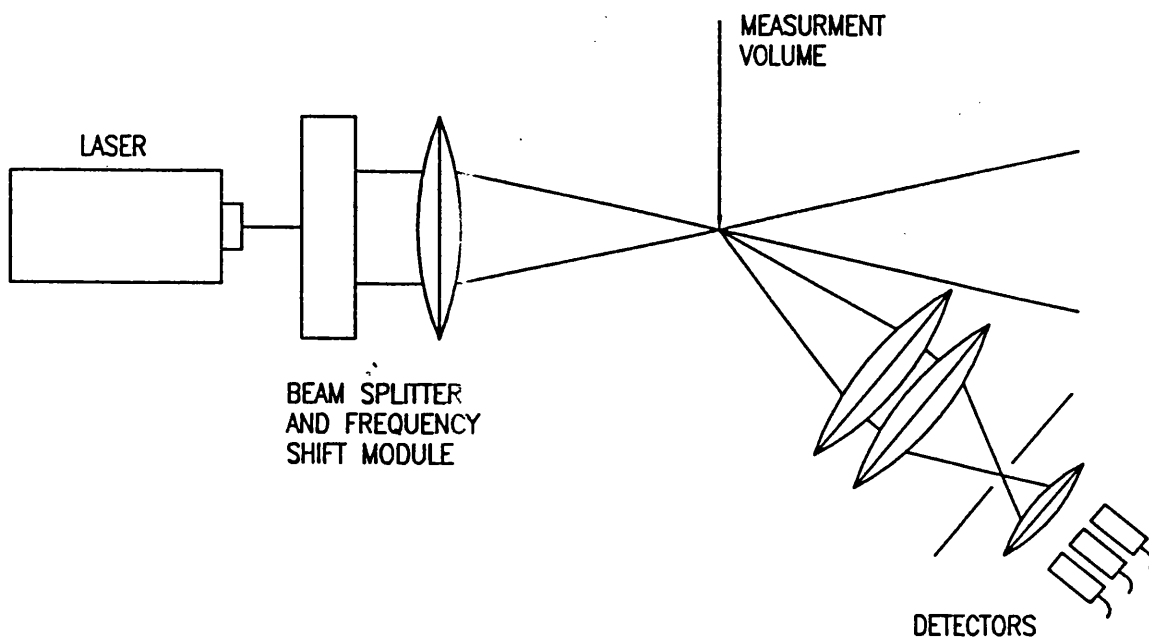
Phase-Doppler Anemometry, PDA, is a temporal drop sizing technique which provides simultaneous measurements of size and velocity distributions within a spray. A small measurement volume, typically of the order of 1 mm^3 , is created at the intersection of two laser beams originating from the same source. Droplets passing through the volume produce a signal of scattered light whose frequency and amplitude may be interpreted to give velocity and diameter measurements respectively.

Since the technique is essentially a single drop counter, accurate particle sizing may only be achieved in relatively dilute sprays, Nightingale, 1985, moreover, ambiguity of the measurement can arise if the edge of the sample volume is traversed by a large

droplet giving the same amplitude of scattered light as a small droplet passing through its centre. Further limitations exist due to the small measurement volume if a complete picture of the spray is required due to the amount of time necessary to traverse more than one plane, though the extent of information generated is immense. Solutions of 'top-hat' light intensity distribution tailoring and 'two colour' LDA are suggested by Ereat & Ungut, 1982, and Yeoman & Azzopari, 1982, respectively as ways of improving accuracy.

PDA has a droplet size range of 3 μm to 5 mm and can measure velocities of the order of 1000 m/s. A typical PDA optical set-up is shown in figure 1.39.

Figure 1.39
Typical PDA optical set-up



1.6.3 Laser diffraction, LD, particle sizing

Laser diffraction particle sizing produces a spatial measurement of the spray. A laser beam is passed through the flow and sizing is achieved by analysing the pattern of light diffracted by the droplets. A characteristic light intensity distribution, known as a Fraunhofer diffraction pattern, is created when a small spherical droplet passes through a parallel beam of monochromatic light. The scattered light, uniquely related to the diameter of the droplet, is focused using a Fourier transform lens onto a detector made up of a series of concentric annular rings, Swithenbank *et al*, 1976, and since the diffraction pattern remains stationary, measurement of the droplet is achieved regardless of its location and velocity within the beam. The light intensity within each ring band is calculated and the measured size distribution obtained for a complete spray by combining the light energy of all the droplets at the point of measurement. In order to obtain a high confidence level of spray characterisation the process is repeated over a number of cycles of a periodic spray. The size distribution is a 'line of sight' average along the full length of the beam passing through the spray. A tomographical transformation of the measured light energy may be performed at a number of radial positions in order to achieve a greater spatial resolution, Yule *et al*, 1980.

The possibility of multiple scattering with the consequence of biased and unreliable light intensity distributions can occur when using light scattering instruments. It was originally indicated that attenuation levels of incident light must be less than 50% to avoid this problem, though experimental and theoretical evaluations by Felton, Hamidi & Aigal, 1985 and Dodge, 1984, have extended this limit to 95% through a series of correction equations.

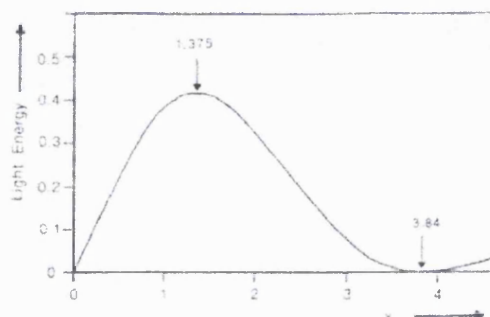
1.6.4 Problems of evaporation

Evaporation of fuel sprays can greatly distort the apparent measured drop size when using LD sizing, Miller, 1992, Fry, 1994 and Dodge & Cerwin, 1984. The laser light

passing through the spray may be refracted in a rapidly varying random manner, due to the density gradients present in the surrounding flow field created by evaporation of the 'light ends' of gasoline mixing with the surrounding air leading to an effect known as beam steering, Dodge & Cerwin, 1984. Undiffracted light will suffer a small angle of refraction and thus partly reproduce the effect of the diffraction by a large droplet.

Williams, 1994, suggested a means of removing the evaporation effects from the light intensity data. The technique was found to be both reliable and reasonably accurate for the type of injectors tested, but it is unknown if this method will be universally applicable to the wide range of injectors now being developed. The method of data manipulation assumed a linear decay from the peak light intensity towards the inner region of the detector, however, the very finely atomised sprays produced using air-assistance will cause the peak to be shifted towards the outer region of the detector. The decay from this point is unknown, though it is likely to be a curve of reducing gradient due to the characteristic energy distribution of diffracted light, shown in figure 1.40. Williams, 1994, examined sprays with associated Smds an order of magnitude greater than those expected from an air-assisted injector. Smaller droplets cause a shift of the light energy distribution peak in the positive 'x' direction accompanied by a similar displacement of the total light energy as seen by the Malvern analyser (an instrument based on the laser diffraction principle). If a linear regression is assumed based upon the portion of the signal where confidence in the accuracy of the measurement is questionable, it is possible for the total light energy distribution to decay to zero before it intersects the y-axis. In this situation, caution is required when applying the method to fuel sprays where evaporation effects are likely to be high.

Figure 1.51
Dimensionless energy distribution
of diffracted light, from Williams, 1994

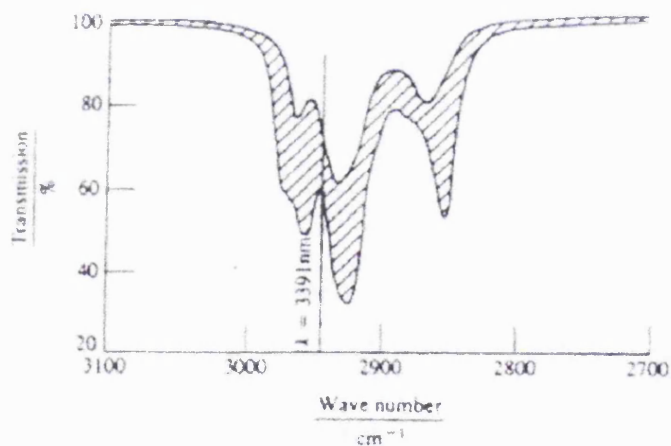


1.6.5 Vapour concentration measurement

A considerable amount of work has been undertaken to quantify the vapour concentration within evaporating sprays by the use of infra-red (IR) absorption techniques, Winklehofer, Fraidl & Plimon, 1992, Chraplyvy, 1981 and Billings & Drallmeier, 1994. Hydrocarbon molecules exhibit absorption bands in the IR part of the spectrum at approximately $3.4 \mu\text{m}$ wavelength. An He-Ne laser is used which has a radiation wavelength of $3.39 \mu\text{m}$, thereby coinciding with the absorption bands of the hydrocarbons, see figure 1.41, and a second laser beam of visible light, He-Ne 632 can be used for droplet detection. The lower wavelength is not absorbed by the

Figure 1.41

Infra-red transmission range of various hydrocarbon molecules, normalised for samples of $1\text{g}/\text{m}^3$ m, from Winklehofer, Fraidl & Plimon, 1992

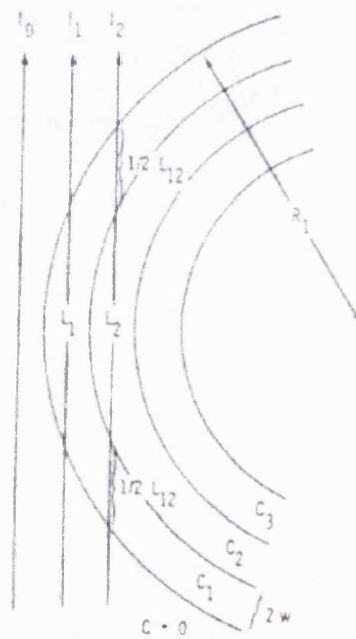


evaporated fuel but is scattered by the liquid droplets. The effects of the droplets passing through the vapour probing laser beam may be calculated once the drop size distribution has been obtained from the diffraction of the visible laser beam and the vapour concentration may then be calculated if a uniform distribution is assumed, Chraplyvy, 1981.

Chraplyvy, 1981, used this method to evaluate the level of vapour concentration within an n-heptane fuel spray. The laser was traversed through the fuel spray,

normal to the spray cone axis of symmetry. This sectioning of the spray formed an axisymmetric geometry which was then partitioned into annular rings, see figure 1.42. Line-of-sight laser intensity measurements were made through the centre of the annular ring band widths with local concentrations provided by the application of deconvolution exhibiting a degree of resolution similar to the band width, see equation 1.8. Figure 1.43 shows the radial variation of the transmission indicating the varying contribution of the droplets to the total attenuation, whilst figure 1.44 describes the relationship between fuel vapour concentration and radial distance from the spray axis. Chraplyvy suggested that the relationship between the vapour concentration and droplet number density was caused by the smaller, sub-20 μm , core droplets being affected by the same fluid transport processes which controlled the dispersion of the of the vapour. It is more likely, however, that the effect was due to the vapour cloud or halo, known to surround each droplet in an evaporating spray.

Figure 1.42
Partition of space into concentric annuli for axisymmetric geometries, from Chraplyvy, 1981



$$C_1 = -\frac{1}{L_1\alpha} \ln \frac{I_1}{I_0}, \quad C_2 = -\frac{1}{L_2\alpha} \left(\ln \frac{I_2}{I_0} + \alpha L_{12} C_1 \right), \text{ etc.} \quad \text{equation 1.8}$$

where, I₀, I₁, I₂ etc. are the light intensities associated with the annular rings C₀, C₁, C₂ etc., whose line of sight average lengths are L_{ij}.

Figure 1.43

Radial variation of total transmission at $3.39\mu\text{m}$ in the axial plane of a 1.48 MPa n-heptane spray, arrow indicates spray edge, from Chraplyvy, 1981

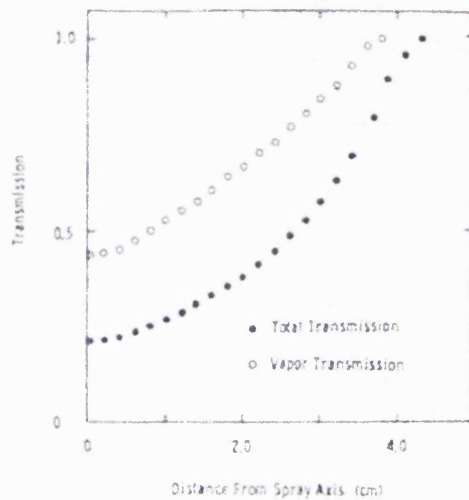
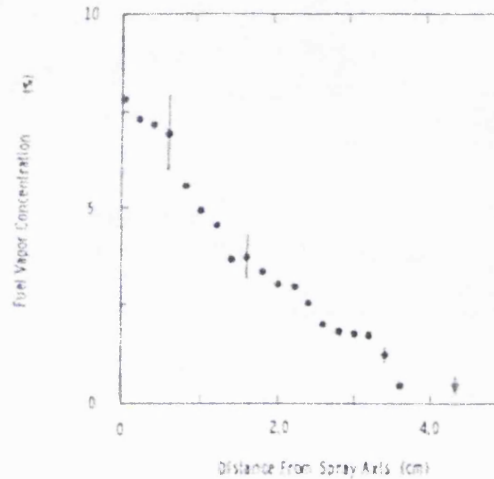


Figure 1.44

Radial variation of the fuel vapour concentration in the axial 1.48 MPa n-heptane spray, arrow indicates spray edge, from Chraplyvy, 1981



Winklhofer applied the IR absorption technique to an optically-accessed engine in order to determine the variation in vapour concentration during inlet and compression strokes. Figures 1.45 and 1.46 show the real-time vapour concentrations within the cylinder for various injection timing strategies and engine temperatures respectively. Some doubt as to the validity of the results must be present in view of the fact that all plots reveal a reduction in the quantity of fuel vapour present within the combustion chamber during the compression stroke, however, it should be noted that the author only makes claims that the results were qualitative.

Both of the IR extinction experiments may have suffered problems from the beam steering phenomenon referred to by Williams, 1994, and consequently incorrect droplet size distributions and size bands may have been assumed during the factoring out of the attenuation of the vapour probing laser.

Figure 1.45

Effects of injector timing on the cycle to cycle repeatability of fuel vapour concentrations, from Winklehofer, Fraidl & Plimon, 1992

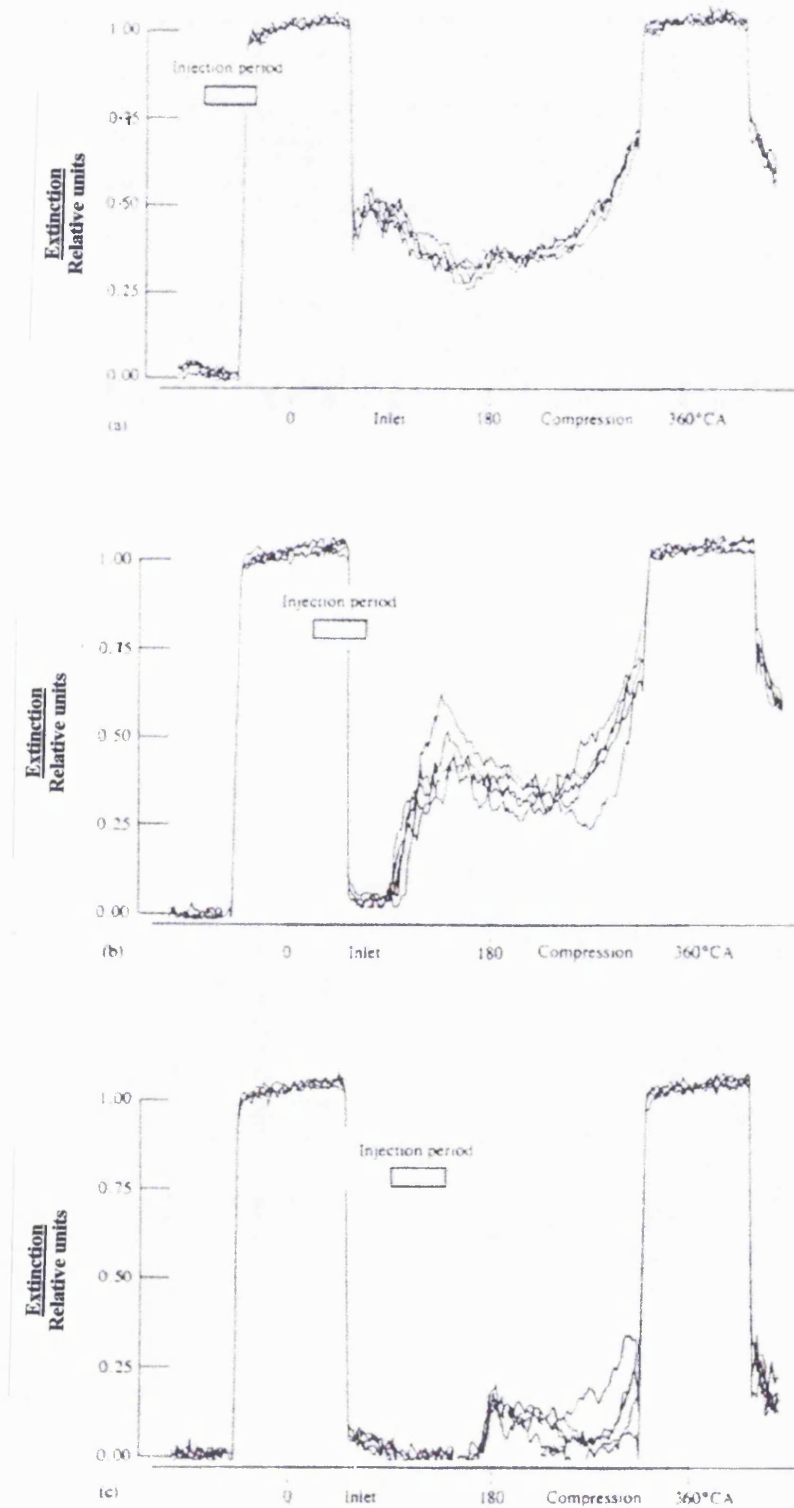
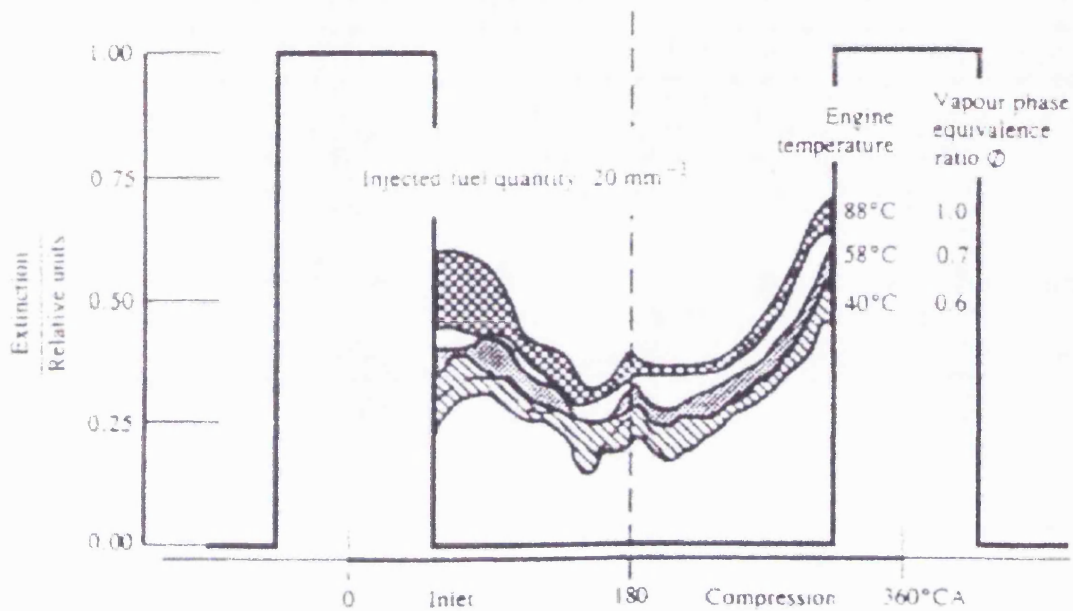


Figure 1.46

Influence of engine temperature on in-cylinder fuel vapour concentration,
from Winklehofer, Fraidl & Plimon, 1992



In an attempt to overcome the problems associated with droplet evaporation, Billings & Drallmeier, 1994, applied the IR extinction technique to non-evaporating droplets in the form of Styrene beads. Methane gas was then introduced into the flow in predetermined quantities allowing an accurate assessment of the abilities and limitations of the technique to be quantified. It was found that for low particle-number-density flows, the vapour mole fraction measured was largely unaffected by the IR scattering from the particles, see figure 1.47, however, a more dense particle population caused significant discrepancies if the scattering effects were not taken into account, see figure 1.48. The author stated that the effect may have increased significance when the particle size approaches the wavelength of the incident radiation.

Figure 1.47

Vapour mole fraction measured as a function of test section position for the light loading case, the input mole fraction was 1%, from Yeoman *et al*, 1982

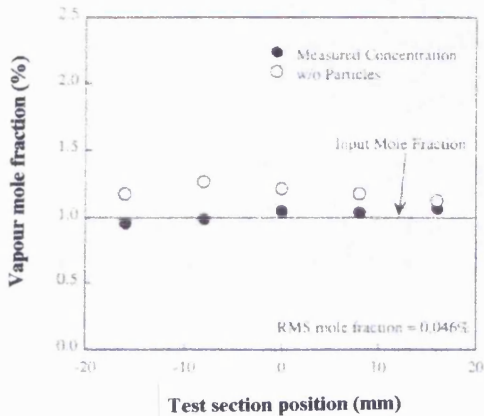
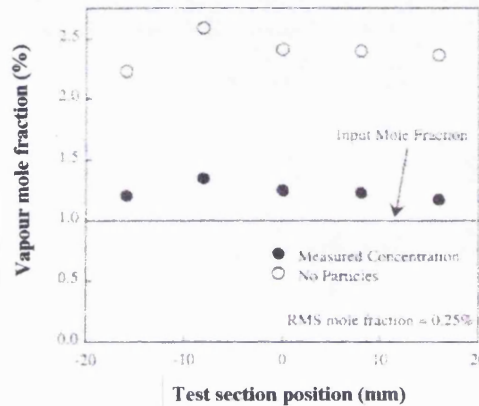


Figure 1.48

Vapour mole fraction measured as a function of test section position for the heavy loading case, the input mole fraction was 1%, from Yeoman *et al*, 1982



1.6.6 Closing comments on spray measurement techniques

Both LD and PDA measurement techniques offer an accurate means of spray measurement and characterisation providing their respective limitations are observed. Other techniques include holography and photography, both of which offer spatial distribution measurements. Holography has the benefit of a three-dimensional characterisation and measurement of the velocity distribution if double-pulsing is used, though it suffers from cost and time penalties, Thompson & Dunn, 1980.

Photographic imaging of fuel sprays used in conjunction with computer image analysis provides quantitative information such as drop size distribution and velocity. Charged Couple Device, CCD, cameras offer an immediate image, though suffer a limited resolution, critical when investigating finely-atomised sprays. A further problem of photographic techniques is caused by the single plane of measurement.

The ideal solution would appear to be a combination of LD particle sizing and infra-red absorption techniques, though even this combination is not fool-proof. It does

however, offer the crucial advantage of being able to measure vapour as well as providing information on droplet size and concentration. That the absorption technique relies on the data provided by LD sizing implies it is prone to the same degree of error unless a means of reliably removing spurious data caused by evaporation can be eliminated from the output. To date, the only known solution to this problem requires an informed judgement to be made as to what proportion of the output signal characterises the actual spray.

1.6.6a Footnote on laser induced fluorescent techniques

Since this literature survey was written, laser induced fluorescence (LIF) techniques have progressed extensively and as such a brief overview is presented.

The fluorescent signal is achieved by tuning a laser light to correspond to a known absorption band of the sample under examination. Detection of the fluorescent signal is detected as a positive signal over a null background.

Crosley & Smith, 1983, showed that LIF was well suited for the detection of reactive intermediates and that OH radicals could be detected in concentrations below 1×10^{-12} . Felton *et al*, 1988, and Tanka & Tabata, 1994 both imaged OH radicals in the combustion flame using propane and gasoline respectively. The primary problem associated with this application of LIF is due to collisional quenching that can occur when the medium is subjected to high pressures.

Fluorescing tracers added to the fuel can overcome the quenching problem and have the benefit that most fluoresce in the visible spectrum, though they cannot be used without complications. The concerns associated with additions to the fuel are the changes that may arise in the fuel characteristics. Deschamps, Synder & Baritauld, 1994, used Biacetyl as a tracer which possessed a similar boiling point to the fuel used, iso-octane, at 88°C compared to 100°C. Reboux, Puechbety & Dionnet, 1994, opted for Toluene mixed with iso-octane.

Further problems are encountered when multi-component gasoline is used due to the large number of chemical species associated, and each with its own boiling point. Consequently only one component can be accurately tracked at any time and as such only limited information of the in-cylinder distribution is known. The aim of LIF is to achieve reliable in-cylinder measurements of the air/fuel ratio, taking into account both liquid and vapour concentrations. Though this has yet to be achieved reliably and accurately, it is felt that LIF techniques point the way towards future in-cylinder liquid and vapour fuel concentration measurements.

1.7 RESEARCH PROGRAMME

The preceding part of this chapter identified the need for improvements to be made to the mixture preparation of spark-ignition engines in order to meet the ever more stringent emissions regulations during cold-start and transient phases of engine operation. Poor mixture preparation manifests itself as liquid deposits on the inlet port walls, a problem which is heightened when the metal surfaces are cold during starting and warm-up due to the low evaporation rate. This requires that the fuel flow rate into the engine is increased such that sufficient fuel vapour is present around the sparking plug at the point of spark initiation to ensure reliable combustion during cold-start and warm-up phases of engine operation. The liquid fuel forms into puddles and rivulets on the port walls, a large proportion of which does not evaporate but flows into the combustion chamber. The consequence of this poor mixture preparation is an increase in tailpipe UHC emissions during the period prior to catalyst light-off temperature

A considerable amount of research is being performed to achieve catalyst light-off temperature at, or just after, the time of starting. However, the techniques under investigation are not without their problems and it is still not certain that they can contain the excessive UHC emissions produced during an engine start and initial period of warm-up. A possible solution is to vaporise the fuel prior to its introduction into the inlet port, as postulated in previous sections.

An injector has been designed by Fry, 1993, patent application number 9314897, with the objectives of providing vaporised fuel during starting and warm-up, and then an air-assisted spray in order to maintain good fuel preparation when the engine is warm.

Fry, 1994, produced an initial prototype (figure 2.1) and performed tests on a single-cylinder engine to demonstrate the unit's potential for vaporising gasoline. The unit, known as the UCL air-assisted fuel vaporiser (AAFV), had certain features which would seem to make it particularly attractive for production: use of standard

automotive components (normal fuel injector and diesel engine glow plug); external dimensions which would enable it to directly replace 'top-feed' injectors; and a power consumption considerably less than that of an electrically-heated catalyst. Fry had not the opportunity to carry out fundamental investigations into the operating mechanisms of the vaporiser nor had he been able to optimise the values of its basic design parameters. The aims of this research programme were set as to take Fry's basic design, investigate its operation, optimise its performance and gather data on its performance under engine operating conditions. In more detail the work included;

(i) characterising the spray produced when operating as an air-assisted atomiser using a Malvern analyser which uses the laser diffraction principle. The work would extend to studying the effects of altering values of the basic design parameters (e.g. exit nozzle diameter). This work is described in chapter 2 along with an investigation into the power requirements for fuel vaporisation.

(ii) cold-start testing using an engine installed in an environmentally-controlled test chamber. The investigation would examine the air/fuel ratios required by the AAFV operating in its vaporising mode and compare the engine-out UHC emissions with the standard fuel system. This work is detailed in chapter 3.

(iii) redesign of the AAFV to incorporate some improvements suggested by the work described in (i) and (ii). The redesign also improved the installation of the device on an engine. Chapter 4 describes the redesign work.

(iv) intake and exhaust port UHC sampling using a high frequency response flame ionisation detector (HFRFID). The work would be performed on a dedicated single cylinder engine during engine operation. The investigation would enable UHC vapour concentration levels to be constantly measured within the intake port and provide information of the fuel transport mechanisms. A novel approach to supplying pressurised air to the AAFV was proposed and tried as earlier testing had suggested that some delay was occurring in the transport of fuel through the device when using a

bleed at atmospheric pressure at low manifold depressions. This work is detailed in chapter 5.

(v) HFRFID testing on a pulsating flow rig to remove the intake port backflow encountered during actual engine operation and so determine its effect on the intake port fuel flow process. Chapter 6 contains this work.

(vi) motored-start and injector interrupt tests to determine the fuel flow and transient response of AAFV compared with a standard fuel system. The exhaust gas UHC concentration would be measured using the HFRFID. This work is contained within chapter 7.

1.8 REFERENCES

- Anon** (1994a), "Heated catalytic converter", *Automotive Engineering*, September 1994
- Anon** (1994b), "Three-way catalysts for ultra-low-emission vehicles", *Automotive Engineering*, October 1994
- Bejan, A** (1993), "Heat Transfer", Pub. John Wiley 1993, chapter 8, Boiling heat transfer, pp 398-443
- Billings, T P & Drallmeier, J A** (1994), "A detailed assessment of the infra-red extinction technique for hydrocarbon vapour measurements in a controlled two-phase flow", *Atomisation and Sprays*, Vol. 4, 1994
- Blackmore, D R & Thomas A** (1977), "Fuel economy of the gasoline engine", Pub. John Wiley, 1977, chapter 6, The effect of mixture preparation on fuel economy, pp 89-118
- Boam, D J & Finlay, I C** (1979), "A computer model of fuel evaporation in the intake system of a carburetted petrol engine", *IMechE*, June 1979
- Boyle, R J, Boam, D J & Finlay, I C** (1993), "Cold-start performance of an automotive engine using prevaporised gasoline", SAE 930710
- Burt, R Roberts, D D & Woodworth, J A** (1979) "A comparison of fuel-economy, exhaust emissions and performance of three European cars operating on homogeneous fuel-air mixtures", *IMechE* 148/79
- Chraplyvy, A R** (1981), "Nonintrusive measurements of vapour concentrations inside sprays", *Applied Optics*, Vol. 20, No. 15, August 1981
- Collins, R** (1980), MEng, Postgraduate fluids mechanic course notes, Department of Mechanical Engineering, University College London

- Crosley, D R & Smith, G P** (1983), "Laser induced fluorescence spectroscopy for combustion diagnostics", *Optical Engineering*, Vol. 22, No. 5, Sept/Oct 1983
- Deschamps, B, Synder, R & Baritauld, T** (1994), "Effect of flow and gasoline stratification on combustion in a four-valve SI engine", SAE941993
- Dodd, A E & Wisdom, J W** (1968), "Effect of mixture quality on exhaust emissions from single-cylinder engines", IMechE conference, November 1968
- Dodge, L G** (1984), "Change of calibration of diffraction based particle sizers in dense sprays", *Optical Engineering*, 1984
- Dodge, L G & Cerwin, S A** (1984), "Extending the applicability of diffraction-based drop sizing instruments", *Liquid particle size measurements*, ASTM STP 848, Edited by J M Tishkoff, R D Ingebo & J B Kennedy, 1984
- Emmenthal, K D, Muller, C, Schafer, O & Strozyk, R H** (1985), "Air-forced injection system for spark ignition engines", SAE850483
- Ereaut, P, & Ungut, A** (1982), "Measurement of drop size and velocity in vaporising sprays", 2nd ICLASS, 1982
- Felton, P G, Hamadi, A A & Aiagal, A K** (1985), "Measurement of drop size distribution in dense sprays by laser diffraction", 3rd ICLASS, London, 1985
- Felton, P G, Mantzaras, J Bomse, D S & Woodin, R L** (1988), "Initial two-dimensional laser induced fluorescence measurements of OH radicals in an internal combustion engine", SAE88163
- Finlay, I C, Boam, D J & Bannell, J L K** (1979), "Computer model of fuel evaporation in air valve carburettors" *Automotive Engineer*, December 1979

- Fry, M D** (1994), "Optimisation of mixture preparation in an SI engine",
PhD Thesis, 1994, Department of Mechanical Engineering, University College
London
- Goldsmith, R** (1989), "Passenger car emissions-part 2", Mechanical Incorporated
Engineer, December 1989
- Habib, I S** (1983), "Instantaneous heating of a flowing spray", AIAA/ASME
November 1983
- Harada, K, Shimizu, R, Kurita, K, Muramatsu, M, Makimura T & Ohashi, M**
(1992), "Development of air-assisted injector system", SAE920294
- Heimrich, M J, Albu S & Osborn, J** (1991), "Electrically-heated catalyst system
conversions on two current-technology vehicles", SAE910612
- Heimrich, M J, Smith, L R & Kitowski, J** (1994), "Cold-start hydrocarbon
collection for advanced exhaust emission control", SAE920847
- Heywood, J B** (1988a), "Internal combustion engine fundamentals", Pub. McGraw
Hill International, 1988, chapter 11, Pollutant formation and control,
pp 567-667
- Heywood, J B** (1988b), "Internal combustion engine fundamentals", Pub. McGraw
Hill International, 1988, chapter 7, SI fuel metering and manifold phenomena,
pp 279-325
- Hires, S D & Overington, M T** (1981), "Transient mixture strength excursions-an
investigation of their causes and the development of a constant mixture
strength fuelling strategy", SAE810495
- Hurley, R G, Hansen, D L, Pawlowicz, R J, Smolinski J M & Ghandi, H S**
(1991), "Experiences with electrically heated catalysts", SAE912384

- Kashiwaya, M, Kosuge, T, Nakagawa, K & Okamoto, Y** (1990), "The effect of atomisation of fuel injectors on engine performance", SAE900261
- Kay, W I** (1978), "Manifold fuel film effects in an SI engine", SAE 780944
- Kays, W M & Crawford, M E** (1980), "Convective heat and mass transfer", Pub. McGraw-Hill, 1980
- Kusumowardhoyo, M A & Subiakto**, "Nucleate boiling performance of ethanol-gasoline mixtures", International Communications Heat Mass Transfer, Vol. 11, November 1994
- Lefebvre, A H** (1989), "Atomisation and sprays", Pub. Hemisphere Publishing, 1989
- Lembke, M** (1988a), "Automotive electric/electronic systems", Pub. Robert Bosch GmbH, 1988, chapter 13, L-Jetronic, pp 232-251
- Lembke, M** (1988b), "Automotive electric/electronic systems", Pub. Robert Bosch GmbH, 1988, chapter 16, Mono-Jetronic, pp 258-261
- Liimatta, D R, Hurt, R F, Deller, R W & Hull, W L** (1971), "Effects of mixture distribution on exhaust emissions as indicated by engine data and the hydraulic analogy", SAE710618
- Lindsay, R, Thomas, A, Woodworth J A, & Zeschmann, E G** (1971), "Influence of homogeneous charge on the exhaust emissions of hydrocarbons, carbon monoxide and nitric oxide from a multi-cylinder engine", SAE710588
- Lindsay, R, Thomas, A & Wilson, J A** (1973), "Heat pipe vaporisation of gasoline-Vapipe", NATO-CNCC, October 1973
- Ma, T, Collings, N & Hands, T** (1992), "Exhaust Gas Ignition (EGI)-A new concept for rapid light-off of automotive exhaust catalyst" SAE920400

- Malvern Droplet Particle Sizer**, Malvern series 2600-User Manual, IM 026, Issue 2,
Malvern Instruments
- Martins, J J G & Finlay, I C** (1992), "Fuel preparation in port-injected engines",
SAE920518
- Martins, J J G & Finlay, I C** (1990), "Heat transfer to air-ethanol and air-methanol
sprays flowing in heated ducts and across heated intake valves", SAE900583
- Matthes, W R & McGill, R N** (1976), "Effects of the degree of fuel atomisation on
single-cylinder engine performance", SAE760117
- Miller, M J** (1992), "Mixture preparation in automotive spark ignition engines", PhD
Thesis, 1992, Department of Mechanical Engineering, University College
London
- Miller, M & Nightingale, C J E** (1990), "Measurement changes in mixture
preparation that occur during flow past the inlet valve on an SI engine",
Proceedings of the IMechE, C394/004, September 1990
- Mires, S D & Overington, M T** (1981), "Transient mixture strength fuelling
strategy", SAE810495
- Mugele, R A & Evans, H D** (1951), "Droplet size distributions in sprays", Industrial
and Engineering Chemistry, Vol 43, No. 6, June 1951, pp 1317-1324
- Nightingale, C J E** (1985), "Internal Combustion Engineering", chapter 6, Mixture
preparation for SI engines, edited by J H Weaving, Pub. Elsevier Science,
1985, pp 173-212
- Nogi, T, Ohyama, Y, Yamauchi, T & Kuroiwa, H** (1988), "Mixture formation of
fuel injection systems in gasoline engines", SAE880558

- Okamoto, Y, Nobukatsu, A, Nakawaga, K, Kosuge, T & Atago, T (1992),**
“Atomisation characterisation of two-stream injector for 4-valve engines”,
SAE920705
- Paganelli, J (1984),** “PTC ceramic heaters in automotive controls” SAE840143
- Peters, D B (1983),** “Laser-video imaging and measurement of fuel droplets in an SI engine”, IMechE, April 1983
- Rao, V K, Bardon, M F & Gardiner, D P (1989),** “A method of assisting cold-starts, improving fuel economy and reducing emissions of engines at cold temperatures”, SAE890001
- Rao, V K, Bardon, M F & Gardiner, D P (1991),** “Improving the cold-start combustion in methanol fuelled spark ignition engines by means of prompt EGR”, SAE910377
- Robison, J A & Brehob, W M (1965),** “ The influence of improved mixture quality on engine exhaust emissions and performance”, Western States Combustion Institute meeting, October 1965
- Reboux, J, Puechbety, D & Dionnet, F (1994),** “A new approach of planar laser induced fluorescence applied to fuel/air ratio measurements in the compression stroke of an optical engine”, SAE941988
- Rogers, G F C & Mayhew, Y R (1980),** “Engineering Thermodynamics Work & Heat Transfer”, Pub. Longman, 1980
- Rokita, R, Bandel, W & Herzog, P (1993),** “Mixture preparation optimisation for gasoline engines on a dynamic flow test rig”, IMechE 032/93
- Simon, N, Arndt, S & Zielger, E (1992),** “Experimental measurement techniques to optimise design of gasoline injection valves”, SAE920520

- Spalding, D B** (1979), "Combustion and mass transfer", Pub. Pergamon Press, 1979
- Stone, R** (1992), "Internal combustion engines", Pub. The MacMillan Press Ltd, 1992, Chapter 3, Combustion and fuels, p74
- Swithenbank, J, Beer, J M, Taylor, D S, Abbot D & McCreath, G C** (1976), "A laser diagnostic technique for the measurement of droplet and particle size distribution", AIAA, 1976
- Tanaka, T & Tabata, M** (1994), "Planar measurements of OH radicals in an SI engine based on laser induced fluorescence", SAE940477
- Thompson, B J & Dunn, P** (1980), "Advances in far-field holography theory and applications", Society of Photo Optical Instrumentation Engineers, Vol 215, Recent Advances in Holography, 1980
- Trayser, D A, Griesike, F A Hazard, J A, Weller, A E & Locklin, D W** (1969), "A study of the influence of fuel atomisation, vaporisation and mixing processes on pollutant emissions from motor-vehicle powerplants", Battelle Memorial Institute, Columbus, Ohio, 1969
- Troy, J S** (1990), "Two-phase flow and heat transfer prediction", SAE901239
- Williams, P A** (1993), "Laser diffraction particle sizing and spark-flash photography techniques for successful measurement of spark ignition engine fuel sprays", IMechE 016/93
- Williams, P A** (1994), "Characterisation of fuel sprays in spark ignition engines" PhD Thesis, 1994, Department of Mechanical Engineering, University College London
- Winklehofer, E, Fraidl, G K & Plimon, A** (1992), "Monitoring of gasoline fuel distribution in a research engine", IMechE Journal of Automobile Engineering, 1992
- Wright, K** (1990), "Trends in transport: the shape of things to go", Scientific American, May 1990

Yeoman, M L & Azzopari, B J (1982), "Optical development and application of a two colour LDA system for the simultaneous measurement of particle size and particle velocity", AERE-R Internal report 10468, UK Atomic Energy Authority, 1982

Yule, A J & Ahseng, C (1980), "A laser tomographic investigation of liquid fuel sprays", 18th symposium on combustion, Canada, 1980

Yun, H J & Lo, R S (1976), "Theoretical studies of fuel droplet evaporation and transportation in a carburettor venturi", SAE760289

CHAPTER 2
CHARACTERISATION OF FUEL/AIR MIXTURE
PREPARATION

CHAPTER 2

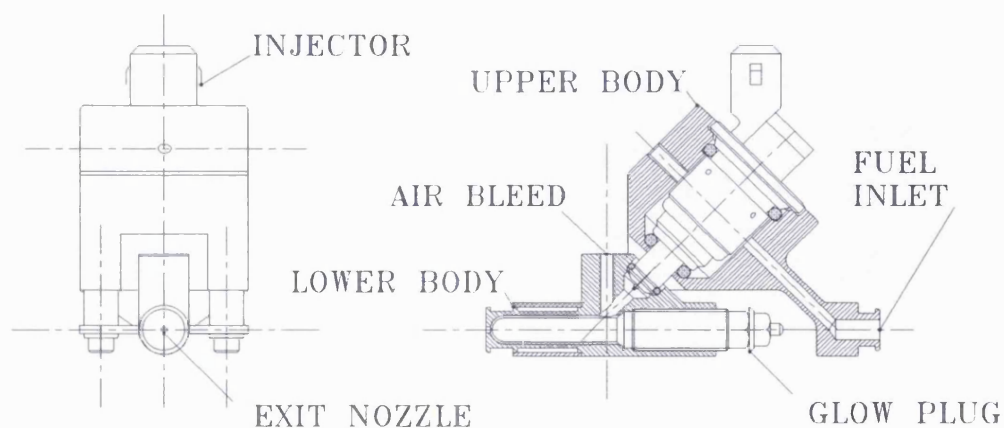
CHARACTERISATION OF FUEL/AIR MIXTURE PREPARATION

2.1 AIR-ASSISTED FUEL VAPORISER (AAFV): DESIGN

Fry's initial design of the AAFV was such that a two-piece construction was used, one housing a side feed type of fuel injector, the other containing the heating element, refer to figure 2.1. The heating element was a modified diesel glow plug, screwed into an aluminium housing incorporating a narrow annular air gap around the heated section length. Air and fuel were combined upstream of the heated chamber and entered through a single orifice. A singular, small diameter exit orifice/nozzle was sized to provide a restriction to the fluid flow. The injector housing was thermally insulated from the heating chamber. Fuel was introduced into the lower body containing the heating element at a 45° angle relative to the glow plug centre line via the tip of the injector which protruded from the upper injector housing. The tip was sealed with a neoprene 'O' ring. At mid-distance between the injector tip and the heating chamber, air was introduced by tapping into the fuel supply transfer drilling.

Figure 2.1

Sectioned view of the UCL air-assisted fuel vaporiser



Air-assistance was provided by metered air at atmospheric pressure drawn from the intake trunking upstream of the throttle, therefore the initial design would only give good fuel preparation at part load operation.

As mentioned previously, two modes of operation of the AAFV were possible, either with or without power supplied to the heating element. Air-assistance was maintained regardless of the mode of operation and ensured fine atomisation of the fuel spray and also provided a means of purging the internal cavity of fuel after each injection event. The terms of 'vaporisation' and 'air-assisted' or 'air-atomisation' are used to describe operation with and without power supplied to the heating element respectively.

The largest nozzle diameter chosen was 2.3 mm. This represented the diameter which would be capable of flowing 100% of the idle air flow requirement of a single cylinder of a 1.8 litre, 4-valve engine of recent design. The smallest diameter chosen was 0.8 mm, capable of flowing 10% of the idle air flow. An intermediate value of 1.5 mm was also used. The diameters were calculated using compressible flow equations, see section 2.2.1, assuming fluid flow composition to be air only and a discharge coefficient of 0.60. The diametral clearance was a compromise between production tolerances of the glow plug units and maintaining a minimal "sac" volume through the heated chamber to reduce transport time and improve heat transfer during vaporisation. Two clearances were used, 0.75 and 1.00 mm. The length of glow plug determined the overall heated surface area. Two industry standard units of 20 mm and 30 mm element length were chosen taking into account installation and availability constraints.

Three test conditions were used, 800 rev/min idle, 1500 rev/min road load and 2000 rev/min full load, see Appendix A2. Data regarding the inlet manifold depression, fuel flow and air flow were obtained from standard engine test data.

2.2 THEORY

In the design of the AAFV, two aspects are of critical importance. The first is the rate of fluid flow through the nozzle restriction and the second is the heat transfer from the heating element to the fuel. The following sections detail some of the theory used to ascribe values to the processes.

2.2.1 Compressible flow equations

The compressible flow equations used to calculate the air mass flow rates through the AAFV nozzles are derived by considering a simplified gas flow in a duct. The flow rate through the nozzles is predominantly a function of pressure ratio and flow area in conjunction with secondary effects such as heat transfer. Taking account of all the flow influences would lead to an overly complex solution, consequently a number of assumptions, correction factors and simplified equations have been used in order to obtain a satisfactory description of the air mass flow rate.

Derivation of the compressible flow equations is achieved by applying continuity and the steady flow energy equation to a one-dimensional steady flow in a duct. The gas is assumed to be isentropic and inviscid. These conditions and assumptions need also to apply to the flow through the nozzle. Any deviation will result in error of the calculated value, however, principal sources of error will arise from the assumption of one-dimensional steady flow. Despite the limitations imposed by the assumptions, it was felt that the accuracy of the predicted values was acceptable for the task of initial sizing of the nozzle diameter.

Since flow leaving the nozzle is in the form of a high speed jet entering a large volume, it may be assumed that there will be no significant pressure recovery of the stream. Hence, if the throat pressure of the nozzle is assumed to be equal to the downstream pressure, the mass flow rate may be calculated from the pressure ratio across the nozzle exit. Empirically-derived correction factors are applied to the

nozzle diameter to take into account the boundary layer effects and the possibility of flow separation. The discharge coefficient, C_d , relates the actual physical nozzle aperture dimension to the true flow or effective area.

Derivation of the compressible flow equations is felt unnecessary and so is quoted directly for subsonic flow as follows:

$$\frac{dm}{dt} = C_d AP_1 \sqrt{\left(\frac{2\gamma_1}{\gamma_1 - 1}\right) \frac{1}{RT_1} \left[\left(\frac{P_2}{P_1}\right)^{2/\gamma_1} - \left(\frac{P_2}{P_1}\right)^{(\gamma_1+1)/\gamma_1} \right]}$$

equation 2.1

Mass transfer reaches an upper limit when flow through the nozzle becomes choked. At this point, the downstream pressure has dropped below a particular value and the flow is then independent of downstream conditions.

In order to determine whether the flow is either sonic or subsonic, consideration of the choked condition is required. By differentiating equation 2.1 with respect to time and equating the result to zero, it can be shown that the mass flow rate is a maximum when:

$$\left(\frac{P_2}{P_1}\right)_{crit} = \left(\frac{2}{\gamma_1 + 1}\right)^{\gamma_1/\gamma_1 - 1}$$

equation 2.2

The maximum flow rate is found by substituting equation 2.2 into 2.1. Hence, the mass flow rate for sonic flow is determined by

$$\frac{dm}{dt} = C_d AP_1 \sqrt{\frac{\gamma_1}{RT_1} \left(\frac{2}{\gamma_1 + 1}\right)^{(\gamma_1+1)/(\gamma_1-1)}}$$

equation 2.3

2.2.2 Heat transfer

An indication of the thermal efficiency of the AAFV during vaporising operation may be obtained by analysis of the power consumption assuming air to be a perfect gas and quasi-steady flow through the device with respect to time. Note that the analysis presented below takes no account of the compressibility of the fluid stream as it passes through the exit nozzle and assumes a reference value for the enthalpy of vaporised gasoline, a more detailed and potentially more accurate approach is presented by Shapiro, 1953. From the First Law of Thermodynamics:

$$Q \equiv E_2 - E_1 + (W) \quad \text{equation 2.4}$$

The energy equation may be written as;

$$Q - W = h_{a2} - h_{a1} + \frac{(\Delta h + h_{gv1} - h_{gv2})}{AFR} + \frac{U_{agv2}^2}{2} \left(1 + \frac{I}{AFR} \right) - \frac{U_{a1}^2}{2} \quad \text{equation 2.5}$$

assuming that the inlet velocities of both the fuel and air are negligible, the air and fuel enter and leave the control volume at the same temperature and that all of the fuel is completely vaporised

2.2.3 Calculation of C_{pf}

Fuel vapour, unlike air, cannot be treated as a perfect gas, i.e. $dh/dT = C_p \neq \text{constant}$. Hence, to evaluate the specific heat capacity of gasoline at constant pressure Heywood, 1988, specifies the following polynomial expression:

$$\tilde{c}_{p,f} = -27.08 + 128.18t^2 - 67.23t^3 + 16.19t^4 - \frac{0.58}{t^5} \quad \text{equation 2.6}$$

In order to perform these calculations, the ratio of specific heats of the mixture, γ_m , is required. C_p may be calculated using dh/dT . To evaluate γ_m the specific heat capacity of fuel at constant volume, C_v , is required in conjunction with the C_p and C_v values of

the mixture passing through the nozzle. This may be achieved using the relationships:

$$C_p - C_v = \frac{\mathfrak{R}}{\omega} \quad \text{equation 2.7}$$

and

$$m_m C_{v_m} = m_a C_{v_a} + m_f C_{v_f} \quad \text{equation 2.8}$$

also

$$m_m C_{p_m} = m_a C_{p_a} + m_f C_{p_f} \quad \text{equation 2.9}$$

Hence the ratio of specific heats of the mixture is simply calculated from:

$$\gamma_m = \frac{C_{p_m}}{C_{v_m}} \quad \text{equation 2.10}$$

2.2.4 Flow restriction

Flow through the AAFV is nominally governed by the flow area at the exit of the heated chamber. However, if the glow plug swells due to heat expansion, it may present sufficient restriction such that the flow becomes governed by the remaining glow plug-chamber wall clearance. The upper limit of glow plug expansion, x , permissible prior to restriction is evaluated from:

$$x \leq 2 \sqrt{\left(\frac{id}{2}\right)^2 - \frac{A}{\pi}} \quad \text{equation 2.11}$$

2.3 DISCUSSION I

2.3.1 Operating criteria

The first series of tests were split into two groups to establish the behaviour of the device during operation in its liquid/air-atomisation and vapour modes and to evaluate the different geometries of AAFV over a range of engine operating conditions. A number of factors will influence the decision of which nozzle geometry to adopt, namely: (1) the time delay between injector pulse and appearance of the spray's leading edge within the test section/inlet tract, (2) the spray duration in relation to the inlet cycle duration, (3) the fuel droplet size, and (4) whether a benefit exists in using a nozzle whose air mass flow rate is such that modulation for operation at idle is necessary.

Fuel spray characterisation was undertaken using a steady flow test rig, with geometry designed to mimic the intake port of a typical 4-cylinder, 2-litre, 4-valves per cylinder engine. Air flow through the rig was induced by a liquid ring vacuum pump. Gasoline was used as the test fuel. The test section incorporated a number of windows. A Malvern 2600c particle sizer was aligned vertically through a pair of windows in the port, near the position normally occupied by the inlet valves. The Malvern sizer uses the patterns of diffracted light formed when the beam encounters droplets to calculate droplet size distribution. This allows the fuel spray to be sampled and measured at the point of entry into the combustion chamber, some 70 mm downstream of the injector. Laser diffraction particle sizing theory and some of the practical limitations of its use are detailed in Appendix A2. Details of the test rig and its installation in the Fuel Systems Test Facility at UCL are contained in Miller, 1992.

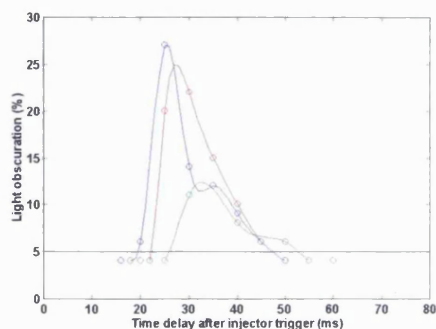
All tests were performed using a fuel pulsewidth and air flow matched to the engine conditions, however, the repetition rate of the injector was decreased such that the test section was clear of any fuel from the previous cycle.

2.3.2 Time delay to leading edge formation

The spray duration was measured using a Malvern particle sizer during the tests by extending the delay between injection events in order to determine the leading and trailing edges of the spray without interaction of fuel from either previous or subsequent injection cycles.

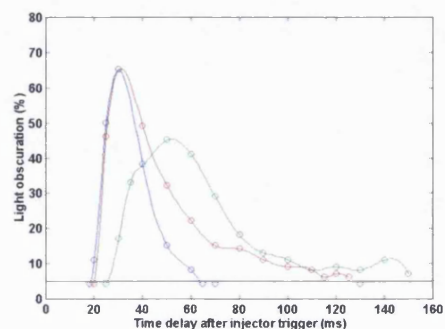
Measurements taken using the Malvern particle sizer include the “obscuration”. This is a measure of laser beam scattering and absorption by the liquid particles within the spray. The obscuration value is related to the particle concentration within the flow and, by setting an arbitrary limit, was used to detect the leading edge of the fuel spray. The limit chosen was 5% obscuration which coincides with the minimum level required by the particle sizer for reliable droplet measurement. The delay time was found to vary with geometric changes of exit nozzle and length of the heated chamber, see figures 2.2-2.4. A 50% increase in length, and therefore sac volume, produced a 5% increase in fuel delay. Changes due to the 25% increase in sac volume created by increasing the diametral clearance around the heating element could not be reliably measured. A 2.3 mm diameter exit nozzle produced a 25% reduction in arrival time of the leading edge when compared with a 1.5 mm exit nozzle. The leading edge of the spray when using the smallest nozzle, 0.8 mm diameter, could not be detected at idle conditions due to the very low levels of obscuration measured.

Figure 2.2
Light obscuration vs. time delay after injector trigger,
0.8, 1.5 & 2.3 mm nozzles, 1500 rev/min,
road load, 450 mm Hg manifold depression,
passive air bleed



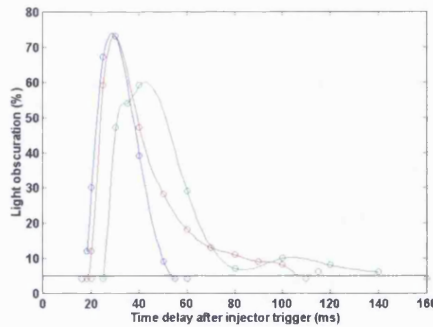
0.8 mm exit nozzle \varnothing , 7.0 mm heated chamber id, 30 mm glow plug length, 1.5 mm exit nozzle \varnothing , 7.0 mm heated chamber id, 30 mm glow plug length, 2.3 mm exit nozzle \varnothing , 7.0 mm heated chamber id, 30 mm glow plug length

Figure 2.3
Light obscuration vs. time delay after injector trigger,
0.8, 1.5 & 2.3 mm nozzles, 2000 rev/min,
full load, 7 mm Hg manifold depression,
35 kPa air bleed pressure



0.8 mm exit nozzle \varnothing , 7.0 mm heated chamber id, 30 mm glow plug length, 1.5 mm exit nozzle \varnothing , 7.0 mm heated chamber id, 30 mm glow plug length, 2.3 mm exit nozzle \varnothing , 7.0 mm heated chamber id, 30 mm glow plug length

Figure 2.4
Light obscuration vs. time delay after injector trigger,
0.8, 1.5 & 2.3 mm nozzles, 2000 rev/min,
full load, 450 mm Hg manifold depression,
70 kPa air bleed pressure



0.8 mm exit nozzle \varnothing , 7.0 mm heated chamber id,
 30 mm glow plug length, 1.5 mm exit nozzle \varnothing ,
 7.0 mm heated chamber id, 30 mm glow plug length,
 2.3 mm exit nozzle \varnothing , 7.0 mm heated chamber id,
 30 mm glow plug length

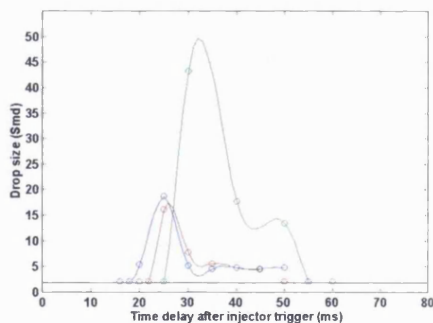
2.3.3 Liquid fuel/air-atomisation operation: Spray duration

If the benefits of an open-valve injection strategy are to be realised, it is important to introduce the majority of the fuel into the air stream just after the inlet valves open such that the air stream entrains a significant proportion of the liquid droplets to reduce impingement on the port wall. Under normal operating conditions, it is therefore desirable for the spray duration to be less than the period of the induction stroke. The 5% obscuration criterion was used to define the leading edge of the spray. The results indicated that all the designs investigated could be purged of fuel within the duration of one inlet stroke at both idle and 1500 rev/min conditions using a passive air bleed (i.e. air bled in from atmosphere), see figure 2.2. During 2000 rev/min full load operation manifold depression is slight, of the order of 1.0 kPa, and therefore a pressurised air supply is required. Two supply pressures, 35 kPa and 70 kPa, were investigated. At the full load condition all the designs failed to purge fully the AAFV device of fuel within the duration of one cycle, see figures 2.3 & 2.4. It is believed that small amounts of fuel adhere to the inside surfaces of the AAFV, and are stripped off at a slower rate than the bulk flow and it is this small amount of fuel that maintains the obscuration levels above the nominal 5% value.

2.3.4 Fuel droplet size

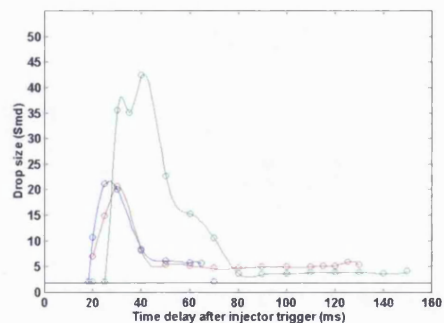
Measurements of droplet diameters were taken at a fixed time interval after the injector was opened. The delay times were set by starting from the point at which the 5% obscuration criterion was exceeded, and then increasing the time delay by increments of 2-5 ms until the obscuration fell below 5%. Beam steering effects known to be caused by evaporation of the liquid fuel, Williams, 1993, were removed prior to processing the raw data. All Malvern readings were taken using a 100 mm lens covering a range of drop sizes from 2 to 188 μm in diameter. This proved to be adequate for all geometric nozzle variations. Both 1.5 and 2.3 mm diameter nozzles produced similar values of droplet Smd with the average value varying between 8 and 9.5 μm , see figures 2.5-2.7. This compares favourably with previous work, Nogi *et al*, 1988, which shows that droplets with diameters of 30 μm or less will remain entrained in the inducted air flow. The droplet size associated with the 0.8 mm diameter nozzle consistently exceeded 40 μm , see figures 2.5-2.7. This was felt to be caused by the exit nozzle becoming “plugged” by the liquid fuel thus reducing the effective air-atomisation.

Figure 2.5
Fuel spray drop size (Smd) vs. time delay after injector trigger, 0.8, 1.5 & 2.3 mm nozzles, 1500 rev/min, road load, 450 mm Hg manifold depression, passive air bleed



0.8 mm exit nozzle \varnothing , 7.0 mm heated chamber id, 30 mm glow plug length, 1.5 mm exit nozzle \varnothing , 7.0 mm heated chamber id, 30 mm glow plug length, 2.3 mm exit nozzle \varnothing , 7.0 mm heated chamber id, 30 mm glow plug length

Figure 2.6
Fuel spray drop size (Smd) vs. time delay after injector trigger, 0.8, 1.5 & 2.3 mm nozzles, 2000 rev/min, full load, 7 mm Hg manifold depression, 35 kPa air bleed pressure

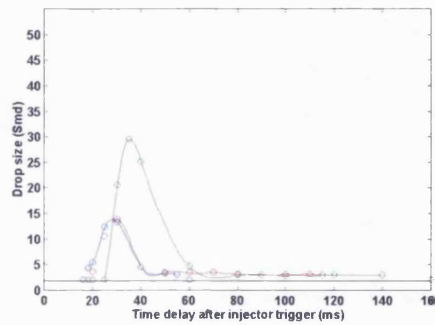


0.8 mm exit nozzle \varnothing , 7.0 mm heated chamber id, 30 mm glow plug length, 1.5 mm exit nozzle \varnothing , 7.0 mm heated chamber id, 30 mm glow plug length, 2.3 mm exit nozzle \varnothing , 7.0 mm heated chamber id, 30 mm glow plug length

The effect of increasing the air-assistance can be clearly seen by comparing figures 2.6 & 2.7. Initially, 35 kPa (relative) air-assistance was used, increasing to 70 kPa.

This change brought about a reduction of approximately 50% of the fuel sprays' Smd. The geometric changes of internal nozzle dimensions had little influence on drop size distributions.

Figure 2.7
Fuel spray drop size (Smd) vs. time delay after
injector trigger, 0.8, 1.5 & 2.3 mm nozzles, 2000 rev/min,
full load, 450 mm Hg manifold depression,
70 kPa air bleed pressure



0.8 mm exit nozzle Ø, 7.0 mm heated chamber id,
 30 mm glow plug length, 1.5 mm exit nozzle Ø,
 7.0 mm heated chamber id, 30 mm glow plug length,
 2.3 mm exit nozzle Ø, 7.0 mm heated chamber id,
 30 mm glow plug length

2.3.5 Modulation of air flow

Table 2.1, contains the calculated nozzle air mass flow rates over the duration of one complete 4-stroke engine cycle, in relation to the engine's required flow rate during the induction stroke. The analysis assumed a constant value of P_1/P_2 , that any reduction to the flow rate due to the presence of fuel was negligible and that the value of γ for the fluid flow remained constant at 1.4. It was felt that, due to difficulties in controlling the engine speed at idle, if the flow through the AAFV was greater than 50% of the idling requirements, some form of modulation would be necessary. The 2.3 mm nozzle fell into this category, its flow rate being some 99% of the idle air flow. Modulation necessitates some form of solenoid valve similar to that employed in the fuel injector with the associated increase in cost for both the hardware and the controlling software and any cost penalty needs to be offset by a significant improvement in the AAFV's operating characteristics. The 2.3 mm nozzle offered both a reduction in the spray's associated Smd and the time delay between injector trigger and its leading edge reaching the intake valve, however, the benefits are

relatively marginal and the vaporising mode efficiency is likely to be poor due to the rapid efflux of the fuel from within the heated chamber.

Table 2.1

**AAFV exit nozzle air mass flow rates for idle and 1500 rev/min road load
(assuming standard temperature and pressure, stp)**

	850 rev/min, idle			1500 rev/min, road load		
Nozzle diameter (mm)	0.8	1.5	2.3	0.8	1.5	2.3
Coefficient of discharge (assumed)	0.6	0.6	0.6	0.6	0.6	0.6
Nozzle flow area (mm²)	0.50	1.77	4.15	0.50	1.77	4.15
Upstream pressure (kPa gauge)	101.3	101.3	101.3	101.3	101.3	101.3
Downstream pressure (kPa gauge)	29.46	29.46	29.46	41.44	41.44	41.44
Gas constant, R (kJ/kg.K)	287	287	287	287	287	287
Air flow temperature (K)	293	293	293	293	293	293
Ratio of specific heats, γ (assumed)	1.4	1.4	1.4	1.4	1.4	1.4
Nozzle mass flow rate (mg/ms)	0.021	0.074	0.174	0.021	0.074	0.174
4-stroke cycle duration (ms)	140	140	140	80	80	80
Air mass required/cylinder/cycle (mg)	22.5	22.5	22.5	25.8	25.8	25.8
Air mass flowed/nozzle/cycle (mg)	2.94	10.36	24.36	2.94	10.36	24.36
Percent of mass required flowed through nozzle (%)	13	46	108	11	40	94

2.4 CONCLUSIONS FROM INITIAL TESTING

The initial tests highlighted that the significant influences on mixture preparation when applying the AAFV in its atomising mode were the exit nozzle diameter and pressure drop across the nozzle. At this stage it was possible to use the results obtained to select a suitable diameter of the exit nozzle. It is logical to assume that, whilst a modest increase in the time between injector trigger and fuel arrival at the intake valve is acceptable, a significant lengthening of the spray duration will lead to problems of fuel mapping for transient operation. With this and the relatively poor mixture preparation borne in mind, it was possible to eliminate the 0.8 mm nozzle geometry from further evaluation. The 2.3 mm nozzle was also be excluded due to the marginal

benefit in both droplet size and delay in fuel arrival at the valve when compared to the 1.5 mm geometry, in conjunction with the penalty associated with its high rate of air consumption.

2.5 DISCUSSION II

2.5.1 Vaporised fuel operation

A number of factors will affect the unit's ability to vaporise the fuel, notably the mass flow rates of both the fuel and air as well as the surface area and temperature to which the fuel is exposed.

Due to the findings of the initial geometry assessment, the second series of tests concentrated on the 1.5 mm nozzle. However, because of the restriction to flow offered by a smaller orifice, it was felt likely that an improved cold start performance could be attained with a smaller exit nozzle diameter due to the increased residence time of the fuel within the heated chamber, consequently, a 1.2 mm diameter nozzle was included in the test programme.

2.5.2 Geometric influences on vaporisation

During testing, it was found that the shorter (19 mm) glow plug variants were incapable of fully vaporising the fuel under any of the specified engine conditions, using the maximum power available of approximately 250 Watts. This indicated that the surface area was insufficient for the air/fuel flow rates investigated. Further testing of the 19 mm glow plug length vaporisers was consequently abandoned.

When testing the 1.2 mm exit diameter nozzles with the longer glow plug, 100 and 200 Watts were necessary to vaporise the fuel at idle and 1500 rev/min road load respectively, however, no significant difference in power requirements for either

internal diametral clearances was identified. The 1.5 mm diameter nozzles produced similar results, see table 2.2. All geometries were unable to produce complete vaporisation at 2000 rev/min full load condition.

Table 2.2

Energy balance results for 1.2 mm & 1.5 mm nozzles at idle and 1500 rev/min road load

	850 rev/min		1500 rev/min	
	1.2	1.5	1.2	1.5
Nozzle diameter (mm)	1.2	1.5	1.2	1.5
Air mass flow rate (mg/s-measured)	106.2 e ⁻³	216.7 e ⁻³	30.33 e ⁻³	151.7 e ⁻³
Fuel mass flow rate (mg/s-calculated)	43.1 e ⁻³	43.1 e ⁻³	148 e ⁻³	148 e ⁻³
Temperature at inlet (K-measured)	294.1	295.1	294.5	295.5
Temperature at outlet (K-measured)	363.6	319.1	402.1	347.1
Specific heat capacity, air (kJ/kg.K)	1.005	1.005	1.005	1.005
Specific heat capacity, fuel @ T_{in} (kJ/kg.K)	1.544	1.548	1.546	1.550
Specific heat capacity, fuel @ T_{out} (kJ/kg.K)	1.849	1.645	1.981	1.760
Latent heat of evaporation, gasoline (kJ/kg.K assumed)	264.2	264.2	264.2	264.2
Electrical energy input (W)	104.22	100	194.63	201.24
Energy rejected to air flow (W)	7.38	5.23	3.28	7.87
Energy rejected to fuel flow (W)	20.79	14.32	89.64	61.73
Energy rejected to surroundings (W)	76.05	80.45	101.71	131.65

2.5.3 Heat transfer

Calculating the energy balance for the AAFV during operation as a vaporiser, see equation 2.5, section 2.2.3, indicated that approximately 20% of the heat energy was transferred to the fuel, 7% to the air flow and 73% rejected to the housing during idling conditions for the 1.2 mm nozzle configurations.

It is interesting to note the fluid stream temperature¹ at exit from the nozzles, see table 2.2. The highest temperature of the flow was achieved during the 1500 rev/min road load test. At low fuel flow rates heat was lost through convection to the air stream passing through the body. The change from idling conditions to road-load, 1500 rev/min brought with it a four-fold increase in the mass flow rate of fuel, as a consequence lower air flows were experienced and a greater proportion of the heat energy was imparted to the fuel.

The energy consumption compares favourably with the alternative technology of electrically-heated catalysts for which Heimrich, Albu & Osborn, 1991, and Hurley *et al*, 1991, measured power requirements greater than 1.0 kW/cylinder for a duration of 30 seconds. The power necessary for AAFV operation was 0.1 kW/cylinder during the period prior to catalyst light off, though it should be stressed that the thermal efficiency of the unit was of secondary importance to the production of fuel vapour at this stage. If the simple measure of modulating the electrical supply to the glow plug could be adopted without loss of vaporising integrity then the unit's efficiency could become even more attractive. The electrically heated catalyst recorded a 65% drop of UHC emissions during bag 1 of the FTP test cycle, though this halved when vehicle battery recharging was included which cannot be ignored in practice. Hurley *et al*, 1991, has shown that EHCs can exhibit rapid deterioration of conversion efficiency with age, with increases of UHC of up to 50% measured during the FTP test cycle after 4,000 miles.

2.5.4 Nozzle mass flow rates

A rotameter was employed to monitor the mass flow rates through the AAFV nozzle. Table 2.3 shows the variation during vaporiser operating conditions. Comparisons between experimental results for the mass flow rates and those calculated using

¹ Note that the temperature was measured via a thermocouple placed 5 mm downstream of the nozzle exit and therefore records the approximate wet bulb temperature of the air/fuel/vapour mixture.

equations 2.1 & 2.3, section 2.2.1, show that agreement between the total measured and predicted flow rates differed sufficiently to prompt further investigation.

Equation 2.3 indicates that four parameters will affect the mass flow rate when the nozzle is choked, namely upstream pressure, upstream temperature, flow area, and γ . The upstream temperature was already measured and included in the calculations, but both pressure variation and the true value for γ were unknown. It was also unknown if the glow plug expansion when heated was sufficient to restrict the flow when the unit operated as a vaporiser.

Table 2.3

1.2 mm nozzle diameter mass flow rates, measured & calculated at idle and 1500 rev/min road load (assuming s.t.p. values for the air flow)

1.2 mm nozzle diameter flow rates, calculated & measured	850 rev/min	850 rev/min	1500 rev/min	1500 rev/min
Mixture preparation	Vapour	Air-atomisation	Vapour	Air-atomisation
Calculated air mass/cycle (mg)	22.72	22.72	12.98	12.98
Calculated fuel mass/cycle (mg)	6.07	6.07	11.84	11.84
Total calculated mass/cycle (mg)	28.79	28.79	24.82	24.82
Measured air mass/cycle (mg)	14.87	26.09	2.64	13.43
Calculated fuel mass/cycle (mg)	6.07	6.07	11.84	11.84
Total measured mass/cycle (mg)	20.94	32.16	14.48	25.27
Calculated mass flow/measured (%)	72.7	111.7	58.3	101.8

Equation 2.11, section 2.2.4, indicates the maximum permissible limit of glow plug expansion that can be tolerated prior to the fluid flow being affected. In order to determine the extent of the expansion experienced under the operating conditions, the glow plug was heated in quiescent air until it achieved a similar temperature gradient along the length to that found during testing. At this point, the diameter was measured and found to be within the limit calculated. Hence, any anomalies between

predicted and experimental values were presumed to be due to either the pressure drop upstream of the nozzle, previously assumed to be at atmospheric conditions, or a significant change in γ . A pressure tapping was introduced to measure the conditions upstream of the nozzle restriction and the value of γ calculated for various air/fuel ratios over a range of temperatures, see Appendix A2, figure A2.1.

Repeat tests were performed with the pressure differential between the air bleed and just upstream of the nozzle exit measured using a micro-manometer. The pressure drop recorded was found to be of the order of 0.5%, and subsequently assumed to be negligible for the purposes of the mass flow rate calculations, however, the variation in γ was found to be up to 75% for the range of temperatures and air/fuel mixtures likely to be experienced during operating conditions. Using the corrected value of γ revealed a better correlation between mixture mass flow rates, the theoretical value corresponding to between 68-93% of that measured, see table 2.4. The error was felt to be due to the fluid stream temperature measurement at the exit of the AAFV and in the measured air mass flow rate, itself having an associated accuracy of approximately $\pm 10\%$. The main inaccuracy in temperature measurement is likely to arise from there being a temperature gradient across the exiting stream. Tables A2.2 & A 2.3, Appendix A2, indicate the glow plug temperature for the level of power drawn² though the values refer to heating within quiescent air.

The equation used to calculate the mass flow rate is not inherently sensitive to errors in γ even though the expression is raised to the power $(\gamma + 1)/(\gamma - 1)$, see section 2.2.1 where γ , at elevated temperatures and low air/fuel ratios, is ≈ 1 .

² The glow plugs were rated to a maximum of 140 W, but this value applies to operation in quiescent air. When operated within the AAFV, both the constant air stream and the injected fuel cools the glow plug and alters its resistive characteristics, thereby allowing the unit to draw more current than the specified maximum as stated by the manufacturer.

Table 2.4

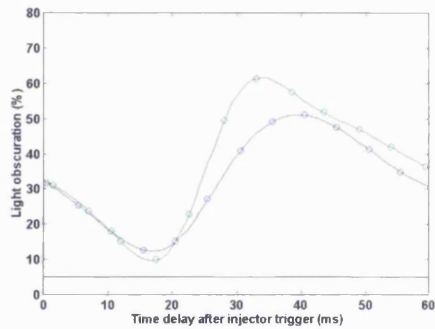
1.2 mm nozzle diameter nozzle mixture mass flow rates at idle and 1500 rev/min road load, measured & calculated (using a calculated ratio of specific heats for the mixture)

	850 rev/min	1500 rev/min
Mixture preparation	Vapour	Vapour
Measured air mass flow/cycle (mg)	14.87	2.64
Fuel mass flow/cycle (mg)	6.07	11.84
Total measured mass flow/cycle (mg)	20.94	14.48
Mixture exit temperature (K)	363.6	402.1
Ratio of specific heats of the mixture based on the measured gravimetric concentration, γ_m	1.222	1.064
Total calculated mixture mass flow/cycle (mg)	19.39	9.8
Calculated mass flow/measured (%)	92.6	67.7

2.5.5 Spray duration

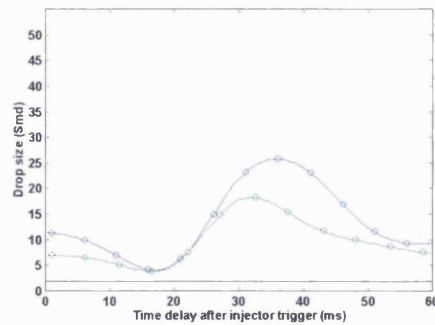
During spray characterisation tests, the injector trigger repetition rate was reduced from that corresponding to the engine condition in order to evaluate the sprays leading and trailing edges without interaction from the previous or subsequent injection event, see section 2.3.1. Throughout the vaporising tests, the fuel flow acts as a coolant for the glow plug element and as such any deviation from the injector repetition rate demanded by the simulated engine operating condition would alter the temperature characteristics of the AAFV. Consequently the injector was triggered corresponding to the associated engine speed for all tests performed using vaporised fuel. Air-atomisation mode testing of the 1.2 & 1.5 mm nozzles was performed in the same manner and drop size measurements were taken in 10 ms delay increments throughout the time period of one four-stroke cycle. Figures 2.8 & 2.9 show the obscuration and fuel spray Smd vs. time delay graphs respectively, which indicate a definite flow pattern implying the presence of leading and trailing edges to the fuel flow in the inlet port.

Figure 2.8
 Light obscuration vs. time delay after injector trigger,
 1.2 & 1.5 mm nozzles, 2000 rev/min,
 full load, 7 mm Hg manifold depression,
 70 kPa air bleed pressure



1.2 mm exit nozzle \varnothing , 7.0 mm heated chamber id, 1.5 mm exit nozzle \varnothing , 7.0 mm heated chamber id

Figure 2.9
 Fuel spray drop size (Smd) vs. time delay after injector trigger, 1.2 & 1.5 mm nozzles, 2000 rev/min,
 full load, 7 mm Hg manifold depression,
 70 kPa air bleed pressure



1.2 mm exit nozzle \varnothing , 7.0 mm heated chamber id, 1.5 mm exit nozzle \varnothing , 7.0 mm heated chamber id

2.5.6 Drop size evaluation

Droplet sizing throughout the spray duration indicated that the larger nozzle, 1.5 mm, generally produced a finer degree of atomisation than the 1.2 mm nozzle with peak Smd values of 22 μm and 30 μm respectively, see figure 2.9. Whilst the percentage difference between the two peak values was substantial, the overall value is of greater interest especially when compared to a pintle or plate type injector with an associated Smd of circa 80-130 μm , Williams, 1994.

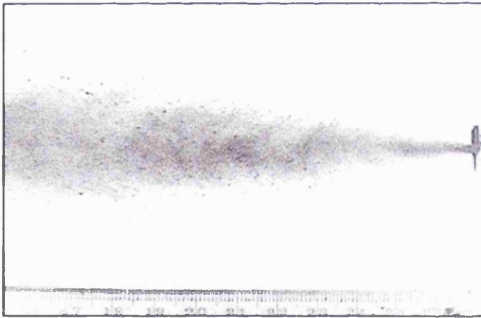
2.5.7 Vapour detection

Attempts were made to perform vapour detection tests by taking Malvern measurements at increasing time delays between injector and Malvern triggering from zero to the duration of one complete engine cycle. Dodge & Cerwin, 1984, drew attention to an effect known as beam steering where the vapour halo that surrounds an evaporating droplet causes density changes in the air which refracts the laser beam used for the drop sizing. No visible change of output signal occurred throughout the period of the engine cycle indicating that there was insufficient density variation to enable detection using the Malvern instrument.

2.5.8 Spray cone angles

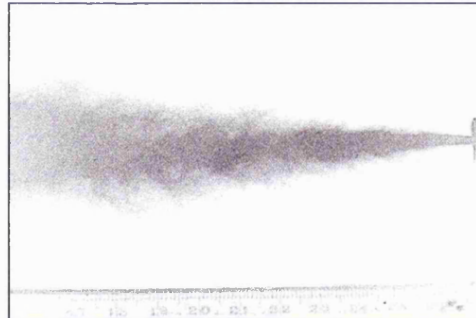
Table A2.4, Appendix A2.3 lists the spray cone angles observed using a charge coupled device, CCD, camera whilst injecting into quiescent air using a range of air-assistance from 12-70 kPa. The minimum and maximum angles found were 23° and 63.5° respectively. In general, the values of cone angle were quite similar for both 0.8 mm and 1.5 mm diameter exit nozzles, and varied little with pressure of supply air. The one exception was the low pressure assistance (ΔP of 14 kPa) with the 0.8 mm diameter nozzle, when the spray angle jumped to the maximum value of 63.5°. The effect of air supply pressure on droplet size can be appreciated to some extent by observing the finer spray in figure 2.11 (ΔP of 70 kPa) compared to figure 2.10 (ΔP of 12 kPa).

Figure 2.10
Image of fuel spray into quiescent air, 1.5 mm nozzle,
12 kPa air assistance



(scale in cm across lower edge of image)

Figure 2.11
Image of fuel spray into quiescent air, 1.5 mm nozzle,
70 kPa air assistance



(scale in cm across lower edge of image)

2.6 CONCLUSIONS FROM VAPOUR TESTING

Tests from the vaporising mode of AAFV operation indicated that the heated surface area of the glow plug was the primary influence on the ability of the design to vaporise the fuel. Little difference in the power requirements to achieve vaporisation of the fuel was measured for either the exit nozzle diameter or internal clearance around the glow plug.

The accuracy of nozzle mass flow rate calculations were found to be sensitive to the fluid flows ratio of specific heats, γ_m .

The included angle describing the spray cone during liquid fuel, air-atomisation mode, was found to exhibit an average of 30° for the 1.5 mm nozzle diameter.

2.7 CONCLUDING STATEMENT

This series of tests indicated the controlling parameters and their effects for the AAFV design. The findings led to recommendations that the geometry adopted for future test work should incorporate a 1.2 mm exit nozzle diameter, a 1.0 mm diametral clearance and a glow plug length of approximately 30 mm. Using this geometry droplet sizes below $30\ \mu\text{m}$ can be expected at either idle or 1500 rev/min road load conditions using a passive air bleed in air-assistance mode.

The tests showed that complete vaporisation of the fuel at a stoichiometric air/fuel ratio could be achieved at idle with a power requirement of 100 Watts/cylinder and that significant, but not full, vaporisation occurs at the 1500 rev/min road load operating condition. The results suggest that this electrical power consumption could be reduced by improving the insulation around the heated chamber and reducing the unit's thermal inertia. By incorporating these two improvements, the use of a modulated power supply is likely to reduce the power requirements without sacrificing the overall performance. The fact that full vaporisation of the fuel was not

possible at 1500 rev/min road load indicated the need to increase the heat transfer from the surface of the glow plug. A possible approach to this could be to modify the fuel entry position so that the fuel tends to follow a helical path across the surface rather than a straight path.

Having identified the main areas for improvement to the design of the AAFV, a redesign was proposed on the basis of the information already gathered. The redesign would incorporate the suggestions already mentioned and also aim to improve the ease of use and serviceability of the design. The redesign is described in chapter 4.

2.8 REFERENCES

Dodge, L G & Cerwin, S A (1984), "Extending the applicability of diffraction-based drop sizing instruments", Liquid particle size measurements, ASTM STP 848, Edited by J M Tishkoff, R D Ingebo & J B Kennedy, 1984

Heimrich, M J, Albu S & Osborn, J (1991), "Electrically-heated catalyst system conversions on two current-technology vehicles", SAE 910612

Heywood, J B (1988), "Internal combustion engine fundamentals", Pub. McGraw Hill International, 1988, chapter 4, Properties of working fluids, pp 100-160

Hurley, R G, Hansen, D L, Pawlowicz, R J, Smolinski J M & Ghandi, H S (1991), "Experiences with electrically heated catalysts", SAE 912384

Shapiro, A H (1953), "Dynamics and thermodynamics of compressible fluid flow", Pub. Ronald, 1953, vol. 1, chapter 8, Generalised one-dimensional continuous flow

Williams, P A (1994), "Characterisation of fuel sprays in spark ignition engines" PhD Thesis, 1994, Department of Mechanical Engineering, University College London

Williams, P A (1993), "Laser diffraction particle sizing and spark-flash photography techniques for successful measurement of spark ignition engine fuel sprays", IMechE 016/93

APPENDIX A2

A2.1 SIMULATED ENGINE CONDITIONS

A2.1.1 Idle

Speed (rev/min)	850
Air flow (g/s)	0.63
Fuel flow (mg/cycle)	6.00
Manifold pressure (kPa absolute)	29.46

A2.1.2 Road load

Speed (rev/min)	1500
Air flow (g/s)	1.29
Fuel flow (mg/cycle)	11.83
Manifold pressure (kPa absolute)	41.44

A2.1.3 Full load

Speed (rev/min)	2000
Air flow (g/s)	4.63
Fuel flow (mg/cycle)	38.34
Manifold pressure (kPa absolute)	97.87

A2.2 GLOW PLUG TEMPERATURE DATA

A2.2.1 Glow plug temperature measurements points

30 mm glow plug

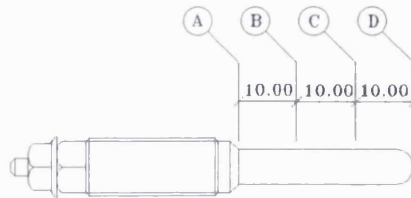


Table A2.1

**Glow plug temperature vs. applied power, 30 mm glow plug
heated in quiescent air**

30 mm glow plug				
Power (Watts)	Temp @ pt A (°C)	Temp @ pt B (°C)	Temp @ pt C (°C)	Temp @ pt D (°C)
16.0	105	160	195	195
22.1	126	200	248	300
30.0	195	280	328	350
42.1	242	306	360	400
54.0	260	400	394	407
66.6	280	383	412	453
80.0	318	465	456	500
97.9	415	505	530	575
112.8	515	530	590	665
130.0	525	630	630	690
148.4	605	735	695	750

20 mm glow plug

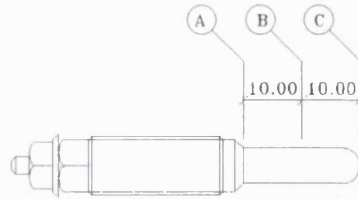


Table A2.2

**Glow plug temperature vs. applied power, 20 mm glow plug
heated in quiescent air**

20 mm glow plug			
Power (Watts)	Temp @ pt A (°C)	Temp @ pt B (°C)	Temp @ pt C (°C)
22.4	185	310	365
35.2	267	392	445
45.0	330	448	490
60.4	410	510	556
75.3	480	625	625
91.5	490	685	703
110.3	560	720	720
131.5	600	728	752

Table A2.3

**Glow plug expansion vs. applied power, 30 mm glow plug
heated in quiescent air**

Power supplied (Watts)	Tip diameter (mm)
0.0	6.10
22.5	6.20
27.0	"
36.0	"
44.9	"
56.2	"
64.9	"
80.0	"
97.0	6.22
108.0	"
127.5	"
140.0	"

A2.3 LASER DIAGNOSTIC PARTICLE SIZING

A2.3.1 Background and limitations

A diffraction pattern is formed when a parallel beam of monochromatic light is interrupted by a circular disc or aperture. A lens may be used to focus the light on a screen. Undelected light has a point focus on the screen's axis and the conically diffracted light is focused concentrically by the lens producing a light intensity pattern characteristic of the size of the disc. The pattern is the two-dimensional Fourier Transform. Parallel light always focuses on the centre line of the lens and the same radial displacement in the focal plane arises from any given conical diffraction, consequently, the light intensity pattern will remain constant regardless of movement of the disc within the light beam. The diffraction patterns, known as Fraunhofer diffraction, only occur when the size of the disc or aperture is larger than the wavelength of the light source thereby setting the lower limit for detection.

Williams, 1994, investigated the problems of applying laser diffraction particle sizing to gasoline fuel sprays using a steady flow rig to mimic intake port conditions during the open intake valve period. Evaporation of volatile fuels such as gasoline creates a vapour halo around liquid droplets which causes an effect known as beam steering arising from refractive index gradients deflecting the light. This signal distortion creates the impression of the presence of large droplets. A method of data conditioning was suggested to overcome the effects of evaporation based on knowledge of the theoretical diffracted light energy signal. Typically, the light energy from non-volatile liquids exhibits a linear decay towards the central rings of the detector unless very large droplets are present. Under these circumstances, any evaporation taking place will lead to a discontinuity in the light energy readings. Williams, 1994, used this knowledge to apply a linear regression program to the measured data using operator experience to determine the minimum position of valid data. He had to back up his laser diffraction measurements with a photographic approach in order to confirm that no large droplets were present.

A2.3.2 Theory

The light intensity distribution measured in the focal plane is evaluated from the Fraunhofer diffraction integral. It can be shown that for a disc or aperture, of radius a , the diffraction amplitude, $U(P)$, can be expressed as:

$$U(P) = CD \left[\frac{2J_1(ka\omega)}{ka\omega} \right] \quad \text{equation A2.1}$$

Where $C =$ a constant

$$D = \pi a^2$$

$k = 2\pi/\lambda$, where λ is the wave length

$\omega = s/f$, a dimensionless radial distance of any point in the diffraction pattern in the focal plane

J_1 is a Bessel Function

The corresponding intensity is:

$$I(P) = I_0 \left[\frac{2J_1(ka\omega)}{ka\omega} \right]^2 \quad \text{equation A2.2}$$

Where $I_0 = ED/\lambda^2$, and E is the incident energy on the disc aperture

Size distributions are difficult to infer from the light intensity though this problem may be overcome by the use of the light energy distribution. The fraction of light energy contained within a circle in the focal plane of radius $\omega_0 = s_0/f$, for particle of radius a is given by

$$L(\omega_0) = 1 - J_0^2\left(\frac{2\pi as}{\lambda f}\right) - J_1^2\left(\frac{2\pi as}{\lambda f}\right) \quad \text{equation A2.3}$$

first obtained by Rayleigh. The expression may be evaluated to find the location of the first maximum (x_{max}) of the energy distribution at $(2\pi as/\lambda f) = 1.375$ and the first

dark ring corresponding to the first minimum (x_{min}) at $(2\pi as/\lambda f) = 3.84$. Eighty percent of the total light energy is contained within the area bounded by the first dark ring. The light energy from N droplets of radius a contained within a ring on the detector, described by radii s_1 and s_2 , is

$$L_{s_1, s_2} = CN\pi a^2 \left[\left(J_0^2 + J_1^2 \right)_{s_1} - \left(J_0^2 + J_1^2 \right)_{s_2} \right] \quad \text{equation A2.4}$$

where C is a constant dependent on the laser power.

Droplet measurement instruments such as the Malvern 2600c particle sizer use the theory of Fraunhofer diffraction to obtain an indication of the droplet size distribution and number contained within a spray. A lens is used to focus the light onto concentric annular photoelectric cells of increasing radii. The light energy contribution at any ring in the focal plane is the sum of the contributions from individual droplets of all sizes. Therefore, for a number of different sized droplet radii, $a_1, a_2, a_3, \dots, a_n$, with differing numbers of droplets contained within each group of $N_1, N_2, N_3, \dots, N_n$, the total light energy within the ring (s_1-s_2) is given by:

$$L_{s_1, s_2} = C \sum_{i=1}^n N_i \pi a_i^2 \left[\left(J_0^2 + J_1^2 \right)_{s_2} - \left(J_0^2 + J_1^2 \right)_{s_1} \right] \quad \text{equation A2.5}$$

The number of droplets within size band N_i is related to the volume fraction by:

$$N_i = \frac{V_i}{\frac{4}{3} \pi a_i^3} \quad \text{equation A2.6}$$

Where V_i = volume distribution

Equation A2.5 then becomes:

$$L_{s1,s2} = K \sum_{i=1}^n \frac{V_i}{r_i} \left[\left(J_0^2 + J_1^2 \right)_{s2} - \left(J_0^2 + J_1^2 \right)_{s1} \right] \quad \text{equation A2.7}$$

Each droplet size will diffract light to all radii, however, the energy distribution will peak at one particular radius.

A2.3.3 Malvern 2600c

The Malvern 2600c is a particular design of laser diffraction particle/droplet sizer manufactured by Malvern Instruments Ltd. To obtain a representation of the drop size distribution the Malvern uses fifteen pairs of concentric detector rings with a small central aperture to allow undiffracted light to pass through onto a further detector used for optical alignment. The light energy incident on each ring is characterised by an equation similar to equation A2.7, consequently the droplet distribution is represented by a set of fifteen simultaneous equations each containing fifteen terms, the derivation of which provides the volume distribution V_i . Equation A2.8 below can then be used to relate the volume distribution to the data D_j

$$D_j = U_{i,j} V_i \quad \text{equation A2.8}$$

where 'i' is the size band index, 'j' is the detector element and $U_{i,j}$ is the relationship between the droplets in size band 'i' and how the light is scattered over element 'j'. The Malvern software utilises a least squares fit to solve equation A2.8, whilst the volume distribution calculation will depend on the analysis model chosen. Analysis models such as Rosin-Rammler, Log-Normal and Normal are specified by two parameters of a characterising equation for the volume distribution. The parameters are the location of the peak droplet size and the distribution width.

Analysis can be made without the two previous assumptions by measuring the light energy data to estimate a volume distribution. Equation A2.8 is then used to calculate

a light energy distribution, the difference between the calculated and the measured values is evaluated from

$$\text{Log. Diff.} = \log_{10} \left(\sum_{j=1}^n (D_j - L_j)^2 \right) \quad \text{equation A2.9}$$

where D_j is the measured data and L_j is the data calculated from the estimated volume distribution. An iterative procedure is then initiated using the difference calculated from equation A2.9 to correct the initial solution until the residual (*Log. Diff.*) reaches a minimum. That the solution remains positive is the only condition that must be satisfied. For a more detailed discussion of the Malvern instrument refer to Williams, 1994.

A2.4 AAFV FUEL SPRAY CONE ANGLES

A2.4.1 Fuel spray cone angle testing

A measurement of the spray cone angle of the emerging fuel spray from the AAFV during air-atomisation mode operation was achieved by capturing an image of the spray using a charge coupled device, CCD, camera. The AAFV was mounted over a funnel connected to a vacuum pump used to draw off the fuel vapour/spray. A Pulnix CCD mono-chrome video camera was used to photograph the fuel spray. Lighting was provided by two Miranda flash units. The flash duration was nominally 1/5000 second. Timing of the lighting was achieved by connecting the flash units to the Malvern Spray Synchroniser and using the delay timing control.

The data was recorded and processed using an Imaging Technologies OFG PC-based frame grabber. The resolution of the screen was 768 x 494 pixels, with each pixel representing 13 x 13 microns (μm). Some blurring of the image was expected due to the flash duration, however, for the purposes of evaluating the spray cone angles, the level of image definition was felt to be sufficient. The cone angle was simply attained by measuring the droplet divergence.

Table A2.4

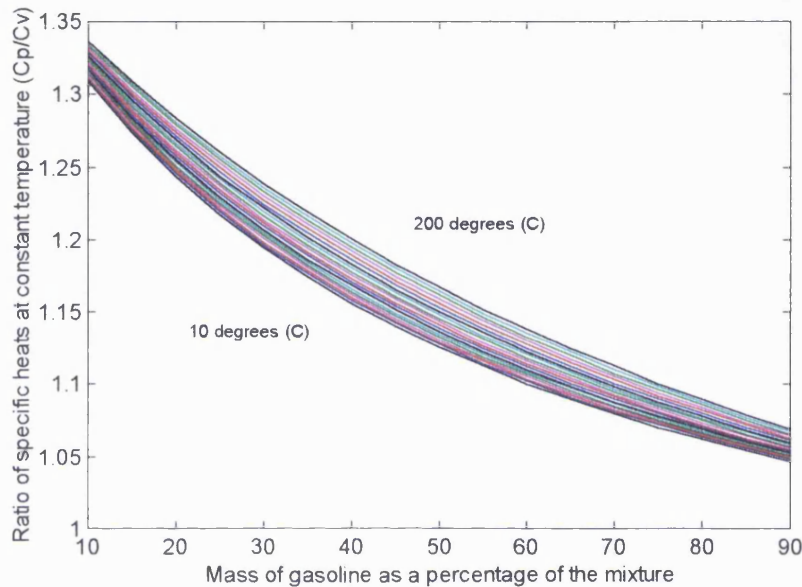
AAFV fuel spray cone angles for a range of ΔP across the exit nozzle

Nozzle type	0.8 mm exit diameter, 1.0 mm diametral clearance			1.5 mm exit diameter, 1.0 mm diametral clearance			
	ΔP (kPa)	70	35	14	70	35	14
Included angle ($^{\circ}$)		23.1	26.45	63.52	28.3	29.7	32.1

A2.5 RATIO OF SPECIFIC HEATS FOR GASOLINE/AIR MIXTURES

Figure A2.1

Variation of γ_{mixture} with respect to air/fuel ratio
across lines of constant mixture temperature



For fuel vapour, $dh/dT = C_p \neq \text{constant}$. Hence, the following equations were used to evaluate the specific heat capacity of gasoline at constant pressure. Heywood, 1988, specifies the following polynomial expression:

$$\tilde{h}_f = -27.08 + 128.18t^2 - 67.23t^3 + 16.19t^4 - \frac{0.58}{t} \quad \text{equation A2.10}$$

Where $t = T(K)/1000$, Heywood, 1988

To evaluate γ_m the specific heat capacity of fuel at constant volume, the relationships stated in section 2.2.3 were written into a computer program using MATLAB. The specific heat capacity was calculated in 10°C increments from 10°C to 200°C and over a gasoline concentration range from 10% to 90%.

CHAPTER 3
COLD-START TESTING

CHAPTER 3

COLD-START TESTING

3.1 INTRODUCTION

The problem of achieving a reliable first-fire from a cold engine should not be underestimated. The amount of fuel vapour entering the cylinder during the first injection event from a conventional injection system is small since only a relatively small proportion will evaporate and because the liquid film present on the port wall during all other operating conditions is not yet established. Consequently, the in-cylinder vapour concentrations occur only due to the evaporation of the airborne spray as it passes through the intake port and the further evaporation of the liquid droplets within the combustion chamber itself during the induction/compression strokes. During subsequent cycles film vaporisation from the inlet port walls increases the in-cylinder HC concentration levels though the evaporation rates from the liquid deposited within the intake manifold will vary with time. This is due to the changing fuel film volume to surface area ratio and fuel temperature as well as the changing port pressure experienced as the engine accelerates to its idling speed. Henein *et al*, 1995, made a cycle by cycle analysis of the processes and parameters controlling engine start-up from ambient conditions. This was performed on a 3.3 litre, port injected, V-6 engine and it showed that the first cycle resulted in a lean misfire in spite of 398 mg/cylinder (equivalence ratio of approximately 7.25) being injected for the first intake valve opening (IVO) event. The in-cylinder equivalence ratio was calculated to be 0.22¹, indicating the problem of achieving adequate evaporation rates such that sufficient fuel vapour exists at the sparking plug at the time of spark initiation.

Horie, Takahasi & Akazaki, 1995, investigated the port wall-wetting characteristics on a modern design of 4-valve engine using a two coefficient model. The coefficients,

¹ The equivalence ratio was calculated by considering the fuel vapour content within the combustion chamber to be equivalent to the fuel emitted into the exhaust.

α and β , represented the ratio of the fuel injected to that which directly entered the combustion chamber and the ratio of indirectly inducted fuel mass from the wetted port surface to the mass residing on the port wall, respectively. The accumulated mass of fuel on the port wall and the rate of evaporation from the liquid deposition were empirically-based and therefore specific to the engine tested. The model suggested that some 70% of the injected fuel was deposited on the port wall and that almost half of the liquid puddling was ingested during each cycle for engine operation at 25°C coolant temperature. Brown & Ladommatos, 1991, estimated that the fuel film mass was up to six times greater than the mass of fuel injected per cycle for a 2-valve engine operating at a fast idle with a coolant temperature of 35°C. This fell to one and a half times the injected mass per cycle when the coolant temperature was raised to 80°C.

A one-dimensional model to predict the intake port fuel-air mixture preparation incorporating unsteady, multi-component and multi phase flow was described by Chen & Aggerwal, 1996. It was claimed, though no experimental data was provided, to be capable of predicting the dynamic behaviour of both the fuel spray and liquid film. The results appear to concur with those obtained by Henein *et al*, 1995, and Horie, Takahasi & Akazaki, 1995, in suggesting that only 10-20% of the fuel vapour entering the combustion chamber is derived from the fuel spray. Perhaps of greater interest is the time taken to establish a steady-state port wall fuel film, the prediction being that some 30 seconds were required after a cold-start. Predictably, the model infers that the heavier ends constitute the majority of the liquid film flow. It was unclear how the fuel mass entering the combustion chamber was evaluated though presumably it was calculated from the predicted components at a certain location downstream of the injector. Whilst the analysis made significant improvements over single component, steady-flow approximations, it must not be forgotten that the extent of fuel impaction will depend greatly upon both the injector timing and targeting. It will also be significantly affected by the backflow into the intake port during the heavily-throttled operating conditions experienced at idle which can

produce significant fuel atomisation, as shown by Shin, Min & Cheng, 1995, and was not included in the analysis of Chen & Aggerwal, 1996.

Schurov and Collings, 1995, attempted to measure the port wall wetting by rapidly stopping the engine between cycles, isolating the intake manifold branch and purging with hot air at a known flow rate. The exhausted mixture from the manifold passed a high frequency response flame ionisation detector probe which measured the UHC concentration from which the values were integrated to achieve a fuel mass. Ratios of the fuel mass injected to that remaining in the intake port after any given number of cycles appeared to be relatively low, 55%, when compared to those already suggested. However, the results still indicated that a significant volume of the injected fuel was deposited on and remained adhered to the port wall following a cold-start.

The difficulties in achieving a stoichiometric in-cylinder mixture during a cold-start were explored by Fox *et al*, 1992, using injected equivalence ratios, ϕ_{inj} , of 1.0-to-1.5, though the test engine was motored at 900 rev/min prior to injector initiation. The in-cylinder HC concentration was measured to increase to $\phi_{inj} \approx 0.5$ within 5 cycles for $\phi_{inj} > 1.0$, at which point sporadic firing occurred. However, to reach a steady firing condition with minimal fluctuation in combustion stability took some 100 or so cycles, which agrees with the time suggested by Chen & Aggerwal, 1996, to achieve a steady state for the liquid fuel film.

3.2 TEST DETAILS

3.2.1 Installation

A 3.0-litre development Jaguar engine, the Emissions Consortium Engine Project 2 (ECEP2) was used for the test programme. The standard fuelling system fitted to the ECEP2 engine utilised port-mounted Bosch top-fed fuel injectors. A Lucas 15CU engine management system (EMS) controlled the fuel system using simultaneous injection timing triggering all six injectors every 360° of crank rotation. Six UCL AAFVs were manufactured to replace the standard injectors and fitted using the existing fuel rail and mounting points. A plenum chamber was incorporated into the design to supply 'metered' air at atmospheric pressure to the AAFVs by a tapping into the induction trunking downstream of the air flow meter and upstream of the throttle plate. For testing purposes an independent battery source was used to power the AAFV's heated elements to avoid unwanted electrical interactions and gain a measure of the power requirements. The AAFVs were thermally and electrically isolated from the engine.

3.2.2 Testbed

The ECEP2 engine was a 24-valve, in-line, 6-cylinder engine incorporating a bore and stroke of 83 mm and 92 mm respectively to achieve a swept volume of 2978 cc with a compression ratio of 11:1. The electrical charging system was disconnected, the operating power for the EMS and engine sensors being provided by a mains driven power supply. Cranking was achieved via a total loss battery system which also powered the fuel pump. The EMS incorporated a 'Dev Aid' allowing user inputs to override the standard engine 'maps'. The Dev Aid was mounted on a PC and was programmed using the computer.

The engine was housed in the UCL Environmental Test Chamber allowing the temperature to be set and controlled down to a minimum of -29°C. Temperature

sensors were mounted in the air intake, induction manifold, engine coolant, exhaust manifold and oil sump.

3.2.3 Operating system

For the purpose of the cold-start tests, open-loop operation was maintained for the duration of each test. The Lucas 15CU EMS includes a number of operating maps covering starting and the subsequent warm-up period. Throughout cranking, defined as any speed up to 500 rev/min, the fuel injector-pulse width is purely a function of coolant temperature. Once the engine exceeds 500 rev/min for a predetermined time, the fuelling switches to the main fuel map which is speed and load dependent. A percentage enrichment is applied throughout, determined by the coolant temperature setting both the initial fuelling level and decay rate. Cranking fuelling is re-introduced if the engine speed should drop below 200 rev/min. A standard automotive type battery was used to provide the electrical power to drive the AAFV's heating elements.

3.2.4 Data-logging system

An 11-channel, 10-bit resolution, analogue to digital converter (ADC) was used to convert the instrumentation signals so that they could be recorded on a computer. The sampling time for each measurement was 200 μ s and measurements were taken every 3 ms for each of the 11 channels providing 25 samples per engine revolution at the target idle speed of 800 rev/min. The response times of the measuring devices and their associated accuracies are tabulated in Appendix A3 which also contains listings of the 11 variables logged during the testing.

3.3 EXPERIMENTAL PROCEDURE

Due to the difficulty in obtaining repeatability during cold-start testing great care was exercised to minimise test-to-test variations. The fuel used throughout the test

programme was drawn from the same delivery. Fuel handling was performed in a manner aimed to reduce the level of evaporative losses of the light ends when refilling the engine's supply tank. Once this tank was full, a small closed reservoir situated within the test facility was filled from the main tank allowing the contents to soak to the same temperature as the test cell. The reservoir contained sufficient fuel to run the engine over the duration of the test cycle. The cold-soak target temperature was considered to have been achieved when the five temperatures listed in section 3.2.2 reached the target temperature, $\pm 1.0^{\circ}\text{C}$, and stabilised for 30 minutes.

Excessive build-up of carbon deposits can occur during the start-up and idling operation of an IC engine, consequently a conditioning cycle was employed after each test. Prior to the conditioning cycle the engine was brought up to its normal operating temperatures for both engine coolant and sump oil by running at 3 bar BMEP, 1200 rev/min, for 5 minutes. Conditioning was achieved by operating the engine at 5.5 bar BMEP, 3000 rev/min, for between 10 and 12 minutes depending on the start temperature for the preceding test. Once the cycle was completed and the engine stopped, the sparking-plugs were removed, non-abrasively cleaned and re-gapped. The fuel reservoir was refilled and shut off from the main supply tank in preparation for the next test. The test chamber was then closed and the refrigeration unit switched on. A 22-point check list was used to reduce the number of aborted tests to a minimum. Data-logging was initiated just prior to cranking and set to record information for a period of 2 minutes of engine operation.

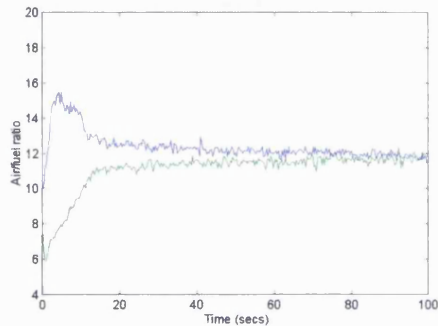
3.4 TEST RESULTS AND DISCUSSION

The tests were split into four groups comprising two test temperatures and two fuel systems. The two temperatures chosen for the tests were 7°C and 0°C, coinciding with the cold-start temperatures adopted for the 1997 European emissions tests, Anon, 1994. The standard injectors were used to gain an overall indication of the emission levels produced by the engine, since the engine was a development unit, the standard of calibration of the open loop maps were not refined to the levels normally associated with a production item. Time was spent to achieve an improvement over the standard calibration, but constraints on the duration of the test programme precluded a fully optimised map.

The tests were repeated until three consistent runs were achieved at each condition. A warm-up period for the AAFVs was required prior to cranking to ensure complete fuel vaporisation. The best start repeatability was achieved using 16 seconds of pre-heat. No attempt was made to reduce this since the primary objective was to achieve a stoichiometric air/fuel ratio² from cranking. Figures 3.1 & 3.2 show that the air/fuel ratio required for the standard injectors was in the region of 7:1, quickly rising to 11:1 after some 15 seconds, and that by using the AAFVs, an approximately stoichiometric mixture was achieved almost immediately. The rich mixture indicated on the extreme left of figure 3.1 and the rapid decay 15 seconds after start-up were due to inaccurate fuel mapping at the beginning of the AAFV test programme. The problem was largely overcome by the start of the AAFV tests at 0°C, as can be seen from figure 3.2, though difficulty was still experienced in achieving a stoichiometric mixture throughout cranking and during engine pick-up due to the complexities of engine mapping during the start-up period of operation.

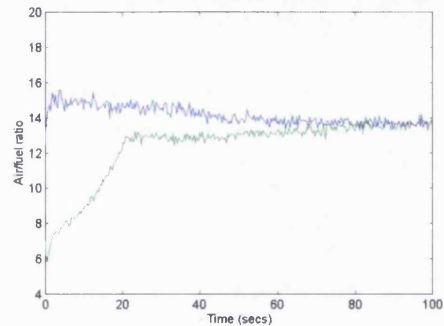
² The air/fuel ratio was calculated from the pulse width of the fuel injector, engine speed and air mass flow rate.

Figure 3.1
Cold-start gravimetric air/fuel ratio, 7° C
start temperature



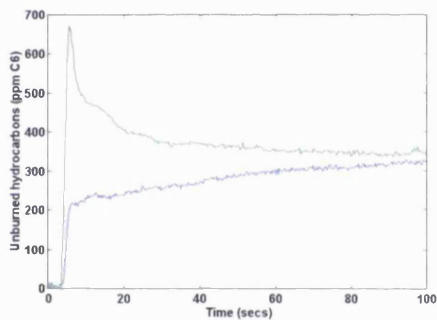
Standard injector, AAFV vaporised fuel

Figure 3.2
Cold-start gravimetric air/fuel ratio, 0° C
start temperature



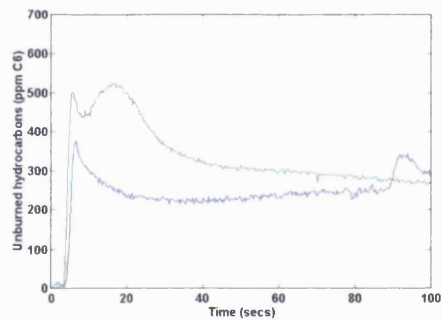
Standard injector, AAFV vaporised fuel

Figure 3.3
Cold-start hydrocarbon emissions, optimum results
from standard injector and AAFV tests, 7° C
start temperature



Standard injector, AAFV vaporised fuel

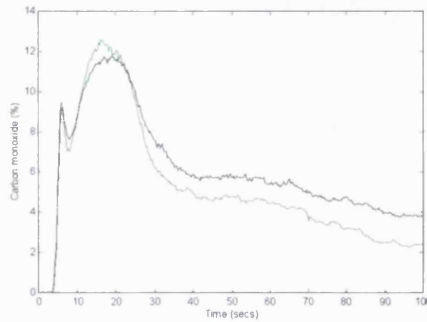
Figure 3.4
Cold-start hydrocarbon emissions, optimum results
from standard injector and AAFV tests, 0° C
start temperature



Standard injector, AAFV vaporised fuel

Comparisons of the best unburned hydrocarbon emission traces for the two fuel systems at both temperatures are shown in figures 3.3 and 3.4 with the AAFV fuelling system achieving a consistent reduction in unburned hydrocarbons of between 45-48% for both temperatures during the first 30 seconds of engine operation. It can be seen from figure 3.3 that no initial peak in the unburned hydrocarbon trace was present when using a vaporised mixture, indicating that the engine started without misfire. The rising nature of the hydrocarbon trace was due to the decreasing air/fuel ratio, see figure 3.1, caused by the approximate engine mapping. The relationship between air/fuel ratio and carbon monoxide production, Newhall & Shahed, 1971, confirmed the calculated air/fuel ratios, see figure 3.5.

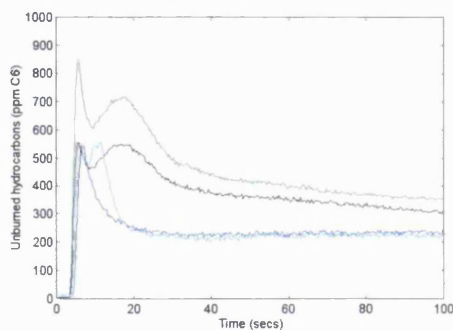
Figure 3.5
Cold-start carbon monoxide emissions, 0° C start temperature



Standard injector, test 1, Standard injector, test 2

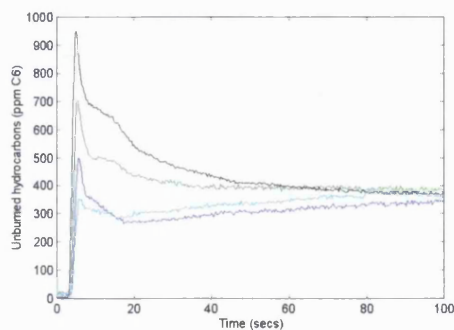
Whilst figure 3.3 indicates a clean engine pick-up from cranking without misfire with the UCL AAFV, figures 3.6 & 3.7 indicate no repetition of this result. To determine the reasons for initial peak of UHC it is necessary to understand the mechanisms by which the fuel vapour is transported from the AAFV into the inlet port and hence to the combustion chamber. The pressure drop between the air reservoir, nominally at atmospheric pressure, and the manifold depression is used to purge the injected fuel from the heated chamber into the inlet port. During cranking this pressure drop varies between 3 and 5 kPa and, as such, is insufficient to purge the heated chamber at the rate required by the engine. Once the engine fires and starts to accelerate, the pressure drop across the AAFV nozzle increases rapidly to between 48 and 76 kPa. During these conditions the nozzle becomes choked providing a rapid change in the

Figure 3.6
Cold-start hydrocarbon emissions, 7° C start temperature



Standard injector, test 1, standard injector, test 3, AAFV vaporised fuel, test 1, AAFV vaporised fuel, test 2

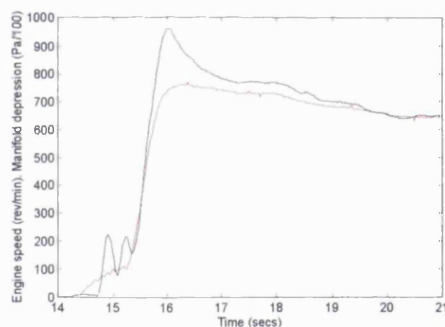
Figure 3.7
Cold-start hydrocarbon emissions, 0° C start temperature



Standard injector, test 1, standard injector, test 3, AAFV vaporised fuel, test 1, AAFV vaporised fuel, test 2

rate at which the heated chamber is purged. Due to the fuelling strategy of the management system, triggering of the injectors occurs every 360°CA without phasing to the intake valve events. It is, therefore, possible that for at least one cylinder the fuel from the two injection events for cycle 1 is not initially delivered to the inlet port/cylinder due to the meagre flow rates through the device caused by the low pressure drop across the AAFV nozzle. If the subsequent injection events for cycle 2 occur once the engine has successfully fired on one or more of the other cylinders, causing the engine to accelerate and consequently reducing the manifold pressure, the AAFV is able to purge itself of the fuel retained within. This sequence of events ensures that the relevant cylinder will contain a mixture far exceeding stoichiometric with the unburned fuel being passed directly into the exhaust causing the UHC spike seen in figures 3.6 & 3.7. The rate at which the inlet manifold depression increases with respect to time and engine speed is shown in figure 3.8.

Figure 3.8
Typical rise of engine speed and manifold depression with respect to time

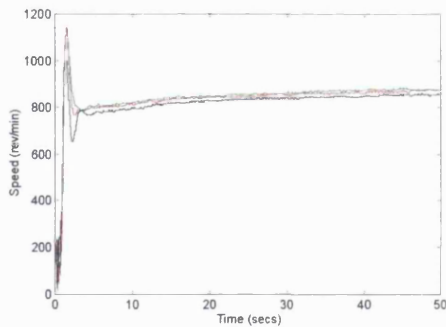


Manifold depression, engine speed

Traces of the engine speed from start are shown in figures 3.9 & 10. These traces appear to indicate a slightly higher level of engine stability when operating with the standard injectors. The variation recorded for the AAFVs was ± 20 rev/min at idle, with the standard injectors indicating a value of ± 5 rev/min. The instability incurred when using the AAFVs may have been caused by running the engine at or about a stoichiometric air/fuel ratio at low coolant temperatures, though it must be remembered that only the 0°C tests actually achieved this condition throughout the

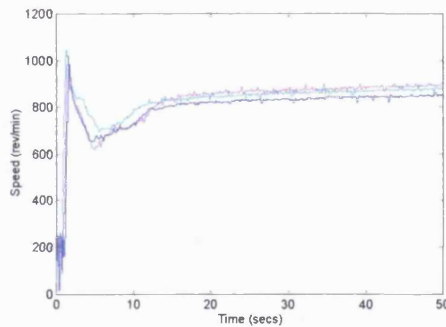
duration of the test, see figure 3.2. The same degree of variation in the speed trace with the AAFVs at the 7°C test temperature with air/fuel ratios significantly below stoichiometric, though still several air/fuel ratios higher than that used for the standard injectors. It is possible the injection strategy creates differences in the transport delay of the fuel vapour from exit nozzle to combustion chamber causing a deterioration in the consistency of the mixture. Consequently, whilst the fuelling strategy is stoichiometric the air/fuel composition within the combustion chamber may vary from cycle to cycle and cylinder to cylinder causing the instability. Coefficients of variation³, COV, of IMEP for the engine operating fully warm at idle for both standard and AAFV fuelling systems, performed by Seabrook, 1995, indicated an increase when using the AAFVs of one percent taking the COV to 11%. Cylinder pressures were recorded throughout the duration of the cold start test programme and the minimum sampling time available was 3 ms, corresponding to one sample every 15°-20° crank angle. This was insufficient to obtain reliable IMEP values and hence COVs could not be calculated for the steady-speed part of this series of tests.

Figure 3.9
Engine speed with respect to time, standard injectors,
7° C start temperature



Standard injector, test 1, standard injector, test 2, standard injector, test 3

Figure 3.10
Engine speed with respect to time, AAFV, 7° C
start temperature

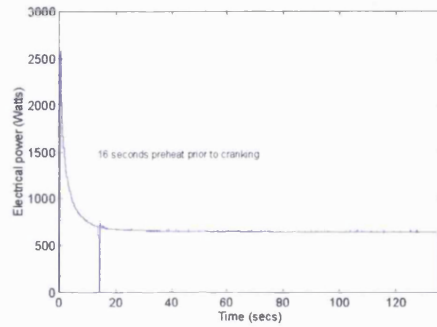


AAFV, test 1, AAFV, test 2, AAFV, test 3

³ COV defined as [(std deviation of IMEP)/mean IMEP] x 100

Electrical power was supplied continuously to the AAFVs. Limitations on the test time available were such that experimentation with power modulation could not be undertaken, consequently, power levels measured during a typical run of 136 seconds, including 16 seconds pre-heat prior to engine cranking, represent a worst case.

Figure 3.11
Typical electrical power requirements for a 6-cylinder installation of the AAFVs



The level of power consumption of all six AAFVs during a typical run was approximately 95 kJ with 650 Watts being drawn after the initial warm-up period, see figure 3.11. Further experimentation is required to investigate the level of power modulation that can be used in association with the AAFVs without incurring a detrimental effect on either unburned hydrocarbons, air/fuel ratio or idle stability. The power demand compares favourably with the levels necessary for an electrically-heated catalyst, see table 3.1. Hiemrich *et al*, 1991, reported power requirements of

Table 3.1
Per cylinder comparison of AAFV & EHCs

AAFV power consumption/cylinder (Watts)	Electrically heated catalyst power consumption/cylinder (Watts)
108.3	1125

4.5 kW over a time span of some 15 seconds, necessitating a current capacity in excess of 700 amps, for a 2.2 litre 4-cylinder installation to obtain a reduction in UHCs of some 66%⁴. The operating system also required that air be pumped into the exhaust system, necessary for controlling the cold-start HC and CO emissions, and incorporated a pre-heat time of 30 seconds. Hurley *et al*, 1991, recorded similar reductions in tail pipe HC emissions but found that the conversion efficiency of the EHC halved within a 4000-mile durability test.

⁴ The reduction is measured in terms of the mass of UHCs produced throughout the duration of bag 1 of the FTP test cycle.

3.5 CONCLUSIONS

Testing using a set of AAFVs in their vaporising mode has shown that stoichiometry can be achieved from start-up and maintained for the period prior to catalyst light-off. The fuelling system has been shown to be a reliable means of reducing unburned hydrocarbon emissions by 45% and 48% at 0°C and 7°C start temperature respectively. This compares well with reductions of 27-60% experienced by Boyle, Boam & Finlay, 1993, during cold-start testing from 20°C with fuel vapour. Electrical power consumption required to achieve vaporisation throughout the duration of the cold-start test was of the order of 15-16 kJ/cylinder with an average current requirement of 10-12 amp/cylinder. The level of power required compares very favourably with the alternative electrically-heated catalyst technology reported by Hiemrich *et al*, 1991, and Hurley *et al*, 1991, who suggest levels of 20-22 kJ/cylinder with an average current requirement of some 175 amp/cylinder and the AAFV does not incur the durability penalty.

With passive air-assistance the manifold depression appeared to be inadequate during cranking to purge the AAFV's heated chamber of injected fuel at a sufficiently high rate, the consequence being that a lean misfire was likely to be experienced during the first few engine cycles. The fuel left within the heated chamber would then combine with the next injection cycle, momentarily creating a rich mixture. These characteristics were felt to be responsible for the initial spike in the unburned hydrocarbon emissions and therefore represented an area in which further development was required. It was thought likely that introduction of an independent pressurised air supply to the AAFVs would reduce or eliminate the initial peak of unburned hydrocarbon emissions. The use of a pressurised air supply may also improve the steady-state engine stability and the transient response of the AAFV. These deductions led to an investigation into a novel means of obtaining a pressurised air supply which is described in chapters 5 and 6.

3.6 REFERENCES

- Anon** (1994), "Emissions 2000 - European exhaust emissions regulations, 1992 to 2000", Ford Power Products, UK
- Boyle, R J, Boam, D J & Finlay I C** (1993), "Cold start performance of an automotive engine using prevaporised gasoline", SAE930710
- Brown, C N & Ladommatos, N** (1991), "The effects of mixture preparation and trapped residuals on the performance of a spark-ignition engine with air-shrouded port injectors, at low load and low speed", IMechE, Part D: Journal of automotive engineering, D02690
- Cheng, G & Aggerwal, S K** (1996), "Unsteady multiphase flow in a port-injected gasoline engine", SAE960074
- Fox, J W, Min K D, Cheng, W K & Heywood, J B** (1992), "Mixture preparation in a S.I. engine with fuel injection during starting and warm-up", SAE922170
- Heimrich, J M, Albu, S & Osborn, J** (1991), "Electrically-heated catalyst conversions on two current-technology vehicles", SAE910612
- Henein, N A, Tagomori, M K, Yassine, M K, Asmus, T W, Thomas, C P & Hartman, P G** (1995), "Cycle-by-cycle analysis of HC emissions during cold start of gasoline engines", SAE952402
- Horie, K, Takahasi, H, & Akazaki, S** (1995), "Emissions reduction during warm-up period by incorporating a wall-wetting fuel model on the fuel injection strategy during engine starting", SAE952478

Hurley, R G , Guttridge, D L , Hansen, L A, Pawlowicz, R J, Smolinski, J M & Gandhi, H S (1991), “Experiences with electrically heated catalysts”, SAE912384

Newhall, H K, & Shahed, S M (1971), “Kinetics of nitric oxide formation in high-pressure flames”, Proceedings of Thirteenth International Symposium on Combustion, pp. 381-390, The Combustion Institute

Schurov, S M & Collings, N (1995), “An experimental investigation of fuel transport in a port injected engine”, SAE952485

Seabrook, J F (1995), “Combustion and emissions optimisation in a high-performance S.I. engine”, PhD Thesis, Department of Mechanical Engineering, University College London

Shin, Y, Min, K & Cheng, W K (1995), “Visualisation of mixture preparation in a port-fuel injection engine during engine warm-up”, SAE952481

APPENDIX A3

A3.1 DATA LOGGING

Variable	Comments
HC/CO	<p>Measured using a Horiba NDIR gas analyser, type MEXA321E, serial n° E40489. The unit's response time to a step change in engine fuelling was measured to establish both time delay and rise time. The response time, measured from step change initiation to a 1% increment of the final peak value was 5.1 sec with rise times to 10% & 90% of the change in 0.45 & 4.44 sec respectively, see figure A3.1. The output of the analyser was calibrated at the start of each test using a 4% span gas after a warm-up period of 1 hour. The calibration was set to ensure the voltage output of the unit remained within the operating range of the data logger, 0-2.5 volts. The voltage output from the analyser is non-linear requiring a curve fit to the output voltages, see figures A3.2 & A3.4. The calibration data was fitted to a third order curve which was used for the HC/CO traces found in the main body of the report.</p>
Cylinder pressure	<p>Measured using a Kistler piezoelectric pressure transducer, type 6121, serial n° 497023. The calibrated range of this transducer is 0-50 bar</p>

with a sensitivity of -14.8 pC/bar and linearity of $\leq \pm 0.1\%$ of the full scale output, natural frequency 55 kHz. The transducer was mounted the cylinder head on cylinder n^o 1. The charge amplifier was located outside the test facility and set to an output scale of 5 mV/pC.

Electrical current

Measured using a Lem Heme current probe, type PR 1001, set on the 0-1000 Amp range. The accuracy of the probe is $\pm 1\%$ of the reading ± 0.5 amps. The output of the device is 1 mV/Amp with a resolution of ± 100 mA. Frequency range for DC measurement is 0-10 kHz.

Port temperature

Measured using a rapid response K-type thermocouple with a 0-800°C temperature range. The response time of the thermocouple was quoted as 5 ms to 63% of a step change. The device was a foil-type, 0.05 mm thickness, mounted in the inlet port approximately 15 mm downstream of the AAFV exit nozzle.

Injector pulse width

An output signal is generated by the EMS relating to the injector pulse width. This signal was recorded and calibrations applied to obtain pulse width (ms). The injectors were calibrated for fuel flow (mg/ms).

Engine coolant temperature

An output signal is generated by the EMS relating to the coolant temperature. This signal was recorded and a calibration applied to obtain the temperature in degrees C.

Air mass flow rate

The air flow meter was calibrated, using a Fischer & Porter rotameter air flow meter, over a range of air flows corresponding to the proposed idle conditions to be used during testing, see figure A3.5. A third-order curve fit was then applied to the output voltage and the calibration curve was used to calculate the mass air flow rates from the recorded data.

Engine speed

Measured using a monolithic frequency to voltage converter in conjunction with a flywheel-mounted magnetic pick-up. Maximum input frequency was 10 kHz with a $\pm 1\%$ linearity up to this value. Minimum reliable input frequency was 3 Hz, consequently an error in the calculation of engine speed would have occurred during cranking.

TDC

A sensor was located on the engine triggered from a flywheel-mounted indicator corresponding to TDC on cylinder n° 1. The sensor was a two-state device switching between 'high' and 'low' outputs with each pass

of the indicator creating a square-wave signal whereby the period of the signal was the duration of the corresponding 4-stroke engine cycle.

Port depression @ cranking speed

Port depression during cranking was measured using a Furness Controls micro-manometer, type MDC, range 0-1000 mm H₂O. The response frequency of this manometer was 200 Hz for pulsating pressures with an accuracy of $\pm 1\%$ of the full scale output.

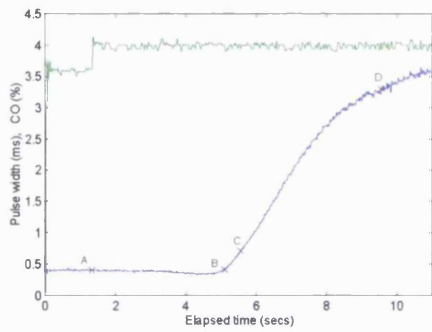
Manifold depression

Measured with a piezoresistive bridge construction pressure transducer, range -2 - 0 Pa. The pressure tapping was placed in the main port manifolding some 250 mm from the inlet valve to avoid pulsation affects.

Battery voltage

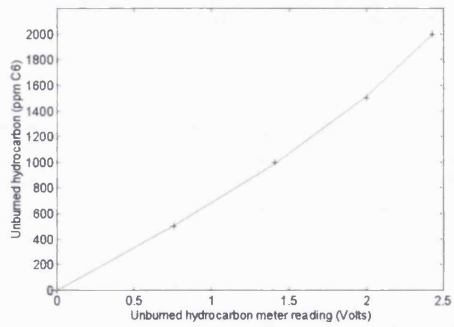
Measured directly across the heating elements and driving circuit.

Figure A3.1
Response characteristics of Horiba HC/CO analyser
to a step change in engine fuelling



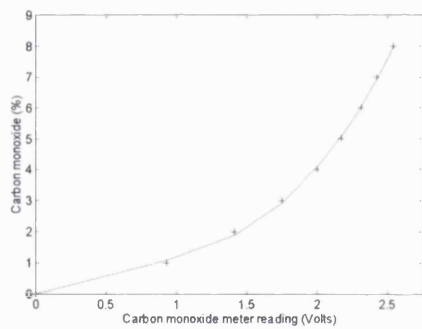
Injector pulse width, Carbon monoxide
 'A' step change @ 1.30 secs
 'B' initial response @ 5.1 secs
 'C' 10% of response @ 5.55 secs
 'D' 90% of response @ 9.54 secs

Figure A3.2
Horiba unburned hydrocarbon calibration,
1500 ppm C₆ spanned to 2.0 V



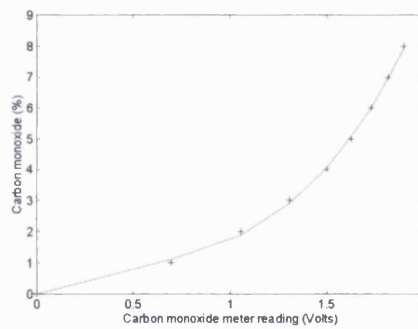
'+' measured data
 Cubic curve fit

Figure A3.3
Horiba carbon monoxide calibration,
4% spanned to 2.0 V



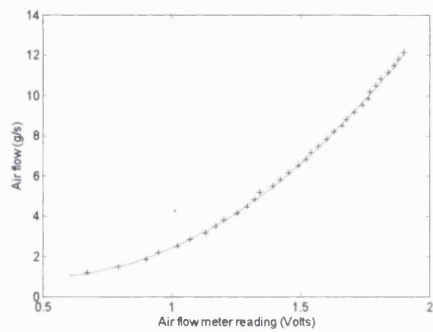
'+' measured data
 Cubic curve fit

Figure A3.4
Horiba carbon monoxide calibration,
4% spanned to 1.5 V



'+' measured data
 Cubic curve fit

Figure A3.5
Jaguar air flow meter calibration



'+' measured data
 Cubic curve fit

CHAPTER 4
AAFV DEVELOPMENT PROGRAMME

CHAPTER 4

AAFV DEVELOPMENT PROGRAMME

4.1 INTRODUCTION

A development programme was initiated to redesign the physical packaging of the UCL AAFV with particular emphasis given to the installation of the units on the Zetec and Sigma engines and to producing a safe and reliable electrical controller. Primary objectives were to reduce the complexity of installation, reduce maintenance time in the event of component failure and reduce the physical size. The reduction in physical size would reduce the thermal inertia of the unit which should bring about a reduced power requirement compared to the initial design investigated in chapters 2.0 and 3.0. It was intended that the design should be generic such that it would require only a change of insulating adapter to fit either of the specified engines.

The re-design was performed using the I-DEAS software 'solid modelling' package which enabled the device to be built up and viewed as a three-dimensional model. The dimensions of all major components such as the cylinder head outline, intake manifold and air box were first obtained and the components modelled using I-DEAS. The new design AAFV was then effectively produced by wrapping a 'skin' around the glow plug, injector and air supply fitting once their positions were established.

4.2 CHANGES TO THE ORIGINAL UNIT

The physical size and complexity of the AAFV was reduced by adopting a 'top feed' fuel injector instead of the 'bottom feed' injector of the original design thereby allowing the upper assembly of the original AAFV to be abandoned. Only two internal changes were made to the unit. The first was to change the fuel entry position to a tangential location on one side of the heater chamber with the intention of promoting a helical flow around the heated element to make better use of the heated surface area. The second alteration arose from a change in glow plug supplier

necessitating a modification in the length of the heated chamber to accommodate in accordance to the dimensions of the standard part. Neither change affected the main design parameters and, as such, it was felt unlikely that the existing spray characteristics would be altered.

Thus, the annular gap around the glow plug was left unchanged as was the diameter of the exit nozzle. The reasons for this were two-fold. The geometry used in the original design had led to the generally satisfactory starting performance referred to in chapter 3.0. Secondly, the lead time associated with any redesign of the controlling geometry and the subsequent testing was considered too great and unnecessary for the task at hand.

4.3 INSTALLATION IMPROVEMENTS

The principal benefit to arise from the redesign was the ease of installation onto both the Sigma and Zetec engines. Three main areas were addressed:

1. The current generation of AAFVs were designed specifically for use on the Ford Sigma and Zetec engines, see figures 4.1-4.5. As far as possible, standard parts were retained for ease of use, each installation being tailored by way of adapters, mounts and fuel rails for the particular engine. The main body of the AAFV was common to both applications and had been reduced in mass by 66%, and was a one-piece design to reduce complexity and ease assembly. The one-piece design allowed major items such as the fuel injector and glow plug to be easily changed in the event of component failure whilst the system remained in-situ on the engine.

2. The electrical connections were simplified and were powered by a modified production unit supplied by Beru, who are manufacturers of glow plugs. The controller is essentially a timed relay designed to power the glow plugs for a 10 second pre-heat time and automatically switch them off if the engine was turned off at the key or if the operator fails to switch on after the pre-heat time has elapsed.

Connection of the glow plugs to the electrical supply retained the industry standard for the original diesel installation with an earth connection common to the engine earth point. The controller/driver for the electrical supply could draw its power from either the standard vehicle electrical system or an external source, if required, provided the source shares a common ground to that of the engine.

3. The electrical driver may be operated automatically through the engine start-up procedure or switched independently if required. During the warm-up period a warning light is activated to inform the operator that the glow plugs have been switched on. Once the light is extinguished, engine cranking may be initiated. Power to the glow plugs will be disabled if for any reason the operator fails to start the engine within 10 seconds of the light going out. Power is maintained for a period of 3 minutes after the initial pre-heating. If the engine is switched off during either pre-heat or post-heat cycles the glow plug supply is automatically disabled. If the heating system is operated by an auxiliary switch, a reset button/switch is required to enable the post-heat cycle, see Appendix A4.

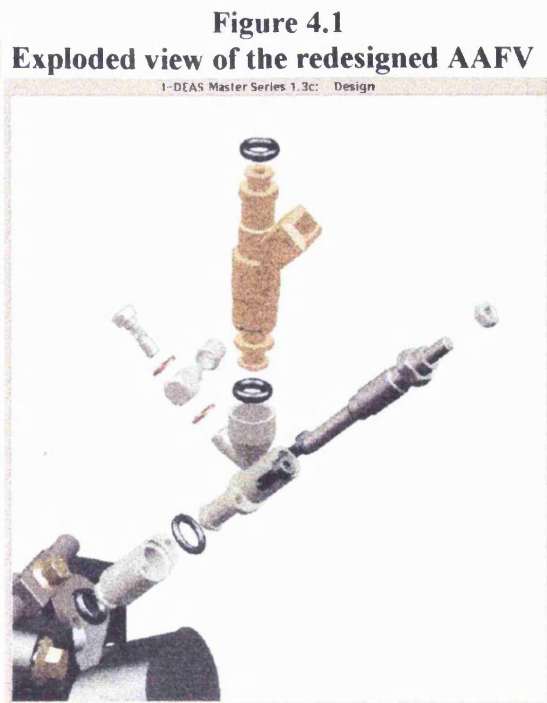


Figure 4.2
Computer generated model of the redesigned AAFV installation
on the Zetec engine

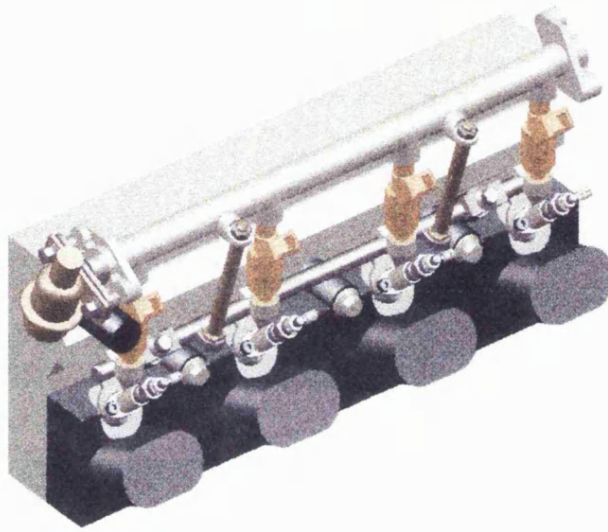
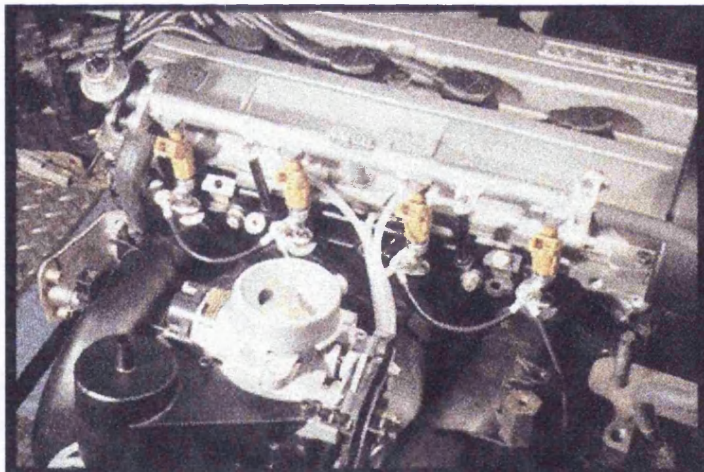


Figure 4.3
Zetec engine equipped with the
redesigned AAFV installation



4.4 CONCLUSIONS

In conclusion, it can be said that the AAFV has been redesigned to incorporate the main changes identified in chapter 2, while improving installation and serviceability.

Figure 4.4
Computer generated model of the redesigned AAFV installation
on the Sigma engine

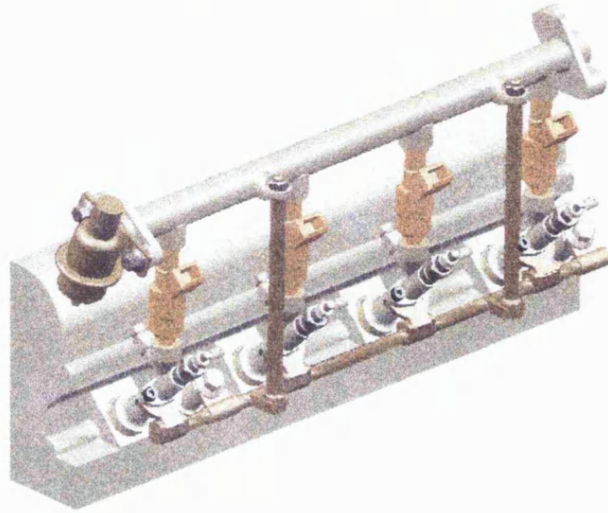
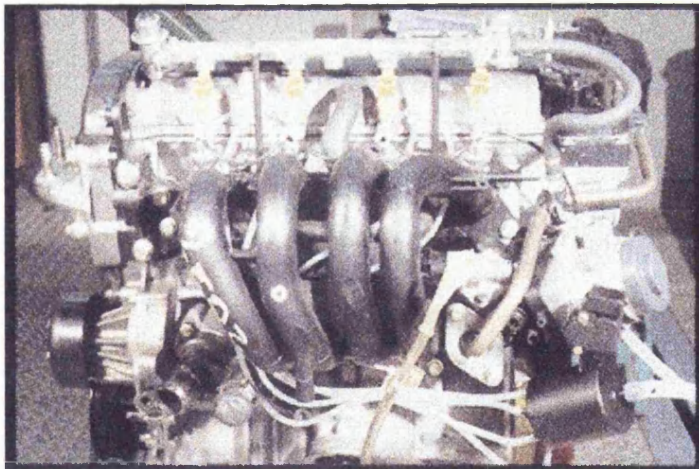


Figure 4.5
Sigma engine equipped with the
redesigned AAFV installation



The design modifications also considerably reduced the thermal inertia of the housing and incorporated a change in the orientation of the injector to the glow plug in order to promote a helical flow around the glow plug surface.

APPENDIX A4

A4.1 GLOW PLUG CONTROLLER FUNCTION

The pre-heat time controller triggers the pre-heat pilot lamp and controls the glow plugs.

The pre-heat time begins with switching in ignition (tml. 86). The pre-heat pilot lamp is lit (tml. L becomes negative) and the glow plugs are fed (tml. 87 becomes positive). After the 10 second pre-heat time has elapsed, the pilot lamp extinguishes and informs the operator that the engine is ready to be cranked. The glow plugs remain on during cranking.

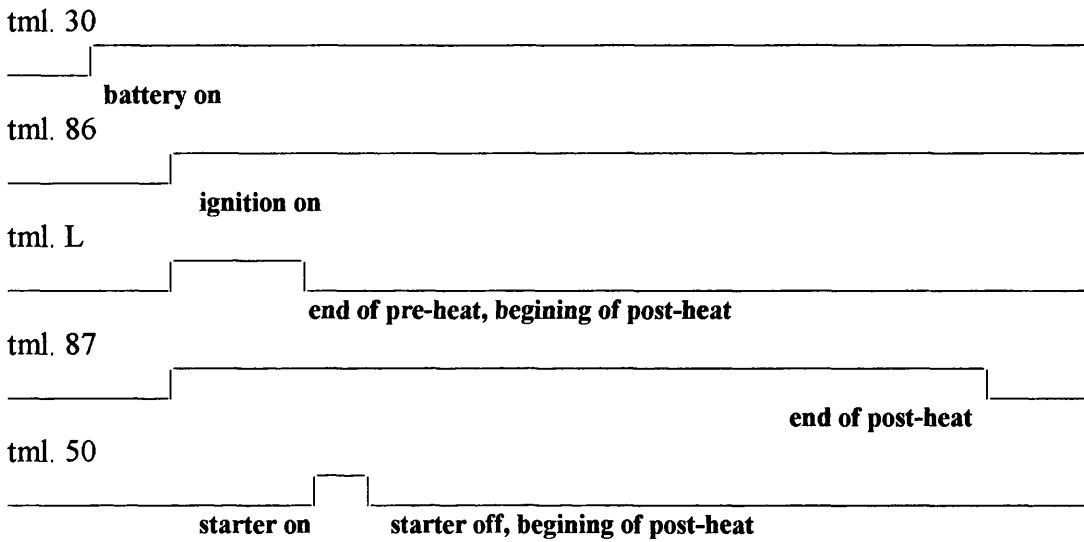
After extinguishing of the pilot lamp, the stand-by time begins (10 seconds). If no start occurs during this time, the controller will cut off the glow plugs after elapse of the stand-by time.

With the release of the starter (tml. 50), the post-heat time begins (180 seconds). After elapse of this time, the controller cuts off the glow plugs.

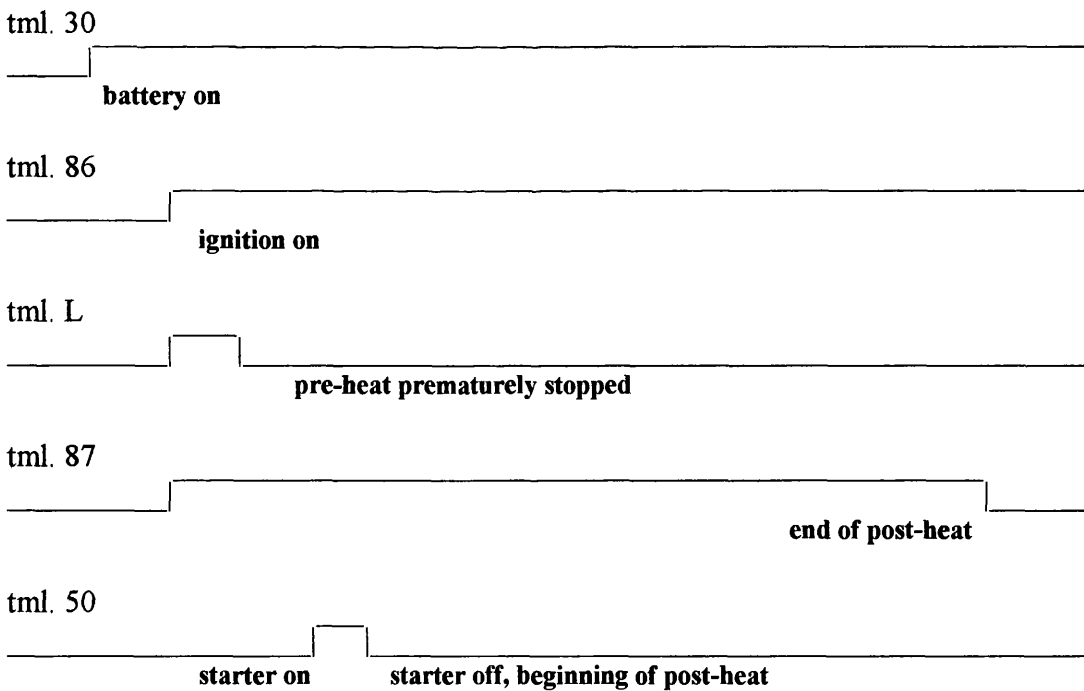
If the engine has not started with the first attempt, ignition must be switched off before a second attempt can be made.

A4.2 FUNCTION DIAGRAMS

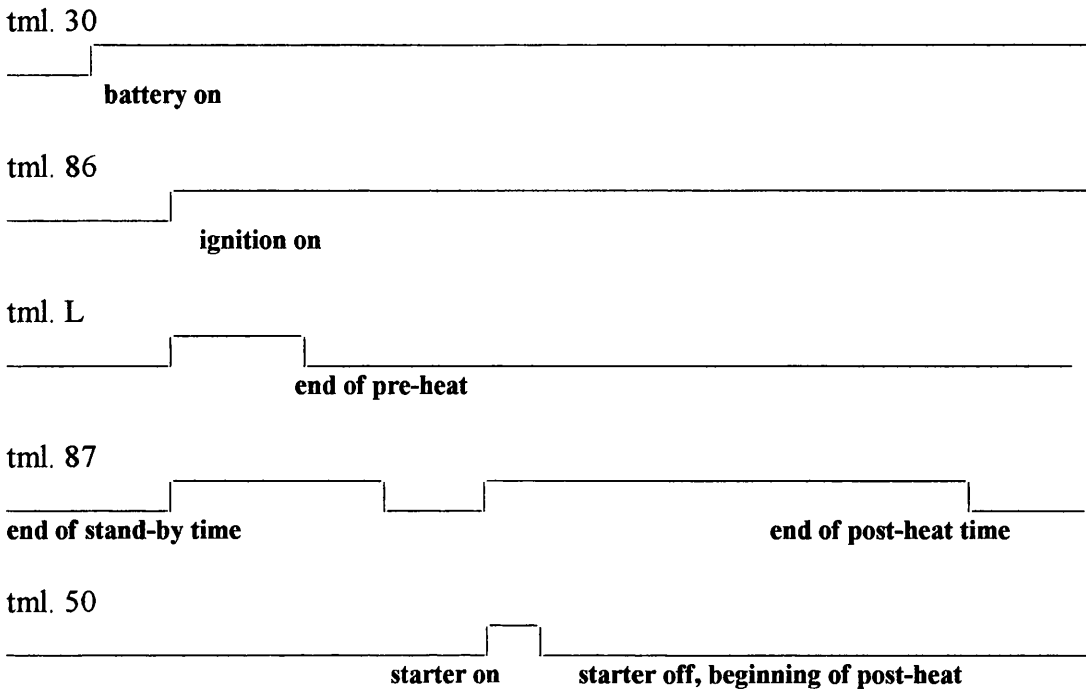
A4.2.1 Normal operation



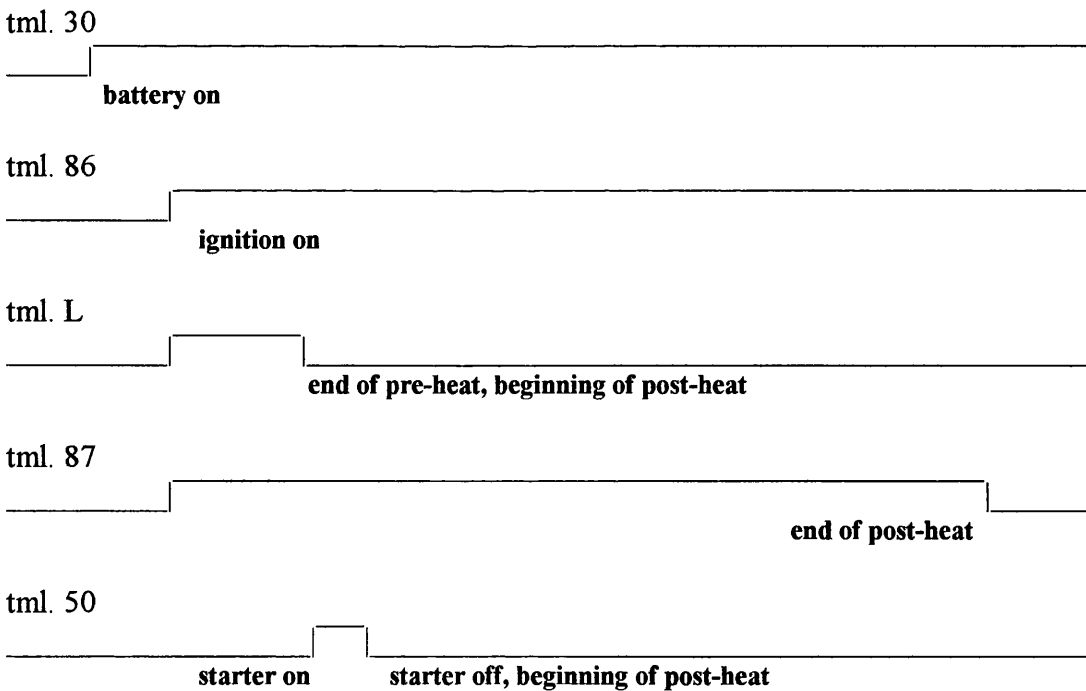
A4.2.2 Premature start



A4.2.3 Start after safety cut-off



A4.2.4 Unsuccessful start²



² Note: as soon as the ignition key is switched off after a unsuccessful start, power is automatically switched off to the glow plugs.

CHAPTER 5

INTAKE & EXHAUST PORT UNBURNED HYDROCARBON CONCENTRATION SAMPLING

CHAPTER 5

INTAKE & EXHAUST PORT UNBURNED HYDROCARBON CONCENTRATION SAMPLING

5.1 INTRODUCTION

The effects on engine performance attained by improving the fuel spray atomisation were examined by Brown & Ladommatos, 1991. A reduction of the mean droplet diameter presented to the intake port was achieved by a means of air-atomisation though little effect on combustion performance was detected with a coolant temperature of 80°C, the largest variation being an increase (< 5%) in the UHC emissions when applied to a 2.9 litre V-6 port injected engine operating at a low speed, light load condition. When the test was repeated using a coolant temperature of 35°C the effects were more distinct with air-atomisation leading to the COV dropping from 10.5% to 9.5%, a decrease in burn duration of between 5° and 10°CA and a reduction in NO_x of 200 ppm when compared with results from the conventional injector. It was suggested that the change in spark timing to obtain MBT (a reduction of ignition advance of 2°CA) could account for the majority of the NO_x reduction.

Brown & Ladommatos, estimated the amount of liquid fuel present on the port walls at coolant temperatures of 80°C and 35°C. They found that at the lower temperature the mass of the liquid film was up to six times greater than the amount injected per-cycle during warm-up, a quantity which was substantially reduced during fully warm conditions, when the film reduced to 1.5 times the injected mass. Little difference of fuel film mass was discernible between either the standard injector or the air-assisted, though since the inclination and position of the injector location was such that the targeted area was the port floor substantially upstream of the intake valve, the result was not altogether surprising. The most significant parameter was the injection timing, with an open valve injection strategy responsible for a reduction of the liquid

mass by almost 50%. Interestingly it was the change in the fuel viscosity which was suggested, in part, for the reduction in the liquid film at the higher coolant temperatures, as it allowed the fuel film to flow more easily along the port walls.

When Pontoppidan & Cristiani, 1993, improved the atomisation of a port injector they found that the ignition advance could be reduced, bringing with it a substantial increase of the exhaust gas temperature. A raised exhaust temperature would engender faster catalyst light off. A further consequence of elevated exhaust temperatures is the increase in the post flame HC oxidation during the expansion and exhaust strokes. However, the fact that the ignition advance could be reduced indicates that the combustion process was more efficient, if the timing represented MBT, and therefore the temperature of the burned gases should be lower. It is felt that the improved mixture preparation allowed the ignition advance to be reduced from the point of MBT associated with the standard injectors, whilst retaining acceptable engine stability and performance thereby prompting the beneficial increase in exhaust temperature. An increased tolerance to open valve injector timing was also established without the increase in UHC emissions associated with the standard pintle injector, due presumably to the improved transport mechanisms whereby more of the fuel droplets were entrained in the air stream and the increased rate of evaporation encountered by the atomised spray prior to spark initiation.

In-cylinder mixture inhomogeneity may contribute to raised engine-out emissions. Shayler, Marshall & Turner, 1990, investigated the influence of differing fuel injectors and their location in an attempt to understand the variations of mixture preparation and the subsequent interaction with the combustion process. By operating the engine at steady state under a range of load and speed conditions, changes in the mixture preparation effects were measured by monitoring the emissions of HC, CO and NO_x. Port injection introduces the fuel at a location close to the intake valve, as such it was felt that insufficient time was available to vaporise fully the fuel prior to its ingestion into the combustion chamber. It was deduced that the mixture within the cylinder could be divided into regions of well mixed fuel vapour, and air and fuel rich pockets

of vaporising liquid droplets. Changes in the mixture preparation can be considered to exert an influence on the relative ratio of these two in-cylinder regions. Introducing the fuel such that there is a higher proportion of liquid to vapour concentration tends to increase HC emissions, leave CO predominantly unaffected and reduce NO_x. The effects of changing the fuel injector type and locations proved difficult to assess since the changes in the measured emissions were often of the same order as the accuracy of the instrument. One of the more intriguing points elucidated was that an improvement in the mixture preparation process could be attained by increasing the wetted port surface area to promote greater evaporation which is in direct conflict with what is required to reduce HC emissions during transients.

The rate of heat transfer to the fuel deposited on the port walls is of great consequence to both transient and steady state operation of an engine. Chen & Aggarwal, 1996, and Horie, Takahasi & Akazaki, 1995, developed models of the intake port injection process incorporating wall wetting. During start-up conditions Horie, Takahasi & Akazaki, 1995, predicted that approximately 30% of the injected fuel directly entered the combustion chamber which is in close agreement with Chen & Aggarwal who suggested that the total liquid flow along the port wall was around 65%. Chen & Aggarwal went on to state that, during steady state operation, the total vapour concentration was made up from a 55% contribution from droplet vaporisation and the remainder provided by wall film evaporation. The model also predicted that the droplets, prior to impaction on the port wall, lost up to 20% of their mass by evaporation. This presumed a specific residence time and was also dependent upon the assumed droplet size, with the model using a mono-sized spray. The intake air temperature will play a significant role in the evaporation of the liquid droplets though the model appears to use an uncharacteristically high value, stated as being 350 K. Whilst Chen & Aggarwal, 1996, stated that their model used a multi-component fuel composition, the results published were for a fuel composition of only two constituents, suggested to represent the heavy and light ends of pump grade gasoline. A useful comparison would have been to show the effects of the predicted vaporisation rates and port wall fuel film volume over a range of fuel compositions as

the fuel type and blend has been shown to have a predominant effect on both evaporation rates and the fuel spray drop size and distribution, Williams, 1993.

Shayler, Colechin & Scarisbrick, 1996, measured the fuel film evaporation from the port wall both with iso-octane and pump grade gasoline, and found that the rate of evaporation was greatly affected by the change in chemical composition of the fuel. The heavy ends of the gasoline remain as a liquid, whilst the iso-octane actually achieved complete evaporation. The experiments indicated that as little as 5% of the wall film evaporated during the warm-up phase of engine operation. Cyclically resolved heat fluxes were presented and indicated that vaporisation tended to occur during two distinct periods. Firstly, a high rate of evaporation occurred just as the fuel landed after the injection event due to the temperature difference between the fuel and port surface. This contribution dominated at coolant temperatures above 50°C. The second period of high convective mass transfer occurred at IVO due to the backflow of hot gases during the initial opening period.

The backflow of hot gases is also responsible for strip atomisation of droplets from the wall film around the valve seat area. Shin, Min & Cheng, 1995, used video techniques to observe the fuel flow in the intake port of a modern 4-valve port-injected engine during throttled, low speed, operation with a view to determining the influence that the fuel injected in one cycle has on subsequent cycles. The images obtained indicated that, during the initial intake valve opening period, the liquid fuel resident around the valve seat was stripped off the port and atomised into droplets which were then driven back into the intake port by the backflow of the in-cylinder gases. It was suggested that the droplets could be pushed back by a distance approaching 200 mm. This figure was specific to the individual engine geometry. Whilst the authors suggested that the process could make a contribution to the mixture preparation, it is thought that it is mainly the increase in port wall temperature which affects the mixture preparation, and that the quantity of fuel actually transported by the backflow is likely to be small. Any droplets that are large enough to constitute a significant contribution to the overall fuelling will be too heavy to

follow the air stream and, as stated by the text, droplets which are small enough to be carried by the air flow are expected to remain suspended and therefore be ingested during the forward flow through the intake valves. It is possible that some of the suspended droplets may impact on the manifold and subsequently evaporate, but the contribution is likely to be negligible. Further investigation of the fuel transportation and subsequent cycle effects were undertaken through a single injection of fuel into a motored engine without triggering the sparking plug. The quantity of fuel entering the combustion chamber was then measured using a high frequency response flame ionisation detector, HFRFID, mounted to sample from the combustion chamber. The in-cylinder UHC concentrations were assumed to be representative of average in-cylinder fuel quantities. 24% of the injected fuel was inducted for the first cycle, and 13% for the second using a fuelling equivalence ratio, ϕ , of 0.92. These values are assumed to be slightly pessimistic since no account was made of liquid deposition, and therefore storage, occurring within the combustion chamber.

Cheng *et al*, 1991, used a HFRFID probe mounted to sample from the intake manifold of a port-injected engine to measure the vapour concentration within the port throughout the cycle duration. The sample was taken from a location just upstream of the injector tip so as to avoid blocking the sample tube with liquid droplets. It was observed that the vapour concentration generally peaked shortly after IVO and that this effect was most pronounced if the injection event was timed to occur on closed intake valves. Under these conditions, liquid deposited around the valve seat was atomised during the initial opening and subsequent backflow, and the hot residual gas vaporised some of the smaller droplets to produce the measured peak in UHC concentration. Whilst the traces are of value in determining the distance that fuel vapour was pushed back into the manifold, it would be of great interest to establish whether the vapour concentration upstream of the injector was representative of the flow entering the combustion chamber. Unfortunately the authors were unable to establish the concentration levels downstream of the injector due to the problems associated with measurements made within a liquid fuel spray.

5.2 TEST PROGRAMME MEASUREMENT APPARATUS

In order to obtain a more comprehensive knowledge of both intake port fuel transport in general and specific characteristics of the AAFV, a series of intake and exhaust port HFRFID sampling tests were undertaken on a single-cylinder version of the Ford Zetec engine that was available for test work. A cylinder head was modified such that access into the inlet port was facilitated at three locations, each with the probe being positioned normal to the flow direction.

Test conditions of 800 rev/min idle and 1500 rev/min road load were chosen for their representation of cold-start engine and warm-up load and speeds, and 1650 rev/min WOT to assess the performance of an alternative air supply to the AAFV.

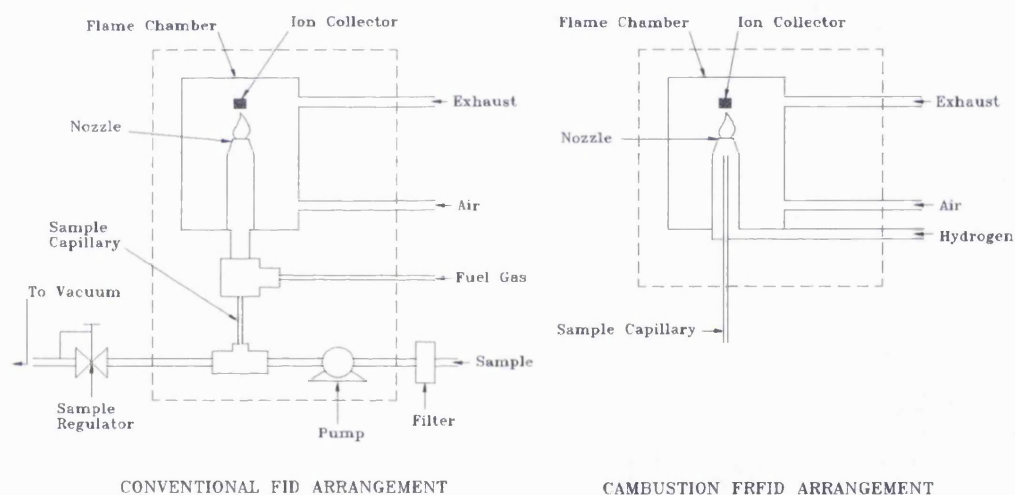
5.2.1 Combustion high frequency response flame ionisation detector, HFRFID

The Combustion instrument is an FID-based device designed to measure unburned hydrocarbon concentrations on a very short time scale to the extent that a crank angle resolved characteristic UHC signature is obtained.

Significant ion formation occurs when a hydrocarbon fuel is burned, the number of ions being very nearly proportional to the number of carbon atoms burned. The quantity of ions produced in the flame of a non-hydrocarbon such as hydrogen is limited to thermal ionisation and as such is very low at normal flame temperatures. The method of production in the hydrocarbon flame is associated with a process called chemi-ionisation. Conventional FID design uses the physical properties of the two ionisation processes by introducing a representative sample of the measured flow into a hydrogen flame. An ion collector is used to measure the concentration of the mass flow of hydrocarbons within the sample. In a conventional FID the necessary gas flows are controlled by capillary tubes and pressure regulators, and the instruments generally have a response time of greater than one second. The Combustion HFRFID differs from a standard FID in that the sample is mixed with the

fuel gas at the nozzle exit, see figure 5.1, drawn directly into the FID by maintaining the flame chamber pressure below that of the sample pressure. Consequently, the chamber normally operates below atmospheric conditions. The accuracy of the chamber normally operates below atmospheric conditions. The accuracy of the measured concentration depends upon the control of the FID chamber vacuum which determines the mass flow rate and pressure fluctuations of sample gas. A typical 10-90% response time of the HFRFID is approximately 4 ms whilst the transport delay, or time constant, is dependent on the capillary tube bore and length used to supply to sample as well as on the pressure differential maintained between the measurement location and the flame chamber.

Figure 5.1
Comparison of a conventional FID and the Combustion HFRFID

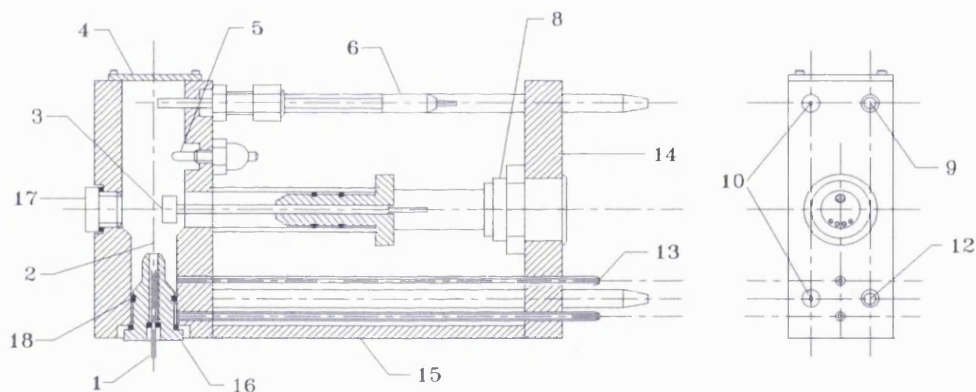


Predictions of the time constant are made using software supplied by the manufacturers. The theoretical estimate takes no account of processes occurring within the flame itself. One-dimensional air flow is assumed at all times and only an approximate correction for compressibility effects is made. A more complete analysis of the equations used within the software may be found within the HFR400 Quick Users Guide.

If pressure fluctuations within the sampling location are more than ± 0.75 Pa, an additional damping chamber is recommended by the manufacturer in order to

minimise oscillation of the flow rate and therefore pressure changes in the flame chamber. Pressure changes over a long time scale are removed by bleed flow regulators, see figure 5.2, and short time scale fluctuations are reduced by making the volume of the damping or constant pressure chamber large by comparison to the fluctuations of the sample pressure. The minimum sample pressure is set by both the limits of the vacuum pump and having an acceptable pressure differential between the HFRFID vacuum chamber and the sample location. The pressure differential is determined by flow requirements of the instrument for accurate measurement and the need to reduce the time delay. For inlet port sampling, the vacuum pump presents a limit to the minimum manifold pressure that can be used, which in practice was found to be approximately 47 kPa (absolute).

Figure 5.2
Sectioned view of the Combustion HFRFID



- | | | |
|---------------------------------|-------------------------|-----------------------|
| 1. Removable nozzle | 8. Electrical connector | 15. Baseplate |
| 2. Flame | 9. FID bleed | 16. Removeable nozzle |
| 3. Collector electrode | 10. Vac supply | 17. Inspection hatch |
| 4. Lid | 11. Air | 18. O ring |
| 5. Glow plug | 12. CP bleed | |
| 6. Thermocouple | 13. Fuel | |
| 7. Collector insulator assembly | 14. Bulkhead | |

A dynamic calibration unit, DCU, allows the sample probe to remain in situ during span gas calibration. This has the benefit of ensuring that all measurements are taken from the same location. The sample line is heated to a controlled temperature, approximately 170°C, to minimise condensation of the UHC sample.

5.2.2 Design of cylinder head sample sites

A Ford Zetec cylinder head was used throughout the duration of the HRFID tests, adapted to fit an existing single-cylinder, cylinder block and crank case assembly. Bore and stroke were matched to the production engine. The cylinder head was a cut-down version of a standard Ford Zetec cylinder head containing a single operating combustion chamber. The head was designed for this project and considerable work was required to develop a method of lubricating the camshafts. The intake manifold was modified to suit with the internal volume reduced by approximately one third compared to the four cylinder item. HRFID probe sites were placed in the intake manifold, inlet port riser and exhaust port. Measurements of cylinder pressure, cylinder head temperature, inlet manifold pressure just upstream of the HRFID sample location, and an AFR meter sensor in the exhaust, see figures 5.3 & 5.4. The option to operate a cylinder pressure bleed tapping for the AAFV was also included, see section 5.3.2. Mention should also be made that the cylinder block and crankcase assembly of the engine had been modified to provide optical access for a previous project. This involved the use of an extended piston with a quartz piston crown. The optical access was not used for the AAFV investigations, but the piston did feature a single low-mounted compression ring. This should not have affected the intake port sampling results, but did provide an unnaturally large crevice volume for the exhaust port sampling tests. This is discussed further in the relevant section. The specification of the test engine is contained in Appendix A5.

Figure 5.3
View of the intake port showing the HRFID
probe sites B & C

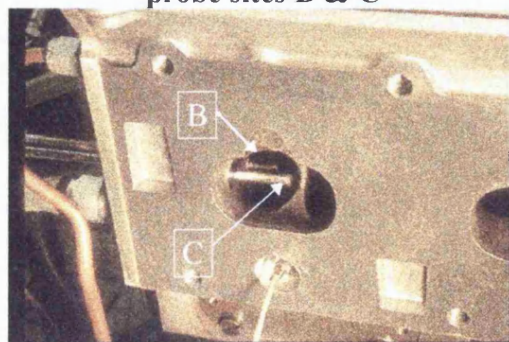
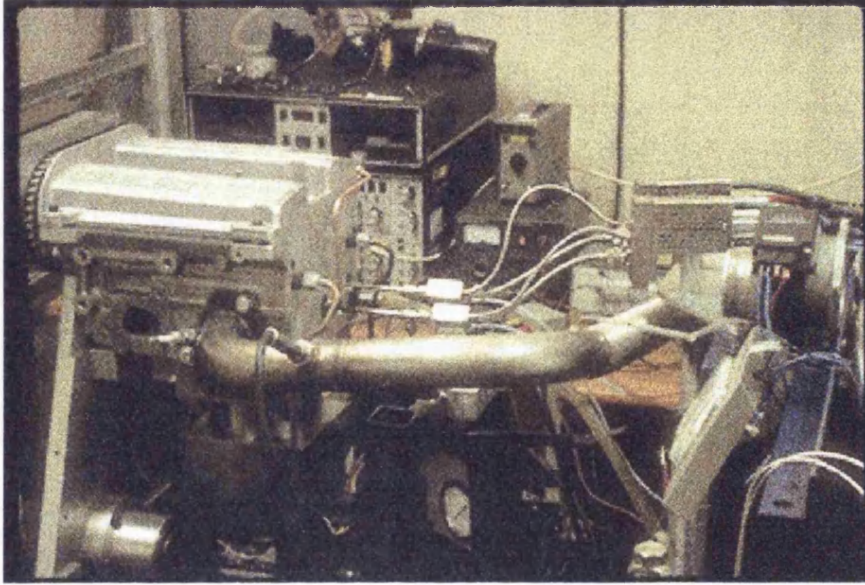


Figure 5.4
Overall view of the engine test bed



The intake HRFID sample sites were located 30, 60 & 120 mm upstream of the intake valve and are identified in the text as locations B, C & D. Location 'A' refers to the exhaust port probe. Site D was positioned 20 mm upstream of the injector location. All intake probes were positioned to align with the central axis of the port normal to the flow direction.

5.3 EXTERNAL AIR-ASSISTANCE FOR THE AAFV

The UCL AAFV had been designed to operate using the pressure drop between the inlet port and the ambient pressure conditions upstream of the throttle. The drop in pressure causes a flow of metered air through the AAFV which has two effects, firstly to purge the internal passages of fuel prior the subsequent injection cycles and secondly to assist in atomising liquid fuel as it leaves the exit orifice. This is referred to within the following text as 'passive air-assistance'. During engine idling and part-load conditions a sufficient pressure differential exists for successful operation (approximately 35 kPa is required to produce droplet Smds of the order of 5-30 μm , see chapter 2). Passive air-assistance, however, becomes negligible as WOT conditions are approached. Under these circumstances the air/fuel ratio is likely to

fluctuate due to the difficulty in adequately purging the internal cavity of the AAFV, the results of which will be observed as rough engine operation, high coefficient of variation, COV, and poor emission performance. Whilst at present the emissions test does not include full-load operation, the level of roughness would be intolerable on a production engine, consequently, the need for a system capable of providing adequate mixture preparation and fuel delivery is fundamental to successful operation of the AAFV.

5.3.1 Air pump

An auxiliary pump could be used to obtain a pressurised air supply, either driven electrically or via a 'v' belt off the crankshaft. However, the problem is quite complex when consideration of the start-up procedure and engine mapping are taken into consideration. If the pump was to be an electrical device the need for it to be activated prior to or during engine cranking would exist, putting an additional load onto the electrical system. The physical size, weight, cost and electrical consumption become significant factors due to the compressibility of the working fluid, air.

5.3.2 Cylinder Pressure Tapping, CPT

A potentially cheaper and simpler alternative approach to obtaining a pressurised supply of air is to take a tapping from the cylinder. This approach has been put forward by Ford, patent application n^o PCT/GB96/01897, but not investigated experimentally until this current test programme. A restrictor needs to be fitted in the line to prevent excessive transfer of gas from the cylinder, and hence loss of cylinder work. A Lee Axial Visco Jet, part n^o VXCA2502140D, was initially used as the in-line restrictor between the combustion chamber and the AAFV. One of the claims for the Lee Visco Jet is that its passages are 'self cleaning' and therefore should be resistant to blockage from particulates being blown through from the cylinder. It may be regarded as consisting of a number of restrictors set in series, separated by small

chambers designed to maintain a significant flow velocity in order to scour the surfaces of any build up of deposits.

The instantaneous mass flow rates through the Visco Jet were calculated using existing cylinder pressure and temperature data and the results then integrated over one cycle duration to obtain the overall mass flow per cycle. At idle, the engine's required air intake is known to be 0.69 mg/ms/cylinder or 55.5 mg per cycle increasing to 214.2 mg at 1500 rev/min road load. The total flow at idle through the restrictor was calculated to be 2.86 mg with a peak of 0.27 mg/ms and at 1500 rev/min the values increased to 11 mg and 1.9 mg/ms respectively.

During the testing, the Visco Jet collapsed internally part way through the test programme due to the heat/pressure experienced at WOT conditions and it was replaced with a straight-through, 0.8 mm diameter restriction approximately 20 mm in length. In the text, the distinction of CPT1 & CPT2 is made referring to the Lee Visco Jet and the straight restrictor respectively. The pressure just upstream of the AAFV air bleed connector was measured throughout the test programme with both restrictors, see figures 5.5a & 5.5b.

Figure 5.5a
CPT schematic

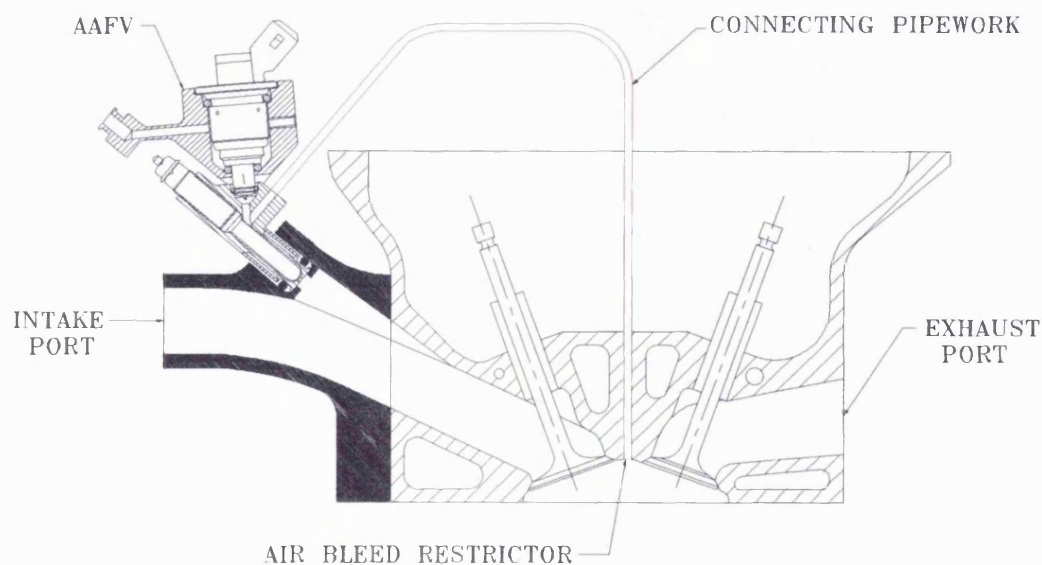
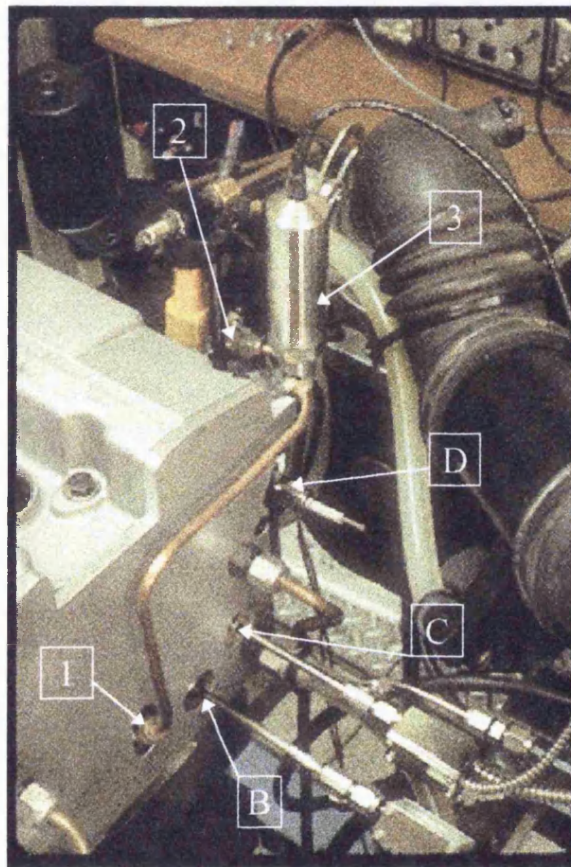
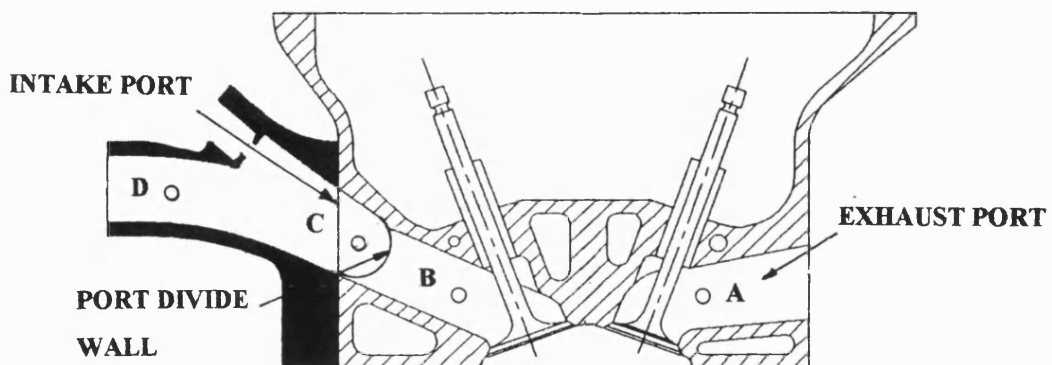


Figure 5.5b
View of the cylinder pressure tapping pipe work cylinder head
and the HFRFID probe sites B, C & D



- 1: connection to cylinder pressure tapping
- 2: connection to AAFV
- 3: pressure transducer

Figure 5.5c
HFRFID sample site locations



5.4 FIGURE GUIDE

Testing was performed on the single-cylinder engine with the AAFV supplied at different times with passive air-assistance and with pressurised air from the cylinder head tapping. Traces from the HFRFID instrument were recorded from four sampling points at three different engine conditions. The following sub-section is included to help the reader interpret the results. Note that a stoichiometric air/fuel ratio calculated using iso-octane would be indicated by a HFRFID reading of approximately 45,000 ppm C₃.

5.4.1 Key to figures

The red vertical lines indicate the start and end of injector triggering, from left to right respectively. The green vertical lines refer to the inlet valve opening and closing events. A blue horizontal line is used, on figures indicating the CPT bleed pressure, for the bleed pressure figures and represents the intake manifold pressure as measured in the intake port riser approximately 30 mm upstream of the injector. All traces are depicted \pm one standard deviation from the mean of approximately 80 cycles with the test repeated to ensure accuracy of the observed results. The engine was running for approximately one minute before recording began.

5.4.2 HFRFID sampling sites:

- A, Exhaust port, 20 mm downstream of the exhaust valve
- B, Inlet port, 30 mm upstream of the inlet valve
- C, Inlet port, 60 mm upstream of the inlet valve
- D, Inlet port, 120 mm upstream of the inlet valve¹

¹ Location D is some 20 mm upstream of the injector tip.

5.5 DISCUSSION

5.5.1 HFRFID tests: 1500 rev/min, road load, 35.9 kPa intake pressure

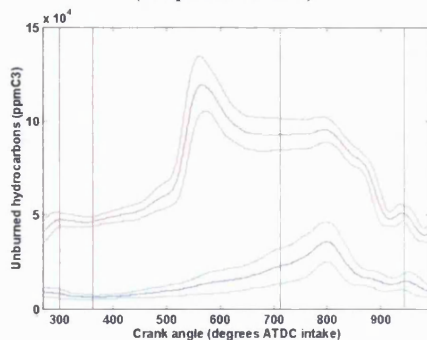
The trends are easier to determine from the 1500 rev/min test condition, consequently these are referred to first with salient points raised for the other operating conditions.

5.5.1a Intake port sampling, vapour, atmospheric bleed

(refer to figures 5.6-5.9)

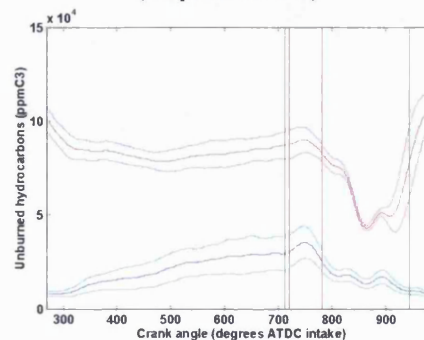
Figures 5.6 & 5.7 show traces taken from sample sites C, red, & D, blue for closed valve injection. The delay in fuel delivery from the AAFV is indicated by the time between start of injection, SOI, and the first UHC peak from the trace at site C. This delay is some 250°CA and compares well with the 225°CA delay suggested by the light obscuration measurements used to evaluate the AAFV performance in chapter 2. Figure 2.2 shows the result for a 1.5 mm diameter exit nozzle (the current diameter is 1.2 mm) using a glow plug of comparable length. There was little detectable variation in UHC level at site C during the backflow period of the valve opening event (around 720°CA) though the probe upstream of the injector (site D) indicates a steady rise up to the point assumed to be the initiation of forward air movement at approximately

Figure 5.6
Closed valve injection, fuel vaporisation, 1500 rev/min
road load, 35.9 kPa manifold depression, $\lambda = 1$
(sample sites C & D)



Sample site C, ± 1 std deviation
Sample site D, ± 1 std deviation

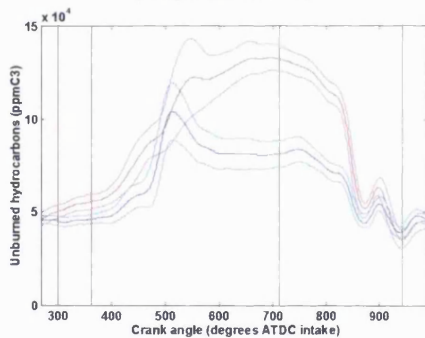
Figure 5.7
Open valve injection, fuel vaporisation, 1500 rev/min
road load, 35.9 kPa manifold depression, $\lambda = 1$
(sample sites C & D)



Sample site C, ± 1 std deviation
Sample site D, ± 1 std deviation

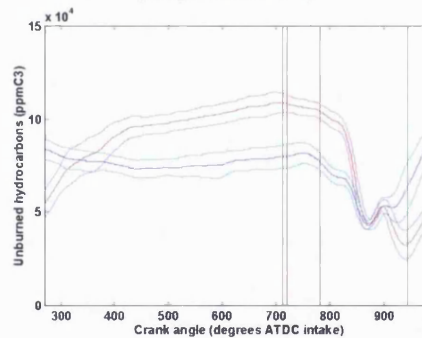
80°C CA ATDC_{intake}, thought to be due to both the constant evaporation of the fuel from the wetted port wall and fuel vapour being purged from the AAFV, pushed upstream of the injector by the backflow. It is somewhat surprising that the UHC levels in the intake port were often higher when open valve as opposed to closed valve injection was adopted, figure 5.7. However, it is clear from the previous discussion, see figure 5.6, that a delay in the fuel transportation exists, consequently with the injection timing shown the bulk fuel flow will occur post IVC, indicated by the sharp rise in the UHC trace from site C at this time, see figure 5.7. The delay appears to be less than that observed during closed valve injection, indicating the increased port velocity during the open valve period and the consequent reduction in bulk flow transport time within the intake port. The delay period appears to be of the order of 150°C CA.

Figure 5.8
 Closed valve injection, fuel vaporisation, 1500 rev/min
 road load, 35.9 kPa manifold depression, $\lambda = 1$
 (sample sites B & C)



Sample site B, ± 1 std deviation
 Sample site C, ± 1 std deviation

Figure 5.9
 Open valve injection, fuel vaporisation, 1500 rev/min
 road load, 35.9 kPa manifold depression, $\lambda = 1$
 (sample sites B & C)



Sample site B, ± 1 std deviation
 Sample site C, ± 1 std deviation

Sampling further downstream during closed valve operation at location B indicates the penetration of the fluid stream after exiting the AAFV. The peak seen in figure 5.8 occurs approximately 50°C CA after that observed during sampling at site C, 30 mm upstream, revealing an apparent fuel vapor transport velocity of 5-6 m/s within the quiescent intake port. Sampling at site B during open valve operation (figure 5.9) did not reveal the clear progression of the UHC peak from site C to site B, observed during closed valve injection. However, there was a fairly rapid increase in the UHC

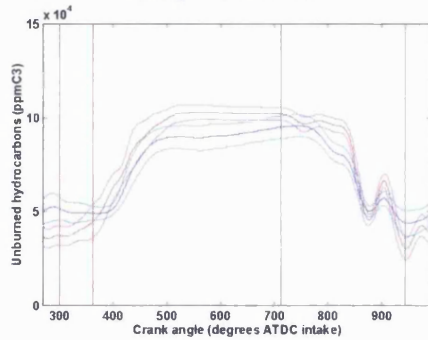
level from IVC up to 400°CA ATDC_{intake} after which the rise was at a reduced rate. It was felt that the initial rise was due to the vapour passing directly from the AAFV into the stationary air stream and that the second rise was created from a combination of continuous purging of the AAFV cavity and evaporation from the port walls of any liquid deposition from a small proportion of fuel escaping vaporisation.

It is worth noting that the software program, see section 5.2.1, used to predict the transport time between passing the HFRFID probe and the constant pressure chamber where the sample is measured presumes that the pressure conditions at the sample location were constant. This assumption leads to a slight smearing along the x-axis of the trace during initial valve opening and to a lesser extent as the manifold pressure recovers throughout the closed valve period, however, the analysis is presented as an overall comparison between mixture preparation processes and not as a specific UHC vs. crank angle investigation.

5.5.1b Intake port sampling, vapour, cylinder pressure tapping 1 & 2 (refer to figures 5.10-5.15)

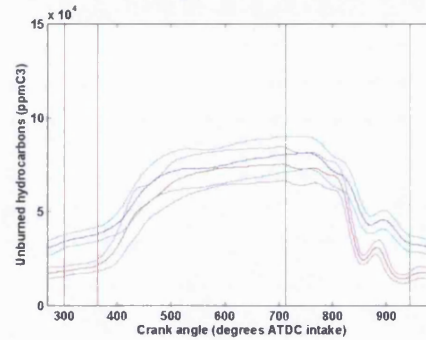
Tests using the cylinder pressure tapping, CPT, were performed with UHC measurements at intake port sites B & C. The transit time through the AAFV appeared to reduce when the CPT was employed to provide the air-assistance which corresponded with an increase in the air supply pressure of between 10 and 30 kPa over the ambient bleed pressure. A sharp increase in the intake port level of UHCs was apparent within 100°CA of triggering the injector and reached a plateau within 200°CA from SOI during operation with a closed valve injection strategy for either CPT, see figures 5.10 & 5.11. This corresponds to a delay duration of 11-22 ms. As in section 5.5.1a, transit times compare well with those indicated from the light obscuration plots in chapter 2. In this case the nearest equivalent test is for the full load condition using 35 kPa external air-assistance (albeit with different manifold pressure), see chapter 2, figure 2.4.

Figure 5.10
 Closed valve injection, CPT1, fuel vaporisation, 1500
 rev/min road load, 35.9 kPa manifold depression, $\lambda = 1$
 (sample sites B & C)



Sample site B, ± 1 std deviation
 Sample site C, ± 1 std deviation

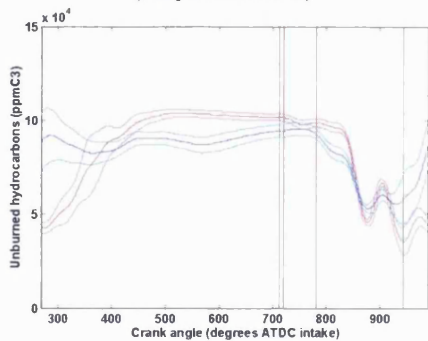
Figure 5.11
 Closed valve injection, CPT2, fuel vaporisation, 1500
 rev/min road load, 35.9 kPa manifold depression, $\lambda = 1$
 (sample sites B & C)



Sample site B, ± 1 std deviation
 Sample site C, ± 1 std deviation

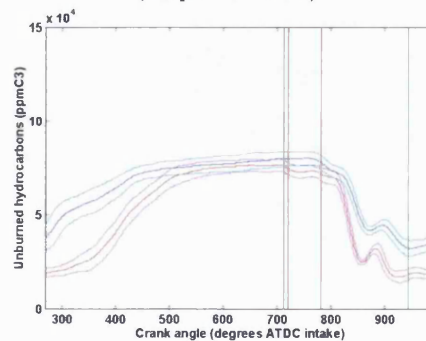
When utilising open valve injection strategy, see figures 5.12 & 5.13, the UHC trace exhibits the characteristics seen when using the atmospheric bleed. The overall shape of the trace was largely unaffected by either injection strategy or pressure tapping though the concentration levels observed when using the second, larger tapping, CPT2, were consistently lower by a difference of 2×10^4 ppm C_3 . The reasons for the reduced concentration levels may be due to a greater volume of gas being bled into the intake port using CPT2. Since both pressure tappings were designed to offer a greater restriction to flow than the AAFV exit nozzle, any change in restriction offered

Figure 5.12
 Open valve injection, CPT1, fuel vaporisation, 1500
 rev/min road load, 35.9 kPa manifold depression, $\lambda = 1$
 (sample sites B & C)



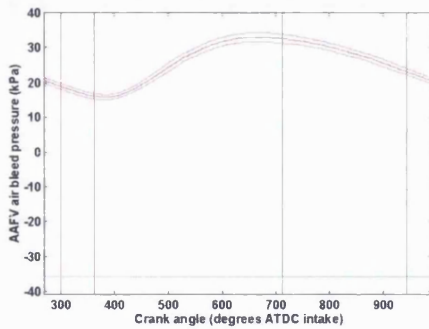
Sample site B, ± 1 std deviation
 Sample site C, ± 1 std deviation

Figure 5.13
 Open valve injection, CPT2, fuel vaporisation, 1500
 rev/min road load, 35.9 kPa manifold depression, $\lambda = 1$
 (sample sites B & C)



Sample site B, ± 1 std deviation
 Sample site C, ± 1 std deviation

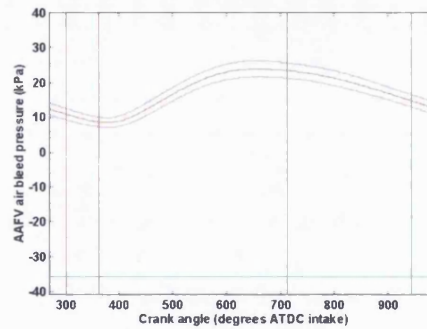
Figure 5.14
CPT1 bleed pressure, fuel vaporisation, 1500 road load,
35.9 kPa manifold depression, $\lambda = 1$



Bleed pressure (gauge), ± 1 std deviation

Manifold pressure (gauge)

Figure 5.15
CPT2 bleed pressure, fuel vaporisation, 1500 road load,
35.9 kPa manifold depression, $\lambda = 1$



Bleed pressure (gauge), ± 1 std deviation

Manifold pressure (gauge)

by the choice of CPT would affect the overall flow rate into the inlet port. Notable exceptions to this observation occurred during open valve injection conditions between IVC, $974^\circ\text{CA ATDC}_{\text{intake}}$, and $400^\circ\text{CA ATDC}_{\text{intake}}$. The UHC level increased more rapidly using CPT1 which benefitted from a bleed pressure 10 kPa higher than produced by CPT2, an increase of some 20%, see figures 5.14 & 5.15.

The level of air-assistance can be measured by the pressure drop across the AAFV exit nozzle. As such, during operation with passive air-assistance, the pressure drop is described by the difference between the manifold pressure, indicated by the light blue trace in figures containing the CPT bleed pressure trace, and the pressure upstream of the throttle, which is virtually atmospheric pressure, indicated as 0 kPa (gauge) in the figures.

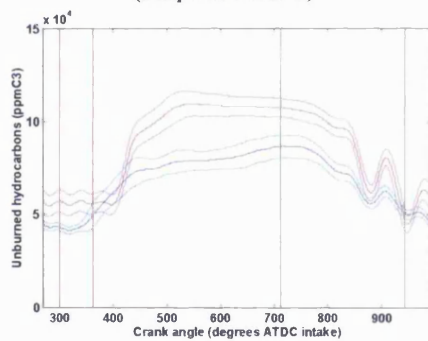
5.5.1c Intake port sampling, air-atomisation (i.e. no heat applied), cylinder pressure tapping 1 & 2

(refer to figures 5.16-5.21)

Figures 5.16 & 5.18 compare the UHC levels obtained from intake port sampling at sites B & C using CPT1 during closed and open valve injection strategies respectively. It is interesting to compare these traces from air-atomised liquid fuel spray with the traces using vapour, see figures 5.10 & 5.12. Whilst the concentration levels

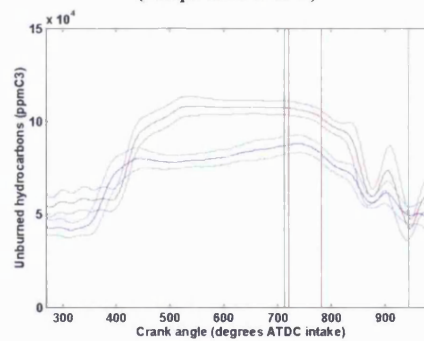
observed at each site when using vapour exhibited little disparity between 400° $ATDC_{intake}$ and IVO at $712^\circ CA_{ATDC_{intake}}$, there was a difference in UHC value of between $2-3 \times 10^4$ ppm C_3 between sites B & C when air-atomisation was used with the sample point closer to the AAFV giving the lower value of the two measurements. The effect did not occur when CPT2 was used, as was the case for the tests using vapour, and again the overall concentration levels observed with CPT2 were significantly lower than those using CPT1, see figures 5.17 & 5.19. The initial rise due to fuel efflux from the AAFV during air-atomisation tests, at around 400° $ATDC_{intake}$, was of the same order of magnitude as measured using vaporised fuel for either pressure tapping, compare figures 5.16 & 5.18 with 5.10 & 5.12 respectively. The UHC level measured in the port 30 mm upstream of the intake valve (site B)

Figure 5.16
 Closed valve injection, CPT1, air-atomisation, 1500 rev/min road load, 35.9 kPa manifold depression, $\lambda = 1$ (sample sites B & C)



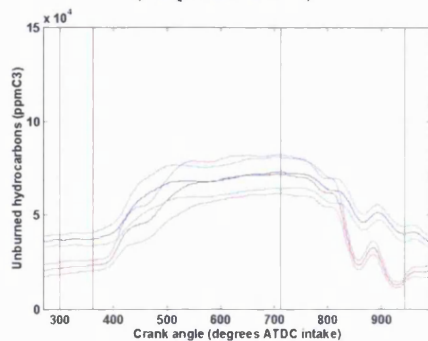
Sample site B, ± 1 std deviation
 Sample site C, ± 1 std deviation

Figure 5.18
 Open valve injection, CPT1, air-atomisation, 1500 rev/min road load, 35.9 kPa manifold depression, $\lambda = 1$ (sample sites B & C)



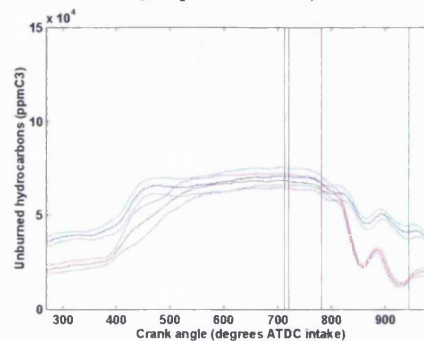
Sample site B, ± 1 std deviation
 Sample site C, ± 1 std deviation

Figure 5.17
 Closed valve injection, CPT2, air-atomisation, 1500 rev/min road load, 35.9 kPa manifold depression, $\lambda = 1$ (sample sites B & C)



Sample site B, ± 1 std deviation
 Sample site C, ± 1 std deviation

Figure 5.19
 Open valve injection, CPT2, air-atomisation, 1500 rev/min road load, 35.9 kPa manifold depression, $\lambda = 1$ (sample sites B & C)

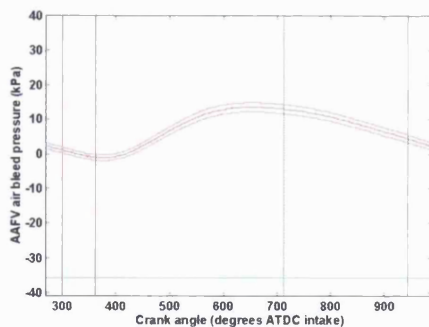


Sample site B, ± 1 std deviation
 Sample site C, ± 1 std deviation

increases beyond the initial rise observed at site C due to evaporation effects which were greater in this location because of the proximity to the combustion chamber and the consequent difference in port wall surface temperature. It must be remembered that whilst the engine was still warming up the metal temperatures at the site closest to the intake valve would be significantly warmer. Using air-atomisation, as opposed to fuel vapour, had the effect of reducing the bleed pressure. This can be seen by comparing figures 5.14 & 5.15 with 5.20 & 5.21 respectively. Previous tests, see chapter 2, table 2.3, using a rotameter to measure the air flow through the device suggested that this is due to the reduced air flow rates through the AAFV when the heating element is enabled. This reduction in flow rate is likely to be caused by the decrease in air and fuel density due to the heat transfer from the heating element as opposed to any differential expansion between the glow plug and AAFV lower body, see chapter 2. The increased restriction to the flow through the device when the heating element was enabled caused a rise of the pressure differential by approximately 40% for both CPT1 & 2, see figures 5.20 & 5.21.

Figure 5.20

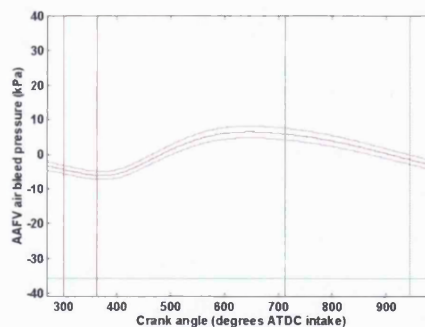
**CPT1 bleed pressure, air-atomisation, 1500 road load,
35.9 kPa manifold depression, $\lambda = 1$**



Bleed pressure (gauge), ± 1 std deviation
Manifold pressure (gauge)

Figure 5.21

**CPT2 bleed pressure, air-atomisation, 1500 road load,
35.9 kPa manifold depression, $\lambda = 1$**



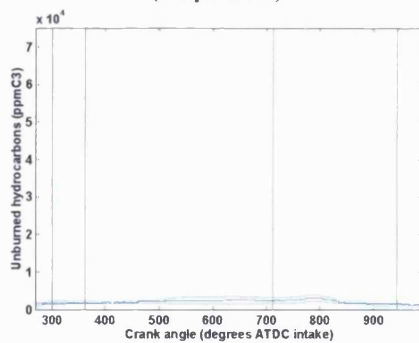
Bleed pressure (gauge), ± 1 std deviation
Manifold pressure (gauge)

5.5.1d Intake port sampling, backflow, standard, air-atomisation & vapour, atmospheric bleed

(refer to figures 5.22-5.27)

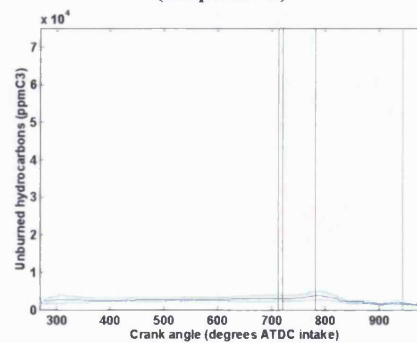
This sub-section concentrates upon the measurement of the UHC concentrations 20 mm upstream of the injector tip at location D. The most dramatic variation in the intake port fuel concentration levels was observed when comparing the AAFV, in either air-atomisation or vapour operation, with the standard 4-hole injector, see figures 5.22-5.27. UHC levels measured during the standard injector tests, figures 5.22 & 5.23, were extremely low to the extent that they fell to around the value expected for exhaust concentration measurements on a fully warm engine. By comparison the traces for both air-atomisation and vapour operation indicate UHC values which are an order of magnitude higher. Figures 5.24-5.27 show that a steady rise in UHC concentration throughout the closed valve period existed upstream of the injector when using the AAFV in either air-atomisation or fuel vaporisation modes, and this was independent of injection timing. It is attributed to continued mixing between the injected mixture and the quiescent air as well as evaporation of liquid deposits from the port walls. The two periods of backflow, i.e., during the initial valve opening and as the piston approaches $BDC_{\text{compression}}$ prior to IVC could be seen

Figure 5.22
Closed valve injection, standard injector, 1500 rev/min
road load, 35.9 kPa manifold depression, $\lambda = 1$
(sample site D)



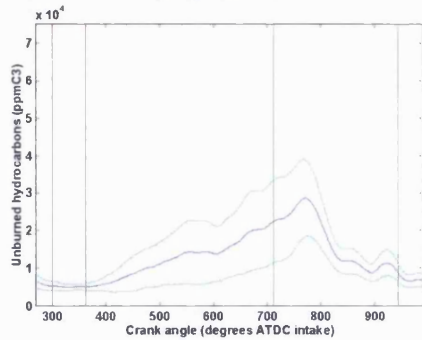
Sample site D, ± 1 std deviation

Figure 5.23
Open valve injection, standard injector, 1500 rev/min
road load, 35.9 kPa manifold depression, $\lambda = 1$
(sample site D)



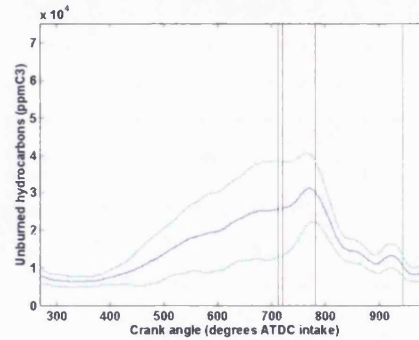
Sample site D, ± 1 std deviation

Figure 5.24
Closed valve injection, air-atomisation, 1500 rev/min
road load, 35.9 kPa manifold depression, $\lambda = 1$
(sample site D)



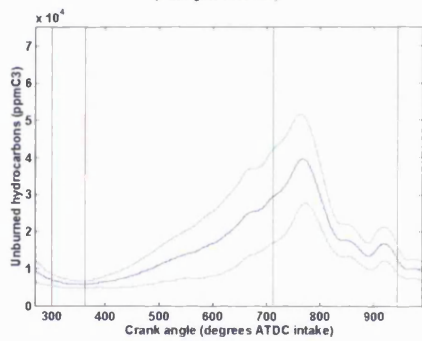
Sample site D, ± 1 std deviation

Figure 5.25
Open valve injection, air-atomisation, 1500 rev/min
road load, 35.9 kPa manifold depression, $\lambda = 1$
(sample site D)



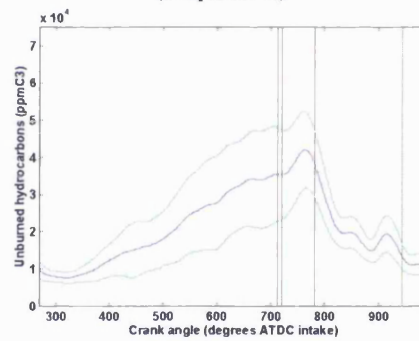
Sample site D, ± 1 std deviation

Figure 5.26
Closed valve injection, fuel vaporisation, 1500 rev/min
road load, 35.9 kPa manifold depression, $\lambda = 1$
(sample site D)



Sample site D, ± 1 std deviation

Figure 5.27
Open valve injection, fuel vaporisation, 1500 rev/min
road load, 35.9 kPa manifold depression, $\lambda = 1$
(sample site D)



Sample site D, ± 1 std deviation

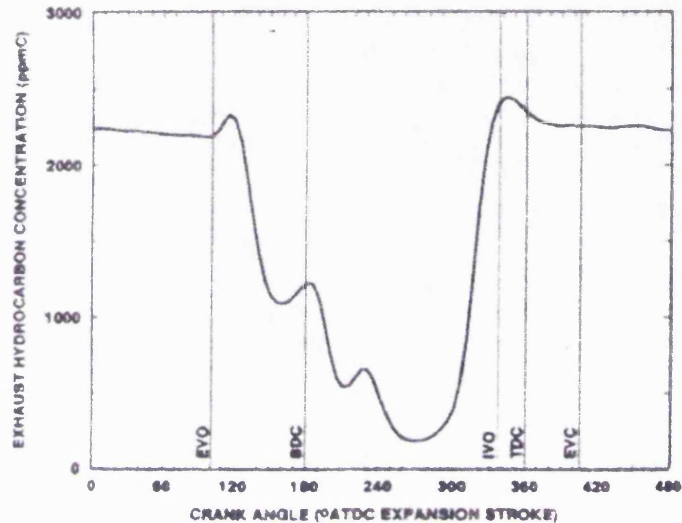
to have an effect on the UHC traces where the AAFV was used. The backflow period pre-IVC could be thought to manifest itself in three ways. Firstly the raised port temperature is likely to increase the evaporation rates from the port surfaces, secondly the physical flow of the in-cylinder mixture back into the intake port will move the entrained fuel back up the port and thirdly the mixing of the port contents should increase as a consequence of the backflow. It is suggested that these mechanisms caused the continuous rise in the concentration levels during the closed valve period mentioned earlier. The initial backflow that occurred as the intake valve opened was thought responsible for the peak in the traces that occurred just after IVO, around $760^\circ\text{CA ATDC}_{\text{intake}}$. This peak in the UHC trace was visible throughout all tests

regardless of the type of mixture preparation employed, though the effect was more pronounced during operation with the AAFV due to the greater fuel vapour concentration established prior to IVO in conjunction with the ability of the vapour to follow the air flow. The period of intake port reverse flow just after IVO carried part of the vapour cloud upstream some distance past the AAFV exit nozzle, the sampling site location being 120 mm upstream of the intake valve. When the standard injector was used the vapour concentration in the port was very much lower, see figures 5.22 & 5.23. Shin, Min & Cheng suggest that small droplets could be blown up to 200 mm back into the intake manifold dependent on operating conditions, consequently it was felt that these droplets with their surrounding vapour cloud were likely to be responsible for the small peak in the UHC trace of the standard injectors just after IVO. These droplets would tend to evaporate in the hot gas stream, and some might impact on the port walls and evaporate into the gas stream. The internal diameter of the HFRFID sampling probe was quite small (approximately 0.5 mm) as this was known to minimise the sampling of droplets rather than vapour. The output of the HFRFID is known to exhibit 'spikiness' when droplets are being sampled; this was not apparent at any stage during the testing and so it is believed that the measurements represent those of the vapour/air mixture.

5.5.2 HFRFID exhaust port sampling

Exhaust port sampling using a HFRFID is now fairly commonplace with the major characteristics having explanations attributed to them. Included here is brief summary of the main features, see figure 5.28, referring predominantly to the text by Thompson & Wallace, 1994.

Figure 5.28
Typical exhaust HFRFID trace, from Thompson & Wallace, 1994



Fast exhaust hydrocarbon concentration versus crank angle at 1800 rpm, 5.0 N-m and $\phi = 1.0$.

Final peak: The peak at 350°CA is the only characteristic that seems to have found universal agreement between researchers “typically attributed to the arrival, at the exhaust valve, of a hydrocarbon rich vortex circulating on the piston top”, Thompson & Wallace go on to state “this tumbling vortex occurs at the corner formed by the edge of the piston crown and the cylinder wall as the piston moves upwards during the exhaust stroke. Its high HC level is thought to be due to the entrainment of the piston-crevice HC laid along the cylinder wall, following the laminar top land crevice outflow, during the expansion stroke”.

The first peak: Caton, Heywood & Mendillo, 1984 suggest that the initial peak just after EVO is made up from two factors, firstly the high HC concentration of the exhaust gases from the end of the previous cycle (see above) which are only displaced at EVO, and secondly a high concentration of the initial gas flow due to crevices in the immediate vicinity of the exhaust valves, i.e., around the valve seats, head gasket and sparking plug. However, Tabaczynski, Heywood & Keck, 1972, and Elechian,

Heywood & Rife, 1977, produced results from tests where the exhaust port was purged with air between exhaust valve opening events and found that the first peak was reduced but still present. Further, Finlay *et al*, 1990, suggest that the leakage around the exhaust valve occurs during combustion/expansion allowing a small amount of UHCs into the port which would mix with the stationary gas from the end of the previous cycle.

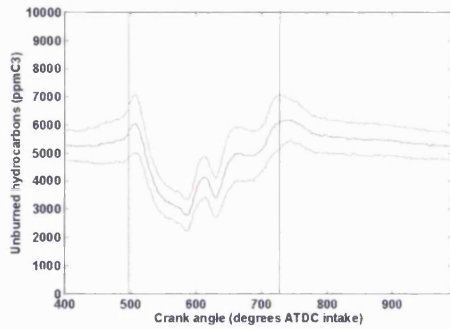
The two peaks near EVO, one at BDC, the other shortly after: During this period, the exhaust mass flow rate is moderate and the HC concentrations are relatively low and therefore only making a small contribution to the overall UHC level. However, Thompson & Wallace “found them to be affected by changes to the piston ring pack and were therefore assumed to stem from the entrainment of a portion of the piston crevice HC by the cylinder bulk gas exhaust flow”.

The valleys, predominantly at 270°CA: “represents the HC concentrations in the bulk gases least contaminated by crevice HC”. Post-combustion oxidation can reduce these valleys to very low levels.

5.5.2a Exhaust port sampling, 1500 rev/min, road load, 35.9 kPa intake pressure, standard, air-atomisation & vapour, atmospheric bleed (refer to figures 5.29-5.34)

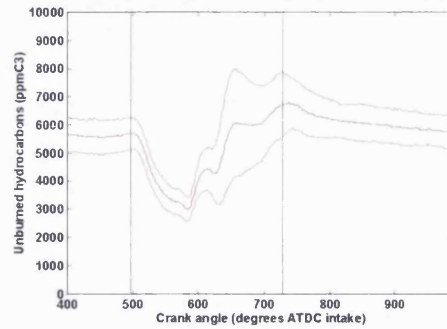
The tests revealed similar characteristics to those suggested by Thompson & Wallace with the notable exception that the valley in the UHC trace at BDC was always greater in magnitude than the valley occurring some 50°CA previously. There was surprisingly little variation in either shape or magnitude between differing mixture preparations or injection strategies. It is presumed that the excessive crevice volume created by the optical piston design was the cause of the higher than expected second peak and also the cause of the UHC levels associated with the ensuing valley.

Figure 5.29
Closed valve injection, standard injector, 1500 rev/min
road load, 35.9 kPa manifold depression, $\lambda = 1$
(sample site A)



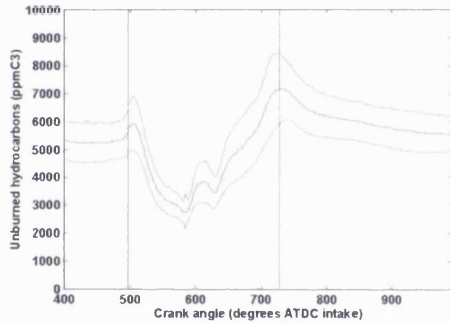
Sample site A, ± 1 std deviation

Figure 5.30
Open valve injection, standard injector, 1500 rev/min
road load, 35.9 kPa manifold depression, $\lambda = 1$
(sample site A)



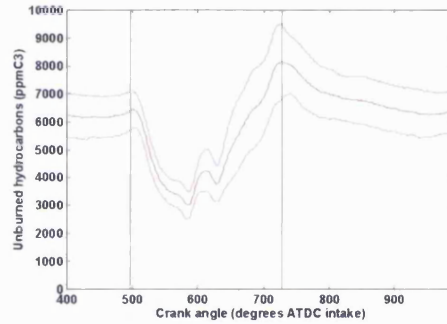
Sample site A, ± 1 std deviation

Figure 5.31
Closed valve injection, air-atomisation, 1500 rev/min
road load, 35.9 kPa manifold depression, $\lambda = 1$
(sample site A)



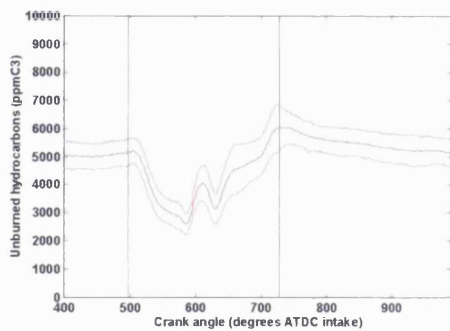
Sample site A, ± 1 std deviation

Figure 5.32
Open valve injection, air-atomisation, 1500 rev/min
road load, 35.9 kPa manifold depression, $\lambda = 1$
(sample site A)



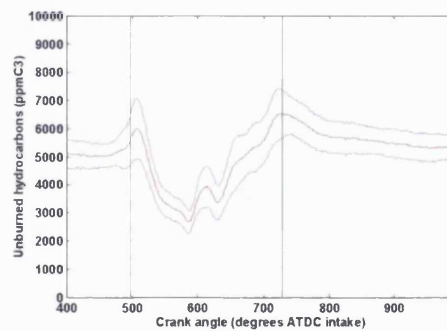
Sample site A, ± 1 std deviation

Figure 5.33
Closed valve injection, fuel vaporisation, 1500 rev/min
road load, 35.9 kPa manifold depression, $\lambda = 1$
(sample site A)



Sample site A, ± 1 std deviation

Figure 5.34
Open valve injection, fuel vaporisation, 1500 rev/min
road load, 35.9 kPa manifold depression, $\lambda = 1$
(sample site A)



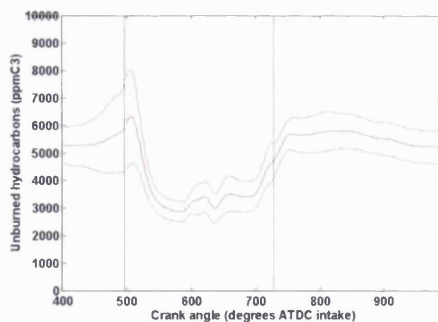
Sample site A, ± 1 std deviation

5.5.2b Exhaust port sampling, air-atomisation, cylinder pressure tapping 1 & 2 (refer to figures 5.35 & 5.36)

Again there was little variation between the UHC traces using the in-cylinder pressure tapping and those from the previous tests, see figures 5.35 & 5.36. It had been assumed that there would be a penalty for having the tapping within the combustion chamber due to the crevice volume effect that it would incur but this was not apparent. However, it is possible that any variation caused by the tapping was masked by the effects of the out-gassing from the excessively-large crevice above the top piston ring. The possibility of fuel entering the tapping during the compression/combustion process does not appear to have materialised since there is no detectable evidence to support this either from the intake or exhaust port sampling.

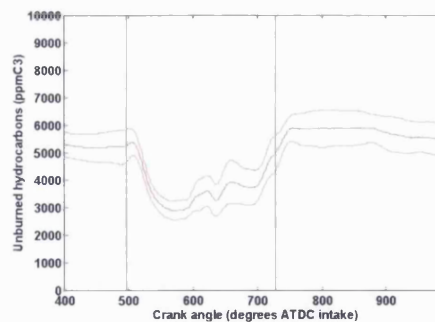
Further analysis of exhaust measurements using the HFRFID are excluded from the main body of text due to the dominant crevice volume effects.

Figure 5.35
Closed valve injection, CPT1, air-atomisation, 1500
rev/min road load, 35.9 kPa manifold depression, $\lambda = 1$
(sample site A)



Sample site A, ± 1 std deviation

Figure 5.36
Open valve injection, CPT1, air-atomisation, 1500
rev/min road load, 35.9 kPa manifold depression, $\lambda = 1$
(sample site A)



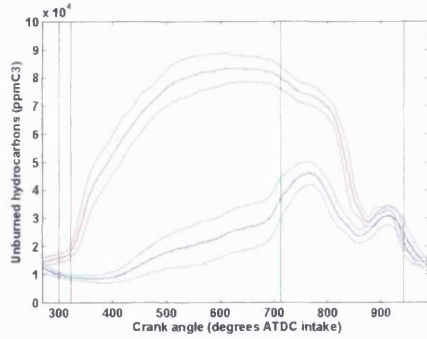
Sample site A, ± 1 std deviation

5.5.3 HFRFID intake port sampling: 800 rev/min, idle, 52.3 kPa intake pressure

5.5.3a Intake port sampling, vapour, atmospheric bleed (refer to figures 5.37-5.40)

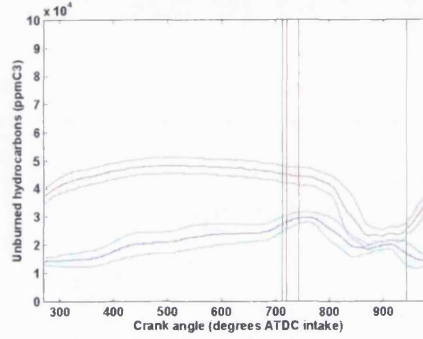
The tests at 1500 rev/min indicated fairly clearly the progression of the fuel vapour through the inlet port, however, this effect was not evident during the idle tests for either open or closed valve injection. The other pertinent variation between the idle and the 1500 rev/min road load operating condition was that HC concentrations observed when an open valve injection strategy was adopted were typically between two-thirds and one-half that of closed-valve levels. This can be observed in figures 5.37-5.40, although it is also visible in other figures. The reduction in UHC for open valve injection can be attributed to the shorter spray duration attained during the idling operation by virtue of the narrower fuel pulse width (Jackson, 1994, suggests a spray exit duration of approximately 20 ms from the AAFV during idling conditions). At 800 rev/min this corresponds to less than 100°CA and the spray duration is therefore well within the duration of the valve opening period. This means that a significant proportion of the fuel will enter the cylinder immediately instead of being held in the manifold for the next intake event. However, a fuel transport delay up to 100°CA was also predicted by Jackson, 1994, consequently, not all of the fuel would have entered the cylinder by the time that reverse displacement flow occurs, compare the UHC concentration levels just after IVC, see figures 5.37 & 5.38 also 5.39 & 5.40. Note that the conditions differ slightly from in-service calibration data in respect of manifold depression and pulse width due to the vacuum pump restrictions of the HFRFID, see Appendices A2 & A5, sections A2.1 & A5.3 respectively. A fuel pulse width of 4.65 ms was used for the idling conditions and the air flow adjusted to achieve a stoichiometric measurement using an exhaust-mounted UEGO sensor. As such the AAFV was operating outside of its design envelope for achieving complete fuel vaporisation and so some liquid deposition may occur. It is interesting to observe the decreasing concentration levels within the intake port for the open valve injection

Figure 5.37
 Closed valve injection, fuel vaporisation, 800 rev/min
 idle, 53.2 kPa manifold depression, $\lambda = 1$
 (sample sites C & D)



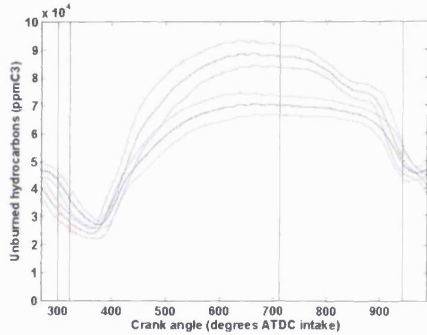
Sample site C, ± 1 std deviation
 Sample site D, ± 1 std deviation

Figure 5.38
 Open valve injection, fuel vaporisation, 800 rev/min
 idle, 53.2 kPa manifold depression, $\lambda = 1$
 (sample sites C & D)



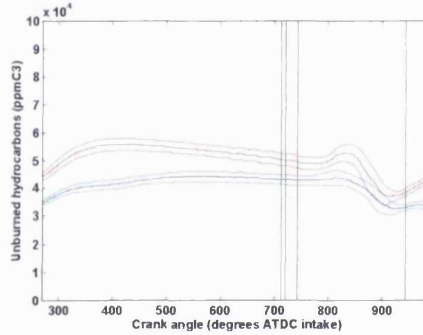
Sample site C, ± 1 std deviation
 Sample site D, ± 1 std deviation

Figure 5.39
 Closed valve injection, fuel vaporisation, 800 rev/min
 idle, 53.2 kPa manifold depression, $\lambda = 1$
 (sample sites B & C)



Sample site B, ± 1 std deviation
 Sample site C, ± 1 std deviation

Figure 5.40
 Open valve injection, fuel vaporisation, 800 rev/min
 idle, 53.2 kPa manifold depression, $\lambda = 1$
 (sample sites B & C)



Sample site B, ± 1 std deviation
 Sample site C, ± 1 std deviation

strategy during the period between TDC_{exhaust} to SOI ($360^\circ\text{CA ATDC}_{\text{intake}}$ and $720^\circ\text{CA ATDC}_{\text{intake}}$). This is thought to be due to the continued dilution of the mixture remaining in the port caused by the air being bled continuously into the port from the AAFV, see figures 5.38 & 5.40. A similar trend can be detected during closed valve injection strategy at sites B and C starting at approximately $600^\circ\text{CA ATDC}_{\text{intake}}$, see figures 5.37 & 5.39

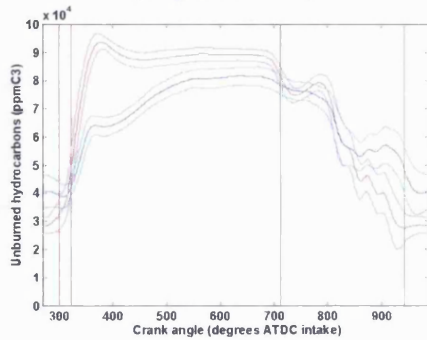
The fuel transport delay time of 20 ms estimated in chapter 2, corresponds well with all traces, though the initial fuel delivery can be seen most clearly during the open valve injection operation by the traces from sample site B, i.e. the site closest to the intake valve, see figures 5.39 & 5.40. A peak occurred during IVO approximately 50 -

100°C_A after the injector was triggered, figure 5.40. Closed valve injection exhibited a sharp rise in the HC concentration levels at around 380°C_A ATDC_{intake}, see figure 5.39, similar to that seen at 1500 rev/min (figure 5.8). However, the peak seen during the closed valve period at 1500 rev/min when using open valve injection strategy (figure 5.9) did not occur, instead the trace reached a maximum which decayed just prior to IVO, possibly due in part to the dilution from the continuous air bleed through the AAFV.

5.5.3b Intake port sampling, vapour, cylinder pressure tapping 1 & 2 (refer to figures 5.41-5.46)

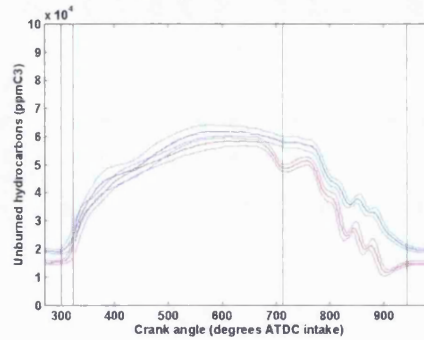
When either of the two cylinder pressure tappings were used the level of air-assistance exceeded that achieved using an atmospheric bleed for a duration of approximately 400°C_A. This was thought to be largely responsible for the fuel being purged from the device at a faster rate than when an atmospheric bleed was maintained. This can be seen by comparing the rise in UHC trace immediately after injection shown in figures 5.39 & 5.40 with 5.41, 5.42 & 5.43, 5.44. Further evidence of the fuel purge rate is implied when the mixture mechanisms within the port are considered by studying the traces recorded from sites B and C. During the closed valve period one can presume that there was little air motion within the intake port, the only agitation being provided by the constant air bleed from the AAFV. The position of the first UHC peaks in figure 5.41, soon after injection, implies a velocity of vapour from the mixture penetration into the port of around 5 m/s with a fuel transport delay of approximately 25°C_A. Assuming the fuel was rapidly purged from the AAFV then it appears logical that the volume of port gases immediately upstream of the intake valve quickly reaches an equilibrium UHC level, whilst the region around the injector takes longer to reach a plateau as it requires the richer mixture to filter back up the intake port. The constant bleed into the port through the AAFV of what was predominantly air after the injection cycle concluded provides two conflicting processes since it simultaneously reduces the mixture concentration but also prompts mixing within the port volume. The CPT pressures can be seen in figures 5.45 & 5.46.

Figure 5.41
Closed valve injection, CPT1, fuel vaporisation, 800
rev/min idle, 53.2 kPa manifold depression, $\lambda = 1$
(sample sites B & C)



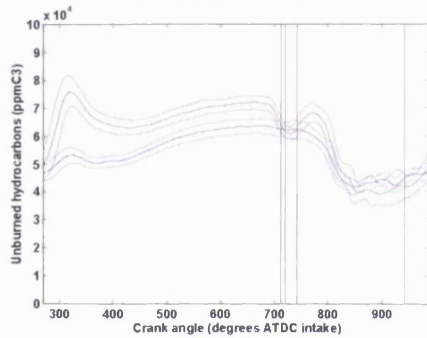
Sample site B, ± 1 std deviation
 Sample site C, ± 1 std deviation

Figure 5.42
Closed valve injection, CPT2, fuel vaporisation, 800
rev/min idle, 53.2 kPa manifold depression, $\lambda = 1$
(sample sites B & C)



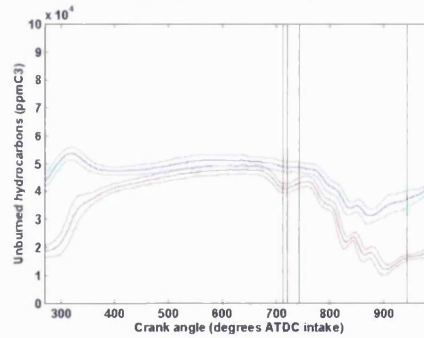
Sample site B, ± 1 std deviation
 Sample site C, ± 1 std deviation

Figure 5.43
Open valve injection, CPT1, fuel vaporisation, 800
rev/min idle, 53.2 kPa manifold depression, $\lambda = 1$
(sample sites B & C)



Sample site B, ± 1 std deviation
 Sample site C, ± 1 std deviation

Figure 5.44
Open valve injection, CPT2, fuel vaporisation, 800
rev/min idle, 53.2 kPa manifold depression, $\lambda = 1$
(sample sites B & C)



Sample site B, ± 1 std deviation
 Sample site C, ± 1 std deviation

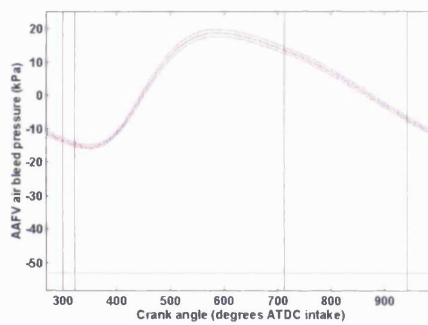
When considering an open valve injection strategy in conjunction with CPT1, see figure 5.43, the most predominant feature was the peak at sample location B which occurs at approximately 300°CA, with the rise starting shortly after IVC. The effect was evident at site C though not to the same extent, giving rise to speculation that the peak in the trace at site B occurred due to the reverse flow blow down. A stronger flow reversal exists at idling conditions due to the lower manifold pressure and the increased time for the event to occur, by comparison to the 1500 rev/min road load traces, manifests itself as a more rapid rise in the UHC concentrations post IVC.

A feature noticeable across the range of intake port measurements at 800 rev/min is the apparent mixture motion that occurs in the port during the valve open period

when compared to the 1500 rev/min road load condition. The flow reversal which occurs towards BDC_{intake} is evident throughout, but the very rapid decay noted during the higher speed tests is somewhat reduced indicating the lower flow rates into the combustion chamber due to the heavier throttling at the idle condition.

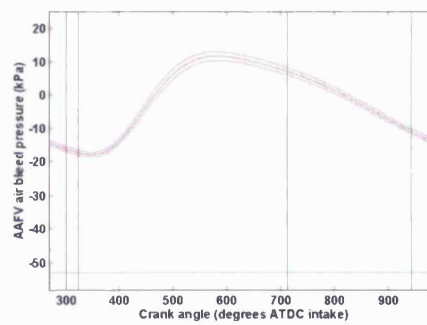
Comparing figures 5.42 & 5.44 with figures 5.41 & 5.43 respectively indicates the effect observed during the 1500 rev/min tests, see section 5.5.1b, whereby the UHC concentration levels in the inlet port are lower during CPT2 tests. Again, the reason is felt to be due to the increased air mass flow rate of the second cylinder pressure tapping.

Figure 5.45
CPT1 bleed pressure, fuel vaporisation, 800 rev/min
idle, 53.2 kPa manifold depression, $\lambda = 1$



Bleed pressure (gauge), ± 1 std deviation
Manifold pressure (gauge)

Figure 5.46
CPT2 bleed pressure, fuel vaporisation, 800 rev/min
idle, 53.2 kPa manifold depression, $\lambda = 1$



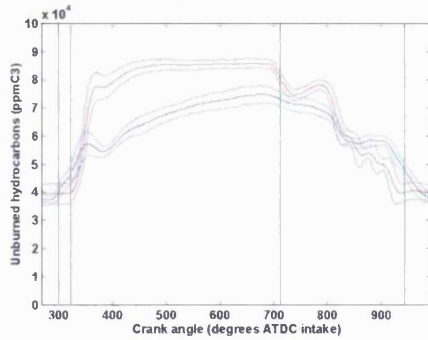
Bleed pressure (gauge), ± 1 std deviation
Manifold pressure (gauge)

5.5.4c Intake port sampling, air-atomisation, cylinder pressure tapping 1 & 2 (refer to figures 5.47-5.50)

The lower UHC concentration previously observed with the CPT2 tapping compared with the CPT1 tapping, see sections 5.5.1b, 5.5.1c & 5.5.4b, was again apparent, see figures 5.47-5.50.

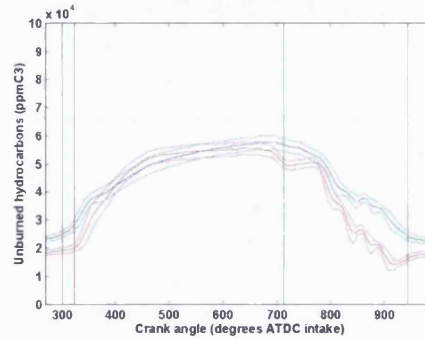
Closed valve injection using air-assistance with either cylinder pressure tapping was little different from the traces obtained operating with a vaporised mixture, compare figures 5.47 & 5.48 with 5.41 & 5.42. This characteristic was also observed

Figure 5.47
 Closed valve injection, CPT1, air-atomisation, 800
 rev/min idle, 53.2 kPa manifold depression, $\lambda = 1$
 (sample sites B & C)



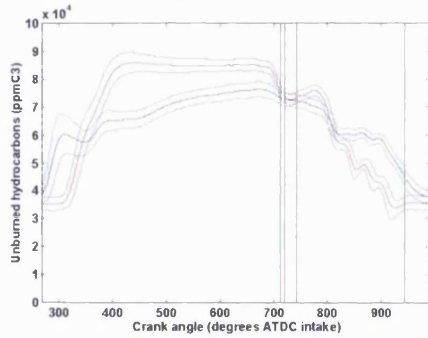
Sample site B, ± 1 std deviation
 Sample site C, ± 1 std deviation

Figure 5.48
 Closed valve injection, CPT2, air-atomisation, 800
 rev/min idle, 53.2 kPa manifold depression, $\lambda = 1$
 (sample sites B & C)



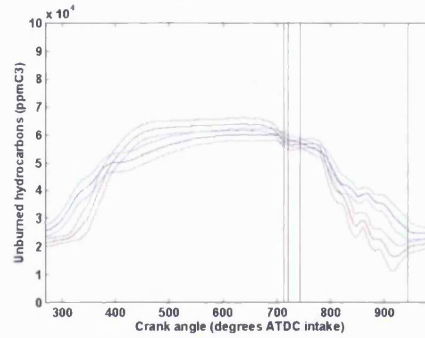
Sample site B, ± 1 std deviation
 Sample site C, ± 1 std deviation

Figure 5.49
 Open valve injection, CPT2, air-atomisation, 800
 rev/min idle, 53.2 kPa manifold depression, $\lambda = 1$
 (sample sites B & C)



Sample site B, ± 1 std deviation
 Sample site C, ± 1 std deviation

Figure 5.50
 Open valve injection, CPT1, air-atomisation, 800
 rev/min idle, 53.2 kPa manifold depression, $\lambda = 1$
 (sample sites B & C)

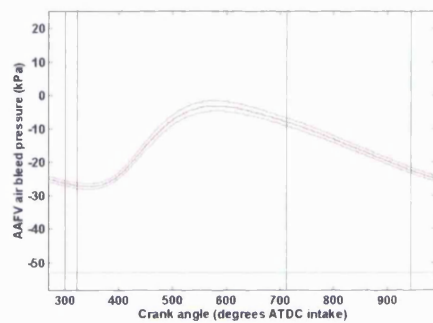


Sample site B, ± 1 std deviation
 Sample site C, ± 1 std deviation

during the 1500 road load and 1650 full load conditions, and was thought to be due to operation outside of the AAFV's vapour operating envelope. When operating at these two conditions in the vaporising mode, there is still a significant quantity of liquid fuel emitted from the AAFV, so that the 'vaporised' and 'air-atomised' mixture preparations become similar. The manifold depression was reduced at the idling condition from that of normal operating values in order that the vacuum pump of the HFRFID could produce a sufficient pressure drop between the flame chamber and the intake port. The fuel flow rate was increased correspondingly in order to maintain a stoichiometric fuelling. The injector pulse width was approximately double the value required for normal idle conditions thereby limiting the vapour concentration attainable. However, since the air supply was at a raised temperature when the

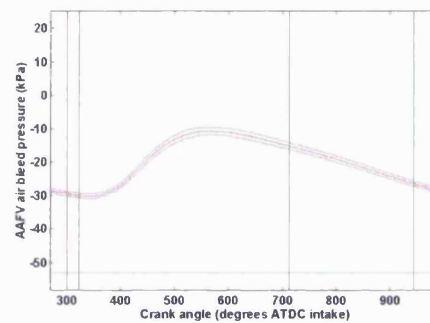
cylinder pressure tappings were used, some increase in the vapour concentration levels was expected. The above operating restrictions, in conjunction with the air-bleed conditions, ensured that little discernible difference existed between operation with either air-atomisation or vaporisation of the fuel, though the bleed pressure attained during the air-atomisation mode was reduced by approximately 40%, compare figures 5.51 & 5.52 with figures 5.45 & 5.46 respectively, as experienced during the 1500 rev/min road load tests.

Figure 5.51
CPT1 bleed pressure, air-atomisation, 800 rev/min idle,
53.2 kPa manifold depression, $\lambda = 1$



Bleed pressure (gauge), ± 1 std deviation
Manifold pressure (gauge)

Figure 5.52
CPT2 bleed pressure, air-atomisation, 800 rev/min
idle, 53.2 kPa manifold depression, $\lambda = 1$

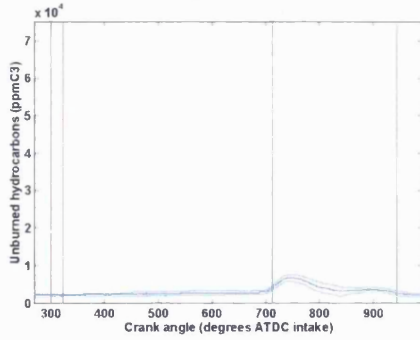


Bleed pressure (gauge), ± 1 std deviation
Manifold pressure (gauge)

5.5.5d Intake port sampling, backflow, standard, air-atomisation & vapour, atmospheric bleed (refer to figures 5.53-5.58)

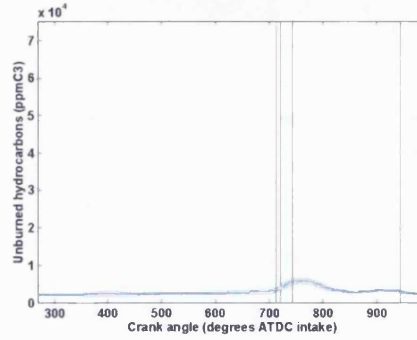
Comparing the intake port backflow during idling conditions by sampling upstream of the injector location with results taken from the tests at the 1500 rev/min condition, it becomes obvious that there was a significantly greater flow reversal with the heavier throttling at idle, compare figures 5.53-5.58 with 5.22-5.27 respectively, though the traces from the standard injectors exhibited only a slight increase. The overall trends were similar to those observed throughout the 1500 rev/min road load measurements, though the second phase of flow reversal from BDC_{intake} to IVC was more pronounced due to the lower manifold pressure. The traces exhibited a greater degree

Figure 5.53
 Closed valve injection, standard injector, 800 rev/min
 idle, 53.2 kPa manifold depression, $\lambda = 1$
 (sample site D)



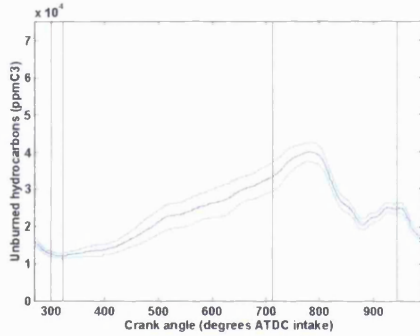
Sample site D, ± 1 std deviation

Figure 5.54
 Open valve injection, standard injector, 800 rev/min
 idle, 53.2 kPa manifold depression, $\lambda = 1$
 (sample site D)



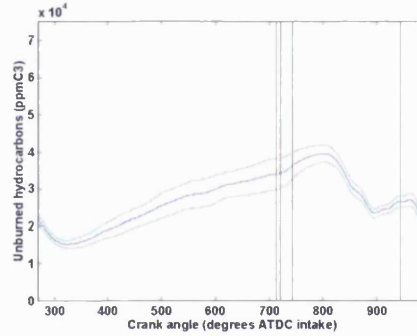
Sample site D, ± 1 std deviation

Figure 5.55
 Closed valve injection, air-atomisation, 800 rev/min
 idle, 53.2 kPa manifold depression, $\lambda = 1$
 (sample site D)



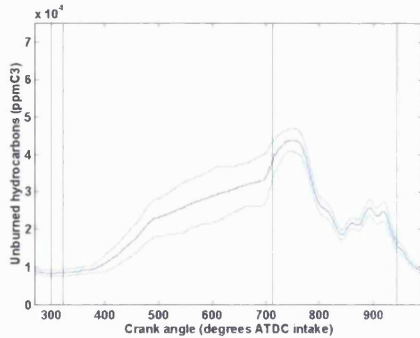
Sample site D, ± 1 std deviation

Figure 5.56
 Open valve injection, air-atomisation, 800 rev/min idle,
 53.2 kPa manifold depression, $\lambda = 1$
 (sample site D)



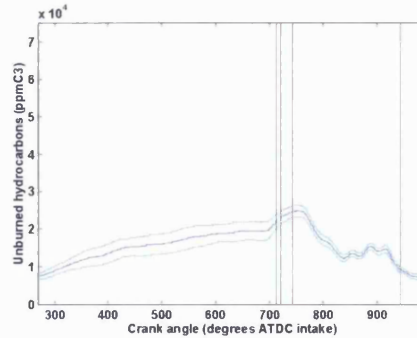
Sample site D, ± 1 std deviation

Figure 5.57
 Closed valve injection, fuel vaporisation, 800 rev/min
 idle, 53.2 kPa manifold depression, $\lambda = 1$
 (sample site D)



Sample site D, ± 1 std deviation

Figure 5.58
 Open valve injection, fuel vaporisation, 800 rev/min
 idle, 53.2 kPa manifold depression, $\lambda = 1$
 (sample site D)



Sample site D, ± 1 std deviation

of repeatability than those at the 1500 rev/min road load condition, which was thought to be due to a more clearly defined forward and reverse flow regimes. It is interesting to note that during idling conditions the trace for the UHCs using an open valve injection strategy and vaporised fuel show a reduction approaching 50% from that measured with closed valve injection, compare figure 5.58 with figure 5.57. The increased mass of fuel, as a percentage of that injected, delivered directly into the combustion chamber during the idling condition leads to a reduction in the UHC level within the intake port prior to IVO, and therefore the backflow concentration was correspondingly reduced. Since the result was not repeated during the air-atomisation tests, see figures 5.55 & 5.56, it can be inferred that the targeting of the injector was such that a significant degree of droplet impaction occurs even with the small droplet sizes associated with air-atomisation, see chapter 2.

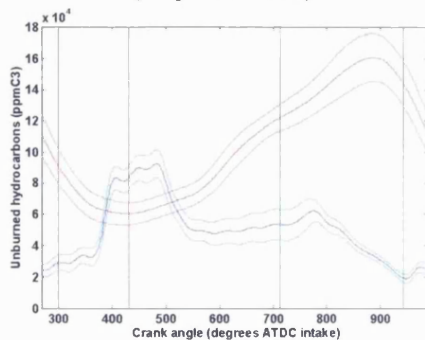
5.5.6 HFRFID intake port sampling: 1650 rev/min, full load, 0 kPa intake pressure

The purpose of this series of tests was to evaluate the ability of a cylinder pressure tapping system to purge the AAFV of fuel at a WOT test condition when passive air-assistance would not normally be available.

5.5.6a Intake port sampling, standard, air-atomisation & vapour, cylinder pressure tapping 2 (refer to figures 5.59-5.65)

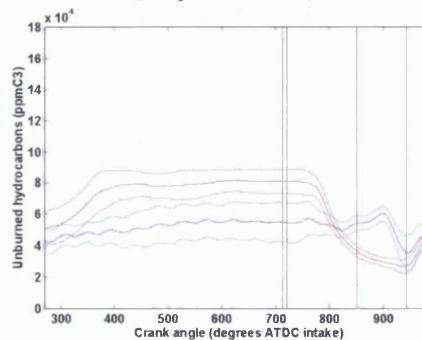
Figure 5.59 shows the fuel vapour moving as a distinct ‘packet’ past the probe at site C which is positioned 40 mm downstream of the injector tip. A delay of approximately 90°CA exists from injector trigger to fuel vapor arrival at the sample site indicating the velocity of the vapour within the intake port to be some 4.0 m/s with the duration of the moving fuel packet remaining close to that of the injector pulse width. There is no indication that the fuel vapour continued to move through the intake port in such a manner since the trace from site B, a further 30 mm downstream towards the inlet valve, did not exhibit a similar ‘square wave’ to that of

Figure 5.59
Closed valve injection, standard injector, 1650 rev/min
full load, 0 kPa manifold depression, 13.5:1 AFR
(sample sites B & C)



Sample site B, ± 1 std deviation
Sample site C, ± 1 std deviation

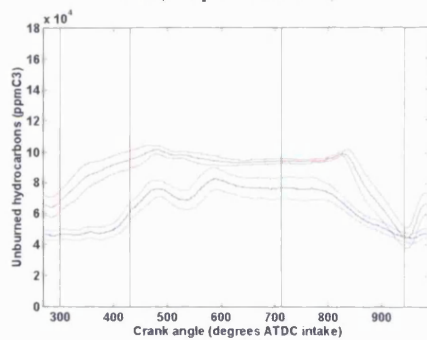
Figure 5.60
Open valve injection, standard injector, 1650 rev/min
full load, 0 kPa manifold depression, 13.5:1 AFR
(sample sites B & C)



Sample site B, ± 1 std deviation
Sample site C, ± 1 std deviation

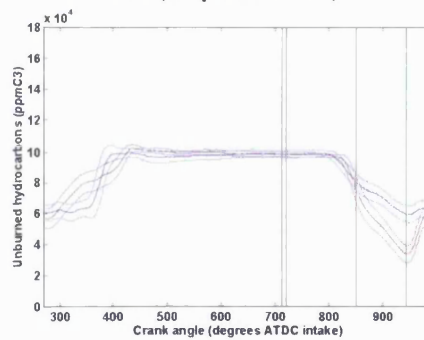
the upstream location. Instead there is a gradual rise in the UHC level which peaks towards the end of the IVO period. It is felt that a significant proportion of the injected fuel was deposited on the port floor and the port divide wall just behind the sample location C and that the slow rise in UHC levels was due to evaporation from the wall films. During open valve operation, see figure 5.60, more of the fuel is entrained into the air stream and therefore passes directly into the cylinder. However, some of the liquid fuel was likely to impact on the back of the intake valve and around the surrounding port surface without entering the combustion chamber. Fuel entering the cylinder will be made up from the liquid deposits on the port walls, fuel droplets emanating from the injector entrained in the air flow and droplets/vapour created from the process of strip atomisation during the initial valve opening period.

Figure 5.61
 Closed valve injection, CPT2, air-atomisation, 1650
 rev/min full load, 0 kPa manifold depression, 13.5:1
 AFR (sample sites B & C)



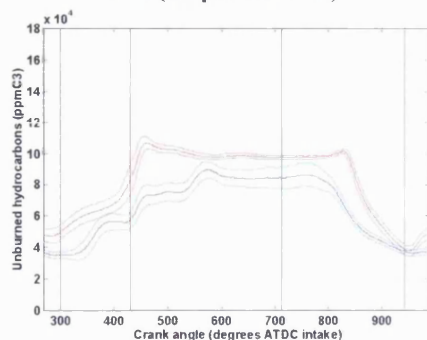
Sample site B, ± 1 std deviation
 Sample site C, ± 1 std deviation

Figure 5.62
 Open valve injection, CPT2, air-atomisation, 1650
 rev/min full load, 0 kPa manifold depression, 13.5:1
 AFR (sample sites B & C)



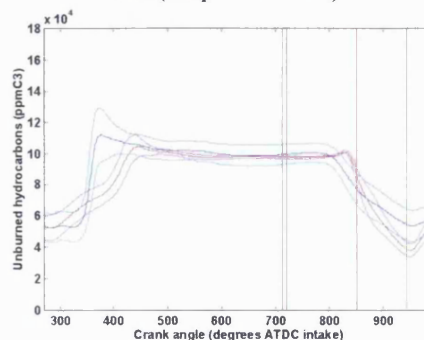
Sample site B, ± 1 std deviation
 Sample site C, ± 1 std deviation

Figure 5.63
 Closed valve injection, CPT2, fuel vaporisation, 1650
 rev/min full load, 0 kPa manifold depression, 13.5:1
 AFR (sample sites B & C)



Sample site B, ± 1 std deviation
 Sample site C, ± 1 std deviation

Figure 5.64
 Open valve injection, CPT2, fuel vaporisation, 1650
 rev/min full load, 0 kPa manifold depression, 13.5:1
 AFR (sample sites B & C)

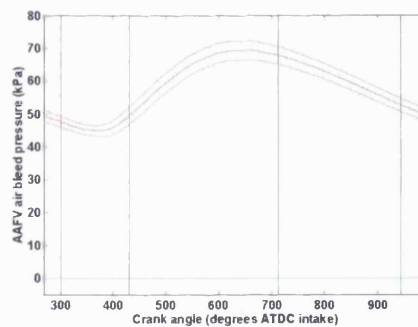


Sample site B, ± 1 std deviation
 Sample site C, ± 1 std deviation

The transport delay associated with the AAFV in either air-atomisation or vapour mode was sufficient for the bulk fuel flow to arrive at the intake valve post IVC with open valve injection strategy with the delay approaching 250°CA, or 25 ms, see figures 5.62 & 5.64. The traces at site B, closest to the intake valve exhibit very little variation between both injection strategies and AAFV mode of operation. The similarity between the UHC levels for vapour and air-atomisation mixture preparations is likely to be due to operation outside of the AAFVs vapour operating range as mentioned previously.

During wide open throttle conditions an atmospheric bleed pressure is insufficient to produce a pressure drop across the exit nozzle of the AAFV. Figure 5.65 indicates the benefit of operating with the cylinder pressure tapping at this condition with an air bleed pressure of approximately 60 kPa above the manifold pressure.

Figure 5.65
CPT2 bleed pressure, air-atomisation, 1650 rev/min full load,
0 kPa manifold depression, 13.5:1 AFR



Bleed pressure (gauge), ± 1 std deviation
 Manifold pressure (gauge)

5.6 CONCLUSIONS

Before any conclusions can be drawn from the data presented, it must be borne in mind that the HFRFID only measures the vapour concentration present around the probe, and as such it cannot indicate the time-resolved intake concentration for any mixture preparation process other than fully vaporised fuel.

Open valve injection at higher load conditions exhibited greater HC vapour residuals within the intake port. This was an indication that the time taken to purge the heated chamber of fuel was greater than the duration of forward flow past the intake valves. Care is therefore required to adopt the most appropriate injection timing strategy such that the majority of the fuel ingested is from the corresponding injection event in order to improve transient engine operation.

Backflow through the intake valve during initial valve opening had a negligible effect on the vapour concentration upstream of the injector location using standard injectors. A far more significant amount was measured when either fuel vapour or air-atomisation was adopted due to the greater propensity for the vapour cloud/small droplets to become entrained with movement of gas.

The cylinder pressure tapping produced an acceptable level of air-assistance and appeared to decrease the sensitivity to injection timing of intake port HC residuals during the closed valve period. Indications from the test programme and results from tests and modelling work by Lam, 1996, are that the reduction in cylinder pressure (and hence work) from the bleed is small. However, further work is required with accurate measurements of the brake specific fuel consumption in order to quantify any variation. The durability of the approach also requires further investigation, though the test programme revealed no deterioration of performance. Of primary concern would be a blockage of the tapping passageway due to carbon deposits, however, it is thought that careful positioning of the tapping within the cylinder and the

installation's inherent ability to operate at higher air/fuel ratios during transients and start-up would help to minimise this problem.

Concerns due to an increase of the crevice volume created by the in-cylinder restrictor and pipe work appeared to be unfounded since the exhaust UHC concentrations were unaffected. Confirmation of this would be required by testing the device on an engine fitted with a standard piston to reveal any trends masked by the crevice volume present with the optically-accessed piston and ring arrangement.

5.7 REFERENCES

- Adamczyk, A A, Kaiser, J A, Calolowsky, J A & Lavoie, G A (1981),** “An experimental study of hydrocarbon emissions from closed vessel explosions”, Eighteenth symposium (International) on combustion, The Combustion Institute, pp 1695-1702, 1981
- Brown, C N & Ladommatos, N (1991),** “The effects of mixture preparation and trapped residuals on the performance of a spark-ignition engine with air-shrouded port injectors, at low load and low speed”, D02690, Proc Instn Mech Engrs, Vol 205, 1991
- Caton, J A, Heywood, J B & Mendillo (1984),** “Hydrocarbon oxidation in a spark ignition engine exhaust port”, Combustion Science & Technology, pp 153-169, 1984
- Chen, G & Aggerwal, S K (1996),** “Unsteady multiphase intake flow in a port-injected gasoline engine”, SAE960074, International Congress & Exposition, Detroit, Feb 26-29, 1996
- Chen, C O, Cheng, W K, Heywood, J B, Martoteaux, D & Collings. N (1991),** “Intake port phenomena in a spark-ignition engine at part load”, SAE912401, International Fuels & Lubricants Meeting & Exposition, Toronto, Oct 7-10, 1991
- Ekchian, A, Heywood, J B & Rife, J M (1977),** “Time resolved measurements of the exhaust from a jet ignition pre-chamber stratified charge engine”, SAE770043

- Finlay, I C, Boam, D J, Bingham, J F & Clark, T A** (1990), "Fast response FID measurement in the exhaust port of a firing gasoline engine", SAE902165
- Horie, K, Takahasi, H & Akazaki, S** (1995), "Emissions reduction during warm-up period by incorporating a wall-wetting fuel model on the fuel injection strategy during engine starting", SAE952478
- Pontoppidan, M & Cristiani, M** (1993), "Consequences of atomisation improvement of port injectors by air-shrouding-theory and industrial solution" SAE930322, International Congress & Exposition, Detroit, March 1-5, 1993
- Shayler, P J, Colechin, M J F & Scarisbrick, A** (1996), "Fuel film evaporation and heat transfer in the intake port of an S.I. engine", SAE961120, International Congress & Exposition, Detroit, May 6-9, 1996
- Shayler, P J, Marshal, W P D & Turner** (1990), "Exhaust emissions: the influence of fuel injection system details", C394/015, Proc Instn Mech Engrs, 1990
- Shin, Y, Min, K & Cheng, W, K** (1995), "Visualisation of mixture preparation in a port-fuel injection engine during engine warm-up", SAE952481
- Tabaczynski, R J, Heywood, J B & Keck, J C** (1972), "Time-resolved measurements of hydrocarbon mass flow rate in the exhaust of a spark-ignition engine", SAE720112
- Williams P A** (1993), "Laser Diffraction particle sizing and spark-flash photography techniques for successful measurement of spark ignition engine fuel sprays", 016/93 IMechE, 1993

APPENDIX A5

A5.1 GENERAL

Three test conditions were used comprising of idle, 1500 rev/min road load and 1650 rev/min full load operation. A stoichiometric air/fuel mixture was maintained for the idle and road load tests with full load being achieved at a 13.5:1 air/fuel ratio.

A5.2 ENGINE SPECIFICATION:

Type:	Ford Zetec, 1.8 litre, 4 cylinder, 4 stroke, S.I.
Bore (mm)	80.6
Stroke (mm)	88
Swept volume (litres)	0.449
Compression ratio	9.80:1
N ^o of cylinders	1
N ^o of valves/cylinder	4 (2 inlet, 2 exhaust)

A5.2.1 Valve timing

Inlet cam	lift (mm)	8.20
	period (°CA)	234
	IVO (°CA BTDC _{inlet})	8
	IVC (°CA ABDC _{inlet})	224
exhaust cam	lift (mm)	7.79
	period (°CA)	234
	EVO (°CA BTDC _{exhaust})	44
	EVC (°CA ABDC _{exhaust})	80

A5.3 TEST DATA

A5.3.1 Engine variables

Injector timing, open valve (degrees CA BTDC _{intake})	0
Injector timing, closed valve (degrees CA BTDC _{intake})	300

A5.3.2 Idle settings

Speed (rev/min)	800
Air flow (g/s)	0.9
Fuel flow (mg/cycle)	10.1
Spark advance (degrees CA BTDC _{compression})	10
Manifold pressure (kPa absolute)	48.2

A5.3.3 Road load setting

Speed (rev/min)	1500
Air flow (g/s)	1.5
Fuel flow (mg/cycle)	14.7
Spark advance (degrees CA BTDC _{compression})	20
Manifold pressure (kPa absolute)	65.5

A5.3.4 Full load settings

Speed (rev/min)	1650
Air flow (g/s)	1.7
Fuel flow (mg/cycle)	28.3
Spark advance (degrees CA BTDC _{compression})	20
Manifold pressure (kPa absolute)	0

CHAPTER 6
INLET PORT UHC TRACES, ENGINE VS. PULSATING
FLOW RIG

CHAPTER 6

INLET PORT UHC TRACES, ENGINE VS. PULSATING FLOW RIG

6.1 INTRODUCTION

Inlet port surface and gas temperatures and the pressure drop across the intake valve will affect the fuel flow processes into the combustion chamber of an SI engine. Heat is introduced to the port via conduction through the metal surfaces from the combustion chamber and by convection from the two periods of intake backflow. The main period of intake backflow occurs during the valve overlap period at part load conditions when the inlet manifold pressure is below the predominantly atmospheric condition within the combustion chamber. A second occurrence of backflow exists just before inlet valve closure when some of the fresh charge is pushed out of the cylinder by the rising piston.

The backflow and temperature effects can be isolated through the use of a pulsating flow rig (PFR). Such a rig was constructed at UCL using the cylinder head used for the engine testing complete with the HFRFID sampling locations. The head was mounted over a dummy cylinder with the intake camshaft driven by an electric motor. The cylinder was attached to a vacuum pump arrangement which provided the manifold pressure conditions experienced during engine testing with the exception that the backflow periods were eliminated, see Miller, 1992, for a more complete description of the installation. Since there was no combustion of the intake mixture the temperature remained at ambient condition. By excluding the temperature variation and flow reversal periods useful information of their effects can be obtained by comparing FRFID results with those measured during engine testing.

It has been suggested, Shin, Min & Cheng, 1995, that the period of flow reversal during the initial valve opening can serve to atomise liquid fuel accumulated around the valve seat area and assists in the evaporation of fuel from within the port since the gases entering the inlet port will be at exhaust gas temperatures. Cheng *et al*, 1991,

measured the inlet port gas temperature using a fine-wire resistance thermometer. The inlet port gas temperature was influenced by the hot gas flow exhausted into the inlet port during the initial valve opening which created a spike in the time-temperature curve. This peaked at nearly 300°C and then fell rapidly to a minimum approaching the ambient temperature once the forward flow was established, approximately 75°CA later. The forward flow actually started before this but contained a high concentration of the expelled gas. During the closed valve period the gas temperature was affected by the displacement backflow of the higher temperature cylinder mixture which occurred just before intake valve closure. The hot residual gas temperature, approaching 140°C, was claimed to be responsible for increasing inlet port vapour concentrations, measured upstream of the injector with an FRFID during the closed valve period prior to injection.

Schurov & Collings, 1995, measured the intake port fuel vapour concentrations during start-up using an axially mounted HFRFID probe, sampling downstream of the injector, though only a handful of cycles were recorded precluding any sensible averaging or estimation of standard deviation to evaluate trends. Sampling during start-up also required that injection timing and pulsewidth were not held constant.

Shayler, Colechin & Scarisbrick, 1996, measured the convective mass transfer of fuel from the port walls by evaporation. The rate of evaporation was found to depend upon the manifold pressure, temperature and air mass flow rates. The investigation also included the effects of fuel composition and revealed that using regular gasoline at low port surface temperatures allowed the light ends to evaporate with heavier fractions remaining in the fuel film, as might be expected.

The concerns of HFRFID signal saturation through droplet deposition on the probe, voiced by Cheng *et al*, 1991, and Schurov & Collings, 1995, dictated that initial engine tests only measured UHC concentrations upstream of the injector at site D. These reservations proved to be unfounded during later investigations, perhaps due to the smaller internal diameter of the sampling probe or its orientation with respect to

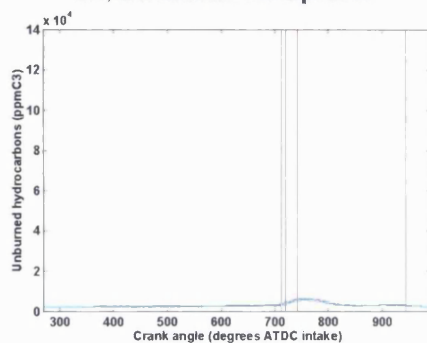
the bulk fluid motion in this work. Time constraints precluded repeating the earlier tests to provide measurements at the downstream locations and, as such, some of the engine test data refers solely to sample site D.

6.2 TEST RESULTS AND DISCUSSION

6.2.1 800 rev/min idle (53.2 kPa manifold depression), sample sites B & D (refer to figures 6.1-6.12)

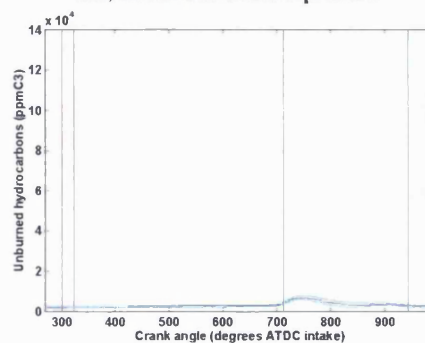
Figures 6.1 & 6.2 indicate the mixture process upstream of the injector at location D during engine testing. It can be seen that using a standard injector, the vapour concentration within the port exhibited little variation during either the backflow or injection events when compared to the other methods of mixture preparation, see figures 6.3-6.4. This trait was attributed to both the coarse atomisation experienced with the standard injectors, Jackson, 1996a, and the spray impacting the port floor around the divide wall which results in a fuel film formation within the inlet port. This fuel film will not easily evaporate in a cold engine. Secondary atomisation may produce droplets small enough to be entrained within the air stream though there was little evidence of a significant effect with the peak of the UHC concentration being some 3000-5000 ppm C₃.

Figure 6.1
Engine test
Open valve injection, standard injector, 800 rev/min
idle, 53.2 kPa manifold depression



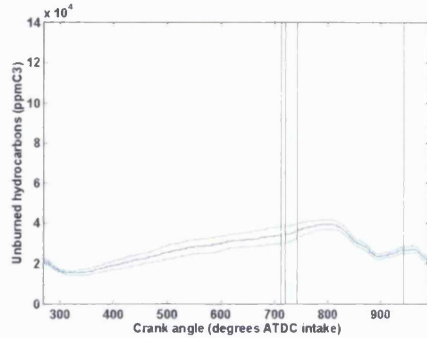
Sample site D, ± 1 std deviation

Figure 6.2
Engine test
Closed valve injection, standard injector, 800 rev/min
idle, 53.2 kPa manifold depression



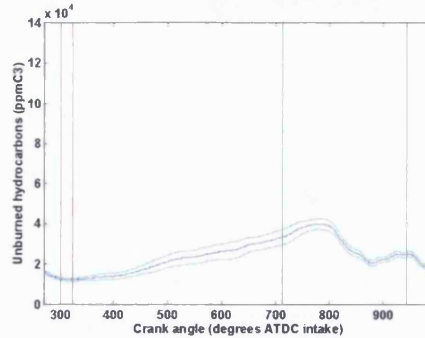
Sample site D, ± 1 std deviation

Figure 6.3
Engine test
 Open valve injection, air-atomisation, 800 rev/min
 idle, 53.2 kPa manifold depression



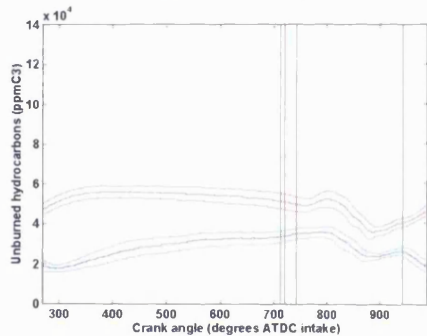
Sample site D, ± 1 std deviation

Figure 6.4
Engine test
 Closed valve injection, air-atomisation, 800 rev/min
 idle, 53.2 kPa manifold depression



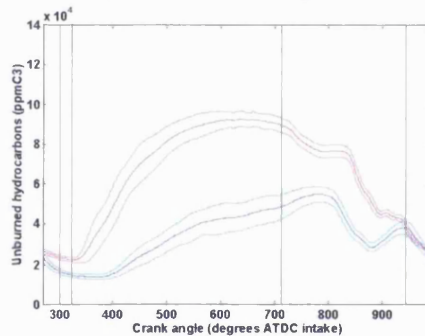
Sample site D, ± 1 std deviation

Figure 6.5
Engine test
 Open valve injection, vaporised fuel, 800 rev/min
 idle, 53.2 kPa manifold depression



Sample site D, ± 1 std deviation
 Sample site B, ± 1 std deviation

Figure 6.6
Engine test
 Closed valve injection, vaporised fuel, 800 rev/min
 idle, 53.2 kPa manifold depression

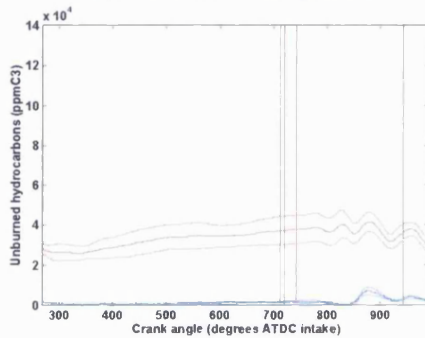


Sample site D, ± 1 std deviation
 Sample site B, ± 1 std deviation

Pulsating flow rig tests for the standard injector gave further indication of the limited evaporation that can arise within the confines of the cold intake port, see figures 6.7 & 6.8. During open valve injection a significant amount of the injected liquid fuel is ingested into the combustion chamber due to primary and secondary atomisation allowing the fuel to follow the air stream and convected fuel vapour from the established liquid film. The remaining liquid is left as deposits in the region of the port divide wall which can only propagate slowly along the port surface towards the downstream sample probe location. Closed valve injection into the quiescent inlet port ensured that the majority of the fuel spray impacted upon the port wall and in so doing provided the mechanism for the liquid to form a continuous wetted surface from the point of initial impaction to the inlet valve. The liquid film was consequently

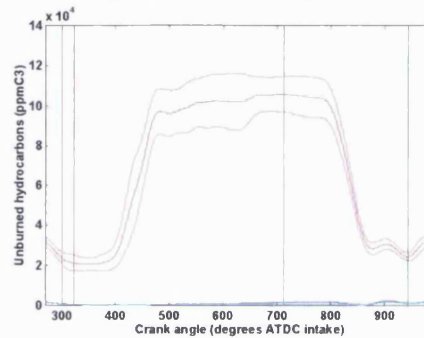
evaporating during the closed valve period close to the vicinity of the HFRFID probe at site B prompting the higher vapour measurements. The UHC trace at site B using closed valve injection during PFR tests, see figure 6.9, remained higher throughout the period from $400^{\circ}\text{CA ATDC}_{\text{intake}}$ to $850^{\circ}\text{CA ATDC}_{\text{intake}}$ ($320^{\circ}\text{CA BTDC}_{\text{intake}}$ to $130^{\circ}\text{CA ATDC}_{\text{intake}}$) than that experienced during open valve injection, see figure 6.3. An increase of some 100,000 ppm C_3 was observed within this period.

Figure 6.7
PFR test
Closed valve injection, standard injector, 800 rev/min
idle, 53.2 kPa manifold depression



Sample site D, ± 1 std deviation
Sample site B, ± 1 std deviation

Figure 6.8
PFR test
Closed valve injection, standard injector, 800 rev/min
idle, 53.2 kPa manifold depression

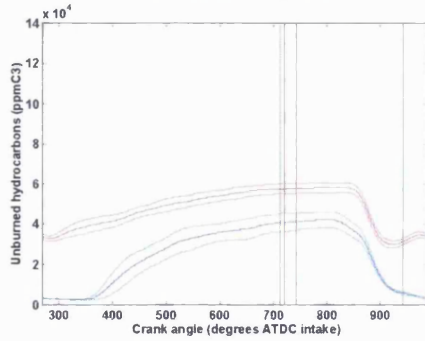


Sample site D, ± 1 std deviation
Sample site B, ± 1 std deviation

Using the AAFV in its air-atomisation mode revealed only slight variation of the UHC concentration between open and closed valve injection during both engine and PFR testing, compare figures 6.3 & 6.4 with 6.9 & 6.10 respectively. Due to relatively efficient atomisation in conjunction with a wide spray cone angle, see chapter 2, it seems likely that there was insufficient concentration of liquid deposits to form the continuous fuel filming inferred during the standard injector tests when a closed valve injection strategy was adopted. Whilst no significant variation at site D was measured, comparison with the results from tests of the standard injectors indicate an increase of the peak fuel vapour concentration at location D by an order of magnitude during both engine and PFR tests, compare figures 6.3, 6.4, 6.8 & 6.9 with 6.1, 6.2, 6.7 & 6.8 respectively.

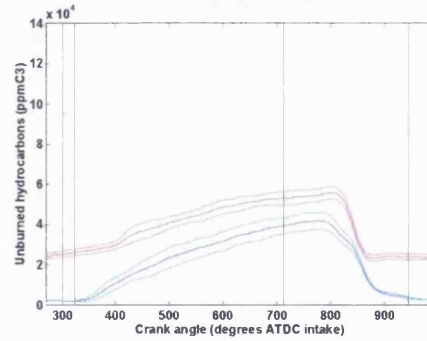
The UHC concentration measurements at site D using air-atomisation showed that from half way through the open inlet valve event, 875°CA (155°CA) $\text{ATDC}_{\text{intake}}$, to approximately $350^{\circ}\text{CA ATDC}_{\text{intake}}$, the engine traces indicated a value approaching

Figure 6.9
PFR test
Open valve injection, air-atomisation, 800 rev/min idle,
53.2 kPa manifold depression



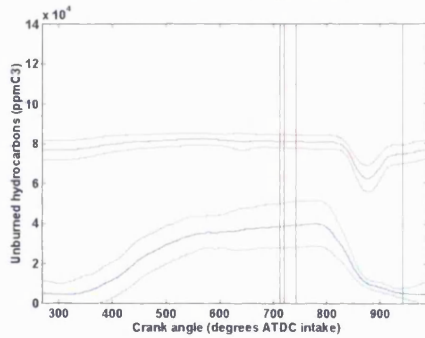
Sample site D, ± 1 std deviation
Sample site B, ± 1 std deviation

Figure 6.10
PFR test
Closed valve injection, air-atomisation, 800 rev/min
idle, 53.2 kPa manifold depression



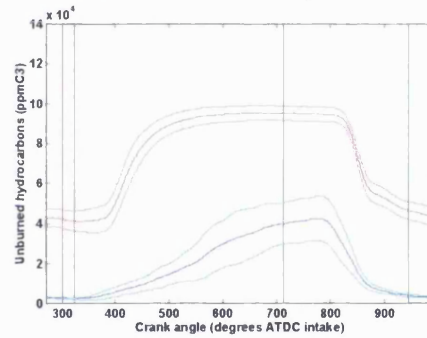
Sample site D, ± 1 std deviation
Sample site B, ± 1 std deviation

Figure 6.11
PFR test
Open valve injection, vaporised fuel, 800 rev/min idle,
53.2 kPa manifold depression



Sample site D, ± 1 std deviation
Sample site B, ± 1 std deviation

Figure 6.12
PFR test
Closed valve injection, vaporised fuel, 800 rev/min
idle, 53.2 kPa manifold depression



Sample site D, ± 1 std deviation
Sample site B, ± 1 std deviation

20,000 ppm C_3 higher than the equivalent PFR trace, see figures 6.3 & 6.10. The period over which the raised concentration manifested itself suggests the cause to be overlap backflow, pushing the most recently ingested air-fuel mixture back into the inlet port along with the increase of the port wall surface and gas temperatures raising the rate of evaporation, these mechanisms being unavailable during the PFR tests. A continuous rise of UHC concentration from 350°CA $ATDC_{intake}$ to 900°CA $ATDC_{intake}$ (370°CA $BTDC_{intake}$ to 180°CA $ATDC_{intake}$) was present during both engine and PFR tests using either open or closed valve injection, see figures 6.3, 6.4, 6.9 & 6.10. Two reasons are suggested. Firstly, since the AAFV bleeds air continually into the intake manifold, constant agitation of the mixture inside the inlet port occurs with the possibility of recirculation within the manifold promoting mixing

of air and fuel vapour. Secondly, because of the targeting imposed by the injector mounting point some liquid deposition would occur realising a significantly higher surface area to volume ratio, due to the extent of atomisation and wide spray cone, than achieved using the standard injector and increase the rate of evaporation from the wetted surfaces. In reality both the above mentioned mechanisms were likely to occur and are felt to be responsible for the rise in UHC during the closed valve period at both sample sites for engine and PFR traces.

Evidence to support the hypothesis of mixture dispersion within the port due to the constant air bleed, postulated above, exists from the vaporised fuel traces, see figures 6.5, 6.6, 6.11 & 6.12. The characteristic UHC concentrations measured upstream of the injector location, site D, using vaporised fuel exhibited similar trends to those identified during atomised mixture preparation. Comparison of the engine and pulsating flow rig tests indicates the effects of the backflow period during intake valve closure on sample site B, some 30 mm upstream of the inlet valve, compare trace for site B in figures 6.5 & 6.6 with that shown in figures 6.11 & 6.12. The vapour's ability to follow the displacement backflow air motion appears to lower the fuel vapour concentration at the downstream sample location, site B, during the initial valve opening, from $700^{\circ}\text{CA ATDC}_{\text{intake}}$ to $800^{\circ}\text{CA ATDC}_{\text{intake}}$ ($20^{\circ}\text{CA BTDC}_{\text{intake}}$ to $80^{\circ}\text{CA ATDC}_{\text{intake}}$). Propagation of the vapour back up the intake port entrained within the backflow during engine tests caused an increase of the UHC level at site D, upstream of the injector, by approximately 20,000 ppm C_3 from $850^{\circ}\text{CA ATDC}_{\text{intake}}$ to $400^{\circ}\text{CA ATDC}_{\text{intake}}$ ($130^{\circ}\text{CA ATDC}_{\text{intake}}$ to $320^{\circ}\text{CA BTDC}_{\text{intake}}$) compared to the PFR results, compare figures 6.5 & 6.6 with 6.11 & 6.12.

**6.2.2 1500 rev/min road load (35.9 kPa manifold depression),
sample sites B & D
(refer to figures 6.13-6.24)**

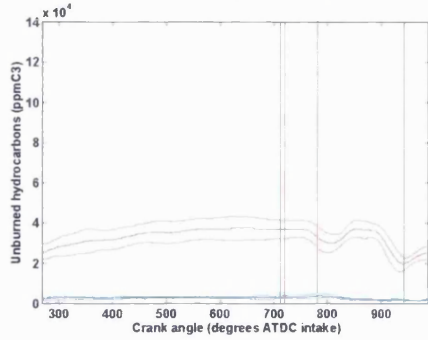
Mixture preparation during closed valve injection with the standard fuel system exhibited UHC peaks of similar magnitudes for both the PFR and engine tests, see

figures 6.20 & 6.14 respectively. The standard fuel system is likely to promote fuel entry into the combustion chamber as droplets, vapour and liquid from the wall film. During pulsating flow rig testing the contribution from the wall film may be significantly increased due predominantly to the absence of the hot port surfaces and to a lesser extent the lack of hot backflow gases. If the wall wetting was to an extent that films and rivulets were established, they may have proceeded towards the inlet valve unabated with little evaporation due to the suppressed port temperatures experienced during PFR tests. The UHC trace from the engine tests at site B during the closed valve period indicated that the fuel film could not establish itself on the hot port surface to the same degree as maintained throughout the pulsating flow rig tests and consequently fuel evaporation was partially hindered.

Tests of the standard fuel system during open valve injection revealed higher vapour concentrations throughout the pulsating flow rig tests than observed during sampling from the running engine. It had been presumed that the raised inlet port surface temperatures of the engine tests would encourage greater rates of evaporation and incur higher vapour concentrations, however, comparison of figures 6.14 & 6.20 indicate that this was not the case. Shayler, Colechin & Scarisbrick's investigation of fuel film evaporation within the intake port, using the same make and model of cylinder head as tested here, suggested that it was possible to evaporate all of the deposited fuel at the lower speed/fuel flow rates if the surface temperature was high enough. During engine tests the temperature immediately around the inlet valve approached 90°C. This temperature was felt to be sufficient to vaporise a significant proportion of the injected fuel which, due to the injection timing, will be carried immediately into the combustion chamber with little being sampled by the FRFID probe due to its location. Whilst complete drying out of the port surface was felt to be unlikely, the reduction of liquid mass accumulated on the wall around the intake valve was thought to be sufficient to lessen the vapour concentration during the closed valve period. A significant volume of the fuel deposition within the intake port during the pulsating flow tests will tend to remain in the liquid state, adhered to the port surface throughout the cycle. The wetted surface around the inlet valve will

Figure 6.13
Engine test

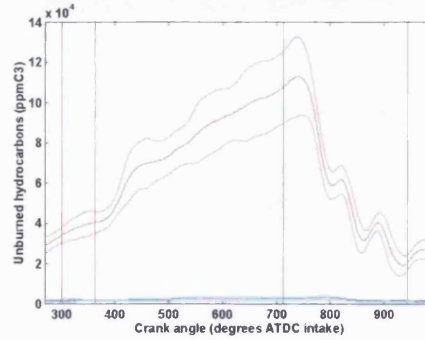
Open valve injection, standard injector, 1500 rev/min
road load, 35.9 kPa manifold depression



Sample site D, ± 1 std deviation
Sample site B, ± 1 std deviation

Figure 6.14
Engine test

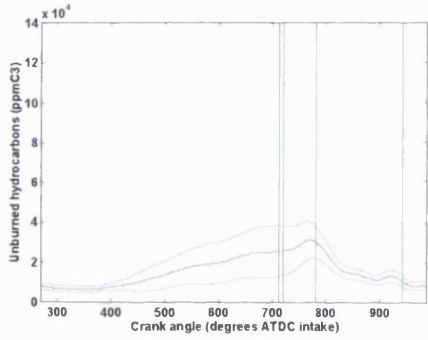
Closed valve injection, standard injector, 1500 rev/min
road load, 35.9 kPa manifold depression



Sample site D, ± 1 std deviation
Sample site B, ± 1 std deviation

Figure 6.15
Engine test

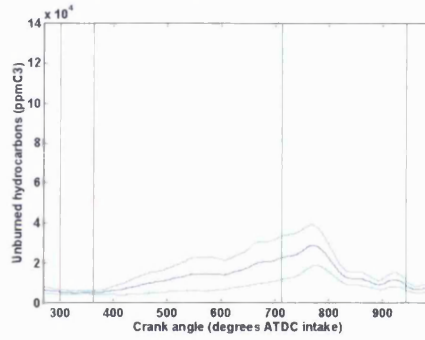
Open valve injection, air-atomisation, 1500 rev/min
road load, 35.9 kPa manifold depression



Sample site D, ± 1 std deviation

Figure 6.16
Engine test

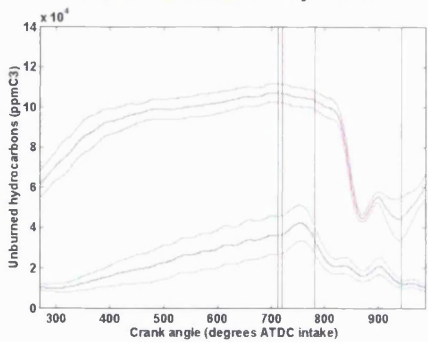
Closed valve injection, air-atomisation, 1500 rev/min
road load, 35.9 kPa manifold depression



Sample site D, ± 1 std deviation

Figure 6.17
Engine test

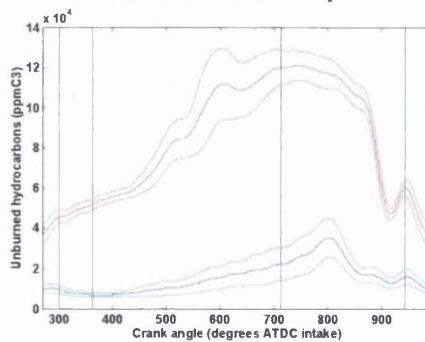
Open valve injection, vaporised fuel, 1500 rev/min road
load, 35.9 kPa manifold depression



Sample site D, ± 1 std deviation
Sample site B, ± 1 std deviation

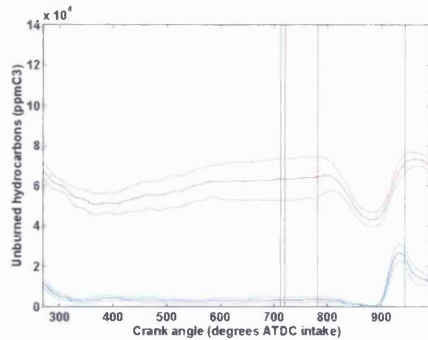
Figure 6.18
Engine test

Closed valve injection, vaporised fuel, 1500 rev/min
road load, 35.9 kPa manifold depression



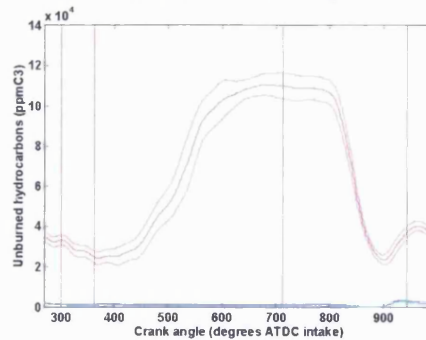
Sample site D, ± 1 std deviation
Sample site B, ± 1 std deviation

Figure 6.19
PFR test
Open valve injection, standard injector, 1500 rev/min
road load, 35.9 kPa manifold depression



Sample site D, ± 1 std deviation
 Sample site B, ± 1 std deviation

Figure 6.20
PFR test
Closed valve injection, standard injector, 1500 rev/min
road load, 35.9 kPa manifold depression



Sample site D, ± 1 std deviation
 Sample site B, ± 1 std deviation

evaporate albeit at a relatively slow rate due to the suppressed temperature. The wet port surface encountered during the PFR tests and the drying out of the port during engine tests are suggested as the reasons for the characteristic vapour concentration levels experienced when the standard fuel injector is employed.

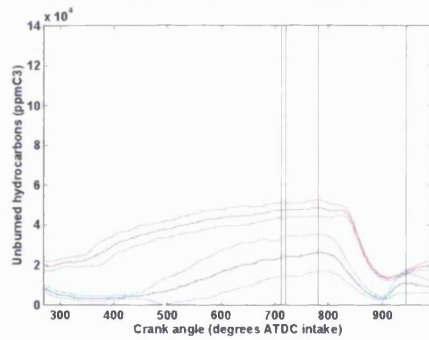
It is worth mentioning that although the PFR tests are able to match the mean engine manifold pressure and air flow rates, each will exhibit different characteristic traces with respect to time expressed on a crank angle scale. The air flow velocity within the port will experience periods of backflow on the engine if throttling is applied, whilst the pulsating flow rig only allows forward motion.

Comparison of the UHC trace between the AAFV using air-atomisation and with fuel vaporisation during the PFR tests, compare figures 6.21 & 6.22 with 6.23 & 6.24 respectively, indicates little difference at the sample site upstream of the injector location, site D. The HC concentration at site B, 30 mm upstream of the inlet valve, however, was greater by 50% at the point of IVO when the vaporiser was employed, see figures 6.21-6.24. The change in peak UHC concentrations was similar to the results obtained at the idle condition.

The principal difference between engine and the PFR tests using a vaporised mixture was that the engine tests exhibited increased UHC concentrations of the order of 75-

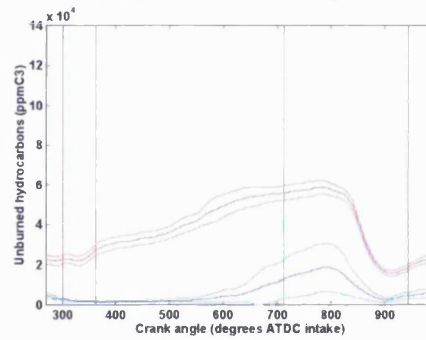
100% greater than those measured on the PFR, compare figures 6.17 & 6.18 with 6.23 & 6.24 respectively. Justification for the higher level of UHC measured during the engine tests can be attributed to the higher metal and inlet port gas temperatures and the fact that at the test condition some fuel will remain in the liquid state, Jackson, 1996b. Engine data was collected during the warm-up period of operation, i.e., the first 2-3 minutes, where the metal temperatures around the cylinder head increased from approximately 60°C to around 90°C. The elevated inlet port temperatures are exacerbated by the operating condition which promoted hot exhaust gas backflow into the port during the initial valve opening which exerts a secondary effect on the rate of evaporation and therefore fuel vapour concentration.

Figure 6.21
PFR test
Open valve injection, air-atomisation, 1500 rev/min
road load, 35.9 kPa manifold depression



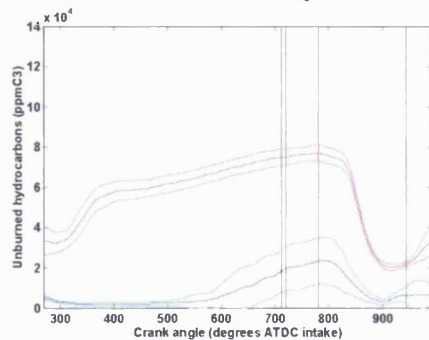
Sample site D, ± 1 std deviation
Sample site B, ± 1 std deviation

Figure 6.22
PFR test
Closed valve injection, air-atomisation, 1500 rev/min
road load, 35.9 kPa manifold depression



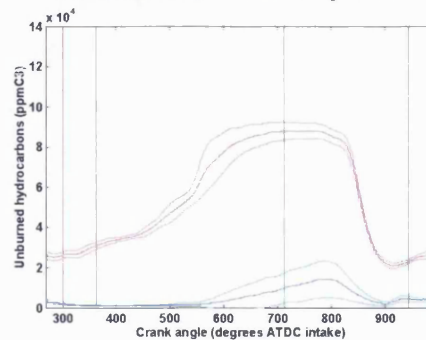
Sample site D, ± 1 std deviation
Sample site B, ± 1 std deviation

Figure 6.23
PFR test
Open valve injection, vaporised fuel, 1500 rev/min road
load, 35.9 kPa manifold depression



Sample site D, ± 1 std deviation
Sample site B, ± 1 std deviation

Figure 6.24
PFR test
Closed valve injection, vaporised fuel, 1500 rev/min
road load, 35.9 kPa manifold depression



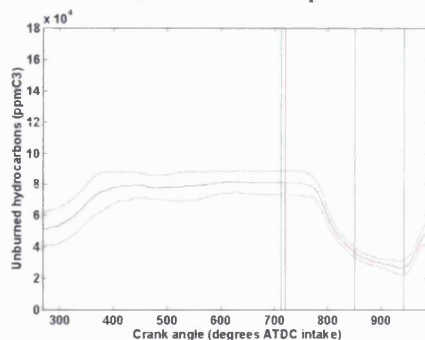
Sample site D, ± 1 std deviation
Sample site B, ± 1 std deviation

6.2.3 1650 rev/min full load (0 kPa manifold depression), sample sites B & D (refer to figures 6.25-6.36)

Comparison of measurements from the pulsating flow rig with engine results using the standard fuel system at the full load condition indicates that the raised inlet port temperature experienced during engine tests does not produce the drying out phenomenon experienced during the 1500 rev/min, open valve injection operating condition, see figures 6.25 & 6.31. The quantity of fuel injected per cycle, approximately 30 mg, was sufficient to maintain the wetted surface throughout the open valve period, whilst the temperature of the surrounding area ensures the vapour concentration exceeds that measured during pulsating flow rig tests.

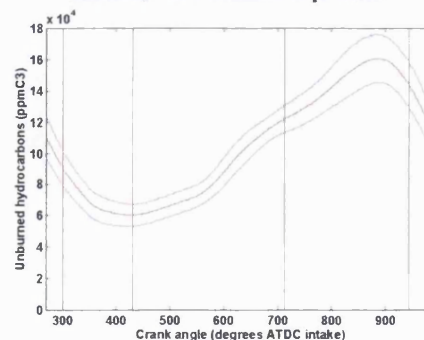
Closed valve injection indicates the effect of the inlet port temperature when sufficient residence time exists in conjunction with the backflow just prior to inlet valve closure by the steady increase of UHC concentration measured during engine testing, figure 6.26. Since a very high concentration of fuel vapour was present during the induction stroke of the engine tests, this period of backflow serves to reintroduce a proportion of the vapour back into the intake port, a mechanism which was clearly not available during pulsating flow rig operation, see figures 6.26 & 6.32.

Figure 6.25
Engine test
Open valve injection, standard injector, 1650 rev/min
full load, 0 kPa manifold depression



Sample site B, ± 1 std deviation

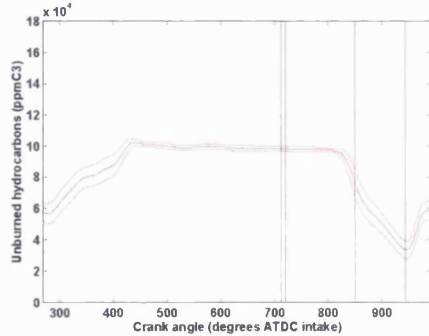
Figure 6.26
Engine test
Closed valve injection, standard injector, 1650 rev/min
full load, 0 kPa manifold depression



Sample site B, ± 1 std deviation

Figure 6.27
Engine test

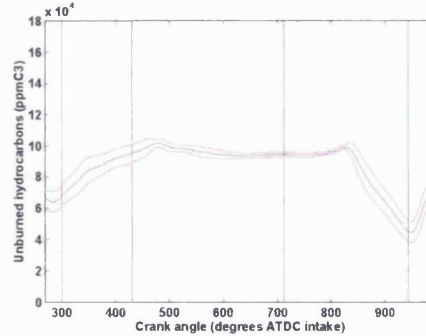
Open valve injection, air-atomisation, 1650 rev/min full load, 0 kPa manifold depression



Sample site B, ± 1 std deviation

Figure 6.28
Engine test

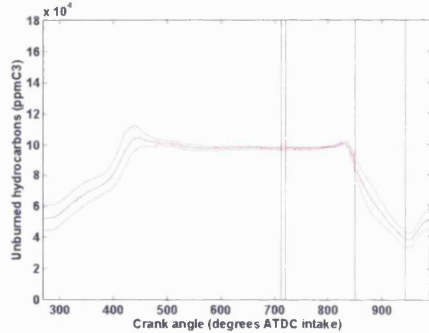
Closed valve injection, air-atomisation, 1650 rev/min full load, 0 kPa manifold depression



Sample site B, ± 1 std deviation

Figure 6.29
Engine test

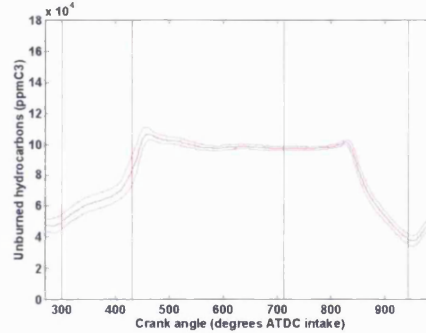
Open valve injection, vaporised fuel, 1650 rev/min full load, 0 kPa manifold depression



Sample site B, ± 1 std deviation

Figure 6.30
Engine test

Closed valve injection, vaporised fuel, 1650 rev/min full load, 0 kPa manifold depression

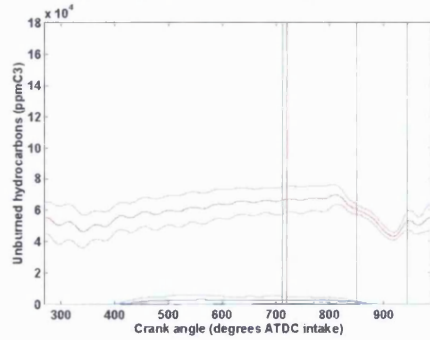


Sample site B, ± 1 std deviation

The predominantly atmospheric pressure conditions within the intake manifold experienced at WOT dictate that the air supplied to the AAFV was required to be at a pressure substantially greater than atmospheric. The cylinder pressure tapping, as described in chapters 5, was used throughout the engine tests whereas the pulsating flow rig employed a regulated external pressurised air supply. The supply pressure was chosen to match as closely as possible that which was measured during engine testing, however, the temperature could not be simulated and as a consequence the density differs between the two tests. It is assumed that though the density will affect the fuel vapour dilution within the intake port its effect will be negligible by comparison to the bleed air temperature. The assumption appears to be vindicated by figures 6.32, 6.34 & 6.36, where the HC concentrations can be seen to rise very quickly just after the injector was triggered, between 400°CA & 500°CA ATDC_{intake},

Figure 6.31
PFR test

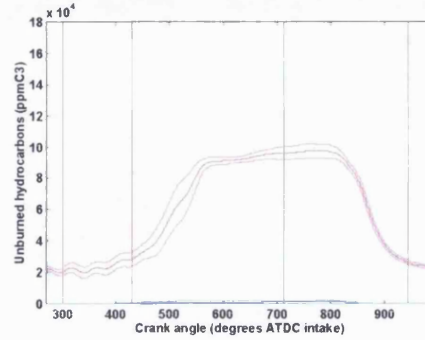
Open valve injection, standard injector, 1650 rev/min
full load, 0 kPa manifold depression



Sample site D, ± 1 std deviation
Sample site B, ± 1 std deviation

Figure 6.32
PFR test

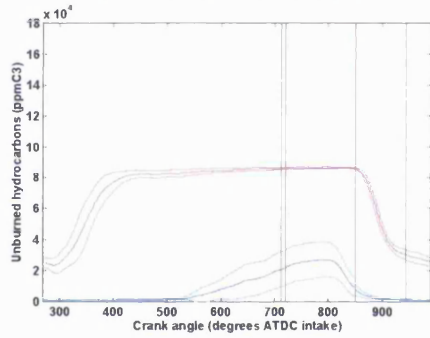
Closed valve injection, standard injector, 1650 rev/min
full load, 0 kPa manifold depression



Sample site D, ± 1 std deviation
Sample site B, ± 1 std deviation

Figure 6.33
PFR test

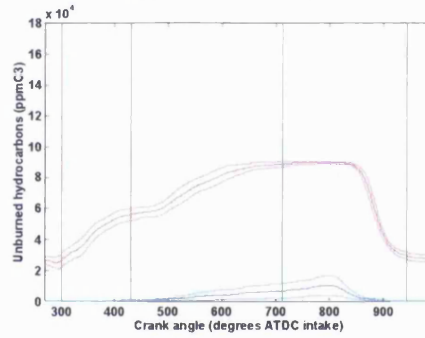
Open valve injection, air-atomisation, 1650 rev/min full
load, 0 kPa manifold depression



Sample site D, ± 1 std deviation
Sample site B, ± 1 std deviation

Figure 6.34
PFR test

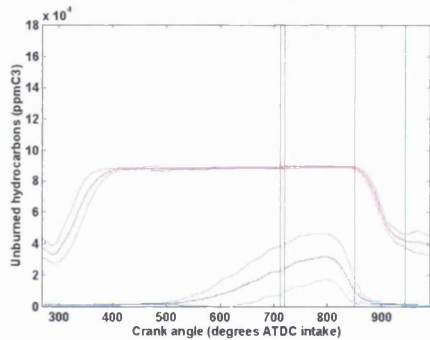
Closed valve injection, air-atomisation, 1650 rev/min
full load, 0 kPa manifold depression



Sample site D, ± 1 std deviation
Sample site B, ± 1 std deviation

Figure 6.35
PFR test

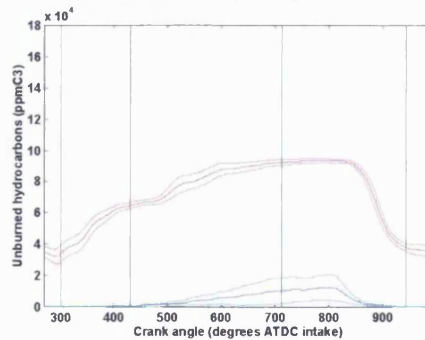
Open valve injection, vaporised fuel, 1650 rev/min full
load, 0 kPa manifold depression



Sample site D, ± 1 std deviation
Sample site B, ± 1 std deviation

Figure 6.36
PFR test

Closed valve injection, vaporised fuel, 1650 rev/min full
load, 0 kPa manifold depression



Sample site D, ± 1 std deviation
Sample site B, ± 1 std deviation

when the cylinder pressure tapping was used. The rate of increase of UHC concentration was significantly impaired over the same period when air at approximately ambient temperature was supplied for the pulsating flow rig tests.

The effect of the raised inlet port temperature was demonstrated by a 25% increase of UHC concentrations during engine testing using the AAFV when compared to the PFR results.

6.3 CONCLUSIONS

The comparison of engine and PFR tests indicated the importance of the port surface temperature and the backflow effects in determining both the magnitude and location of fuel vapour in the inlet port. Using the improved mixture preparation processes of either vaporised fuel or air-atomised fuel, the periods of intake port backflow were able to push some of the vapour/small droplets upstream beyond the fuel injector location. The coarse spray of the standard injector and the impaction of the fuel tended to reduce the backflow of fuel considerably. It was apparent that the air bleed incorporated into the AAFV design served to agitate the intake port mixture during the closed valve period due to the constant air flow through the device again leading to the backflow of fuel with the AAFV.

Engine testing at 1500 rev/min road load with an open-valve injection timing had revealed lower UHC concentrations than obtained during the PFR tests, measured at the intake valve sampling point with standard injectors. This suggested that the fuel film was substantially reduced due to the increased port surface temperature around the inlet valve. It was also an indication of the mixture problem likely to occur during operation from a cold-start.

One of the benefits of the cylinder pressure tapping is that the temperature of the bleed air through the AAFV is increased and the effects of this were particularly apparent in the increase in port vapour concentration measured at the 1650 rev/min WOT condition. This, and the raised port temperature, provided a 25% increase in UHC concentrations over the PFR tests.

6.4 REFERENCES

- Cheng, C O, Cheng, W K, Heywood, J B, Marteaux, D & Collings, N (1991),**
“Intake port phenomena in a spark-ignition engine at part load”, SAE912401
- Jackson, S D (1996a),** “Development of a fuelling system to reduce cold-start hydrocarbon emissions in an SI engine”, SAE961119
- Jackson, S D (1996b),** “Intake port vapour concentrations sampling using a Cambustion fast response flame ionisation detector”, University College London internal report, October 1996
- Miller, M J (1992),** “Mixture preparation in automotive spark-ignition engines”, PhD Thesis, Department of Mechanical Engineering, University College London
- Schurov, S M & Collings, N (1995),** “An experimental investigation of fuel transport in a port injected engine”, SAE952485
- Shayler, P J, Colechin, M J F & Scarisbrick, A (1996),** “Fuel film evaporation and heat transfer in the intake port of an S.I. engine”, SAE961120, International Congress & Exposition, Detroit, May 6-9, 1996
- Shin, Y, Min, K & Cheng, W, K (1995),** “Visualisation of mixture preparation in a port-fuel injection engine during engine warm-up”, SAE952481

CHAPTER 7
MOTORED-START & INJECTOR INTERRUPT TESTS

CHAPTER 7

MOTORED-START & INJECTOR INTERRUPT TESTS

7.1 INTRODUCTION

Liquid deposition within the intake port causes significant transient and start-up fuelling problems due to both the volume of fuel resident on the surface and the rate at which it enters the combustion chamber with respect to the air flow. Combustion within an SI engine is directly related to the vapour concentration around the sparking plug at the point of spark initiation, consequently it is necessary to provide an air fuel ratio close to stoichiometric in this vicinity. The ability to achieve this criterion is affected by the accuracy with which fuel flow into the cylinder matches the inducted air mass. During rapidly opening throttle operation, significant enrichment is required in order to maintain the appropriate in-cylinder air/fuel ratio. Drive by wire throttle control eases the problem of matching the fuel and air flows by regulating the speed with which the throttle is opened. However, this will not solve the problem of having a slow moving fuel wall film, it will only reduce its significance.

Closing throttle transients are somewhat harder to overcome. Whilst it is possible and sometimes advantageous for throttle opening to lag the operator input, any delay incurred in closing the throttle would be unacceptable to the user due to safety considerations. When the throttle closes the intake manifold suffers a rapid pressure drop which increases the rate of fuel evaporation from the wall film whilst reducing the air flow. This sequence of events produces a rich spike in the air/fuel ratio with the consequent increase in UHC emissions. Time is also required once the transient has passed to re-establish the fuel film. Clearly the problem of fuel deposition is significant if UHC emissions are to be reduced to a minimum. Fuel shut-off can be employed, but again it does not solve the problem, it just minimises its impact.

Brown & Ladommatos, 1991, attempted to measure the fuel mass accumulated on the port wall of a 2.9 litre V-6 engine by disabling the injector and monitoring the

decaying in-cylinder UHC level for the subsequent 50 cycles using a Combustion HFRFID. The results indicated that the accumulated fuel represented between 3 & 7 times the fuel injected per cycle using engine coolant at 35°C. A slight reduction was obtained through the use of air-atomisation of the fuel spray though injector location ensured a high degree of impaction regardless of the fuel preparation.

Fox *et al*, 1922, took in-cylinder measurements using a HFRFID probe on a motored test rig, to monitor the in-cylinder fuel equivalence ratio from a motored start. The lean limit of the in-cylinder fuel equivalence ratio for first fire at a manifold pressure of 0.5 bar (absolute) was measured to be ≈ 0.6 with this value being obtained within the first 6 to 20 cycles dependent upon the fuelling enrichment. This observation was consistent with the findings of Horie, Takahasi & Akazaki, 1995, who estimated that only 30% of the fuel injected per cycle directly entered the combustion chamber during cold-start conditions. Stable IMEP_{gross} was achieved by Fox, *et al*, at an in-cylinder value of $\phi = 0.8$. Note that HFRFID results only indicate the fuel vapour concentrations around the sample location. The range of inlet equivalence ratios tested was 1.0 to 1.5. The primary factor influencing the in-cylinder mixture composition is the intake manifold pressure which largely determines the in-cylinder residual gas fraction and the degree of intake backflow during inlet valve opening and closing periods. The residual gas fraction will typically be of the order of 15 to 20% at light load and low speed operation, Brown & Ladommatos, 1991, consequently during a motored start the composition of this gas will be unburned air creating a lean mixture within the cylinder for stoichiometric inlet conditions. Tests using vaporised gasoline were undertaken though lamentably only at WOT conditions. Valve overlap backflow is likely to have a significant effect on in-cylinder UHC concentrations if the fuel is able to follow the air motion back into the intake port during part load operation.

Henein *et al*, 1995, performed a wide range of cold-start testing from cranking speed using liquid fuel and calculated the in-cylinder equivalence ratio from the mass of fuel

burned and emitted. First fire always required a fuel-rich charge, varying between $\phi = 1.08$ to 1.75 which compares with the vapour concentration results from Fox *et al* which indicated a range of $\phi = 0.6$ to 0.8 , the residual was presumably the quantity of fuel which remained in the liquid state, the amount of this would be dependent upon engine design and operating factors.

The effects of improved mixture preparation during cold-start and warm-up were reported by Takeda *et al*, 1995. A purpose-built engine was employed allowing the valves to be closed at any time. Hot air was then fed into the combustion chamber through a valve near the sparking plug location at a known flow rate. The gas was bled out of the cylinder via another valve past a FID sample site and the integral of the output curve was used to calculate the mass of fuel. A similar method was used for the intake port. Using a pressurised air-assisted injector, compared to the same injector unassisted, a claimed 40% reduction of both intake port and in-cylinder wall wetting was calculated for the first cycle. The corresponding reduction in the Smd of the fuel spray was from $320 \mu\text{m}$ to $10 \mu\text{m}$ with a pressure drop across the injector nozzle of 200 kPa . It proved possible to reduce the engine fuelling by some 35% due to the improved mixture preparation.

Kashiwaya *et al*, 1990, developed a swirl-type injector which, it was claimed, converted the fuel pressure energy into swirling energy thereby assisting atomisation of the spray. The actual difference in measured fuel spray Smds was a reduction from $176 \mu\text{m}$ to $85 \mu\text{m}$. The mean droplet size was found to exert a strong influence on the engine response time to a step change of throttle opening with a 15% reduction of the lag time associated with the reduced droplet diameter, presumably due to a reduction of the port wall wetting.

7.2 TEST PROGRAMME

The engine described in chapter 5 was used to establish the transient response of the AAFV in both its operating modes compared to a conventional fuel injector. One of the approaches applied was similar to that of Brown and Ladommatos, 1991, that of monitoring the decaying UHC level, though the point of UHC measurement was moved from the combustion chamber to the exhaust port.

The tests were split into two groups: injector interrupt and motored start. During the motored start tests the engine was motored at a constant speed with the fuel injector disabled. A HFRFID probe mounted in the exhaust monitored the UHC concentration. The time taken to reach a combustible in-cylinder air/fuel ratio is related to the quantity of fuel ingested into the combustion chamber, the rate of evaporation and the residual gas composition. The HFRFID was used to detect a firing cycle.

During the injector interrupt tests the engine was operated (firing) at idling conditions for a short period after which the injector and sparking plug were disabled, whilst continuing to motor the engine at the idling speed (800 rev/min). The fuel stored in the manifold and cylinder was then drawn through the engine during subsequent cycles. The UHC trace, again measured in the exhaust port with a HFRFID probe, initially rose to a peak before decaying. The rate of decay indicated the amount of fuel resident within the intake port/manifold and combustion chamber.

7.3 DISCUSSION

7.3.1 Motored-start tests, (idling conditions, 52.3 kPa manifold depression), standard fuel system, open & closed valve injection strategy (refer to figures 7.1-7.6)

A notable feature that occurred during the standard injector tests was that the HFRFID trace saturated within the first 3 cycles regardless of the air/fuel ratio, denoted on the results from the standard injector tests as a 'flat line' response at a concentration of approximately 35,000 ppm C₃¹, signifying HFRFID saturation. This indicates that significant quantities of fuel were entering the combustion chamber and that either sparking plug wetting or poor mixture preparation prevented combustion.

With the standard four-hole plate type injector, and using an open valve injection strategy, an air/fuel ratio of 10.5:1 was required to achieve reliable combustion within the first five cycles, see figure 7.1. A closed valve injection strategy extended the time to achieve reliable combustion using the same air/fuel ratio to seven cycles, figure 7.2. During the cycles prior to combustion when the injector is triggered, the in-cylinder air/fuel ratio increases cycle-by-cycle due to increasing amounts of fuel vapour evaporated from port wall deposits. The process is obviously dependent on the elapsed time and quantity of fuel injected per cycle. The required amount of fuel injected for stoichiometric operation will change with the varying trapped residual composition within the combustion chamber during start-up. The manifold depression established for motored start tests dictated that the trapped residuals would be of the order of 20% (Brown & Ladommatos, 1991 and Fox *et al*, 1992). For the first cycle, the residuals will be air. As injection starts, the composition will change to a lean air/fuel mixture until combustion commences and the residuals will be trapped exhaust gases. For the purpose of the motored start tests, it is the air/fuel concentration of the trapped residuals which are of interest.

¹ Note that a stoichiometric air/fuel ratio calculated using iso-octane would be indicated by a HFRFID reading of approximately 45,000 ppm C₃.

Trace in black indicates EVO event for each cycle
 Each figure shows the results from five tests at the same condition

Figure 7.1
 Motored start unburned exhaust hydrocarbon concentration vs. time after injector enabled, standard injector, 800 rev/min, open valve injection, 360 mm Hg manifold pressure (absolute), 10.5:1 air/fuel ratio

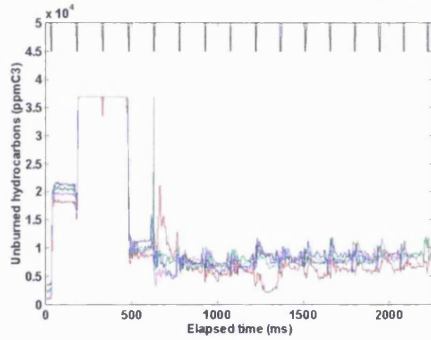


Figure 7.2
 Motored start unburned exhaust hydrocarbon concentration vs. time after injector enabled, standard injector, 800 rev/min, closed valve injection, 360 mm Hg manifold pressure (absolute), 10.5:1 air/fuel ratio

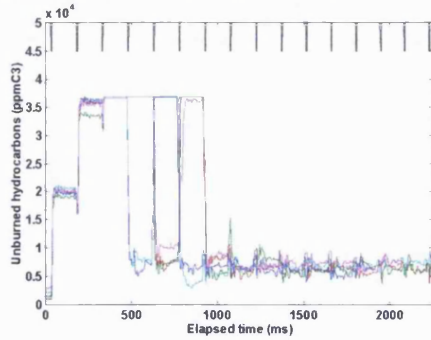


Figure 7.3
 Motored start unburned exhaust hydrocarbon concentration vs. time after injector enabled, standard injector, 800 rev/min, open valve injection, 360 mm Hg manifold pressure (absolute), 11.5:1 air/fuel ratio

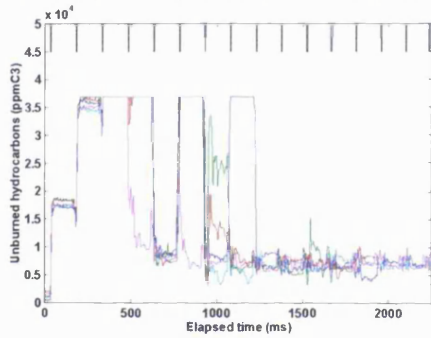


Figure 7.4
 Motored start unburned exhaust hydrocarbon concentration vs. time after injector enabled, standard injector, 800 rev/min, closed valve injection, 360 mm Hg manifold pressure (absolute), 11.5:1 air/fuel ratio

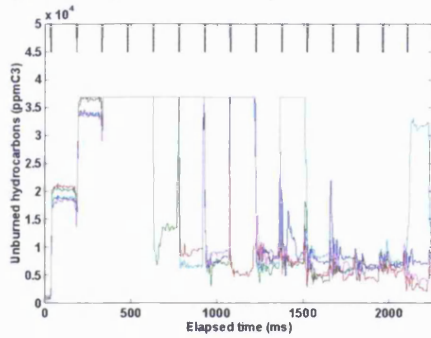


Figure 7.5
 Motored start unburned exhaust hydrocarbon concentration vs. time after injector enabled, standard injector, 800 rev/min, open valve injection, 360 mm Hg manifold pressure (absolute), 12.5:1 air/fuel ratio

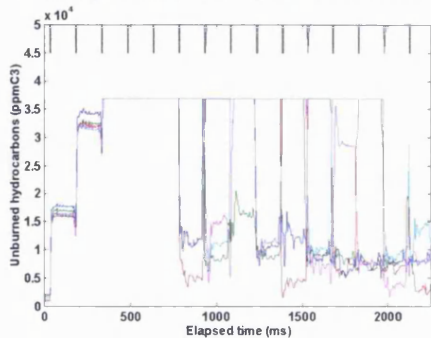
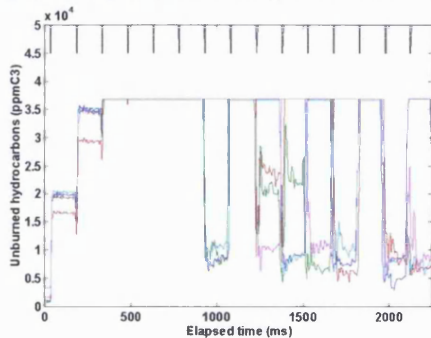


Figure 7.6
 Motored start unburned exhaust hydrocarbon concentration vs. time after injector enabled, standard injector, 800 rev/min, closed valve injection, 360 mm Hg manifold pressure (absolute), 12.5:1 air/fuel ratio



Figures 7.3-7.6 indicate the corresponding unburned hydrocarbon concentrations within the exhaust port for 11.5:1 & 12.5:1 air/fuel ratios, open and closed valve injection. During the tests at 10.5:1 air/fuel ratio it was observed that open valve injection produced a more rapid means of attaining a combustible in-cylinder mixture, a characteristic also evident during the tests at 11.5:1 air/fuel ratio, figures 7.1 & 7.2. The reduction of time to first fire is due to the reduced rate of liquid deposition in the port that occurs with open valve injection and the corresponding increase of airborne fuel delivered to the cylinder. Brown & Ladommatos, 1991, measured a 50% reduction in the fuel film mass by adopting open as opposed to closed valve injection, a result that is also consistent with the pulsating flow rig tests, see chapter 6, which indicated significantly lower vapour concentrations during open valve injection, commensurate with reduced impaction and limited evaporation due to the cold surfaces. Adopting an open valve injection strategy in conjunction with a 12.5:1 air/fuel ratio procured reliable combustion within the first nine cycles, closed valve injection required at least two further cycles, see Figures 7.5 & 7.6.

7.3.2 Motored-start tests, (idling conditions, 52.3 kPa manifold depression), AAFV, air-atomisation, open & closed valve injection strategy (refer to figures 7.7-7.12)

Improving the mixture preparation through the use of the AAFV, as an air-atomised injector, produced a number of interesting results. The maximum exhaust trace UHC level recorded for the open valve injection was close to 30,000 ppm C₃, some 5,000 ppm C₃ lower than observed during tests with the standard fuel injectors. Referring back to chapter 6, inlet port HFRFID measurements performed on the running engine with air assisted fuelling indicated that fuel vapour was displaced upstream of the injector location (figures 6.3 & 6.4). In addition, the corresponding pulsating flow rig tests at idle conditions (figures 6.9 & 6.10) indicated that the closed valve UHC concentration level was dependent upon the displacement backflow that occurs prior to the end of intake valve closure. Putting this information together, one conclusion that can be drawn from this is that the displacement backflow can reduce both the in-cylinder and, following a non-firing cycle, the exhaust UHC measurement.

Figure 7.7
Motored start unburned exhaust hydrocarbon concentration vs. time after injector enabled, air-atomisation, 800 rev/min, open valve injection, 360 mm Hg manifold pressure (absolute), 10.5:1 air/fuel ratio

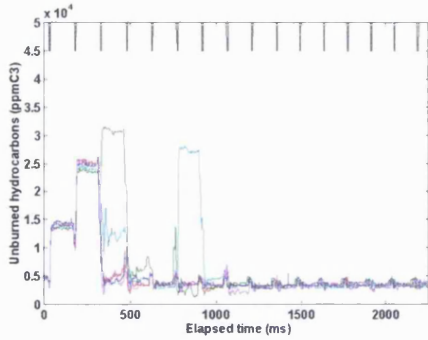


Figure 7.8
Motored start unburned exhaust hydrocarbon concentration vs. time after injector enabled, air-atomisation, 800 rev/min, closed valve injection, 360 mm Hg manifold pressure (absolute), 10.5:1 air/fuel ratio

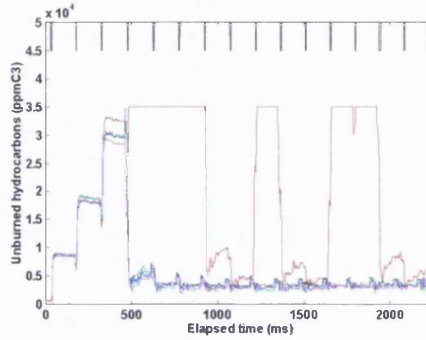


Figure 7.9
Motored start unburned exhaust hydrocarbon concentration vs. time after injector enabled, air-atomisation, 800 rev/min, open valve injection, 360 mm Hg manifold pressure (absolute), 11.5:1 air/fuel ratio

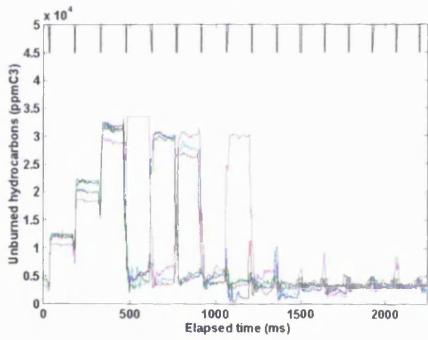


Figure 7.10
Motored start unburned exhaust hydrocarbon concentration vs. time after injector enabled, air-atomisation, 800 rev/min, closed valve injection, 360 mm Hg manifold pressure (absolute), 11.5:1 air/fuel ratio

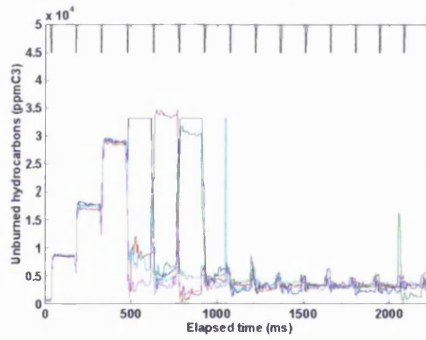


Figure 7.11
Motored start unburned exhaust hydrocarbon concentration vs. time after injector enabled, air-atomisation, 800 rev/min, open valve injection, 360 mm Hg manifold pressure (absolute), 12.5:1 air/fuel ratio

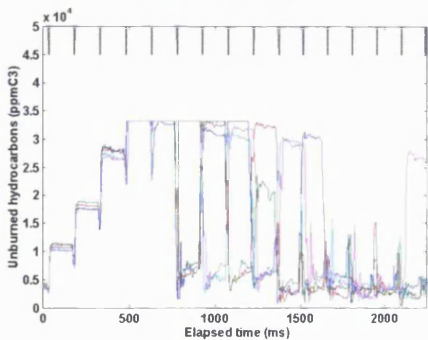
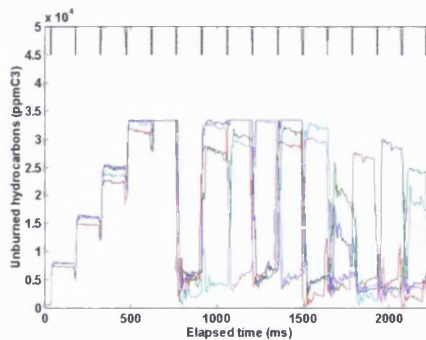


Figure 7.12
Motored start unburned exhaust hydrocarbon concentration vs. time after injector enabled, air-atomisation, 800 rev/min, closed valve injection, 360 mm Hg manifold pressure (absolute), 12.5:1 air/fuel ratio



Comparison of exhaust traces measured after the initial start between the standard injectors and the air-atomised mixture demonstrated a significant reduction of test-to-test variability using the AAFV, an indication of the improved in-cylinder mixture.

Improving the mixture preparation appears to offer an increased tolerance to injection strategy with both open valve and closed valve injection requiring the same number of cycles to achieve first fire, three and seven for the 10.5:1 and 11.5:1 air/fuel ratios respectively, compare figures 7.7 & 7.9 with 7.8 & 7.10. This characteristic was also noted during the intake port sampling tests of the air-atomised mixture on the pulsating flow rig (compare chapter 6, figures 6.7 & 6.8 with figures 6.9 & 6.10 respectively) where injection timing had little effect on the inlet port UHC concentrations.

Figures 7.11 & 7.12 indicate that an air/fuel ratio of 12.5:1 was insufficient to promote reliable combustion within the test duration, some fifteen cycles after injector initiation.

7.3.3 Motored-start tests, (idling conditions, 52.3 kPa manifold depression), AAFV, fuel vaporisation, open & closed valve injection strategy (refer to figures 7.13-7.16)

The same degree of tolerance to injector timing was noted for the vaporised mixture as observed during tests with air-atomisation of the fuel spray, see figures 7.13 & 7.14. Importantly, it was possible to achieve combustion with higher air/fuel ratios than those used in the previous (standard and air-atomisation) tests. First fire was achieved generally within four cycles using the vaporised mixture operating with a 13.5:1 air fuel ratio and continuous firing was reached within the first eight cycles.

During stoichiometric tests first fire was obtained by cycle 6, though continuous firing was not achieved within the duration of the test, some 15 cycles after fuelling started. Problems of attaining a stoichiometric in-cylinder mixture with vaporised fuel, as

Figure 7.13
Motored start unburned exhaust hydrocarbon concentration vs. time after injector enabled, fuel vaporisation, 800 rev/min, open valve injection, 360 mm Hg manifold pressure (absolute), 13.5:1 air/fuel ratio

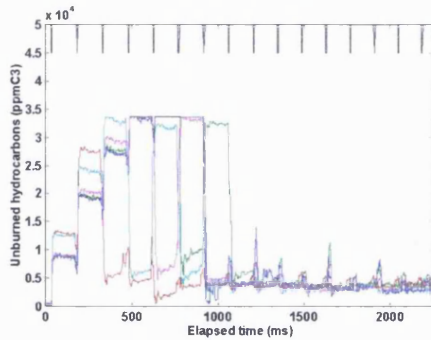


Figure 7.14
Motored start unburned exhaust hydrocarbon concentration vs. time after injector enabled, fuel vaporisation, 800 rev/min, closed valve injection, 360 mm Hg manifold pressure (absolute), 13.5:1 air/fuel ratio

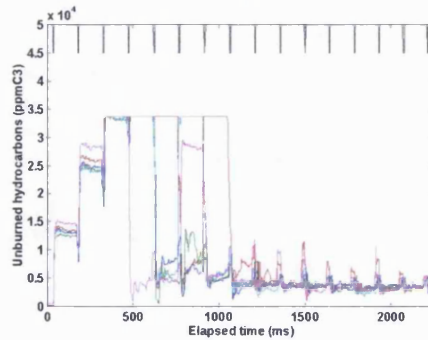


Figure 7.15
Motored start unburned exhaust hydrocarbon concentration vs. time after injector enabled, fuel vaporisation, 800 rev/min, open valve injection, 360 mm Hg manifold pressure (absolute), stoichiometric air/fuel ratio

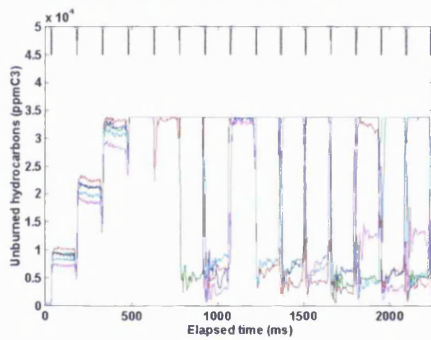
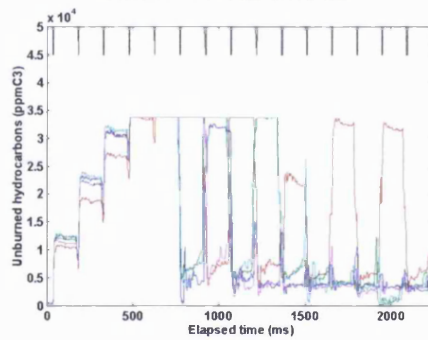


Figure 7.16
Motored start unburned exhaust hydrocarbon concentration vs. time after injector enabled, fuel vaporisation, 800 rev/min, closed valve injection, 360 mm Hg manifold pressure (absolute), stoichiometric air/fuel ratio



opposed to a liquid, are brought about by the vapour's ability to follow the air flow. Intake backflow displaces a significant quantity of fuel with the air stream and the trapped residual would consequently be at a lower UHC concentration. Figures 7.15 & 7.16, highlight the difficulty in retaining the fully vaporised fuel within the combustion chamber at the point of intake valve closure in conjunction with the appropriate composition of trapped residual gases.

The test results clearly indicate the reduced fuelling required using the AAFV in its vaporising mode. In order to achieve a similar number of cycles to first fire, the standard fuel system required a 10.5:1 air/fuel ratio and the air-atomised mixture preparation an 11.5:1 air fuel ratio compared to the vapour's 13.5:1.

7.4 INJECTOR INTERRUPT TESTS

7.4.1 Curve fitting program as applied to injector interrupt test measurements

Raw data was corrected for the time response of the HFRFID using the proprietary software package SATFLAP, and split into individual engine cycles, noting the point of injector interrupt. Processing the data was only performed if the injector was disabled before the injection event for the current cycle and after combustion of the previous cycle. This ensured a constant point of reference for each cycle, because if the criterion was not met then the exhaust concentration for the first exhaust event post interrupt would represent a fuelled misfiring cycle, distorting the results. The mean UHC level was then calculated for each cycle.

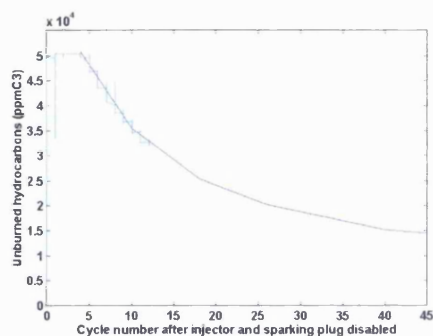
The characteristic of the exhaust UHC concentration post interrupt was to ramp up to a maximum within 2-5 cycles as the majority of the liquid fuel was drawn into the combustion chamber and passed directly into the exhaust port after which the concentration decayed exponentially due to the diminishing fuel reserves contained within the intake system. A computer program was written in MATLAB, which fitted an exponential decay to the raw data of the cycles that occur after the initial ramp peaks. A cubic spline was used to fit the mean UHC trace that was then plotted on a log-log scale. Since the UHC decayed exponentially, a straight line curve fit was used to extrapolate the data beyond the measurement limit, typically beyond 10-15 cycles post interrupt. The gradient was calculated by differentiating the curve along its length and finding the mean, and the curve was then plotted using Cartesian coordinates. The accuracy of the assumptions and curve fitting approximations are shown in figures 7.17-7.19 where the raw data and the fitted curve are drawn.

Injector interrupt tests allow an appreciation of both the fuel within an engine upstream of the exhaust valve and the rate at which the fuel is purged from the wetted surfaces. Typical UHC decay rates produced by the different mixture preparation processes can be seen in figures 7.17-7.19. The curve fit was applied to the raw data

measured for fifteen cycles after the spark and injector were interrupted. The initial ramp up to the peak, from which point the traces are shown, is not included in this analysis as the decay rate was of primary interest here.

Figure 7.17

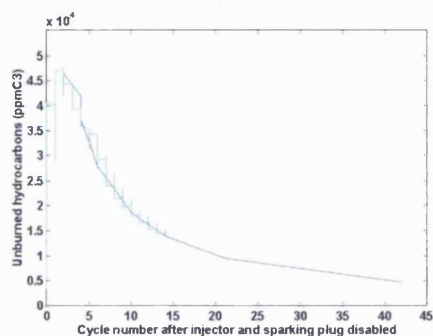
Typical UHC decay after injector interrupt, raw data & curve fit, standard injector, closed valve injection, 360 mm Hg manifold pressure (absolute), 800 rev/min, stoichiometric fuelling



Raw HFRFID data, Exponential decay curve fit

Figure 7.18

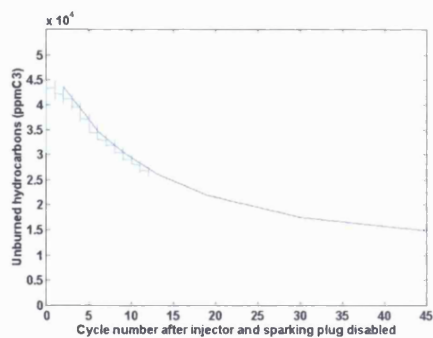
Typical UHC decay after injector interrupt, raw data & curve fit, air-atomisation, closed valve injection, 360 mm Hg manifold pressure (absolute), 800 rev/min, stoichiometric fuelling



Raw HFRFID data, Exponential decay curve fit

Figure 7.19

Typical UHC decay after injector interrupt, raw data & curve fit, vaporised fuel, closed valve injection, 360 mm Hg manifold pressure (absolute), 800 rev/min, stoichiometric fuelling



Raw HFRFID data, Exponential decay curve fit

7.4.2 Injector interrupt tests, (idling conditions, 52.3 kPa manifold depression), standard fuel system, open & closed valve injection strategy (refer to figures 7.20-7.25)

Using the standard injector, as the UHC level decayed from its peak value (beyond the saturation measurement of the HFRFID) an exhaust concentration of approximately 52,000 ppm C₃ was measured, some five cycles after the fuel injector was disabled, see figure 7.20. This compares with 42,000 and 35,000 ppm C₃ for the air-atomised and vaporised fuel mixture respectively after the same number of elapsed cycles, see figures 7.21 & 7.22. Normalising results against the standard injector reveals that air-atomisation of the liquid fuel represented a 19% reduction and the vaporised fuel a 33% reduction in the UHC concentration of the air flow through the engine. The results effectively indicate the extent of liquid deposition produced by the standard fuel injector and the slow rate at which that fuel was both drawn through the engine and continues to evaporate from the port surfaces when compared with the other systems.

The presence of substantial liquid fuel deposits when testing with standard fuel injectors have already been inferred both from previous tests, see chapters 5 & 6, and through independent research, Shayler, Colechin & Scaribrick, 1996, Brown & Ladommatos, 1991. Fuel has two mechanisms by which it can be inducted into the combustion chamber post injector interrupt, either direct induction of the liquid film or through continued evaporation from the liquid deposits. The high initial concentration levels measured during tests of the standard injector were felt to be due to liquid fuel directly entering the combustion chamber. This mechanism can only be sustained for one or two cycles as the reserve of the liquid deposit was not being replenished. Approximately 45,000 ppm C₃ represents a stoichiometric unfired exhaust concentration (based on calculations for iso-octane). By cycle fifteen, the concentration can be seen to have dropped to 30,000 ppm C₃ for the standard injector tests, a reduction of 42% from the UHC level measured at cycle five. The air-atomisation and vaporised fuel tests indicated UHC concentrations of 26,000 ppm C₃

Each figure shows the scatter for 10 tests at the same condition.

Note: open valve injection strategy only shows results for 3 tests due to data acquisition problems.

Figure 7.20

UHC decay after injector interrupt, exponential decay curve fit, standard injector, closed valve injection, 360 mm Hg manifold pressure (absolute), 800 rev/min, stoichiometric fuelling

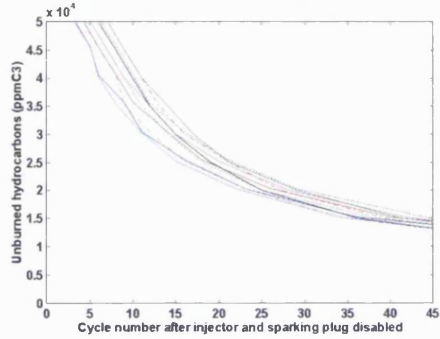


Figure 7.23

Calculated cumulative UHC, standard injector, closed valve injection, 360 mm Hg manifold pressure (absolute), 800 rev/min, stoichiometric fuelling

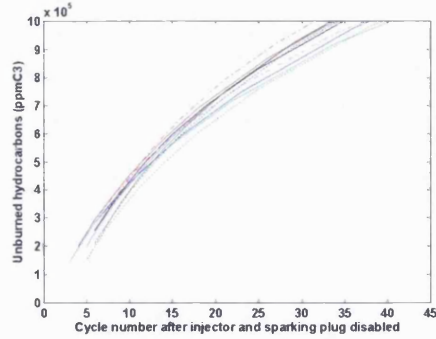


Figure 7.21

UHC decay after injector interrupt, exponential decay curve fit, air-atomisation, closed valve injection, 360 mm Hg manifold pressure (absolute), 800 rev/min, stoichiometric fuelling

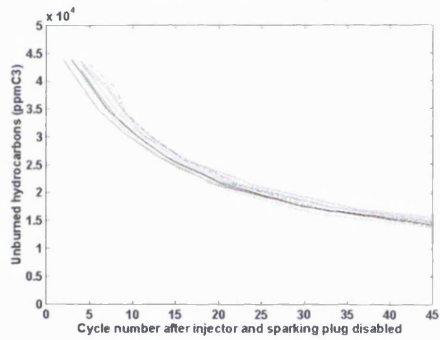


Figure 7.24

Calculated cumulative UHC, air-atomisation, closed valve injection, 360 mm Hg manifold pressure (absolute), 800 rev/min, stoichiometric fuelling

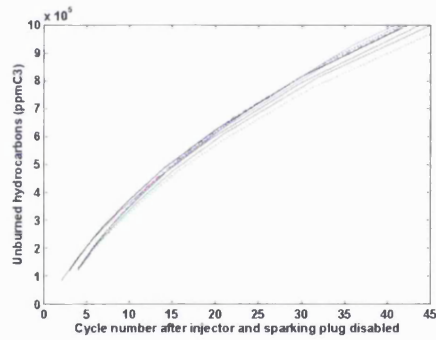


Figure 7.22

UHC decay after injector interrupt, exponential decay curve fit, vaporised fuel, closed valve injection, 360 mm Hg manifold pressure (absolute), 800 rev/min, stoichiometric fuelling

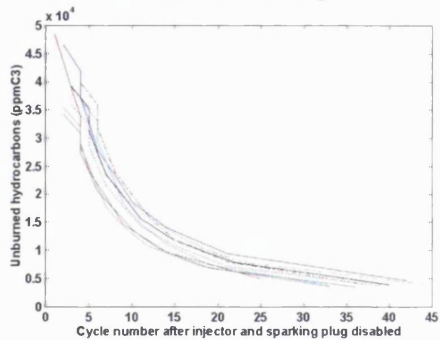
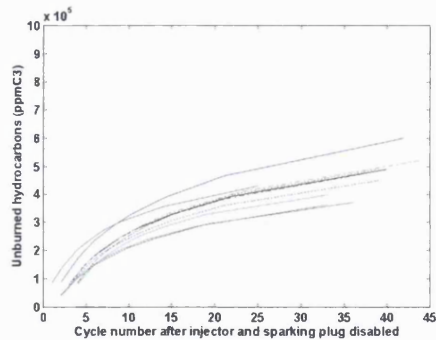


Figure 7.25

Calculated cumulative UHC, vaporised fuel, closed valve injection, 360 mm Hg manifold pressure (absolute), 800 rev/min, stoichiometric fuelling



and 12,000 ppm C₃ respectively. These values represent reductions of 38% and 65% from levels measured at the fifth cycle for the air-atomised mixture and vaporised fuel respectively.

It is interesting to note the similarity of decay rates for the standard injector and the air-atomised tests. The difference in the initial concentration levels immediately after the injector was disabled is symptomatic of the larger wall film required by the standard mixture preparation process during steady state operation. Once readily available direct liquid intake was depleted, the rate of decay converges, presumably since the fuel remaining after this initial purge is similar for both the standard injectors and the air-atomised mixture.

The initial concentration of approximately 35,000 ppm C₃ at cycle five for the vaporised mixture has reduced to 12,000 and subsequently 7,500 ppm C₃, representing decays of 65% and 78%, by cycles fifteen and twenty five respectively. Integrating the unburned hydrocarbon curve with respect to time provides a useful indication of the cumulative fuel mass exhausted by the engine, see figures 7.23-7.25. Note that the results presented within the text refer specifically to closed valve injection timing, however, no discernible difference was measured between open and closed valve injection strategies. Appendix A7 contains the figures referring to open valve injection testing. The HFRFID measures hydrocarbon concentration levels and therefore accurate mass calculations cannot be made without knowing the instantaneous mass flow rates through the exhaust valve. Again, by normalising the results from the standard fuel system a 50% reduction of the quasi-cumulative UHC mass was predicted using vaporised fuel and a 12.5% decrease for the air-atomised tests over the first 40 cycles.

A number of mechanisms exist that are responsible for the diminishing rate of decay seen throughout the test results. Once the majority of direct liquid flow into the combustion chamber has occurred, which will depend upon the operating condition, fuel evaporation from the port walls will be the predominant source of unburned

hydrocarbons. Evaporation will be from a decreasing quantity of fuel, and therefore incur a continuously reducing volume to surface area ratio slowing down the process. Conduction of the combustion heat to the intake port will cease and the back flow of gases, previously responsible for a significant degree of evaporation of the liquid film, refer to chapter 6, will cool dramatically.

The process of evaporation itself will reduce the temperature of the liquid deposits due to the latent heat of evaporation of the fuel. As the cycling continues, the lighter ends of the fuel composition will vaporise first leaving a residue of the heavier ends with a higher associated boiling point that necessarily take longer to evaporate. Finally, even if no deposition occurs, some time to purge the engine of vapour will be required due to the backflow process within the intake manifold during inlet valve closure displacing, albeit an ever decreasing concentration, some of the ingested fuel vapour.

7.5 CONCLUSIONS

The degree of port wall wetting was minimised by the AAFV in vapour mode such that the engine achieved continuous firing from a motored-start with a leaner injected mixture than either the AAFV in air-atomised mode or the standard injector by 17% and 28%, respectively.

The injector interrupt tests confirmed the port wall wetting characteristics of the differing mixture preparations, with the AAFV in vaporising mode exhibiting the lowest residuals post interrupt and an increased rate of UHC decay. The air-atomisation mode of the AAFV gave lower residuals than the standard injector, though the rate of UHC decay was broadly similar.

Whilst it was somewhat disappointing that a degree of 'wetting' was evident with the vaporised fuel, it must be remembered that it is difficult to evaporate the 'heavy ends' of the fuel. Some of the fuel vapour will have been absorbed in the cylinder oil film and forced down crevices, to be released later, and this will also account for some of the UHC emissions post interrupt.

7.6 REFERENCES

- Brown, C N & Ladommatos, N** (1991), "The effects of mixture preparation and trapped residuals on the performance of a spark-ignition engine with air-shrouded port injectors, at low load and low speed", IMechE, Part D: Journal of automotive engineering, D02690
- Fox, J W, Min K D, Cheng, W K & Heywood, J B** (1992), "Mixture preparation in a S.I. engine with fuel injection during starting and warm-up", SAE922170
- Henein, N A, Tagomori, M K, Yassine, M K, Asmus, T W, Thomas, C P & Hartman, P G** (1995), "Cycle-by-cycle analysis of HC emissions during cold start of gasoline engines", SAE952402
- Horie, K, Takahasi, H, & Akazaki, S** (1995), "Emissions reduction during warm-up period by incorporating a wall-wetting fuel model on the fuel injection strategy during engine starting", SAE952478
- Kashiwaya, M, Kosuge, T, Nakagawa, K & Okamoto, Y** (1990), "The effect of atomisation of fuel injectors on engine performance", SAE 900261
- Shayler, P J, Colechin, M J F & Scarisbrick, A** (1996), "Fuel film evaporation and heat transfer in the intake port of an S.I. engine", SAE961120, International Congress & Exposition, Detroit, May 6-9, 1996
- Takeda, K, Yaegashi, T, Sekiguchi, K, Saito, K & Imatake, N** (1995), "Mixture preparation and HC emissions of a 4-valve engine with port fuel injection during cold starting and warm-up", SAE950074

APPENDIX A7

A7.1 INJECTOR INTERRUPT DECAY AND CUMULATIVE UHC TRACES

Each figure shows the scatter for 10 tests at the same condition.

Note: open valve injection strategy only shows results for 3 tests due to data acquisition problems.

Figure A7.1

UHC decay after injector interrupt, exponential decay curve fit, standard injector, open valve injection, 360 mm Hg manifold pressure (absolute), 800 rev/min, stoichiometric fuelling

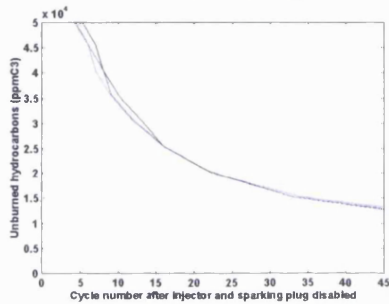


Figure A7.4

Calculated cumulative UHC, standard injector, closed valve injection, 360 mm Hg manifold pressure (absolute), 800 rev/min, stoichiometric fuelling

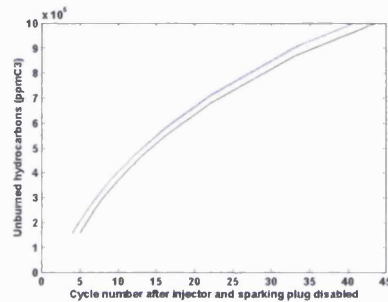


Figure A7.2

UHC decay after injector interrupt, exponential decay curve fit, air-atomisation, open valve injection, 360 mm Hg manifold pressure (absolute), 800 rev/min, stoichiometric fuelling

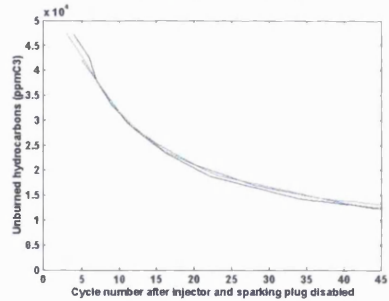


Figure A7.5

Calculated cumulative UHC, air-atomisation, open valve injection, 360 mm Hg manifold pressure (absolute), 800 rev/min, stoichiometric fuelling

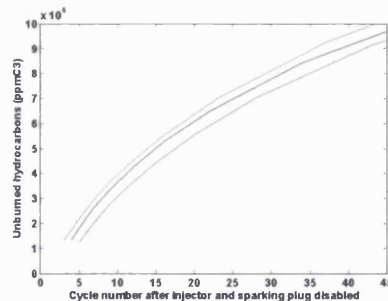


Figure A7.3

UHC decay after injector interrupt, exponential decay curve fit, vaporised fuel, open valve injection, 360 mm Hg manifold pressure (absolute), 800 rev/min, stoichiometric fuelling

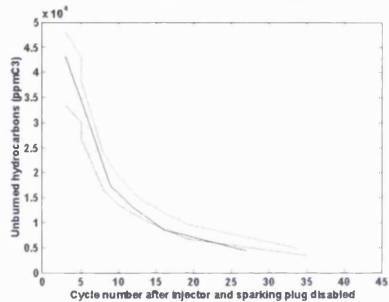
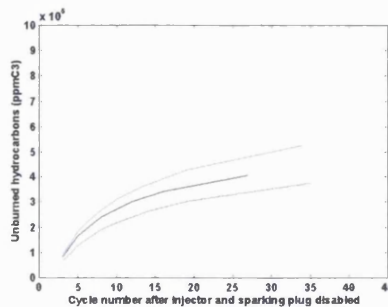


Figure A7.6

Calculated cumulative UHC, vaporised fuel, open valve injection, 360 mm Hg manifold pressure (absolute), 800 rev/min, stoichiometric fuelling



CHAPTER 8

CONCLUSIONS AND SUGGESTIONS FOR FUTURE WORK

CHAPTER 8

CONCLUSIONS AND SUGGESTIONS FOR FUTURE WORK

8.1 SUMMARY OF CONCLUSIONS FROM PRECEDING CHAPTERS

8.1.1 Steady flow rig tests

The initial steady flow rig tests highlighted the exit nozzle diameter and pressure drop across the nozzle of the AAFV as the significant influences on mixture preparation when operating in its atomising mode. Testing the AAFV during vaporising mode indicated that the heated surface area of the glow plug was the primary influence on ability of the design to vaporise the injected fuel. The tests showed that complete vaporisation of the fuel at a stoichiometric air/fuel ratio could be achieved at idle with a power requirement of 100 Watts/cylinder and that significant vaporisation occurs at the 1500 rev/min road load operating condition. The test results suggested that the following values of the critical dimensions should be adopted for subsequent work: 1.2 mm exit nozzle diameter, 1.0 mm diametral clearance and a glow plug length of approximately 30 mm. Using this geometry, mean droplet diameters below 30 μm can be expected at either idle or 1500 rev/min road load conditions using a passive air bleed to the AAFV in air-assistance mode.

8.1.2 Cold-start engine tests

Engine testing with a set of AAFVs in their vaporising mode showed that a stoichiometric air/fuel ratio can be achieved from a cold-start and maintained for the period prior to catalyst light-off, reducing the total engine-out unburned hydrocarbon emissions by 48% from a start temperature of 7°C compared with results obtained using the standard fuel system. The level of power required compares very favourably with an alternative technology, the electrically-heated catalyst. Further, the AAFV does not incur the durability penalty.

The engine tests indicated that passive air-assistance was unable to generate a sufficient pressure drop across the AAFV exit nozzle during cranking for satisfactory operation.

8.1.3 Intake port HFRFID sampling: engine tests

An open valve injection strategy was shown to exhibit greater UHC vapour residuals within the intake port at higher load conditions than closed valve injection. This characteristic indicated that the time period required to purge the AAFV of fuel was greater than the period of forward flow through the inlet valves.

HFRFID sampling upstream of the standard injectors indicated that the intake backflow during initial valve opening gave very low levels of vapour concentration compared to the levels measured using the AAFV in either of its operating modes. This was due to the vapour cloud/small droplets associated with the AAFV mixture preparation becoming more easily entrained in the gas flow. The vapour concentrations were an order of magnitude greater with the AAFV.

An acceptable pressurised air supply for the AAFV was achieved through use of a combustion chamber tapping, and it appeared to decrease the sensitivity to injection timing of intake port residuals during the closed valve period. No durability problems were encountered during the short test programme. Exhaust UHC concentrations were not affected by any increased crevice volume associated with the tapping or pipe-work.

8.1.4 Intake port HFRFID sampling; PFR tests

The effects of intake port temperature and backflow were isolated and found to affect both the location and concentration of fuel vapour within the intake port. Constant air flow through the AAFV was found to promote vapour migration upstream of the injector location in the normally quiescent intake port during the closed valve period.

Lower UHC levels with an open valve injection timing were measured around the intake valve during engine tests using standard injectors at 1500 rev/min road load. This indicated that the temperature of the inlet port surface reaches a temperature sufficient to reduce substantially the liquid deposition around the valve seat area. Vapour concentrations within the intake port at the 1650 rev/min WOT condition were up to 25% greater during engine tests using the AAFV with the cylinder pressure tapping, demonstrating the effects of both the warm intake port surface and the increased temperature of the air bleed.

8.1.5 Motored-start and injector interrupt tests

Vaporised fuel reduced the intake port wall wetting to a minimum and allowed the engine to fire on a 13.5:1 air fuel ratio within the first 5-8 cycles after enabling the injector. This represented reductions of fuel flow of 17% and 28% by comparison with air-assisted and the standard injector mixture preparation processes.

Injector interrupt tests confirmed the port wall wetting characteristics of the differing mixture preparations. The lowest residuals post interrupt were measured using the AAFV in vaporising mode coupled with the fastest rate of UHC decay measured over the subsequent cycles. The air-atomisation mode of the AAFV gave lower residuals than the standard injector, but with an approximately similar UHC decay rate.

8.2 FURTHER DEVELOPMENT POSSIBILITIES FOR THE AAFV

The benefits of reducing engine-out UHC emissions through use of the AAFV are clear. The continual movement towards more stringent emissions requirements will mean that untreated exhaust gases, even from a successful stoichiometric start, will have unacceptably high UHC levels. Thus, the AAFV will not alone provide the answer to cold-start emissions and its future will lie in being a possible additional measure, rather than a replacement, for fast warm-up catalyst systems. However, the power requirement of the device necessary for fuel vaporisation is relatively modest, approximately 100W/cylinder. This offers the possibility of eliminating the starting peak on the UHC trace, thus requiring the catalyst to deal with a relatively modest UHC concentration, rather than the exceptionally high level normally associated with this period of engine operation. An important additional consideration is that for a fast warm-up catalyst to reduce tail-pipe UHC emissions a stoichiometric mixture must be achieved quickly for effective operation which is likely to be before the engine is warm. The driveability (smoothness) of the engine will be unacceptable to the driver unless the mixture preparation of its fuel system is exceptionally good. The faster that catalysts warm up, the greater the challenge that this sets. Again the AAFV would have a role to play.

Further justification for adoption of the AAFV may be provided in terms of overall efficiency. Assuming that the average air/fuel ratio required by a four-cylinder engine equipped with a conventional fuel system for a cold start would be of the order of 12:1 for the first 30 seconds, whereas the AAFV can start at 14.7:1, then the fuel saving is (assuming an air flow rate of 1.0 g/s/cylinder):

$$4 \times 1.0 \left(\frac{1}{12.5} - \frac{1}{14.7} \right) \times 30 = 1.44 \text{ g}$$

taking the calorific value of the fuel to be 43 MJ/kg, this is equivalent to 61.9 kJ or 2 kW for 30 seconds. The power consumption of the AAFVs fitted to a 4-cylinder engine would be 400 Watts over a period of approximately 30 seconds, and this must be weighed against the potential fuel saving.

The effectiveness of the AAFV as an air-assisted atomiser during the period of operation when the engine is warm should not be forgotten. It also offers the potential to reduce wall film and hence improve the transient response of an engine.

Overall, it can be said that a strong case can be made to continue development of the AAFV.

8.2.1 Recommendations for further research

The steady flow tests described in chapter 2 showed that a surprisingly high proportion of the electrical energy was not being transferred to the fuel. Some improvement would be expected if the outside of the AAFV was thermally insulated.

One criteria that limited the design of the unit was the need to use a standard diesel glow plug. The move to a dedicated design of heating element would allow further optimisation of the design to improve the rate of heat transfer, while making a useful reduction to the thermal inertia. An electrical power modulation system was designed and built, though time constraints precluded development, see Appendix A8. This development must also be seen as a high priority.

The cylinder pressure tapping used to provide air-assistance for the AAFV requires investigation on a multi-cylinder engine to establish both the durability and to determine the effects on the engine's fuel consumption and UHC emissions. Ideally, this would encompass a design of tapping that allowed cross linking between cylinders in order to match the pressure pulse to the injection timing strategy.

The use of a Lee 'visco-jet' type restriction within the tapping may also be advantageous due to the claimed reduction of clogging through the swirl-inducing passages within the restrictor. However, it would have to be manufactured out of a different material if it were to withstand IC engine operating temperatures.

8.3 CLAIMS OF ORIGINALITY

The original contributions made through this research are:

- (i) Taking a novel design of fuel system and optimising its dimensions for performance in vaporising and air-assisted modes of operation.
- (ii) Demonstrating the potential reductions in UHCs available from using vaporised fuel for the starting and warm-up of a modern multi-cylinder SI engine.
- (iii) Redesigning the novel fuel system to make it more efficient in operation and practical in use.
- (iv) Investigating a novel idea for a pressurised air supply and obtaining satisfactory performance from it.
- (v) Investigating the mixing of air and vaporised fuel in the intake port using HFRFID probes, and comparing the results with those obtained from air-assisted and standard injection. Relatively little was known about the behaviour of vaporised fuel in the inlet manifold before this work, and its movement upstream from the injector location has been clearly demonstrated.
- (vi) Quantifying the improvement from the new fuel system in terms of UHC held in store between the injector and exhaust port, by using injector interrupt tests. Also quantifying the benefits in starting with the new fuel system.

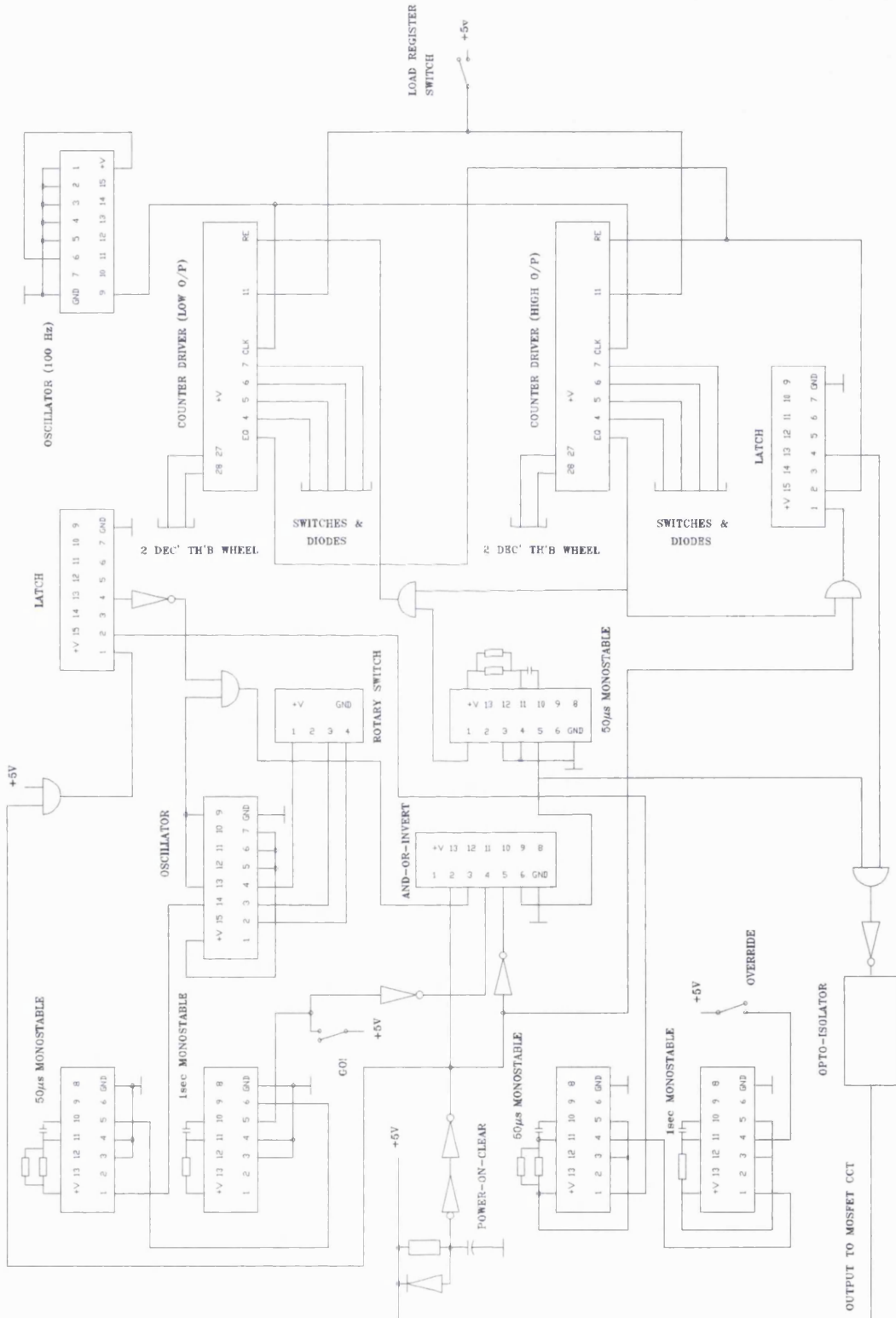
APPENDIX A8

A8.1 GLOW PLUG POWER CONTROLLER

A purpose-designed electronic controller was designed to allow the duration of time the elements were switched on for to be varied with the capability of modulating the power by supplying the heating elements via a square-wave driving voltage throughout this period. The duration and frequency of the square-wave is varied independently, with the supplied current controlled by the square-wave voltage amplitude. The controller output is used to switch a series of high power, metal-oxide, semi-conductor field effect transistors (MOSFETs) which are connected in series with the heating elements, see figures A8.1 & A8.2.

Figure A8.1

Circuit diagram for glow plug modulation



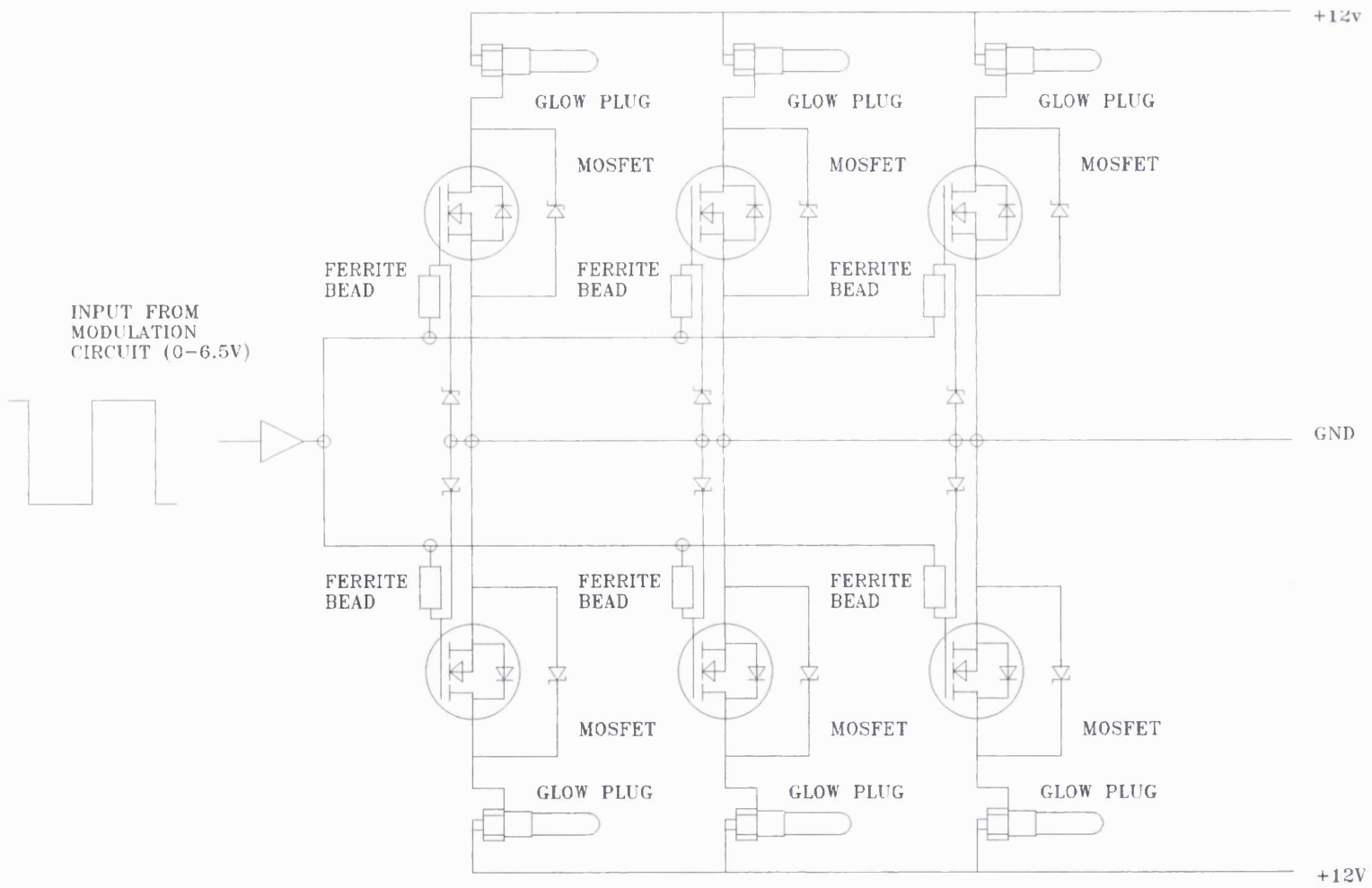


Figure A8.2
Glow plug driver circuit